UNIVERSITY OF CATANIA

DEPARTMENT OF BIOMEDICAL AND BIOTECHNOLOGICAL SCIENCES

INTERNATIONAL PhD PROGRAM IN NEUROSCIENCE

XXXII CYCLE

Maria Gaetana Giovanna Pittalà

Structural characterization of the Voltage-Dependent Selective Anion Channels (VDACs)

PhD Thesis

Tutor: *Prof. Vito De Pinto*

Co-tutors: *Prof. Rosaria Saletti*

Prof. Angela Messina

PhD Coordinator: *Prof. Claudio Bucolo*

A C A D E M I C Y E A R S 2 0 1 7 / 2 0 1 9

There is only one way to access Science: to meet a problem, to be fascinated by its beauty, to fall in love with it, to generate child-problems, to start a new family of problems.

Karl Popper

A mio fratello Salvatore,

la mia parte migliore…

Abstract

Cysteine and methionine residues are unique amino acids in proteins for their property to undergo several redox reactions as part of their normal function. Mitochondria are the cell source of most chemical energy obtained as the end-product of the aerobic oxidation of glucose. Mitochondria are also the source of an abundant production of radical species and it is surprising that such a large availability of highly reactive chemicals is compatible with viable and active organelles, needed for the cell functions. In this work I show the studies of post-translational modifications (PTMs) of cysteine and methionine residues, both sulfur amino acids, in the Voltage-Dependent Selective Anion Channel Isoforms (VDACs), the most abundant proteins of the Outer Mitochondrial Membrane (OMM) where they form aqueous pores which allow the passage of ions and small molecules. VDACs are involved in complex interactions regulating organelle and cellular functions and thus contribute to homeostasis maintenance. Because of their central role in metabolism and interactions with several cytosolic enzymes and apoptotic factors, VDACs have emerged as key players in cancer and in neurodegenerative diseases such as Alzheimer's disease (AD), Parkinson's disease (PD) and Amyotrophic Lateral Sclerosis (ALS).

This interesting protein family carries several cysteinesin the loop regions exposed to the oxidative inter-membrane space (IMS) and it is reasonable to suppose that the redox state of VDACs can be modified in this peculiar environment.Through UHPLC/High Resolution nESI MS/MS and the development of a new "in solution-digestion" protocol, cysteine and methionine PTMs were precisely determined in rat and human VDAC proteins obtaining very consistent results.

These analysis show that cysteine residues, in physiological state, can be subject to several oxidization steps, ranging from the permanently reduced state, that indicates the possibility of disulfide bridges formation, to the most oxidized, the sulfonic acid, one. Noteworthy, this last oxidative state is irreversible in the cells and itis an exclusive feature of VDAC proteins becauseit was not detectable in other mitochondrial membrane proteins, as defined by their elution at low salt concentration by a hydroxyapatite (HTP) column. Furthermore, methionine residues are detected both in normal form and oxidized to methionine sulfoxide.

The large spectra of VDAC cysteine oxidations, indicate that they could have both a regulative function and a buffering capacity able to counteract excess of mitochondria ROS load. The quest for the complete identification of disulfide bridges is the next, highly challenging, from the technical point of view, goal of this research.

Finally, other PTMs of cysteines such as succination or the presence of selenocysteines and phosphorylation of serine, threonine and tyrosine residues were investigated.

The results of my PhD thesis are reported in papers published in important impact factor journals.

Tableofcontents

LIST OF ABBREVIATIONS

1-DE	one-Dimensional Electrophoresis
2-DE	two-Dimensional Electrophoresis
2SC	S-(2-succino)cysteine
ACN	Acetonitrile
AD	Alzheimer'sDisease
Ala	Alanine
ALS	AmyotrophicLateralSclerosis
Arg	Arginine
Asn	Asparagine
CHAPS	3-[(3-cholamidopropyl)dimethylammonio]-1-propanesulfonate
CI	ChemicalIonization
CID	CollisionInducedDissociation
CLM	ChronicMyelogenousLeukemia
Cys	Cysteine
DAO	D-amino acid oxidase
DTT	Dithiothreitol
DUB	DeubiquitylatingEnzyme
EDTA	Ethylenediaminetetraacetic acid
EGTA	Ethyleneglycoltetraacetic acid
EI	Electron Impact
ETD	Electron-transfer dissociation
FA	Formic Acid
FALS	FamilialAmyotrophicLateralSclerosis
FBS	Fetal Bovine Serum
FDR	False Discovery Rate
FWHM	Full Width at Half Maximum
GAPDH	Glyceraldehyde-3-phosphate dehydrogenase
Gln	Glutamine
Glu	Glutamic acid
GSH	Glutathione
GSK3β	GlycogenSynthase kinase-3β
HCD	High-energyCollisionDissociation
HEPES	4-(2-hydroxyethyl)-1-piperazineethanesulfonic acid
His	Histidine
HPLC	High-Performance Liquid Chromatography
HTP	Hydroxyapatite
IAA	Iodoacetamide
IEF	IsoelectricFocusing
IMDM	Iscove'sModifiedDulbecco's Medium
IMM	Inter Mitochondrial Membrane
IMS	Inter-Membrane Space
INSR	InsulinReceptorTyrosineKinase
IPG	ImmobilizedpHGradient
IT	Ion Trap

LC	Liquid Chromatography
Lys	Lysine
MALDI	Matrix-Assisted Laser Desorption/Ionization
MD	MolecularDinamic
MDVs	Mitocondria-DerivedVesicles
Met	Methionine
MIA	MitochondriaIntermembrane Space Assembly
MPTP	MitochondrialPermeabilityTransitionPore
MuDPIT	MultidimensionalProteinIdentification Technology
NADH	Nicotinammide adenine dinucleotide
Nek1	NIMA-RelatedProteinKinase
nESI	nano ElettroSprayIonization
NMR	NuclearMagneticResonance
Nt	N-terminal
OMM	Outer mitochondrial Membrane
OXPHOS	MitochondrialOxidativePhosphorylation
Ox-PTM	Oxidative-Post-TranslationalModification
P/S	Penicillin-streptomycin
p38MAPK	p38 Mitogen-Activated Protein Kinase
PBS	PhosphateBuffered Saline
PD	Parkinson'sDisease
PDI	ProteinDisulfideIsomerase
PINK1	PTEN-inducedkinase 1
PKC	ProteinKinase C
PKC	ProteinKinase A
PKI	ProteinKinaseInhibitor
PMSF	Phenylmethylsulfonylfluoride
PTM	Post-translationalModification
Q	Quadrupole
Q-OT-qIT	Orbitrap Fusion Tribrid
ROS	ReactiveOxygenSpecies
RP-HPLC	Reverse Phase-High Performance Liquid Chromatography
SDS	Sodio Dodecilsolfato
SDS-PAGE	Sodium Dodecyl Sulphate - PolyAcrylamide Gel Electrophoresis
Sec	Selenocysteine
Ser	Serine
SOD1	SuperoxideDismutase 1
TEM	Transmission electron microscope
TFA	Trifluoroacetic acid
Thr	Threonine
TM	Trans Membrane
TOF	Time-Of-Flight
Tris	Tris(idrossimetil)amminometano cloridrato
Tyr	Tyrosine
Ub	Ubiquitin
Unspec	UnspecificKinase

1. General introduction

1.1 The mitochondrion

Mitochondria are intracellular organelles present in all eukaryotic cells. They play a vital role in cell metabolism since they are involved in many cellular processes such as ATP synthesis[1], redox state adjustment, osmotic regulation, pH control, cytosolic calcium homeostasis, cellular signaling, apoptosis[2,3] and aging[4].

The mitochondrion is structurally defined by its two membranes (Figure 1) which are different in composition and function: a limiting outer membrane that enwraps the energy-transducing inner membrane, which in turn encloses a dense and protein-rich matrix.

The double mitochondrial membrane system divides thus the mitochondrion into four main sub-compartments each with its own chemical-physical characteristics: Outer Mitochondrial Membrane (OMM), Inner Mitochondrial Membrane (IMM), Inter Membrane Space (IMS) and matrix.

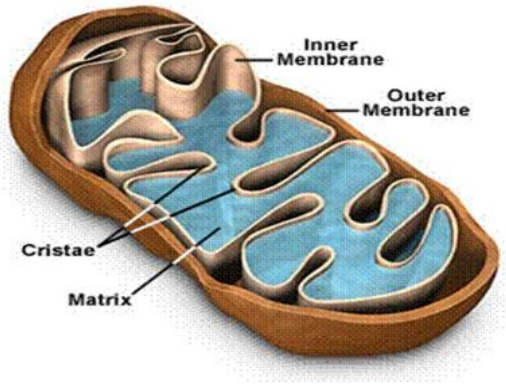

Figure 1. Internal structure of mitochondrion.

The OMM is topologically simple and characterized by the presence of mitochondrial porins, that form large and unspecific channels to allow the passage of ions and molecules with a molecular weight up to 5,000 Da. Thanks to the presence of porins, the OMM regulates the complex interactions between mitochondrial systems and other cellular compartments and separates the cytosol from the mitochondrial IMS that has physical-chemical properties distinct from the mitochondrial matrix and cytosol: the pH

is more acidic than cytosol by 0.2-0.7 units and the glutathione redox buffer is more oxidizing[5,6] (Figure 2).

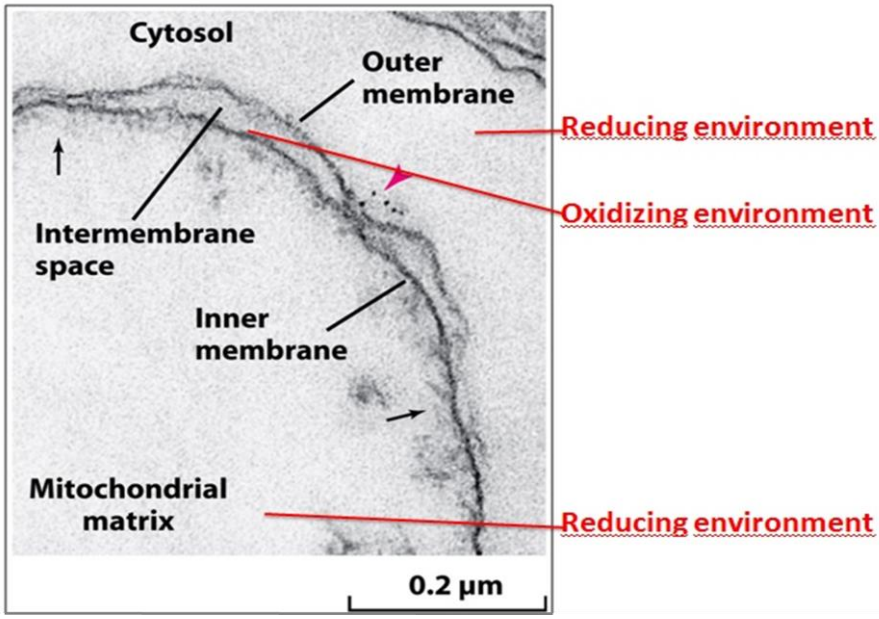

Figure 2. Detail in electron microscopy (TEM) of the mitochondrial structure (from Molecular Cell Biology, Sixth Edition, 2008, W. H. Freeman and Company).

The IMM has a larger surface area than the OMM. This is due to presence of "cristae" which are not simply random folds of this membrane but rather real internal compartments[7]. In this membrane are contained many protein complexes necessary for the production of energy (ATP)[8].

The matrix is particularly rich in proteins with enzymatic activity: several of them are involved in mitochondrial DNA replication and energy production. The matrix also contains the ATP-stimulated Mitochondrial Lon proteases that play an important role in the degradation of oxidized proteins and thus in oxidative stress control[9]. In general, many mitochondrial proteins are used as possible target for therapeutic interventions[10] because they are key regulators of mitochondrial quality control pathways[11,12] and thus are required to maintain a functional and healthy pool of mitochondria within the cells. The loss of function of these proteins leads to various disorders, such as ischemia, viral infections, neurodegenerative diseases (e.g. Huntington's chorea, Parkinson's disease, Alzheimer's disease, Familial and Sporadic Amyotrophic Lateral Sclerosis), cancer and toxicity.

Therefore, the mechanisms that regulate the intrinsic quality of mitochondria play a crucial role in dictating the global fate of cells. The importance of these well-regulated mechanisms is highlighted in disease scenarious and this makes mitochondria and its proteins a fervent and promising field of research.

1.2 The Voltage-Dependent Anion Channel: general features

Voltage-Dependent Anion Channel (VDAC) proteins, also known as mitochondrial porins, represent the most abundant proteins of the OMM where they play a vital role in various cellular processes, in the regulation of metabolism and in cell death. They mediate the ions and metabolites exchange between cytosol and mitochondrion, ensuring good functionality of mitochondrial complexes and energy production[13]. Their name indicates that the conductance may vary as well as the selectivity in dependence of the voltage applied when proteins are reconstituted in a planar lipid bilayer[14] (Figure 3).

VDAC proteins were discovered in 1974 in *Paramecium aurelia* and were believed to have evolved directly from the OmpF porins of the membrane of Gram-Negative bacteria. Although the bacterial and eukaryotic porins gene sequences share a similarity of only about 13%, they both have a well conserved secondary structure. The OmpF subunits (which assemble to form a trimer) have a β-barrel structure of 16 β-strands with hydrophobic amino acids in contact with the membrane and hydrophilic amino acids that protrude towards the aqueous pore. The similarities go beyond the structure because electrophysiological characterizations in artificial membranes of these porins have shown that they are able to modulate their opening and closing, showing a voltage dependence similar to eukaryotic porins[15].

In higher eukaryotes there are three VDAC isoforms VDAC1, VDAC2 and VDAC3 (so named by the chronological order of their discovery). From the evolutionary analysis, it is generally accepted that VDAC3 is the oldest protein, while VDAC1 is considered the most recent mitochondrial porin[16,17].

The pore-forming proteins have a molecular weight of about 30 kDa and conserved sequences of about 280 amino acids with the exception of VDAC2 that has the N-terminal fragment 11 residues longer than the other isoforms.

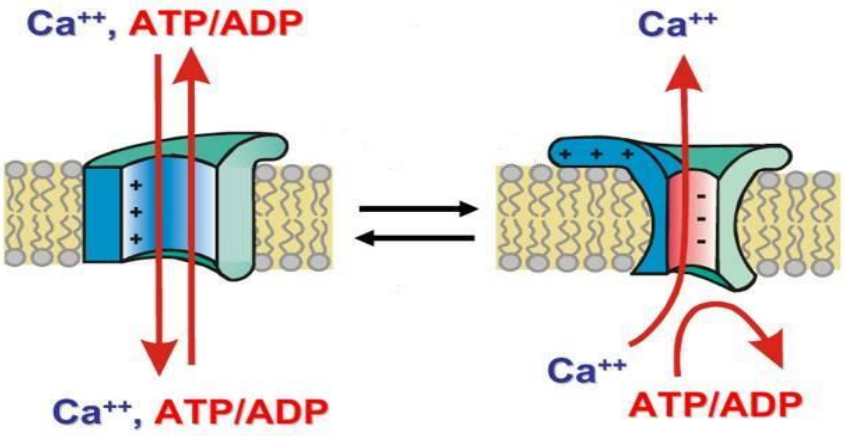

Figure 3. Voltage-dependence of mitochondrial porins. VDAC proteins present an open state at lower membrane potentials (between ± 0-10 mV) selective for anions (phosphate, chloride, adenine nucleotides) while at applied membrane potentials greater than ± 30-40 mV the pore switches to the so called "closed" state, which is not completely closed, the selectivity shifts to the cations and the channel becomes impermeable to ATP and ADP (From R. Benz et al., 1994).

The organization of the three VDAC genes is very similar: genes, located on different chromosomes, are made of the same number of coding exons, sharing exactly the same size, with the VDAC2 gene containing an additional first exon encoding for the N-terminal short pre-sequence[18].

The experimental 3D structures of mouse and human VDAC1 isoform have been determined using X-ray crystallography and NMR[19,20,21]. These analysis revealed a structure constituted by 19 β-strands arranged to form a trans-membrane β-barrel and by a region of α-helix at the N-terminus of the protein. Each strand features a regular alternation of hydrophilic and hydrophobic residues, the former pointing to the water-accessible lumen of the channel and the latter interacting with the non-polar membrane environment. The barrel is organized as a regular antiparallel array of β-strands with the exception of strands 1 and 19 that run in parallel. The amphipathic α-helix tail is located inside the pore (Figure 4). However, the exact position and local structure of this segment are still elusive since these features are different in the available X-ray and NMR structures. The biophysical structural model of the VDAC protein has been subject of several criticisms. Among them, the consideration that the artificial folding procedure used to prepare enough material for the crystallization efforts might produce two or more populations of stable VDAC structures and the proposed crystallized structure might be just one of the available alternatives. In this

respect other structural organizations of the sequence have been proposed[22]. This quarrel still calls for further experimental evidence, to be definitely solved such as the crystallization of VDAC purified from mitochondria and not from recombinant DNA.

Recently, the structure of zebrafish VDAC2 was solved at high resolution confirming the same β-barrel arrangement as VDAC1[23]. Zebrafish VDAC2 has no cysteine residues in the sequence and lacks the 11 amino acid longer N-terminal sequence present in mammalian VDACs.

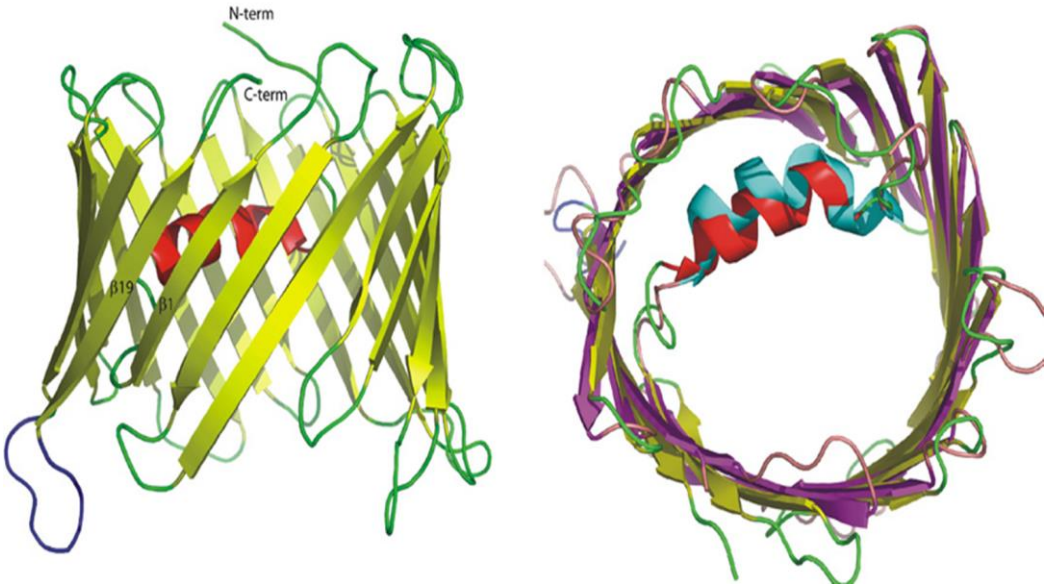

Figure 4. Three-dimensional structure of VDAC1.Left: Side view of the structure of human VDAC1 solved using a combined NMR/X-ray approach. β-strands 1-19, the N-terminal α-helix and the loops are colored yellow, red and green, respectively. The longest loop, which connects β-strands 18 and 19 is highlighted in blue. β-strands 1 and 19 are parallel and close the VDAC1 barrel. N- and C- terminal are indicated. **Right:** Top view of a superposition of the NMR/X-ray (PDB code: 2JK4) of human VDAC1 (helix in red) with the crystal structure (PDB code: 3EMN) of mouse VDAC1 (helix in cyan). Figures of this panel were prepared using PyMOL software (From V. Shoshan-Barmatz et al., 2010).

The VDAC3 structure has not yet determined. Several bioinformatic predictions, based on the large sequence similarity, proposed a barrel core such as the other VDAC isoforms[24].

These data converge on the clear observation that the three isoforms have a very similar protein sequence and structure. Moreover, comparison between human and yeast VDAC1 homologous, POR1, suggests a sequence conservation of porins through

evolution[17]. Despite this, the three VDAC isoforms display different functional properties.

VDAC isoforms 1 and 2 are expressed more or less ubiquitously in all eukaryotes and co-localized within the same area of the OMM while VDAC3 is more abundant in celebral cortex, liver, heart, testis and spermatozoa[25] and it is distributed all over the surface of the mitochondrion. Analysis of the expression levels of human VDAC isoforms in HeLa cells, determined by Real-Time PCR, have shown that VDAC1 is the most abundant isoform, 10 times more abundant compared to VDAC2 and hundred times more abundant compared to VDAC3, the least characterized of the isoforms. In addition, the over-expression of each single VDAC isoform affects the mRNA levels of the other two isoforms, suggesting that the ratios between VDAC isoforms are subject to a reciprocal control that avoids an imbalance among these proteins[26].

VDAC1 and VDAC2 have a pro-apoptotic and anti-apoptotic function, respectively; in fact VDAC2 is upregulated in several debilitating diseases including Alzheimer's and cancer[27,28,29]. This property is probably due to the unique ability of VDAC2 to sequester the pro-apoptotic protein Bak in the OMM and maintain it in the inactive state[30].

VDAC3 plays roles in sperm motility by microtubule doublet formation[31] and in ciliary disassembly during the cell cycle by targeting Mps1 protein kinase to centrosomes[25].

Several experiments have demonstrated that VDAC isoforms have similar electrophysiological characteristics, with some distinct features. Reconstitution experiments carried out in planar lipid bilayers or in liposomes demonstrated that both native (purified from mitochondria) and recombinant VDAC1 and VDAC2 are able to form similar pores in lipid bilayers. Instead, VDAC3 turned out to be poorly active as pore-forming protein either after reconstitution in artificial bilayers or incorporation in liposomes[32] and this isoform did not exhibit typical voltage-dependent channel gating. Furthermore, in a recent work it was demonstrated that VDAC3, in certain conditions, forms very small pores compared to the other isoforms, with a lower conductance[33]. The treatment of VDAC3 with DTT restores the pore-forming ability and the voltage dependence, probably following the reduction of predicted disulfide bridges that can bind the N-terminal helix to the bottom of the channel[34]. Moreover, it was also reported that swapping of the N-terminal region of VDAC3 with that of VDAC1 increased the channel activity[35,36]. This result again points to the relevance of the

residues located in this sequence, like one or two cysteines. The functional difference between the VDAC isoforms was also tested by yeast complementation assay. In this experiment, *Δporin1* yeast strains were transformed with plasmids expressing the mammalian VDAC isoforms, to assess their ability to restore normal growth phenotype. The results showed that VDAC1 and VDAC2 were able to restore the wild-type growth phenotype on not-fermentable carbon sources at 37°C while VDAC3 was not, or it was at a very low level[37]. Over-expression of human VDAC isoforms in yeast strains lacking endogenous porin 1 gene revealed that VDAC3 has a very weak protective activity against ROS, unlike the other isoforms[26]. These features have suggested unknown and peculiar role for this isoform.

1.3 Location and role of cysteine residues in VDAC isoforms

Although the general organization of the three isoforms is similar, different molecular weights and isoelectric points in addition to a different amino acid composition may confer specific functions to these proteins. It is interesting to observe that the most relevant difference in amino acid composition of VDAC isoforms is the number and distribution of cysteines and it is reasonable to assume a key role for this residues in protein activities (Table 1). In Figure 5 a multi-alignment of human and rat VDAC protein sequences and cysteine residues position is reported.

Table 1. Isoelectric points, molecular weight and cysteine content in human and rat VDAC isoforms. These figures do not take into account possible PTMs.

	Organism	**VDAC1**	**VDAC2**	**VDAC3**
I. P. estimated	Human	8.68	8.06	9.05
	Rat	8.62	7.44	8.81
Molecular weight (Da)	Human	30770	31563	30656
	Rat	30624	31651	30667
Number of cysteines	Human	2	9	6
	Rat	2	11	7

As we have already highlighted, VDAC3 is considered the oldest isoform while VDAC1 and VDAC2 diverged more recently[17]. Starting from isoform 3, evolution has taken two different pathways: on the one hand, there is a decrease in the number of Cys residues, as for isoform 1, which shows a robust pore-forming activity and a pro-apoptotic function; on the other hand the number of cysteines increases with the isoform 2 which has associated an anti-apoptotic function[38].

Figure 5. Multi-alignments of human (top) and rat (bottom) VDAC protein sequences. Sequences show high levels of identity, which can be calculated to be around 70%. The asterisks indicate the identical residues (Clustal Omega). In yellow the position of Cys residues is outlined.

Furthermore, due to their position on the OMM, VDACs have the peculiar situation to have moieties exposed towards two different aqueous compartments with different chemical-physical characteristics: the cytosol, a reducing environment, and the IMS, a more oxidizing environment. Many of the Cys residues of the VDAC channels are located in the loops which extend towards the IMS and therefore could be more easily subject to oxidation. Indeed, the pore-forming structure in the OMM is main way of escape from the mitochondria of an aliquot of the superoxide radical ($O^{2-\bullet}$) produced, in particular, by the Complex III of respiratory chain. Superoxide radical, $O^{2-\bullet}$, is very active but has a short life, while hydrogen peroxide (H_2O_2), a catabolite produced by the SOD1 (Superoxide Dismutase 1) in the IMS, is permeable to the membranes and able to oxidize cysteines[39].

In VDAC1 Cys 127 is located in the β-strand 8 and faces the hydrophobic layer of the phospholipidic membrane while Cys 232 is in the strand 16 pointing towards the aqueous lumen of the pore. Several studies suggest that VDAC1 cysteines, due to their position, cannot be involved in intramolecular but possibly in intermolecular disulfide bridges and could participate in oligomerization[40]. Under physiological conditions, VDAC1 forms contacts between single forming units, at strands 19, 1 and 2[41]. When apoptosis is induced, VDAC1 undergoes conformational changes, which initiates the formation of higher order oligomers involving other weakly stabilized strands, such as strand 16[41]. The migration patterns of VDACs in SDS-PAGE analysis are different, though the estimated molecular weights are similar. In particular, it was reported that although VDAC1 has a shorter N-terminus than VDAC2, it shows the same migration in gel electrophoresis[42]. When the two VDAC1 cysteines are both mutated, this isoform shows a faster migration than VDAC2. The formation of an intermolecular disulfide bridge could explains this different result[43] Instead, delection of both cysteines does not affect the activity of the pore, its voltage-dependence features and apoptosis induction. It has been proposed that the conductance of VDAC1 can be controlled by dynamic movement of the N-terminal helix and it is independent of the cysteines[44].

The additional extension of 11 amino acids at the N-terminal of VDAC2 sequence is particularly rich in Cys residues (two in hVDAC2 and four in rVDAC2). Recent studies suggest that this extension is critical to allow VDAC2 folding, voltage-gated channel function, equilibrium thermodynamic stability to the barrel structure[45] and to confer

higher helicity to this segment[46,47]. Moreover, interactions between OMM lipids and certain amino acids (such as Cys residues) are crucial for the proper functioning of the protein[48]. The Cys residues can participate in several enzymatic reactions, metal binding and the tertiary fold by modification of their redox state[49]. The crystal structure of VDAC2 from zebrafish reveals a broader dimerization interface in this protein, which can be mapped to strands 17, 18, 19, 1 and 3[22]. These oligomerization events do not seem to occur through disulfide bond formation. In fact the zebrafish VDAC2 has no cysteine residues and, using human VDAC2 C0, in which cysteine residues have been replaced with other amino acids, it was possible demonstrate that protein oligomerization can be obtained, suggesting that oligomer formation is independent of cysteines[50].

In VDAC2, only one Cys residue (Cys 138 in hVDAC2 and Cys 139 in rVDAC2) faces the hydrophobic layer of the phospholipidic membrane as Cys 127 in VDAC1; another cysteine residue (Cys 227 in hVDAC2 and Cys 228 in rVDAC2) is exposed to the cytosol. The other cysteines are located in loops oriented towards the IMS (Cys 8, 13, 47, 76, 103, 133, 210 in hVDAC2 and Cys 4, 5, 9, 14, 48, 77, 104, 134, 211 in rVDAC2).

Based on bioinformatic transmembrane model, in hVDAC3 and rVDAC3 only Cys 8 is located inside the channel and, in rat isoform, Cys 165 is exposed to the cytosol. As for VDAC2, the most of VDAC3 Cys residues populate loop segments located in the ring region oriented towards the IMS. The oxidizing properties of this cellular compartment can render cysteines highly reactive and susceptible to modifications. Several data, obtained in my laboratory by mass spectrometry analysis and which are part of my master's thesis, confirmed that cysteines in VDAC3, extracted from rat liver mitochondria, can exist in different oxidation states[51] and have differentiated roles, as these results unequivocally demonstrate. In particular, Cys 36, 65 and 165 are oxidized to a remarkable extent to sulfonic acid[51], a redox state irreversible in the cell. This irreversible oxidation of cysteines, also termed over-oxidation, introducing distinct negative charges, can result in changes in protein structure or at least can modify the electrostatic surface of the protein accessible to water. Over-oxidation can also be required to target a protein to degradation[50].

Cys 2 and 8, located in the same N-terminal peptides, are present exclusively in the carboxyamidomethylated form both in tryptic and chymotryptic digestions (alkylated

with IAA, see section “Materials and methods”) which means they are in the cell as free thiol group or oxidized to disulfide bridges[51]. Indeed, mass spectrometry analysis confirmed that a disulfide bridge is formed between Cys 2 and Cys 8. The removal of selected cysteines (Cys 2, 8 and 122 in different combinations) and substitution with alanine residues, by site-directed mutagenesis, reduced the range of oxidation state, modified the electrophoretic migration and strongly affected the protein activity both *in vivo* and *in vitro*[49]. In particular, the deletion of Cys 2 together with Cys 8 and Cys 122 completely changed the electrophysiological features of VDAC3 that became able to easily insert into a phospholipid bilayer and adopt a higher conductance state than the wild type protein. Moreover, these mutants are able to complement the absence of porin 1 in yeast cells[49]. The results with the cysteine mutants, have been obtained, at the same time, both by my research group and by another independent group[35] which stated that the decreased channel gating observed for VDAC3 was due to fixation of the N-terminal domain to the bottom of the pore through a disulfide bridge between residues Cys 2 and Cys 122.

In my thesis work, I have found only one disulfide bridge between Cys 2 and Cys 8. In the mass spectrometry data, the bond between Cys 2 and 122 was not found. Moreover, no peptide containing Cys 122 was identified because its large molecular weight was not included in the m/z range selected and also because, in this position, unknown post-translational modifications (such as a disulfide bridge) of the protein might exist.

In a work in progress, the development of a new protocol for the disulfide bridges identification is already giving the first results.

Indeed, preliminary results indicate that in VDAC3 it is not possible to exclude that beside Cys 2-8, other disulfide bonds can form between other cysteine pairs. But the way is still long as the interpretation of the MS/MS spectra is very complex.

Various VDAC3 intra-chain disulfide bridges were simulated by molecular dynamics[52]. The bioinformatic analysis was also useful to calculate the measured reduction of the current flow in the presence of a disulfide bridge. The bonds between Cys 2 and Cys 8, found in my mass spectrometry data, and between Cys 2 and Cys 122, found in the other work[35], only slightly occlude the channel diameter and hinder the N-terminal

protrusion towards the exterior of the pore. The predicted disulfide bridge between Cys 8 and Cys 122 leads to a 20% conductance reduction.

It was instead proposed that the formation of disulfide bridges may change the exposition of N-terminal sequence residues, thus changing the presentation and the docking state of VDAC3[52].

An interesting feature of isoform 3 is the presence of a Cys residue in position 2 which, after PTMs, becomes the N-terminal residue. The over-oxidation of this residue can trigger the N-End Rule Pathway, a ubiquitin-dependent proteolytic system, in which destabilizing N-terminal residue function as determinant of degradation signal. This pathway has been found in all organisms examined, from prokaryotes to eukaryotes. The N-terminal Asn and Gln can function as destabilizing residues and, through deamidation by N-terminal amidohydrolases, form Asp and Glu, respectively. Glutamic and aspartic acids are arginylated by ATE1 R-transferases and subsequent ubiquitin-dependent degradated[53,54]. In VDAC3, the removal of Met 1 exhibits Cys 2 at the N-terminal of the protein that becomes a destabilizing residue. The over-oxidation makes cysteine structurally similar to Asp and thus can be arginylated by R-transferases. This mechanism suggests that the oxidation of N-terminal Cys is a specific modification to create a destabilizing residue.

In my work I have never detected the oxidated form of Cys 2: this can mean that the potentially Cys 2 oxidated, if existing, is a marker used to remove the protein from the membrane for degradation.

VDAC3 has been identified as a Parkin interactor and subjected to ubiquitination by Parkin in defective mitochondria[12]. The PINK1/Parkin system is responsible for the elimination of damaged mitochondria by autophagy. PINK1 is a kinase present, at very low levels, in the OMM, that is able to phosphorylate Parkin upon its recruitment from cytosol to the OMM. The phosphorylated Parkin starts ubiquitination of selected targets in the mitochondria and this event is considered preliminary to mitochondrial quality control pathway (or to mitophagy). By mass spectrometry, VDAC isoforms have been found to be the most abundant Parkin-associated proteins, indicating their role as mitochondrial docking site for Parkin. Interestingly, while VDAC3 was found ubiquitinated, VDAC2 can bind Parkin but it was not detected ubiquitinated[12]. This difference can be due to the lack of the N-terminal cysteine in the mature form of

VDAC2. When the Cys 2 is reduced or forms a disulfide bridge, the VDAC3 protein can follow the same degradation pathway followed by the other isoforms.

1.4 The chemistry of cysteine and its Oxidative Post-Translational Modifications (Ox-PTMs)

In proteins, Cys residues have important functions and are unique amino acids for their property to undergo reversible redox reactions as part of their normal function[39]. These properties depend on the characteristics of the sulfur atom.

Sulfur is the second-row element of group VIa of the periodic table with an electron configuration of [Ne] $3s^2$ $3p^4$. The availability of d-orbitals allows expansion to valencies of 4 and 6 at oxidation states ranging from 2^- to 6^+.

The amino acid cysteine is characterized by a thiol functional group, which contains a sulphur atom and a hydrogen atom (RSH); the sulfur atom is fully reduced with an oxidation state of 2^-. The large, polarizable sulfur atom in a thiol group is electron-rich and enough nucleophilic. Its reactivity is enhanced in the deprotonated form of the thiol, also known as the thiolate anion (RS^-). About this, the thiol group is mildly acidic and the pK_a value is dependent on the structure and local environment. In peptides the pK_a is typically about 9, but in proteins this value can be as low as 3.5. Although the molecular basis remains incompletely understood, empirical observations indicate that not all cysteine residues in an individual protein are equally sensitive to oxidation. The thiolate anion reacts with “hard” electrophilic groups (carbonyl, phosphoryl and sulfuryl groups) and with “soft” electrophiles such as saturated carbon. Due to its high reactivity and its low redox potential in proteins (from -0.27 to -0.125 V) the thiol group of cysteine plays important biological roles in catalysis, metal binding and detoxification of xenobiotics[55] Furthermore, the thiol side chain of cysteine is widely used as a nucleophile for many PTMs including disulfide bonds (RS-SR), S-acylation, S-Glutathionylation (SSG), S-nitrosylation (SNO), S-sulfhydration (SSH), sulfenylation (SOH), sulfinylation (SO_2H), and the formation of sulfonic acid (SO_3H). Except for this last, all the reported Ox-PTMs are readily reversible and ruled by specific enzymatic activities. Sulfiredoxin (Srx1), for example, acts on oxidative states up to sulfinic acid by reducing them back to thiol in an ATP-dependent manner. The biological significance of

most of these reversible modifications has been amply investigated under physiological and non-physiological conditions. On the contrary, the knowledge about the impact of irreversible Ox-PTMs on cell physiology is quite restricted.

Disulfide bonds (RS-SR) and pathways for disulfide bond formation

The most commonly known thiol oxidation reaction is disulfide formation. The formation of disulfide bonds between cysteine residues is a crucial component in the process of protein folding and plays an important role in stabilizing the tertiary and quaternary structures of proteins. Therefore, characterizing the exact positions of disulfide bonds is an important aspect of proteomics, especially for a comprehensive understanding of protein folding and three-dimensional structure. Moreover, in the use of protein therapeutics (e.g. antibodies), it is also of interest to monitor the reshuffling of disulfide bonds during formulation, storage, and usage, which reflects the antibody structure, stability, and biological function[56].

The reaction of disulfide bridge formation is in principle spontaneous (but not always, because specific enzymes are required with the function of forming disulfide bonds) and thus it is genetically pre-determined since spatial proximity to another cysteine is a prerequisite for disulfide formation. Disulfide formation indeed requires the proximity of two cysteines but also chemical conditions (structure and local environment) favoring this process such as modifications of the thiol group reactivity. Disulfide bonds are formed between thiol groups in two independent free thiols that are in close proximity, either within a protein or between proteins (termed an intra- or inter-molecular disulfide bond, respectively). Disulfides can also form through reaction with a sulfenic acid in the presence of high concentration of ROS that will that convert SOH groups to thiyl radicals (RS•) which react with other thiolates preferentially to form a disulfide bond.

Recent work has suggested that some disulfide bonds are dynamic and can confer changes in protein structure and function. Indeed disulfides will undergo nucleophilic cleavage and thiol-disulfide exchange especially under neutral and alkaline condition[57].

The identification and characterization of protein disulfide bonds is a challenging task. Several methods are used to determine the pattern of disulfide bond linkage. Among

them, X-ray crystallography and NMR spectroscopy are excellent tools that can identify disulfide bond linkages with minimal disulfide bond inter exchange. However, the application of both techniques is limited by large sample requirements and protein size. Edman degradation can also be used for the identification of disulfide bonds. But this technique requires ultra pure samples, digestion, and further purification of the peptides for protein sequencing[58].

Mass spectrometry is gaining importance in the identification and characterization of protein disulfide bridges both in solution and from gels. Some advantages of MS-based approaches include relatively easy sample preparation, short analysis time, and the capability to deal with more complex protein mixtures from endogenous sources. Researchers have successfully demonstrated that disulfide bridge patterns can be identified by mass spectrometry analysis, following protein digestion either under partial reduction or non-reducing conditions[59]. In partial reduction approach, the protein is digested under controlled conditions using different reduction and alkylated kinetics. The analysis is performed by mass spectrometry. When a protein has many disulfide bridges, multiple reductions and separations are necessary for complete disulfide mapping and thus this approach requires large sample amounts. Instead, protein digest under non-reducing condition can identifies disulfide bonds pattern in a single run.

In the cells reduction and oxidation of disulfide bonds is mediated by a variety of thiol-redox enzymes, which permit fast and reversible thiol-disulfide exchange (figure 6). In prokaryotic cells disulfide bond formation is catalyzed in the oxidative environment of the periplasm. Here, the catalyst DsbA (protein of the oxidoreductases family with a thioredoxin-like domain) donates its disulfide bonds to target periplasmic proteins and as a consequence is released in a reduced form. To start a new oxidation cycle DsbA must be subsequently reoxidized and its partner protein DsbB accomplishes this reoxidation step. Moreover, in *E. coli* the isomerases DsbC and DsbD that catalyse the shuffling of incorrectly arranged disulfide bonds were found. DsbD is responsible for maintaining DsbC in a reduced state, permits the rescue and proper maturation of such proteins.

In eukaryotic cells catalysts necessary to promote disulfide bond formation are found within the Endoplasmic Reticulum (ER) and mitochondrial IMS. In the ER there are

many oxidoreductases with a thioredoxin-like domain, but the most important and most well characterized of this group is the Protein Disulfide Isomerase (PDI). This enzyme has the ability to catalyze both the oxidation of free thiols and the isomerization of existing disulfides. The redox state of PDI *in vivo* is determined by its interaction with Ero1 and Erv2 (essential membrane protein in the ER) and oxidizing equivalents flow from Ero1 or Erv2 to PDI to secretory proteins in the ER.

The pathway for disulfide bond formation in mitochondria was recently discovered.

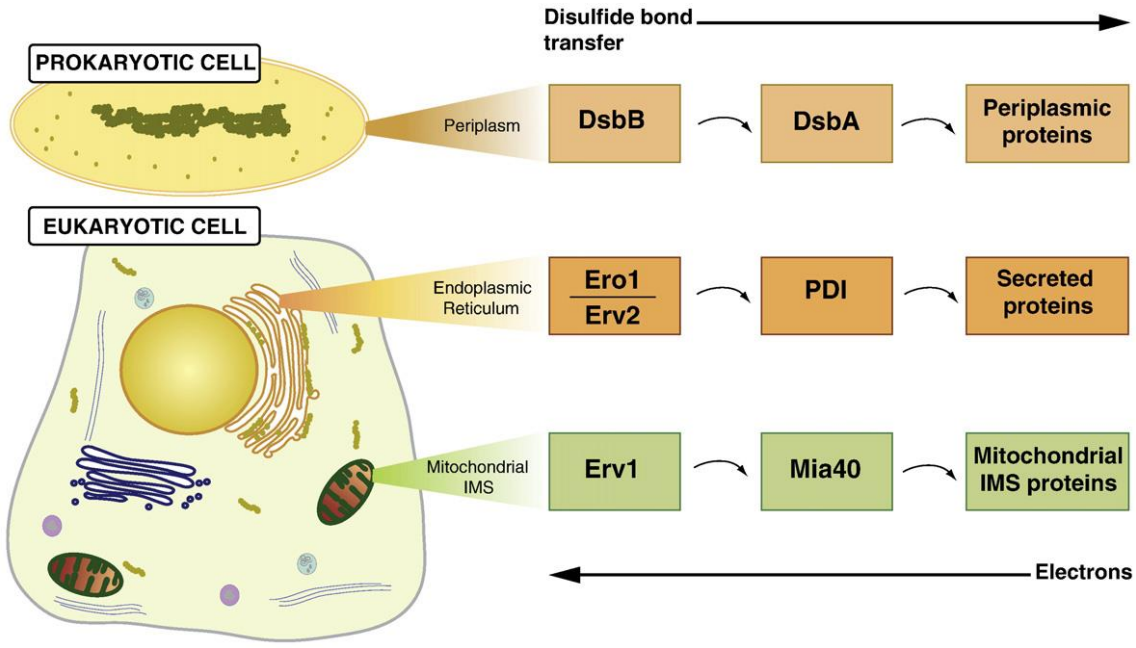

Figure 6. Pathways for disulfide bond formation. In prokaryotic cells disulfide bond formation is catalyzed in the oxidative environment of the periplasm. Here, the catalyst DsbA donates its disulfide bonds to target periplasmic proteins and as a consequence is released in a reduced form. To start a new oxidation cycle DsbA must be subsequently reoxidized and its partner protein DsbB accomplishes this reoxidation step. In eukaryotic cells catalysts necessary to promote disulfide bond formation are found within the ER and mitochondrial IMS. Oxidizing equivalents flow from Ero1 or Erv2 to PDI to secretory proteins in the ER, or from Erv1 to Mia40 to IMS proteins in the mitochondria. The direction of disulfide bond transfer and electron flow is shown (From D. Stojanovski et al., 2008).

The regulated transfer of disulfide within the mitochondrial IMS was indeed an unexpected event because it was believed that the IMS was continuous with the reducing environment of the cytosol through the mitochondrial porins.

The formation and interchange of disulfide bridges in mitochondria are possible thanks to the MIA (Mitochondria Intermembrane Space Assembly) pathway[60]. This pathway plays a crucial role in post-translational events of IMS-directed proteins from their translocation across the OMM to their subsequent folding and maturation. Many

mitochondrial IMS proteins contain conserved cysteine residues that are involved in binding of cofactors, metals and the formation of disulfide bonds. The formation of these bridges is associated to the MIA system.

The reactions that mediate protein import into the IMS initiate with an association of incoming precursors with the receptor Mia40 through the formation of a transient disulfide intermediate. Mia40 is ubiquitously expressed in eukaryotes and contains six essential cysteines, four of which arranged in two Cys-X_9-Cys motifs. The donation of disulfides by Mia40 to substrates permits their folding and retention within the IMS and results in the release of Mia40 in a reduced form. The sulphydryl oxidase Erv1 maintains Mia40 in an oxidized state and thus competent for subsequent cycles of protein precursor import through the donation of electrons to cytochrome c. Electron flow from cytochrome c is coupled to respiratory chain complexes within the IMM.

Sulfenic acid (RSOH)

Among the different modifications generated by thiol oxidation, sulfenic acids are implicated in a wide variety of important biochemical reactions. Sulfenic acids are unstable and highly reactive functional groups, which have traditionally been viewed as intermediates to additional cysteine modifications. The formal oxidation state of the sulfur atom in a sulfenic acid is zero, enabling it to function as both a weak nucleophile and a soft electrophile. In recent years sulfenic acids have been identified in a growing list of proteins and they have received intense interest for their roles in enzyme catalysis and cell signalling[61]. Sulfenic acids are formed by the reaction of a thiol or thiolate anion with hydrogen peroxide and other biological oxidants such as peroxynitrite. Sulfenic acids can also result from the hydrolysis of S-nitroso-thiols, after the reaction of thiol or thiolate anions with thiol-sulfinates, and the condensation of a thiyl and hydroxyl radical. Finally, sulfenic acids are generated via reaction of a thiol or thiolate anion with hypochlorus acid, which is enzymatically produced in human immune cells during the inflammatory response[55]. In kinetic studies, the pK_a for the sulfenyl group of cysteine sulfenic acid has been estimated to be between 6 and 10. The reactivity of the thiol side chain is a function of its ionization state and thiolate ion stability, which is modulated by the surrounding protein environment. Several proteins

contain cysteine residue in the active site and they are inhibited or activated by the oxidation of these key cysteine thiols. Oxidative activation and inactivation can be reversible or irreversible, depending on how the cysteine oxidation state is formed. The presence of polar residues as well as the presence of His and Thr are important factors for cysteine oxidation. The reaction of condensation between sulfenic acid and a nearby cysteine thiol on a protein or a low-molecular-weight thiol such as the GSH forms a disulfide bridge. The intramolecular and intermolecular disulfide formation from sulfenic acid plays an essential protective role because that modification may prevent the irreversible over-oxidation of cysteine residues to sulfonic acid.

Cysteine S-sulfenylation provides redox regulation of protein functions, but the global cellular impact of this transient PTM remains unexplored. Different cysteines in the same proteins displayed dramatic differences in susceptibility to *S*-sulfenylation. This PTM is favored at solvent-exposed protein surfaces and is associated with sequence motifs (such as CxxE, CxxxE, and KxC) that are distinct from those for other thiol modifications.

S-sulfenylated sites are present on the functional domains of protein kinases, phosphatases, acetyltransferases, deacetylases and deubiquitinases, suggesting the possibility of regulatory cross-talk between S-sulfenylation and other major PTM events. Indeed, other recent studies[62] suggest the potential regulatory impact of reversible cysteine oxidation on protein phosphorylation, acetylation, and ubiquitylation. In addition, Gene Ontology annotations show that these S-sulfenylated proteins are present in all major cellular compartments and are involved in various biological processes such as cell signaling, response to stress, cell cycle, and cell death[63].

The formation of sulfenic acid is associated in particular to the presence of hydrogen peroxide (H_2O_2). In fact, the treatment of cells with H_2O_2 determines changes in the total quantities of sulfenic acid identified by mass spectrometry. This reactive oxygen species acts as a sort of intracellular messenger that can oxidize the cysteines. The amount of H_2O_2 must be finely regulated and there are also physical barriers in the cell that oppose its high diffusibility, in addition to antioxidant enzymes. The reversible formation of sulfenic acid provides the cell with an alarm signal about its general redox state. In certain cases, the initial sulfenic acid may it self be stabilized within the protein

micro-environment. However, this potentially leaves the protein sulfenic acid vulnerable to hyperoxidation to the largely irreversible sulfinic or sulfonic acids further modifications that could also provide an alarm signalling regarding cellular redox status[64].

The sulfenic acid modification has been observed in the catalytic cycle of multiple enzymes including Peroxiredoxin (Prx)[65] (Figure 7) and NADH Peroxidase, using tandem mass spectrometry.

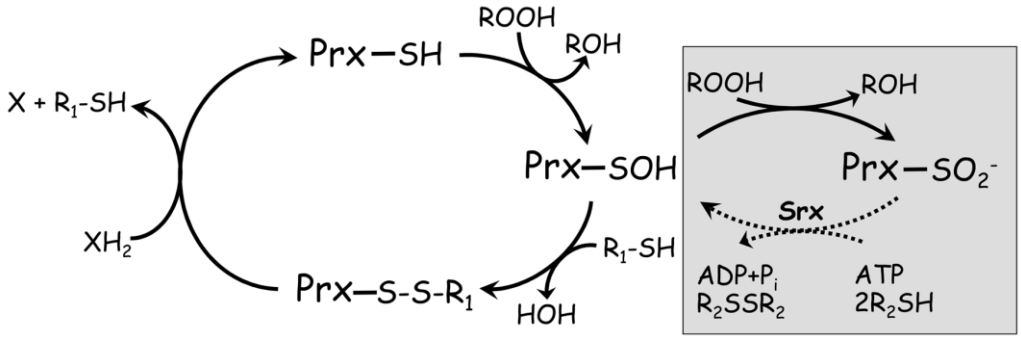

Figure 7. Peroxiredoxin catalytic and regulatory redox cycles. Peroxiredoxins (Prx) with the active site cysteine thiol (in its thiolate form) attack the hydroperoxide substrate, releasing the corresponding alcohol and the enzyme in its sulfenic acid (SOH) form. For catalytic recycling, a resolving cysteine (R1-SH) in the same or another subunit, typically forms a disulfide bond with the peroxidatic cysteine, and the enzyme is regenerated by small molecule or protein electron donors. The sulfenic acid can also act as a redox-sensitive switch, converting the enzyme to an inactive sulfinic acid form in the presence of excess hydroperoxide substrate (gray box). Enzymes called Sulfiredoxins (Srx) can regenerate activity in some Prx through an ATP-dependent reduction (dotted line) (From L. B. Poole et al., 2008).

Peroxiredoxin enzymes catalyse the reduction of hydroperoxide substrates via a catalytic cysteine at the active site and show high sensitivity and specificity towards H_2O_2. Their activity is indeed regulated by phosphorylation, oligomerization and oxidation state[66]. The cysteine thiol (in its thiolate form) in the active site attacks the hydroperoxide substrate, releasing the corresponding alcohol and the enzyme in its sulfenic form which then undergoes one or more steps of inter- or intra-subunit disulfide bond formation and disulfide exchange with other thiols in order to return to its reduced and activated state. The sulfenic acid can also act as a redox-sensitive switch, converting the enzyme to an inactive sulfinic acid form in the presence of excess hydroperoxide substrate. Sulfinic acid can form sulfonic acid or can undergoes an ATP-dependent reduction.

Sulfinic acid (RSO_2H)

In the presence of excess oxidant, sulfenic acid can be oxidized to sulfinic acid. The formal oxidation number of the sulfur atom in sulfinic acid is +2. On this basis, this oxyacid might be expected to have enhanced electrophilicity compared to sulfenic acid. However, sulfinic acid does not undergo self-condensation or nucleophilic attack by thiols. This can be explained by the increase in partial positive charge on the sulfur in sulfinic acid, which converts the sulfur atom into a harder electrophile making it less prone to reaction with soft nucleophiles, such as thiols. With a pK_a of 2, sulfinic acid is deprotonated at physiologic pH and can exist in two resonance forms. Sulfinic acids function as nucleophiles and will undergo alkylation, as well as nucleophilic addition to activated alkenes, aldehydes, lactones and α,β-unsaturated compounds to forme the corresponding sulfones[64]. If activated by a keto functional group, sulfinic acid will hydrolyze to sulphite (SO_3^{2-}). For example, the spontaneous hydrolysis of β-sulfinyl pyruvate is a key reaction in cysteine catabolism.

The biological function of sulfinic acid has also been hotly debated, largely owing to a general consensus that this modification could not be reduced under physiological conditions. This observation led many to conclude that sulfinic acids in proteins were irreversible or caused by random cysteine oxidation during isolation. However, this idea was challenged by the discovery that peroxiredoxin enzymes were reversibly inactivated by oxidation of the catalytic cysteine to sulfinic acid in cells[67,68]. Soon after, an ATP-dependent enzyme with sulfinic acid reductase activity, Sulfiredoxin (Srx), was isolated from yeast and a human homolog was subsequently identified[69] (Figure 7). To date, Peroxiredoxin isoforms 1–4 (Prx 1–4), which reduce hydrogen peroxide and alkylperoxides to water and alcohol, are the only confirmed Srx substrates. The reaction of Srx with sulfinic acid is slow (kcat = 0.2 min^{-1}), and it is currently unknown whether any accessory proteins enhances this reaction *in vivo*. Individual studies have identified a functional role for sulfinic acid modification or S-sulfinylation in a growing list of proteins[70], including the D-Amino Acid Oxidase (DAO), Parkinson's Disease Protein, DJ-1 and the Copper-Zinc Superoxide Dismutase 1 (SOD1)[71]. Cysteine oxidation

to sulfinic acid can modulate protein metal binding properties. In matrix metalloproteases, the oxidation of a cysteine to sulfinic acid activates protease function and is essential for catalytic activity. Despite its regulatory potential and association with diseases linked to ROS[72] generation, including cancer, the scope, dynamics, and function of sulfinic acid is essentially unknown, owing to major challenges of detection. Antibodies have been generated for monitoring sulfidic acid, but have limited affinity and specificity. Alternatively, a difference of +32 Da has been used to detect sulfinic acid by mass spectrometry[73]. However, this approach presents several problems such as the protein oxidation during sample preparation and the existence of other modifications with the same nominal mass shift, like S-sulfhydration (-SSH). Despite their limitations, these approaches have revealed many S-sulfinylated proteins associated with diverse cellular pathways, pointing towards a more complex role for this Ox-PTM in biology, while also highlighting the need for more advanced methods to detect and quantify S-sulfinylated proteins from cells.

Sulfonic acid (RSO_3H)

The sulfinic acid modification is relatively unstable and can undergo further oxidization to give sulfonic acid, the irreversible and highly oxidized thiol species. Due to their relative stability compared to the reversible thiol modifications, they can be detected directly by high resolution mass spectrometry, although with some difficulties.

The sulfur atom in sulfonic acid has a formal oxidation number of +4 and, as sulfinic acid, functions as a hard electrophile and does not undergo self-condensation or nucleophilic attack by thiols. Strong oxidizing agents such as halogens, hydrogen peroxide and nitric acid can generate sulfonic acids from thiols. In addition to proteins, sulfonic acids are found in many naturally occurring, low-molecular-weight compounds such as taurine and methansulfonic acid[55].

With a $pK_a<2$, the sulfonic acid is both strong acid and a weak base. Owing to the stability of the conjugate base, which can stabilize the negative charge through resonance localization, sulfonic acids are strong acids comparable to sulfuric acid. As weak bases, sulfonates are good leaving groups in S_N1, S_N2, E1 and E2 reactions. In

organic synthesis, the sulfonic acid group is often used as a directing group or is installed on hydrophobic molecules as a method to improve solubility of a compound[55].

To date, the role of cysteine sulfonic acid on protein function and conformation is still controversial since it is not completely clarified if this strong oxidation can be counted as an oxidative damage or a signalling modification. Literature contains just a few examples in this regard.

Sulfonic acid was detected in the active-site Cys of Peroxiredoxin1 (Prx1) and its presence has been associated to enhance chaperone activity of protein which represents a marker of the cumulative oxidative damage to the cells[74]. In particular the quantitative measurement of both the native and oxidized forms of Prxs is a relevant indicator of oxidative stress: the oxidized form is prevalent in pathological conditions[75]. Interestingly, over-oxidation of Prxs cysteines follows a precise circadian rhythm in human blood cells[76].

In the active site of GAPDH, Cys residue 149 is rapidly over-oxidized to sulfonic acid by hydrogen peroxide and this hyperoxidized form is associated with the inhibition of glycolysis and numerous other activities including the induction of apoptosis[77].

A pathophysiological relevance of sulfonation has been observed also in PD. Mass spectrometry analysis demonstrates that in Parkin protein there is an accumulation of Cys residues in the form of sulfonic acid following the treatment with hydroxide peroxide. Mutations of redox state in these cysteines alter Parkin solubility, its intracellular localization and sensitivity to stress. Moreover, the presence of this Ox-PTM induces Parkin auto ubiquitination and its aggregation[78].

In human mutant SOD1 the over-oxidation of Cys 111 to sulfonic acid has been implicated in the pathology of the neurodegeneration disease of Familial Amyotrophic Lateral Sclerosis (FALS). Immunohistochemical analysis, using antibodies that selectively recognize a cysteine redox state, proved indeed the accumulation of mutant SOD1 with over-oxidized Cys 111 residue in the Lewy body-like hyaline inclusions and vacuole rims of the spinal cord of FALS-transgenic mice. Mass spectrometry analysis of several redox state of SOD1 separated by two dimensional gel electrophoresis (because oxidized form of SOD1 has slower electrophoretical mobility) confirms that result[79,80].

In the field of endocrinology, sulfonation represents a particularly explored biological phenomenon. Pregnenolone sulfate is considered an important neurosteroid and

cholesterol sulfate plays a key role in keratinocyte differentiation and development of the skin barrier. Over-oxidations were found also in other hormones such as Thyroglobulin and Catecholamines but their role is unknown[81].

Irreversible oxidation of N-terminal Cys to sulfonic acid can impact protein function and homeostasis in many ways. In fact, the introduction of highly oxidized sulfur species with distinct negative charge distribution and steric requirements result in changes to protein structure. We have already underlined the involvement of over-oxidized N-terminal Cys residues in the N-End Rule Pathway and in mitochondrial quality control mechanisms.

Mass spectrometryc analysis revealed the presence of Cys residues in the form of sulfonic acid in VDAC3 extracted from rat liver mitochondria but their biological roles in still little known. This Ox-PTM in VDAC could be associated with mechanisms that regulate the activity of these trans-membrane porins and with pathways involved in mitochondrial quality control[50].

1.5 Other Post Translational Modifications (PTMs)

Selenocysteines

Selenium is an essential trace element that is incorporated into proteins as the amino acid selenocysteine (Sec), the 21st amino acid in the genetic code. The incorporation of this amino acid turns out to be a fascinating problem in molecular biology because Sec is encoded by a stop codon, UGA. Sec is a Cys residue analogue with a selenium-containing selenol group in place of the sulfur-containing thiol group in Cys. The selenium atom gives Sec quite different properties from Cys. The most difference is the lower pK_a of Sec, and Sec is also a stronger nucleophile than Cys. Other unique features of Sec, non shared by any of the other 20 common amino acids, derive from the atomic weight and chemical properties of selenium and the particular occurrence and properties of its stable and radioactive isotopes. Indeed, six stable isotopes and a number of radionuclides with different characteristics exist for selenium.

Selenoproteins exist naturally in all kingdoms of life, eubacteria, archaea and eukaryotes. Only 20% of the genomes sequenced in eubacteria encode the machinery for inserting Sec into protein and in archaea about 10% have this machinery. In eukaryotes, the Sec insertion machinery has been found in a number of lower organisms, such as algae, and it is widespread in animals but absent in fungi and higher plants[82].

Computational and experimental approaches have identified 25 selenoproteins in the human proteome[83]. Proteins naturally containing Sec are often enzymes, employing the reactivity of the Sec residue during the catalytic cycle and therefore Sec is normally essential for their catalytic efficiencies. The selenoproteins can be classified according to their biological function into six different groups: 1) peroxidase and reductase activities, 2) hormone metabolism, 3) protein folding, 4) redox signaling, 5) Sec synthesis, and 6) selenium transport.

Some selenoproteins are of major importance for mammalian life and that was unequivocally demonstrated by the mouse knockout of the selenocysteinyl-tRNA gene (necessary for Sec incorporation and thereby selenoprotein synthesis), which shows

early embryonic lethality. Mutagenic studies revealed a dramatic decrease in the enzymatic activity of rat Thioredoxin reductase when Sec was replaced by Cys[84].

The highly increased reactivity of selenoproteins compared to their Cys-dependent counterparts is generally regarded as an evolutionary pressure for the development of selenoproteins. The other point of view is that Sec would be an ancient amino acid, to a major extent lost during evolution due to its high reactivity. Whatever the true reason is for selenoprotein existence, it is clear that the insertion of a Sec residue in a protein constitutes a metabolically costly synthesis machinery. It is also clear that selenoenzymes generally have higher catalytic efficiencies than their Cys-containing counterparts.

In this scenario, it is legitimate to ask some questions: why did some selenoproteins maintain Sec while others evolved with Cys? What is the advantage of having an energetically expensive machinery for Sec synthesis and incorporation if Cys active sites are possible? Has it been developed a new "chemico-biological" hypothesis that posits a biological convenience rather than a chemico-enzymatic advantage as the reason for selecting Sec over Cys [83]?

This biological convenience could be the ability to resist enzymatic inactivation by irreversible oxidation. Sec in selenoproteins ($R–Se^-$) is oxidized to R–SeOH and can readily be recycled back to $R–Se^-$, while Cys cannot be recycled once it is over-oxidized to sulfinic or sulfonic acid. Therefore, Sec in selenoproteins prevents over-oxidation and enzyme inactivation while the Cys-homologs, by virtue of their catalytic role and/or biological function, might not require resistance to irreversible oxidation.

Succination

Protein succination is a stable and irreversible chemical modification that occurs when fumarate, a Krebs cycle intermediate, reacts by a Michael addition with cysteine residues to generate S-(2-succino)cysteine (2SC)[85,86]. Succination appears to be specific for cysteine, as we have been unable to detect succination of other candidate nucleophilic amino acids.

The increase in fumarate develops as result of excess fuel supply, accumulation of NADH, and feedback inhibition of the Krebs cycle. Mitochondrial stress results in the

accumulation of fumarate and subsequently in the succination of Cys residues that alters protein structure or function. In particular, fumarate and succinated cysteines are increased in adipocytes in diabetes, disturbing protein function and turnover[87]. Inactivation of GAPDH is a critical, early step in the metabolic derangements that lead to the development of diabetic complications. Inactivation of this enzyme causes an increase in intracellular concentrations of glucose and glycolytic intermediates, leading to enhanced activity of other pathways. Recent study *in vitro* indicate that GAPDH is not activated by reactive oxygen species but by the succination of its cysteine residues, in particular Cys 149[86]. Therefore, the presence of 2SC is a biomarker of glucotoxicity driven mitochondrial stress in the adipocyte. Mass spectrometry analysis reveals that also chaperone Protein Disulfide Isomerase (PDI) presents cysteines succinated in the adipocytes. Succination significantly lowers PDI reductase activity that is no longer able to re-fold proteins within the adipocyte[88].

This irreversible PTM of cysteine is an early step in the response to excess glucose concentration in cell culture or *in vivo* in diabetes but accumulation of ATP also leads to an increase in mitochondrial Nicotinamide Adenine Dinucleotide (NADH) and then to hyperpolarization of the IMM, as seen in adipocytes. The increase in NADH would then led to accumulation of Krebs cycle intermediates, including fumarate, causing an increase in succination of proteins. The accumulation of NADH may also trigger the production of ROS. Eventually, damage to the integrity of the mitochondrial membranes would open the mitochondrial permeability transition pore, precipitating a series of events culminating in apoptosis[86].

Cys 149, in GAPDH, was also found oxidized to sulfenic acid. This suggests that sulfenation, which can lead to glutathionylation, and succination may be competing processes. Glutathionylation is both protective and reversible, while, succination is an irreversible modification of proteins and 2SC, *in vivo*, is neither absorbed nor recycled.

The relationship between succination and oxidative stress is complex, because processes that are associated with succination are also associated with oxidative stress. Several evidences indicate that antioxidants may inhibit oxidative damage and formation of sulfenic acids without affecting the high mitochondrial fumarate concentration and resultant increase in succination of proteins[86].

Protein N-Terminal Acetylation

Protein N-terminal (Nt) acetylation is a major modification of eukaryotic proteins which involves the transfer of an acetyl group from acetyl coenzyme A to the α-amino group of the first amino acid residue of a protein[89]. This reaction, catalyzed by N-terminal acetyltransferases associated with ribosomes, is irreversible and occurs co-translationally.

Despite being discovered over 50 years ago, the biological relevance of this modification is only known for a few substrates. The functional implications of N-terminal acetylation include regulation of protein-protein interactions and targeting to membranes. Moreover, this PTM affects accumulation on the mature proteins in target organelles and confers metabolic stability on the protein by providing general protection from peptidases and the Ubiquitin-mediated pathway on protein degradation. Experimental data indeed indicated that proteins with acetylated N-terminal were more stable *in vivo* than non-acetylated proteins. One explanation for this might be the discovery that another N-terminal modification (ubiquitination) involving direct attachment of the small protein Ubiquitin to the N-terminal amino acid residue promotes the subsequent degradation of the protein[90]. Thus, blocking the N-terminus by Nt-acetylation potentially prevents N-terminal ubiquitination, and thus stabilizes the protein. A naturally occurring N-terminally acetylated protein has not yet been found, however, that is N-terminally ubiquitinated and degraded when lacking its acetylation modification. A naturally occurring N-terminally acetylated protein has not yet been found, however, that is N-terminally ubiquitinated and degraded when lacking its acetylation modification. An unacetylated N-terminus may still contribute to protein destabilization by a mechanism independent of Ubiquitin. In contrast to the general idea that Nt-acetylation protects proteins from degradation, recently Nt-acetylated amino acid sequences in certain proteins were found to be involved in creating degradation signals: a Ubiquitin ligase, Doa10, recognizes Nt-acetylated proteins and marks them with Ubiquitin for destruction[91].

Although these two hypotheses predict opposite functional outcomes for Nt-acetylation and thus appear to be contradictory, both mechanisms may take place side by side in the cell, each applying to specific subsets of proteins under defined

conditions. The N-terminal acetylation is a signal that is part of a quality control mechanism to degrade unfolded or misfolded proteins and to regulate *in vivo* protein stoichiometries and it is depending on cellular state[89].

Phosphorylation

Protein phosphorylation is a very common PTM that is involved in regulating protein functions. However, protein phosphorylation in eukaryotes only occurs on the side chains of amino acids containing free hydroxyl groups. Amino acids such as Ser, Thr, and Tyr residues of proteins carry free hydroxyl groups. Hence, phosphorylation is very commonly found in eukaryotic proteins containing Ser, Thr, and Tyr residues. Very rarely in some eukaryotic proteins and most commonly in prokaryotic proteins, phosphorylation is also found on His, Lys, and Glu residues. Protein phosphorylation is mediated by protein kinases. For this mechanism, universal phosphoryl donor is Adenosine Triphosphate (ATP).

Protein phosphorylation is a reversible process in which phosphorylation and dephosphorylation act as molecular switch for the biological functions of many proteins. Dephosphorylation is mediated by a group of enzymes called phosphatases that catalyzes the hydrolysis of phosphate groups and converts the phosphate carrying groups back in to hydroxyl groups. Extremely large number of protein kinases and phosphatases exists in living cells. For example, in yeast approximately 3% of all proteins are kinases and phosphatases[92]. Many of the kinases and phosphatases are highly specific, but some kinases and phosphatases have very broad specificity. Known targets of phosphorylation include enzymes, receptors, ion channel proteins, structural proteins, signaling molecules, etc. Phosphorylation and dephosphorylation may occur continually on a protein, and this cycle allows protein to rapidly switch from active state to inactive state and viceversa. The phosphorylation and dephosphorylation have many unique advantages for the cells because these processes are rapid, do not require cells to make new proteins or degrade the old proteins; and the reactions are easily reversible. Specific protein kinases are involved in transferring phosphoryl group to hydroxyl groups of specific amino acids such as Ser, Thr and Tyr residues. They are independently called as serine/threonine kinases and tyrosine kinases.

Phosphoryl group is a negatively charged functional group and is hydrophilic in nature. Hence, phosphorylation introduces a very strong negative charge to protein that influences the changes in protein interactions with nearby amino acids as well as with other proteins. Phosphorylation of a hydrophobic protein domain converts into highly polar and hydrophilic domain of the protein. This change in hydrophobic into polar and hydrophilic nature may also induce conformational change in higher-order structure of proteins.

Phosphorylation regulates many protein functions including regulation of thermodynamics of biological reactions that involves energy, protein–protein interactions, protein degradation, enzyme inhibition. Approximately 90% of all phosphorylated proteins are believed to be phosphorylated on multiple sites[93].

The most current methods to analyze protein phosphorylation includes electrophoresis with chemical detection or immunodetection, phosphoprotein enrichment, mass spectrometry.

Oxidation of methionine

Methionine (Met) is a sulfur containing amino acid, such as Cys, normally found in protein. Researchers in the life sciences are generally familiar with the major functions of cysteine residues in proteins but the functions of methionine residues are still little known[94].

The role of Met as initiator in protein synthesis is well-known and, in recent years, other functions have been proposed. Available studies lead to the conclusion that Met, like Cys, functions as an antioxidant and as a key component of a system for regulation of cellular metabolism[95].

Met is readily oxidized to methionine sulfoxide by many reactive species. The oxidation of surface exposed methionines thus serves to protect other functionally essential residues from oxidative damage. Met Sulfoxide reductases have the potential to reduce the residue back to Met, increasing the scavenging efficiency of the system. Reversible covalent modification of amino acids in proteins provides the mechanistic basis for most systems of cellular regulation[96]. Inter-conversion of Met and Met sulfoxide can

function to regulate the biological activity of proteins, through alteration in catalytic efficiency and through modulation of the surface hydrophobicity of the protein[95].

Oxidized methionine residues may be reduced by a variety of enzyme systems, known as Met Sulfoxide reductases, which often involve Thioredoxin. These enzymes exist in most organisms, from bacteria to mammals.

The potential of Met Sulfoxide reductase to contribute to the antioxidant defense of the cell is clear. Oxidative stress also causes a dramatic increase in protein-bound Met sulfoxide as well as free Met sulfoxide in the mutant yeast cells[97]. Conversely, overexpression of Met Sulfoxide reductase in yeast or a T-lymphocyte cell line provided an improved response to oxidative challenges[95,98].

Cyclic Met oxidation/MetO reduction possesses the characteristics required to function as a regulator[99]. There are several examples in which reversible oxidation of Met may function as a regulatory mechanism, although none are yet convincingly documented to operate *in vivo*. The absence of detailed experimental investigations is due in good part to the lack, until recently, of methodology for the detection of methionine sulfoxide in intact proteins.

Recently, advances in mass spectrometric techniques have permitted to reveal the presence of oxidized methionine in numerous proteins[100]. The presence of this Ox-PTM could indicate which proteins are destined for proteolytic degradation by the proteasome via Ubiquitin-dependent and independent routes.

1.6 Advances in proteomic for membrane protein analysis

Biological membranes form an essential barrier between living cells and their external environments. They also serve to compartmentalize intracellular organelles within eukaryotes and, in this function, they include membranes that envelope the nucleus, the outer and inner membranes of mitochondria, membrane *cisternae* complex of the ER, Golgi apparatus, as well as lysosomes and secretory vesicles. Depending on their localizations in the whole organism and also within the cell, these membranes have different, highly specialized functions.

Membrane proteins can be classified into three groups based on their location and interaction with membranes: integral (membrane penetrating); peripheral (attached via non-covalent bonds); lipid-anchored (attached through covalent bonds). Peripheral membrane proteins are attached to one side of the membrane in several ways, such as for example through an α-helix, while the lipid-anchored membrane proteins are attached to one side of the membrane through covalent bonds to lipid groups[101].

The integral membrane proteins span across the lipid bilayer and are amphipathic. Their hydrophilic regions protrude into the cytosol, the inner of organelles or the extracellular environment for interaction with soluble proteins and molecules whereas the hydrophobic regions work for the embedding of the proteins into the lipid bilayer. Moreover, integral membrane proteins comprise of single or multiple transmembrane domains and thus they can be classified as type 1, type 2 or multipass proteins. Type 1 proteins are oriented with their N-terminal facing the luminal or extracellular space in an organelle, whereas type 2 proteins have the opposite orientation. Multipass proteins can have either or both of their N and C-terminal facing either the luminal (such as VDAC proteins) or extracellular space.

Membrane proteins have a wide variety of functions required for normal development and physiology and when disrupted lead to a range of diseases. Identification of membrane proteins with aberrant properties can result in discovery of novel therapeutic targets. It is reported that about 60% of approved drugs target membrane proteins[102]. The sub-cellular localizations of membrane proteins determine their functions. Proteins at the plasma membrane act as receptors, relaying information from the environment to the cell, thus enabling the cell to alter its behavior in response to external signals. Still other proteins at the cell membrane provide anchors for cytoskeletal proteins and extracellular matrix that give the cell its shape. IMM contains protein complexes of the respiratory chain that produce energy for the cell, as well as proteins which form the apoptosome involved in the trigger of cell suicide. Furthermore, still many others function as carriers and channels involved in the transport of various ions, molecules, and even other proteins in and out of the organelles or cells (for example VDAC isoforms in the OMM).

Despite constituting 30% of the total genome, membrane proteins are under-represented in many proteome profiles and that is dependent to the presence of a high

dynamic range of cellular protein expression. The under-representation of membrane proteins from proteome studies is mainly due to the heterogeneous, hydrophobic and limited solubility, restricted enzyme accessibility and low abundance of these proteins which limits their detection and identification. To overcome these limitations, various strategies have been applied in the enrichment, solubilization, separation, and digestion steps involved in membrane protein studies.

The major difficulty of membrane proteome analysis still lies in the preparation of membrane proteins. The first essential step is the membrane protein enrichment for which several strategies have been developed, including sub-cellular fractionation delipidation, affinity purification and removal of non membrane proteins[103].

Sub-cellular fractionation of membranes is usually achieved by centrifugations at increasing speeds. Isolating membrane proteins in single-cell organisms requires only lysis of the cells before sequential centrifugation steps. In multicellular organisms, there is another level of separation that is necessary for isolating tissues, organelles and proteins.

Density gradient centrifugation (using sucrose or sorbitol) has amply been used to enrich various cellular organelles. During the isolation of membrane proteins, there are potential contaminations from other organelles or non-membrane proteins that associate with membrane proteins, such as the high abundance cytoskeletal proteins. Hence, it is crucial to have minimal contamination from non-membrane proteins using sub-cellular fractionation to enrich membrane proteins[104].

It essential to couple an efficient solubilization procedure with the enrichment of membrane proteins. It can be utilized a two-phase system, detergent/polymer: in this case, the soluble proteins are isolated in the polymer phase whereas membrane proteins are enriched in the detergent phase. Enrichment of membrane proteins can also be achieved via sequential extraction of proteins from cells and tissue lysate using different extraction buffers containing progressively stronger solubilizing agents. This method separates soluble cytosolic proteins from hydrophobic membrane proteins and it is based on differential solubility properties of the cells[105] Membrane proteins can also be enriched using affinity chromatographic purification (hydroxyapatite chromatography in the case of VDAC proteins) or membrane biotinylation reagents that bind to membrane proteins exposed at the cell surfaces. These biotinylated

membrane proteins can be affinity purified using avidin or streptavidin resin. Alkaline solutions such as sodium carbonate can be used to strip peripheral membrane proteins from the lipid bilayer. Another enrichment method known as the membrane protein "shaving" approach disregards the trans-membrane domains and analyzes the exposed hydrophilic regions of membrane proteins using high pH and proteinase K that yields peptides of 6-20 amino acids which are ideal for LC/MS-MS analisys.

In the "Bottom-Up" proteomic approach, a complex mixture of proteins is separated by mono (1-DE) or two-dimensional electrophoresis (2-DE). Subsequently, the protein of interest is excised from the gel and subjected to enzymatic digestion. This is followed by mass spectrometry analysis and bioinformatics research. Although 2-DE is the main platform used in proteomics and has been used in studies on profiling of membrane proteins, membrane proteins have been under-represented in 2-DE gels due to difficulties in extracting and solubilizing them in the isoelectric focusing sample buffer. Typical buffers for isoelectric focusing (IEF) include non ionic detergents such as urea, thiourea and CHAPS. Unfortunately, these chemicals can interfere with mass spectrometry analysis. However, membrane proteins, especially those with multiple TM domains, are insoluble in these solutions. The most effective solubilizing agent for highly hydrophobic membrane proteins is SDS but this detergent is incompatible with 2-DE. Besides the difficulties in entering the IPG (Immobilized pH Gradient) gels, membrane proteins tend to precipitate at their isoelectric point during IEF. Furthermore, their tendency to absorb to the IPG matrix impedes their migration into the SDS-PAGE gel. Hence, conventional 2-DE is only able to resolve membrane proteins with no more than two TM domains whereas those with multipass TM domains could not be identified by 2-DE. Moreover, there is also an under-representation of peptides from TM domains of membrane proteins resolved in gel-based separation methods. This is due to the inherent lack of trypsin cleavage sites in these domains, poor accessibility to proteases in these regions, tendency of the hydrophobic domains to aggregate and precipitate after the removal of SDS, and difficulties in extracting these peptides from the gels[106].

The mono dimensional electrophoresis (1-DE) solely relies on the size of the protein for separation. This approach has less resolution than two-dimensional techniques but also has fewer associated technical problems.

Due to the limitations of 2-DE and 1-DE in separating membrane proteins, various alternative techniques have been employed in membrane proteomics, such as the MuDPIT commonly named "Shotgun" approach. It is a gel-free platform that use solution-based separation techniques and it has helped to minimize the problem of insolubility encountered in membrane proteins studies. In Shotgun proteomics, the peptides derived from proteins digest are separated and analyzed in a liquid phase. This also avoids the difficulty of extracting hydrophobic proteins from gels. Several Shotgun approaches have circumvented the low solubility and high hydrophobicity limitation of membrane protein by using organic solvents, organic acids or detergent-containing aqueous solution. The use of both detergents and organic solvents (for example chloroform/methanol) has shown to enhance the solubility and membrane proteome coverage. However, the use of such detergents and organic solvents for membrane proteins solubilization must not interfere with subsequent protein separation, enzymatic digestion and MS analysis. Otherwise, precipitation is usually performed to remove the interfering reagents but this often leads to yield loss. The digestion of membrane proteins has also been shown to improve by using combinations of proteases (including the non-specific protease proteinase K) and chemical cleavage (e. g. cyanogen bromide/TFA). For effective digestion, the backbone of the proteins must be accessible for the proteolytic cleavages. However, access to certain parts of membrane proteins is often blocked due to the same protein folding or presence of sugar and lipid. Trypsin digestion (specific cleavage after Arg and Lys residues) is a typical specific way to digestion. However, some membrane proteins tend to lack trypsin cleavage sites and it leads to large peptide fragments which keep up their hydrophobic nature and are not detected by mass spectrometer. Unspecific chymotrypsin and proteinase K enzymes can be used to obtain additional information but peptides generated are difficult to predict because of the random location of cleavage sites.

Top-down proteomics analyzes intact proteins using “soft-ionization” mass spectrometry. The protein ions are fragmented within the instrument without previous digestion to identify the native state of the membrane proteins. This last method need of highly purified proteins and thus it cannot be used for complex mixtures.

Tandem mass spectrometry analysis equipped with a MALDI or ESI ion source is often used for membrane protein identification. Peptides were analyzed and obtained mass spectra. Subsequently, the bioinformatics tool and software are used for membrane protein identification.

Structural assignment of proteins is usually performed using X-ray crystallization, NMR and electron microscopy, which all require large amount of high quality protein samples. However, the determination of membrane protein structures has been challenging due to difficulties faced in expressing, solubilizing and purifying these hydrophobic proteins. The inability to obtain sufficient native membrane proteins for crystallization necessitates the need to over-express them as recombinant proteins. These hydrophobic proteins are harder to express as recombinant proteins than soluble proteins, particularly for eukaryotic membrane proteins. This is due to the difficulty encountered in expressing adequate amounts of functionally folded membrane proteins, and the toxicity and aggregates formation associated with over-expression of membrane proteins. Furthermore, the requirement of strong detergents for membrane protein solubilization affects the stability of the proteins which may lead to unfolding or alteration of the protein structure. Several new or improved approaches in the production of membrane proteins have been developed, including cellular and cell-free expression systems. In particular, the cell-free expression technologies have avoided many problems faced by over-expression of membrane proteins, such as toxicity induced in the host cells.

Providing that membrane proteins make up 30% of naturally occurring proteins and because they are implicated in a wide variety of functions, the ability to perform specific proteomic analyses is crucial for understanding their function[107]. Future advances in technology will also play a critical role for the field of proteomics. New instrumentation that performs faster scanning speeds and higher mass accuracy will also allow for more peptide identifications and ultimately higher proteome coverage which will facilitate the analysis of membrane proteins.

2. Aim of the work

VDAC proteins in mammals have a high sequence homology. The three-dimensional structure is known only for VDAC1 (in mouse and human) and a reduced variant of VDAC2 (in zebrafish), while the structure of VDAC3 was predicted by homology modeling. Several studies indicate differential functions for each isoform and in particular these differences are evident for VDAC3, the least known isoform[17]. Variations in molecular weight, isoelectric points and amino acid composition could determine these functional differences, such as the ability to form pores in artificial membranes and the size of channels. In particular, VDAC isoforms have a different content in cysteine residues, amino acids that can have multiple redox states: in rat isoforms, VDAC1, 2 and 3 have 2, 11 and 7 cysteines, respectively; in human isoforms, VDAC1, 2 and 3 have 2, 9 and 6 cysteines, respectively[38]. Furthermore VDAC proteins, being integral membrane proteins, have the characteristic of having fragments exposed to environments with different chemical-physical properties: cytosol, OMM and IMS.

Most of the cysteine residues in VDAC2 and 3 are located in loops that extend into the IMS. In a first study carried out on rat isoform 3 we wanted to verify, through the use of high resolution mass spectrometry, whether the strongly oxidizing environment of the IMS could influence the redox state of the cysteine residues[51]. If the redox state depended exclusively on the environment in which the residues are immersed, all the residues protruding towards the IMS should be oxidized in the same way and with similar oxidation ratios. Instead, the results showed that the Cys residues localized in the IMS show a variable oxidation pattern[51] (Supplementary Article 3) which could be connected with the intrinsic mechanisms of regulation of the activities of these trans membrane proteins.

In this context, the aim of my work has been to extend the study of the oxidation states of Cys residues to the other rat VDAC isoforms and to the VDAC isoforms extracted from human cells (HAP cells). The comparison of the oxidation states of cysteine residues in different organisms is important to understand the function of these peculiar post-translational modifications. Furthermore, the possible conservation of the redox states of cysteine residues in different organisms could indicate that these are

not random events or associated with technical artifacts, but modifications related to the normal functioning of the mitochondrial porins.

Furthermore, many proteins (e. g. Sod1, Bax, Bak, Bcl-xl and Hexokinase) are associated with the cytosolic face of the OMM by binding to the VDAC proteins. Thus several cytoplasmatic proteins use the same docking protein in the surface of the OMM. Competition for the same or few docking sites can be a central paradigm for aggregation on the OMM. The formation of protein aggregates on the OMM characterizes the tissues of patients affected by specific neurodegenerative diseases[108].

Since VDACs represent the key proteins of the bioenergetics metabolism and interact with several proteins on the surface of mitochondria, they are considered involved in any mechanism where the access to the mitochondria energetic production is reduced or hindered, as it looks to be the case in neurodegenerative diseases like, in particular, AD, PD[109] and ALS[110].

For all of these reasons, the goal of my research has been the elucidation of structural details and chemical modifications in VDAC proteins that could support functional explanation of their role.

3. Article 1

Post-translational modifications of VDAC1 and VDAC2 cysteines from rat liver mitochondria

Rosaria Saletti, Simona Reina, Maria G.G. Pittalà, Andrea Magrì, Vincenzo Cunsolo, Salvatore Foti and Vito De Pinto

BBA-Bioenergetics 1859 (2018) 806-816

BBA - Bioenergetics 1859 (2018) 806–816

Contents lists available at ScienceDirect

BBA - Bioenergetics

journal homepage: www.elsevier.com/locate/bbabio

Post-translational modifications of VDAC1 and VDAC2 cysteines from rat liver mitochondria☆

Rosaria Saletti[a,1], Simona Reina[b,c,1], Maria G.G. Pittalà[c,d], Andrea Magrì[b,c,d], Vincenzo Cunsolo[a], Salvatore Foti[a,*], Vito De Pinto[c,d,**]

[a] Department of Chemical Sciences, Organic Mass Spectrometry Laboratory, University of Catania, Viale A. Doria 6, 95125 Catania, Italy
[b] Department of Biological, Geological and Environmental Sciences, Section of Molecular Biology, University of Catania, Viale A. Doria 6, 95125 Catania, Italy
[c] National Institute for Biomembranes and Biosystems, Section of Catania, Viale A. Doria 6, 95125 Catania, Italy
[d] Department of Biomedicine and Biotechnology, Section of Biology and Genetics, Viale A. Doria 6, 95125, Catania, Italy

ARTICLE INFO

Keywords:
Cysteine over-oxidation
Orbitrap fusion tribrid
Mitochondria
Mitochondria quality control
ROS
Hydroxyapatite

ABSTRACT

VDACs three isoforms (VDAC1, VDAC2, VDAC3) are integral proteins of the outer mitochondrial membrane whose primary function is to permit the communication and exchange of molecules related to the mitochondrial functions. We have recently reported about the peculiar over-oxidation of VDAC3 cysteines. In this work we have extended our analysis, performed by tryptic and chymotryptic proteolysis and UHPLC/High Resolution ESI-MS/MS, to the other two isoforms VDAC1 and VDAC2 from rat liver mitochondria, and we have been able to find also in these proteins over-oxidation of cysteines. Further PTM of cysteines as succination has been found, while the presence of selenocysteine was not detected. Unfortunately, a short sequence stretch containing one genetically encoded cysteine was not covered both in VDAC2 and in VDAC3, raising the suspect that more, unknown modifications of these proteins exist. Interestingly, cysteine over-oxidation appears to be an exclusive feature of VDACs, since it is not present in other transmembrane mitochondrial proteins eluted by hydroxyapatite. The assignment of a functional role to these modifications of VDACs will be a further step towards the full understanding of the roles of these proteins in the cell.

1. Introduction

In the outer mitochondrial membrane of all eukaryotes, VDACs (Voltage Dependent Anion Selective Channel) are the main responsible for the cross-talk between the organelle and the rest of the cell [1, 2]. As aqueous channels, VDACs mediate the transport of ions and metabolites across the OMM. In addition, the interactions of VDACs with several cytoplasmic proteins like hexokinase [3] tubulin [4, 5], dynein [6], actin [7], synuclein [8], mutated forms of SOD1 [9], pro-apopototic and antiapoptotic factors [10, 11], highlight a crucial function of VDAC in several biological processes ranging from mitochondrial bioenergetics to apoptosis. In mammals, the presence of three isoforms (VDAC1-VDAC2-VDAC3) with a relatively high sequence similarity and structural homology, contrasts with the different roles that have been proposed within the cell. Indeed, along with their common involvement in cellular bioenergetics maintenance, VDAC1 and VDAC2 have been proposed to have opposite functions in programmed cell death (pro-apoptotic the first one [2, 10, 12] and anti-apoptotic the second one [13]), while recent evidences suggest VDAC3 as a player in ROS metabolism control [14, 15].

The three-dimensional structure obtained by NMR and X-ray crystallography techniques [16–18] revealed VDAC1 as a transmembrane β-barrel containing an α-helix N-terminal segment that, according to the protein arrangement within the membrane [19], protrudes towards the cytosol. Interestingly, the high sequence similarity with the other two isoforms suggests the existence of a common structural pattern in the pore organization, as confirmed by the crystallographic structure resolved for VDAC2 from zebrafish [20] and the in silico prediction of

Abbreviations: VDAC, voltage-dependent anion selective channel; OMM, outer mitochondrial membrane; PTM, post-translational modification; ROS, reactive oxygen species; MS, mass spectrometry; HTP, hydroxyapatite

☆ This article is part of a Special Issue entitled 20th European Bioenergetics Conference, edited by László Zimányi and László Tretter.

* Correspondence to: V. De Pinto, Department of Biomedicine and Biotechnology, Section of Biology and Genetics, University of Catania, Campus S. Sofia, Building 2, Viale A. Doria 6, 95125 Catania, Italy.

** Correspondence to: S. Foti, Department of Chemical Sciences, Organic Mass Spectrometry Laboratory, University of Catania, Campus S. Sofia, Building 1, Viale A. Doria 6, 95125 Catania, Italy.

E-mail addresses: rsaletti@unict.it (R. Saletti), vcunsolo@unict.it (V. Cunsolo), sfoti@unict.it (S. Foti), vdpbiofa@unict.it (V. De Pinto).

[1] These authors equally contributed to the article.

https://doi.org/10.1016/j.bbabio.2018.06.007
Received 3 February 2018; Received in revised form 4 June 2018; Accepted 7 June 2018
Available online 08 June 2018

human VDAC3 structure [15].

It is widely reported that in its native environment, VDAC exhibits several post-translational modifications such as phosphorylation [21], acetylation [22], tyrosine nitration [23] whose role in protein activity has been only partially clarified. For instance, VDAC1 phosphorylation has been associated to the modulation of channel gating properties [24], prevention of cell death [25], sensitization to apoptosis [26, 27] and/or various physiopathological conditions [28]. However, information regarding the modifications of sulfur-containing amino acids is rather limited. It is known, for example, that S-nitrosylation of VDAC modulates sperm function [29] and correlates with enhanced calcium-induced mitochondrial swelling and cytochrome *c* release [30]. Given the emerging role of redox signaling in numerous cellular processes [31] we focused on unraveling the modifications of VDAC's cysteine and methionine residues under physiological conditions. Through the combination of the UHPLC/High Resolution ESI MS/MS with the "in-solution" digestion of VDACs purified from rat liver mitochondria, we recently succeeded in defining a complete and detailed profile of oxidations of VDAC3 cysteines and methionines [32], discovering that cysteines may reside in a wide range of oxidation states. In this work, we thus report for the first time an accurate survey of the oxidative states of sulfur containing amino acids of VDAC1 and VDAC2 isolated from rat liver mitochondria. As for VDAC3, we found cysteines over-oxidized to sulfonic acid also in VDAC1 and VDAC2. A comparison with highly hydrophobic mitochondrial proteins eluted from hydroxyapatite shows that this modification happens specifically in VDAC isoforms. To complete the survey of the most common cysteine modifications, also the presence of succination (i.e. the addition of fumarate to reduced cysteines) and selenocysteine was examined in the three isoforms VDAC1–3. Possible consequence or a rationale of such VDAC modifications in the cell context is discussed.

2. Materials and methods

2.1. Chemicals

All chemicals were of the highest purity commercially available and were used without further purification. Ammonium bicarbonate, TrisHCl, Triton X-100, Sucrose, EDTA, HEPES, formic acid (FA), phenylmethylsulfonyl fluoride (PMSF), dithiothreitol (DTT), iodoacetamide (IAA) and chymotrypsin were obtained from Sigma-Aldrich (Milan, Italy). Modified porcine trypsin was purchased from Promega (Madison, WI, USA). Water and acetonitrile (OPTIMA® LC/MS grade) for LC/MS analyses were provided from Fisher Scientific (Milan, Italy).

2.2. Isolation of intact rat liver mitochondria and proteins reduction and alkylation

Rat liver mitochondria were prepared as already reported [33, 34]. Briefly, 5 livers of male Sprague-Dawley rats weighing 300–500 g (Envigo) were resuspended into buffer A (0.25 M sucrose, 10 mM HEPES, 0.1 mM EDTA, 0.15 μM PMSF, pH 7.0) in ratio (v/w) 3:1 and homogenized with a glass Potter-Elvehjem pestle. Homogenate was diluted 1:1 (v/v) in buffer A and centrifuged for 5 min at 1000 ×*g* at 4 °C. After repeating this step on the pellet obtained in the first homogenization, the supernatants were reunited and subjected to differential centrifugations. Final mitochondria-enriched fraction was resuspended in buffer B (sucrose 0.25 M, HEPES 10 mM, 0.15 μM PMSF) and total yield was determined by micro-Lowry method. Reduction/alkylation was carried on before VDACs purification in order to avoid any possible artifacts due to air exposure. 70 mg of intact mitochondria were incubated for 3 h at 4 °C in Tris-HCl 10 mM (pH 8.3) containing 0.7 mmol of DTT, which corresponds to an excess in the order of 50:1 (mol/mol) over the estimated thiol groups. The temperature was kept at 4 °C in order to avoid possible reduction of methionine sulfoxide to methione by methionine sulfoxide reductase. After centrifugation for 30 min at 10,000 ×*g* at 4 °C, alkylation was performed by addition of iodoacetamide at the 2:1 M ratio over DTT for 1 h in the dark at 25 °C. Mixture was centrifuged for 30 min at 10,000 ×*g* at 4 °C and the pellet was stored at −80 °C until further use.

2.3. Preparation of VDAC1 and VDAC2 enriched fractions from rat liver mitochondria

VDAC1 and VDAC2 were purified from rat liver mitochondria as in [32]. 70 mg of reduced and alkylated intact mitochondria were lysed in buffer A (10 mM TrisHCl, 1 mM EDTA, 3% Triton X-100, pH 7.0) in ratio 5:1 (mitochondria mg/buffer volume) [33] for 30 min on ice and centrifuged at 17,400 ×*g* for 30 min at 4 °C. The supernatant containing mitochondrial proteins was subsequently divided onto 12 glass Econo-column 2.5 × 30 cm (Biorad), each packed with 0.6 g of dry hydroxyapatite (Bio-Gel HTP, Biorad). Columns were eluted with 5 mL of buffer A at 4 °C and fractions from each column were collected and precipitated with 9 volumes of cold acetone at −20 °C.

2.4. In-solution digestion of the hydroxyapatite eluate

Pellets from the hydroxyapatite eluate was purified from non-protein contaminating molecules with the PlusOne 2-D Clean-Up kit (GE Healthcare Life Sciences, Milan, Italy) according to the manufacturer's recommendations. The desalted protein pellet obtained was suspended in 100 μL of 50 mM ammonium bicarbonate (pH 8.3) and incubated at 4 °C for 15 min. After, 100 μL of 0.2% RapiGest SF (Waters, Milan, Italy) in 50 mM ammonium bicarbonate were added and the sample was put at 4 °C for 30 min. Protein amount, determined using fluorometer assay kit, resulted 1 μg (Invitrogen Qubit™ Protein Assay kit, ThermoFisher Scientific, Milan, Italy). The reduction was carried out by adding 2.6 μg of DTT dissolved in the same buffer for 3 h in the dark at 25 °C. Subsequently, alkylation was performed by addition of iodoacetamide at the same molar ratio over total thiol groups and the reaction allowed to proceed for 1 h in the dark at 25 °C. Finally, reduced and alkylated proteins were subjected to digestion using modified porcine trypsin or chymotrypsin in ammonium bicarbonate (pH 8.3) at an enzyme-substrate ratio of 1:50 and 1:25, respectively, at 37 °C for 4 h. The protein digests were then dried under vacuum, dissolved in 20 μL of 5% FA and analyzed by nano UHPLC/High Resolution ESI-MS/MS.

2.5. Liquid chromatography and tandem mass spectrometry (LC–MS/MS) analysis

Mass spectrometry data were acquired on an Orbitrap Fusion Tribrid (Q-OT-qIT) mass spectrometer (ThermoFisher Scientific, Bremen, Germany) equipped with a ThermoFisher Scientific Dionex UltiMate 3000 RSLCnano system (Sunnyvale, CA).

Samples obtained by in-solution digestion were reconstituted in 20 μL of 5% FA aqueous solution and 1 μL was loaded onto an Acclaim®Nano Trap C18 column (100 μm i.d. × 2 cm, 5 μm particle size, 100 Å). After washing the trapping column with solvent A (H_2O + 0.1% FA) for 3 min at a flow rate of 7 μL/min, the peptides were eluted from the trapping column onto a PepMap® RSLC C18 EASY-Spray, 75 μm × 50 cm, 2 μm, 100 Å column and were separated by elution at a flow rate of 0.250 μL/min, at 40 °C, with a linear gradient of solvent B in A from 5% to 20% in 32 min, followed by 20% to 40% in 30 min, and 40% to 60% in 20 min.

Eluted peptides were ionized by a nanospray (Easy-spray ion source, Thermo Scientific) using a spray voltage of 1.7 kV and introduced into the mass spectrometer through a heated ion transfer tube (275 °C). Survey scans of peptide precursors in the *m/z* range 400–1600 were performed at resolution of 120,000 (@ 200 *m/z*) with a AGC target for Orbitrap survey of 4.0×10^5 and a maximum injection time of 50 ms. Tandem MS was performed by isolation at 1.6 Th with the quadrupole, and high energy collisional dissociation (HCD) was performed in the

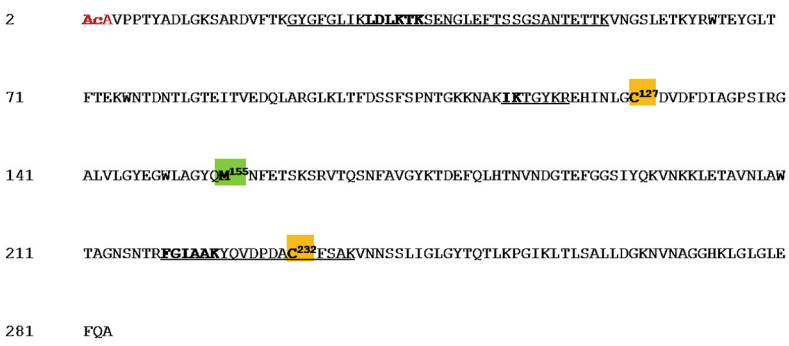

Fig. 1. Sequence coverage map of rVDAC1 obtained by tryptic digestion. Solid lines indicate unique tryptic peptides originated by missed-cleaveges, used to cover sequences shared by isoforms. Sequences shared by isoforms are reported in bold. The oxidized cysteine residues are highlighted in yellow and the oxidized methionine residues are highlighted in green. The N-terminal acetylated alanine is shown in red.

Ion Routing Multipole (IRM), using a normalized collision energy of 35 and rapid scan MS analysis in the ion trap. Only those precursors with charge state 1–4 and an intensity above the threshold of $5{\cdot}10^3$ were sampled for MS^2. The dynamic exclusion duration was set to 60 s with a 10 ppm tolerance around the selected precursor and its isotopes. Monoisotopic precursor selection was turned on. AGC target and maximum injection time (ms) for MS/MS spectra were 1.0×10^4 and 100, respectively. The instrument was run in top speed mode with 3 s cycles, meaning the instrument would continuously perform MS^2 events until the list of non-excluded precursors diminishes to zero or 3 s, whichever is shorter. MS/MS spectral quality was enhanced enabling the parallelizable time option (i.e. by using all parallelizable time during full scan detection for MS/MS precursor injection and detection).

Mass spectrometer calibration was performed using the Pierce® LTQ Velos ESI Positive Ion Calibration Solution (Thermo Fisher Scientific). MS data acquisition was performed using the *Xcalibur* v. 3.0.63 software (Thermo Fisher Scientific).

2.6. Database search

LC–MS/MS data were processed by Proteome Discoverer v. 1.4.1.14 (Thermo Scientific) and PEAKS software (v. 8.5, Bioinformatics Solutions Inc., Waterloo, ON Canada). Data were searched against the SwissProt database (release July 2016, containing 550,552 entries) using the MASCOT algorithm (Matrix Science, London, UK, version 2.5.1). The search was performed against *rattus* sequences database (7961 sequences). Full tryptic or chymotrypsin peptides with a maximum of 3 missed cleavage sites were subjected to bioinformatic search. Cysteine carboxyamidomethylation was set as fixed modification, whereas acetylation of protein N-terminal, trioxidation and succination of cysteine, presence of selenocysteine, oxidation of methionine, and transformation of N-terminal glutamine and N-terminal glutamic acid residue in the pyroglutamic acid form were included as variable modifications. The precursor mass tolerance threshold was 10 ppm and the max fragment mass error was set to 0.6 Da. Peptide spectral matches (PSM) were validated using Target Decoy PSM Validator node based on q-values at a 1% FDR.

Identification of the other transmembrane mitochondrial proteins eluted by hydroxyapatite was obtained using Proteome Discoverer v. 1.4.1.14 software with the following filters: Mascot significance threshold 0.05; peptide confidence: high; peptide score: > 20. A protein was considered identified with minimum of two peptides.

3. Results

3.1. Mass spectrometric analysis of VDAC1 from rat liver mitochondria

In this work, the primary structure of VDAC1 from *Rattus norvegicus* (rVDAC1) has been investigated by tryptic and proteinase K digestion, and MALDI and ESI-MS/MS mass spectrometric analysis [35]. When combining the coverage obtained in all the experiments, a total coverage of 99% (279 of 282 amino acids) was achieved. The N-terminal methionine was never found, indicating that it is removed during protein maturation. The protein tract not covered in this analysis included the sequence Gly^{94}-Lys^{96}.

To exclude the possibility that any unspecific and undesired oxidation could happen during the purification protocol, we added DTT to the buffer used to suspend the mitochondria and in the purification steps, as described in the Experimental Section. In-solution tryptic digestion of the hydroxyapatite (HTP) eluate of Triton X-100 and mass spectrometry analysis was then performed. Note that in this experiment every protein present in the HTP eluate was digested, producing a very complex peptide mixture. rVDAC1 peptides found in the analysis of mitochondria lysate incubated with DTT are reported in Supplementary Table 1.

UHPLC/High Resolution ESI-MS/MS of the tryptic digest allowed the coverage of 100% of the rVDAC1 sequence (Fig. 1 and Supplementary Table 1), thus chymotryptic digestion was not required. Although some predicted tryptic peptides of the rVDAC1 sequence are shared by two or three isoforms, unequivocal sequence coverage was obtained by the detection of unique peptides originated by missed-cleavages. The sequences of these unique peptides are underlined in Fig. 1.

The results also confirmed that the N-terminal Met, reported in the SwissProt database sequence (Acc. N. Q9Z2L0), is absent in the mature protein and that the N-terminal Ala is almost totally present in the acetylated form (Supplementary Fig. 1, Supplementary Table 1, fragments 2 and 3).

Data analysis was particularly focused on the investigation of the oxidation state of Met and Cys residues. The sequence of rat VDAC1 comprises one methionine in position 155, and two cysteines in position 127 and 232. It should be noted that the numeration adopted in the discussion starts from Met^1, which, actually, has been found to be absent.

Among the peptides identified, besides the fragment containing Met^{155} in the normal form (Supplementary Table 1, fragment 26), a peptide with this residue in the form of methionine sulfoxide was also detected (Supplementary Table 2, fragment 3).

The full scan and fragment ion mass spectrum of the molecular ion of the peptide G^{140}ALVLGYEGWLAGYQMNFETSK^{161} with Met^{155} as methionine sulfoxide are reported in Supplementary Fig. 2. The MS/MS spectrum presents the characteristic neutral loss of 64 Da corresponding to the ejection of methanesulfenic acid from the side chain of MetO [36].

Although from these data a precise determination of the amount of methionine and methionine sulfoxide respectively present in the digestion mixture cannot be obtained, a rough estimation of their relative abundance can be derived from the comparison of the absolute intensities of the multiply charged molecular ions of the respective peptides. These calculations for the doubly charged molecular ion of the fragment G^{140}-K^{161}, detected in the tryptic digest, indicate a ratio of 65:1 MetO/Met (Table 1).

Analysis of the mass spectral data oriented to the determination of

Table 1
Comparison of the absolute intensities of molecular ions of selected sulfur containing tryptic peptides found in the analysis of rVDAC1 reduced with DTT, carboxyamidomethylated and digested in-solution. The ratio reported was determined from a single experiment.

Peptide	Position in the sequence	Measured monoisotopic *m/z*	Absolute intensity	Ratio Ox/Red
EHINLG**C**DVDFDIAGPSIR	121–139	1059.9929 (+2)	$1.10 \cdot 10^6$	0.12
EHINLG***C***DVDFDIAGPSIR		710.0099 (+3)	$9.10 \cdot 10^6$	
EHINLG**C**DVDFDIAGPSIR	121–139	1050.9885 (+2)	$1.62 \cdot 10^6$	0.26
EHINLG***C***DVDFDIAGPSIR		1055.5061 (+2)	$6.19 \cdot 10^6$	
GALVLGYEGWLAGYQ**M**NFETSK	140–161	1225.5898 (+2)	$1.07 \cdot 10^7$	65
GALVLGYEGWLAGYQMNFETSK		1217.5914 (+2)	$1.64 \cdot 10^5$	
YQVDPDA**C**FSAK	225–236	696.2938 (+2)	$4.18 \cdot 10^6$	0.1
YQVDPDA***C***FSAK		700.8118 (+2)	$4.06 \cdot 10^5$	

M: methionine sulfoxide; ***C***: cysteine carboxyamidomethylated; **C**: cysteine oxidized to sulfonic acid. **E**: pyroglutamic acid form.

oxidation state of cysteines showed that for both the cysteines 127 and 232, besides the peptides containing these residues carboxyamidomethylated (Supplementary Table 1, fragments 23, 24, 25, 33, and 34), peptides with these amino acids in the form of sulfonic acid were also identified (Fig. 2, Supplementary Table 2, fragments 1, 2 and 4).

Again, a rough estimation of the relative abundance of the cysteines oxidized to sulfonic acid with respect to the Cys in the carboxyamidomethylated form can be derived from the ratio of the absolute intensities of the multiply charged molecular ions of the corresponding peptides. From these comparisons (Table 1), a ratio Cys-oxidized-to-sulfonic-acid/Cys-carboxyamidomethylated ranging from about 0.1:1 to 0.26:1 is observed. In the evaluation of these results, it should be considered that the oxidation of cysteine to cysteine sulfonic acid introduces a strong negative charge in the peptide, thus hampering the formation of positive ions. However, even taking into account these considerations, the data in Table 1 suggest that a sizeable amount of cysteines is oxidized to sulfonic acid.

3.2. Mass spectrometric analysis of VDAC2 from rat liver mitochondria

3.2.1. Tryptic digestion

As for rVDAC1, also the sequence of VDAC2 from *Rattus norvegicus* (rVDAC2) has been characterized by tryptic and proteinase K digestion, and MALDI and ESI-MS/MS mass spectrometric analysis [35] reaching a total coverage of 89,5% (263 of 294 amino acids). The N-terminal methionine was found to be removed in the mature protein and the region Gly^{138}-Thr^{168} was not covered.

In our work, the analysis of tryptic digest of the hydroxyapatite eluate of Triton X-100 solubilized rat liver mitochondria analyzed by UHPLC/High Resolution ESI-MS/MS allowed to identify 84.35% of the protein (248 of 294 amino acids) (Fig. 3 and Supplementary Table 3).

Although some predicted tryptic peptides of the rVDAC2 sequence are shared by two or three isoforms, unequivocal sequence coverage was obtained by the detection of unique peptides originated by missed-cleavages.

Also in rVDAC2, the N-terminal methionine, reported in the SwissProt database sequence (Acc. N. P81155), was found to be absent and the Ala^2 resulted present in the acetylated form (Supplementary Table 3, fragment 1 and Supplementary Fig. 3).

In the rVDAC2 there are one methionine in position 167, and eleven cysteines in position 4, 5, 9, 14, 48, 77, 104, 134, 139, 211, and 228. The oxidation state of the Met residue could not be determined in the analysis of the tryptic digest because the peptide containing the Met residue was not found. Instead, the partial oxidation of Cys^{48} (Table 2 and Fig. 4), Cys^{77}, Cys^{104}, Cys^{211}, and Cys^{228} (Supplementary Table 4, fragments 1–6 and Supplementary Figs. 4–6) to sulfonic acid, and the presence of the cysteines 4, 5, 9, and 14 exclusively in the carboxyamidomethylated form was detected (Supplementary Table 3, fragment 1, and Supplementary Fig. 3).

The relative abundance of the peptides containing the cysteines oxidized to sulfonic acid in comparison with peptides containing "normal" cysteines (i.e. carboxyamidomethylated cysteines), was estimated from the ratio of the absolute intensities of the respective multiply charged molecular ions. Table 2 shows that the cysteines 48 and 77 are oxidized to sulfonic acid in considerable amount, whereas cysteines 104, 211 and 228 oxidized to sulfonic acid are present only in trace amount.

Peptides including Cys^{134} and Cys^{139} resulted undetectable, so it was not possible to evaluate their oxidation state.

3.2.2. Chymotryptic digestion

To increase the sequence coverage, chymotryptic digestion of rVDAC2 was also performed. When combining the results obtained in the tryptic and chymotryptic digestions, the coverage of the sequence of rVDAC2 was extended to 96, 26% (283 out of 294 amino acids) (Fig. 3 and Supplementary Tables 3, 5). Although some predicted chimotryptic peptides of the rVDAC2 sequence are shared by two or three isoforms, unequivocal sequence coverage was obtained by the detection of unique peptides originated by missed-cleavages, except for the sequence GYEGWLAGY, which was not possible to cover by unique peptides (shown in bold in Fig. 3).

The region still not covered corresponds to the sequence Glu^{133}-Phe^{143}, a part of the stretch not determined in a previous work [35] (Fig. 5). In the chymotryptic digest, Met^{167} was identified either as normal methionine (Supplementary Table 5, fragments 12 and 13) and as methionine sulfoxide (Supplementary Table 6, fragments 1 and 2 and Supplementary Fig. 7). Because the peptide LAGYQM is shared by all the three isoforms, a rough estimation of the Ox/Red Ratio can be derived from the comparison of the absolute intensities of the multiply charged molecular ions of the peptide **QM**TFDSAKSKL, which is unique of the rVDAC2 sequence. As shown in Table 3, the two forms appear present in approximately equal amounts. Instead, cysteines oxidized to sulfonic acid were undetectable. (See Fig. 5.)

3.3. Presence of selenocysteines and identification of succination in VDAC isoforms

Mass spectral data were also analyzed in order to detect the presence of selenocysteines and the occurence of cysteine succination. Selenocysteines were not observed in all the rVDAC isoforms. Succinated cysteines were not found in rVDAC1, whereas in rVDAC2 only Cys48 was identified as succinated in very low amount (Supplementary Table 7 and Supplementary Fig. 8) (Table 4). In rVDAC3 three cysteines (8, 36 and 229) were succinated (Supplementary Table 8 and Supplementary Fig. 9), with two of them (36 and 229) in very low amounts (Table 5).

3.4. No other protein carrying over-oxidized cysteine was identified in mitochondrial HTP eluates

Many works have outlined the power of HTP as a chromatographic

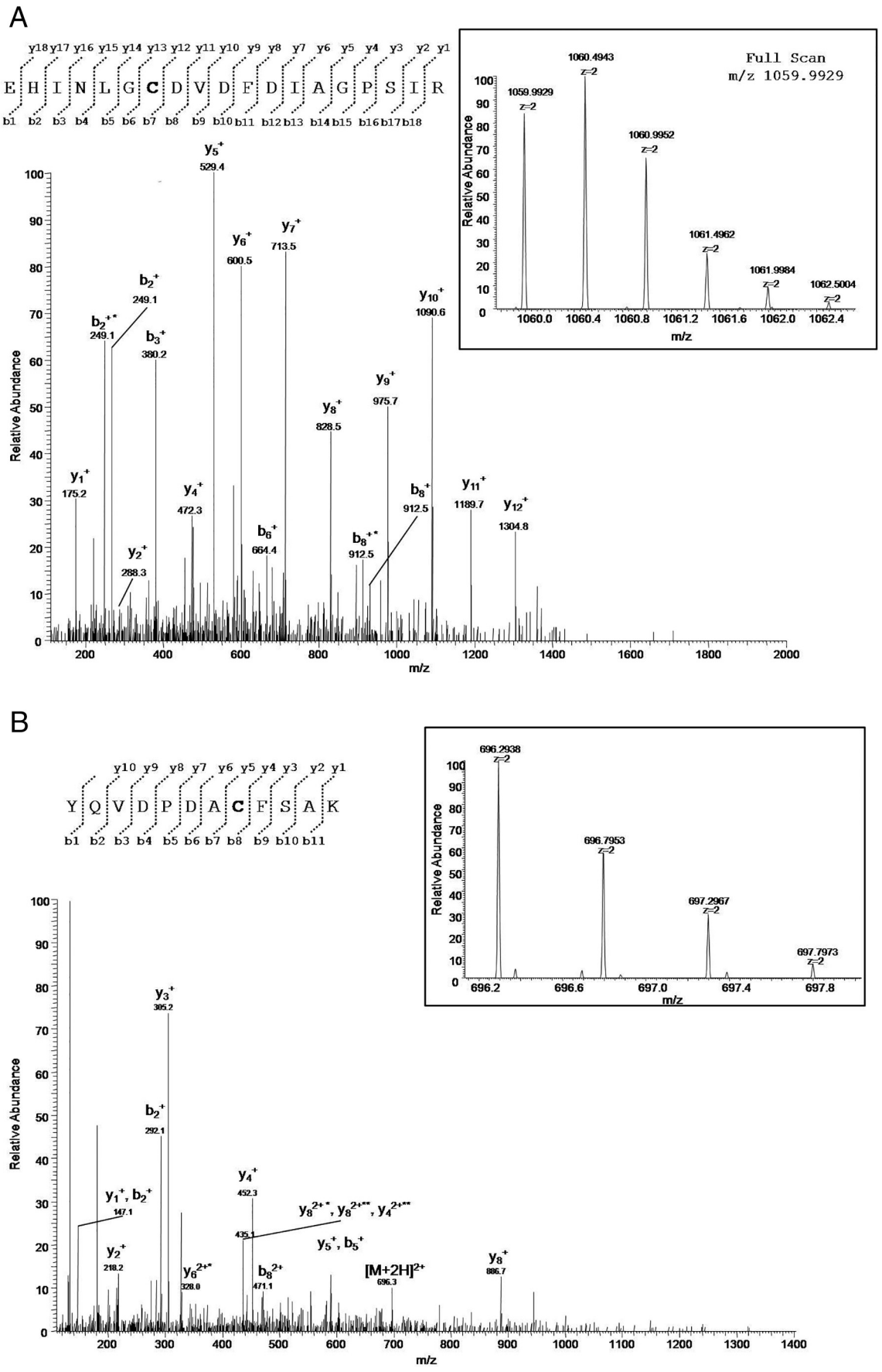

(caption on next page)

Fig. 2. Top: MS/MS spectrum of the doubly charged molecular ion at *m/z* 1059.9929 (calculated 1059.9919) of the VDAC1 tryptic peptide from *Rattus norvegicus* containing cysteine residue 127 in the form of sulfonic acid. Bottom: MS/MS spectrum of the doubly charged molecular ion at *m/z* 696.2938 (calculated 696.2938) of the VDAC1 tryptic peptide from *Rattus norvegicus* containing cysteine residue 232 in the form of sulfonic acid. The insets show the full scan mass spectrum of molecular ions. Fragment ions originated from the neutral loss of H_2O are indicated by an asterisk. Fragment ions originated from the neutral loss of NH_3 are indicated by two asterisks.

matrix able to selectively allow the purification of integral membrane proteins. This was also proved true for VDACs [33, 34]. Consequently, the HTP eluate from Triton X-100 solubilized rat liver mitochondria has been the starting material for the preparations used in this work. The HTP eluate (or pass-through, since the analyzed proteins are only those not retained by the chromatography) results enriched in VDAC isoforms, but many other proteins are also present. The power of the deep Mass Spectrometric analysis reported us a list of other proteins, identified by the concordance between the peptide masses and the sequences in the databases (Table 6). We were interested to know whether other mitochondrial membrane proteins carried similar over-oxidations as those found in VDAC3 [32]. Although in some of the proteins reported in Table 6 (shown in bold) tryptic peptides containing cysteines residues were identified, no evidence of over-oxidized cysteines was found. This is a strong indication that the cysteine over-oxidation in the inter-membrane space is peculiar of VDACs. Instead, several of the proteins reported Table 6 present methionines in the oxidized form.

Among the other proteins found in the HTP pass-through, and not being transmembrane proteins, only the mitochondrial matrix protein thiosulfate sulfur-transferase (UniProtKB - P24329), the mitochondrial import factor for the cytosolic 5S rRNA, was reported to be oxidized from our analysis, outlining how rare and peculiar is this modification.

4. Discussion

Using the same techniques that allowed the deep characterization of human and rat VDAC3 [32], we succeeded in obtaining a good sequence coverage of VDAC1 and VDAC2 from rat liver mitochondria, together with the accurate determination of the oxidative states of their cysteine and methionine residues. The association of the "in-solution" digestion of the eluates obtained from hydroxyapatite chromatography with the high-resolution mass spectrometry has indeed permitted to overcome the remarkable difficulties associated with the analysis of membrane proteins. In particular, it is worth to note that the digestion in solution of the HTP eluate allowed bypassing the SDS-electrophoresis step with its potential dangers of unwanted oxidations. Unfortunately, even though the techniques applied are the most updated available, it is striking that a short amino acid stretch in the sequences of both VDAC2 and VDAC3 could not be identified, leaving a small leak in the sequence coverage of the two proteins (Fig. 5). Interestingly these two short stretches do contain a cysteine and are located in a very close position with respect to the whole sequences. Although it is possible that peptides present in the digested mixture may remain undetected in the mass spectrometric analysis, it is tempting to speculate that parts of sequences not matched by the mass spectral data hide sequence modifications, presently unknown but possibly of structural and functional importance.

4.1. VDAC1 and VDAC2 show evidence of oxidized sulfur-containing amino acids

A particularly intriguing result was the identification, also in VDAC isoforms 1 and 2, of oxidized methionines and of cysteine residues over-oxidized up to sulfonic acid, an irreversible state, at least in the cell, of the sulfur-containing amino acid. These modifications, affecting cysteines 127 and 232 in rVDAC1, and 48, 77, 104, 211, and 228 in rVDAC2, respectively, are however, present in relatively smaller amount than in rVDAC3, previously characterized [32]. There are interesting differences among the cysteine oxidation patterns affecting the VDAC isoforms.

In the case of VDAC1 the only two cysteine residues in the sequences are not either close one another nor in a highly hydrophilic environment (see the 3D structure of the protein in Fig. 6). However, in the physiological state, a consistent amount of cysteines in VDAC1 is present in the reduced form or can be involved in disulfide bridges formation, which, if present, must be necessarily intermolecular in nature, owing to the position of the two cysteines in the protein. VDAC1 sulfur residues do not play any special function in the protein pore-forming activity.

VDAC2 is particularly rich of cysteines. In the rat there is the highest number of cysteines, 11 against 9 in human and mouse. In the critical N-terminal sequence, or very close to it, there is an abundance of 4 cysteines very much clustered. It is very indicative that these cysteines, in our analysis, did not show any presence of oxidization, i.e. they were found as carboxymethylated residues: in chemical terms this means that these cysteines are in a reversible oxidation state, i.e. they can oscillate between a reduced and a mild oxidized state, like in the case of disulfide bridge formation. In the remaining sequence four cysteine containing peptides were detected and they were found both over-oxidized and reduced. A rough estimation of the ratio between the two peptides was attempted, with the aim to get at least a broad indication of the amount of cysteines found in any oxidized or reduced state. From this survey (see Table 2) Cys 48 and Cys 77 were present in an approximately 1:10 ratio oxidized/reduced, while Cys 104 and Cys 211/228, both on the same peptide, had a rough ratio of 1:100 oxidized/reduced, i.e. the reduced state is more an exception than a rule. Cys 134 and Cys 139 are on a sequence stretch that was not detected, and it thus presently impossible to state their oxidation state (discussed above).

In front of these results, in rat VDAC3 we found that four cysteines

Fig. 3. Sequence coverage map of rVDAC2 obtained by enzymatic digestions. Solid lines indicate the coverage obtained with tryptic peptides; dotted lines the coverage obtained with chymotryptic peptides. The sequence stretch not covered by unique peptides is reported in bold. The carboxyamidomethylated cysteine residues are highlighted in gray; the oxidized cysteine residues are highlighted in yellow and the oxidized methionine residues are highlighted in green. The N-terminal acetylated alanine is shown in red.

Table 2
Comparison of the absolute intensities of molecular ions of selected sulfur containing tryptic peptides found in the analysis of rVDAC2 reduced with DTT, carboxyamidomethylated and digested in-solution. The ratio reported was determined from a single experiment.

Peptide	Position in the sequence	Measured monoisotopic *m/z*	Absolute intensity	Ratio Ox/Red
TKS**C**SGVEFSTSGSSNTDTGK	45–65	1064.4547 (+2)	$5.01{\cdot}10^4$	0.08
TKS***C***SGVEFSTSGSSNTDTGK		712.9837 (+3)	$6.03{\cdot}10^5$	
S**C**SGVEFSTSGSSNTDTGK	47–65	949.8823 (+2)	$1.09{\cdot}10^5$	0.41
S***C***SGVEFSTSGSSNTDTGK		954.4005 (+2)	$2.67{\cdot}10^5$	
YKW**C**EYGLTFTEK	74–86	858.3899 (+2)	$7.98{\cdot}10^4$	0.75
YKW***C***EYGLTFTEK		862.9038 (+2)	$1.06{\cdot}10^5$	
W**C**EYGLTFTEK	76–86	712.8052 (+2)	$1.22{\cdot}10^5$	0.030
W***C***EYGLTFTEK		717.3243 (+2)	$4.05{\cdot}10^6$	
WNTDNTLGTEIAIEDQI**C**QGLK	87–108	1255.5902 (+2)	$9.98{\cdot}10^4$	0.007
WNTDNTLGTEIAIEDQI***C***QGLK		1260.1088 (+2)	$1.36{\cdot}10^7$	
V**C**EDFDTSVNLAWTSGTN**C**TR	210–230	1207.9841 (+2)	$3.16{\cdot}10^4$	0.008
V***C***EDFDTSVNLAWTSGTN***C***TR		1217.0264 (+2)	$3.90{\cdot}10^6$	

C: cysteine carboxyamidomethylated; **C**: cysteine oxidized to sulfonic acid.

upon six detected (Cys 36, 65, 165, and 229) are oxidized to sulfonic acid in a considerable amount [32] and Cys 2 and Cys 8 were not heavily oxidized, showing instead carboxyamidation and thus the possibility of a reduced and mildly oxidizable state as a disulfide bridge [15]. Cys 122 could not be detected because the corresponding peptide was not identified.

4.2. In mitochondria, cysteine over-oxidation is a specific feature of VDACs

The observation that over-oxidation, mainly in VDAC2 and VDAC3, only affects certain cysteines, ensures the absence of artifacts. Oxidation of thiols to sulfonic acid is not attributable to a simple oxidation by air, but, chemically, arises from exposure to strong oxidizing agents such as halogens, hydrogen peroxide, and nitric acid [37]. The presence of oxidative modifications in VDACs could be explained by their localization within the cell, since they are exposed to the intermembrane space (IMS) [15], a cellular compartment where oxidative protein folding occurs [38–40]. Anyhow, despite the existence of a dedicated machinery for the introduction of disulfide bonds, many proteins and protein domains of the IMS contain reduced cysteine residues, probably due to special reductases (i.e. the thioredoxin and the glutaredoxin systems [41–43]). This would primarily explain the carboxyamidomethylated cysteines in VDAC2 and VDAC3 N-terminal regions, likely involved in disulfide bridge formation. What is surprising is the fact that only another mitochondrial protein, found in the HTP eluate, has been identified as sulfonated. It is the mitochondrial matrix protein thiosulfate sulfur-transferase (UniProtKB - P24329) that acts as a mitochondrial import factor for the cytosolic 5S rRNA, involved in the

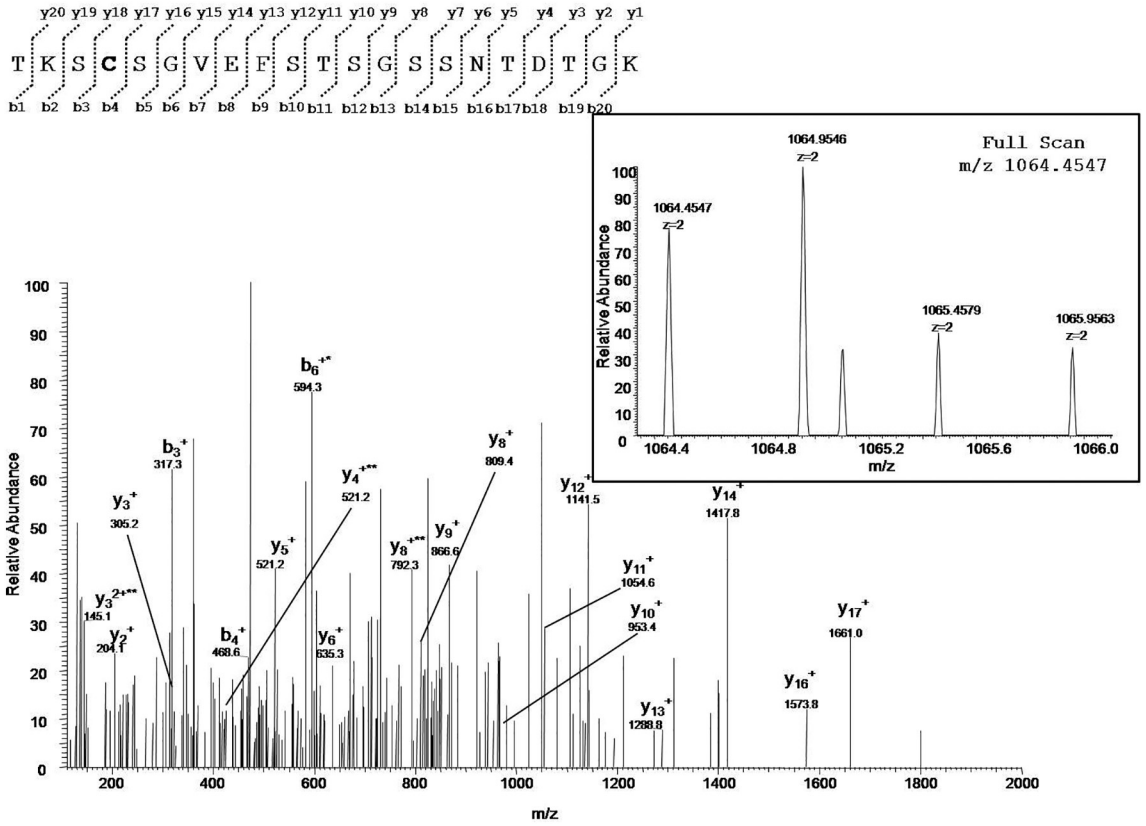

Fig. 4. MS/MS spectrum of the doubly charged molecular ion at *m/z* 1064.4547 (calculated 1064.4530) of the VDAC2 tryptic peptide from *Rattus norvegicus* containing cysteine residue 48 in the form of sulfonic acid. The inset shows the full scan mass spectrum of molecular ion. Fragment ions originated from the neutral loss of H_2O are indicated by an asterisk. Fragment ions originated from the neutral loss of NH_3 are indicated by two asterisks.

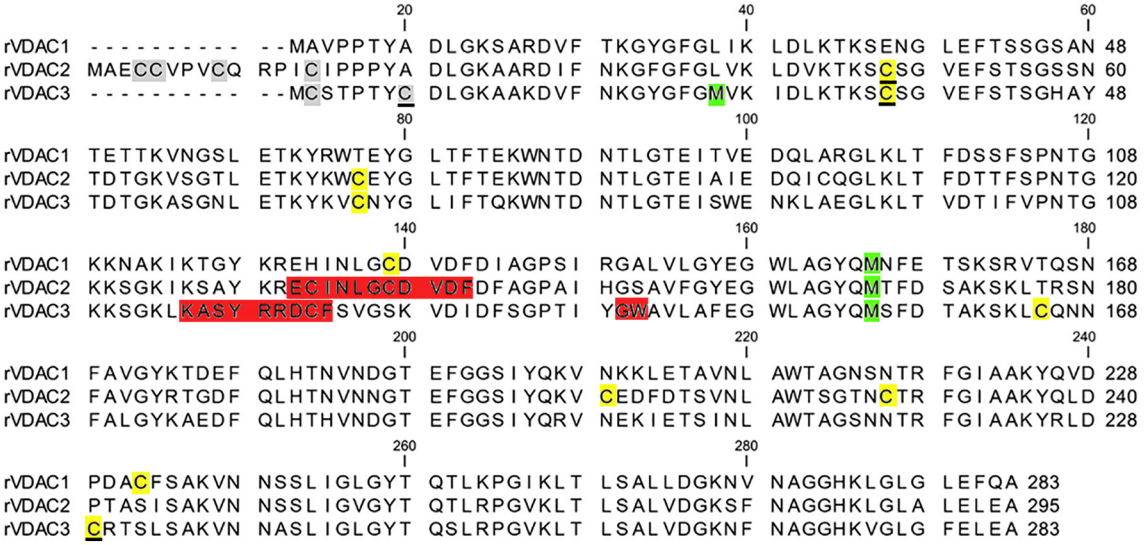

Fig. 5. Multi-alignment of rat VDAC proteins. The cysteine residues identified as carboxamidomethylated are highlighted in gray; the cysteine residues found over-oxidized to sulfonic acid in yellow. In green the methionine residues identified as oxidized; solid lines indicate cysteines identified as succinated. In red the sequences not covered by the mass spectrometric analysis.

Table 3
Comparison of the absolute intensities of molecular ions of a selected sulfur containing chymotryptic peptide found in the analysis of rVDAC2 reduced with DTT, carboxyamidomethylated and digested in-solution.

Peptide	Position in the sequence	Measured monoisotopic *m/z*	Absolute intensity	Ratio Ox/Red
QM**M**TFDSAKSKL	166–176	627.8057 (+2)	$7.91 \cdot 10^4$	3.2
QMTFDSAKSKL		619.8083 (+2)	$2.46 \cdot 10^4$	

M: methionine sulfoxide; **Q**: pyroglutamic acid form.

Table 4
Comparison of the absolute intensities of molecular ions of succinated peptides found in the analysis of rVDAC2 reduced with DTT, carboxyamidomethylated and digested in-solution.

Peptide	Position in the sequence	Measured monoisotopic *m/z*	Absolute intensity	Ratio Succinat/ Norm
TKS**C**SGVEFSTSGSSNTDTGK	45–65	732.6460 (+3)	$2.38 \cdot 10^4$	0.039
TKSCSGVEFSTSGSSNTDTGK		712.9837 (+3)	$6.03 \cdot 10^5$	

C: cysteine succinated.

formation of iron-sulfur complexes, cyanide detoxification or modification of sulfur-containing enzyme and possess a weak mercaptopyruvate sulfurtransferase (MST) activity. This finding defines the sulfonation of cysteine residues as a non-random event that affects specific components and not the entire universe of IMS-exposed mitochondrial proteins. Beside reports that claim the negative effects of such over-oxidations (i.e. the sulfonic acid modification of mammalian Cu, Zn-SOD has been speculated to play an important role in diseases like familial amyotrophic lateral sclerosis [44]), others seem to say otherwise. Lim, J. et al. have indeed shown that sulfonation of a specific residue of Peroxiredoxin activates a "super-chaperone" activity that may be induced during oxidative stress [45].

Moreover, Poderoso and coworkers have demonstrated that the redox state modulates the mitochondrial interaction of MAPKs to MAPKKs by oxidation of conserved cysteine domains of MAPKs to sulfinic and sulfonic acids [46]. Is it therefore possible that the oxidative modification of cysteine residues is the basis of a fine regulation of VDAC pore-forming activity? Considering the different Cys-oxidized-to-sulfonic-acid/Cys-carboxyamidomethylated ratios of the three isoforms, it is tempting to speculate that the redox state "modulates" the specific activity of each isoform according to the cellular needs. In this regard, we have previously demonstrated that the removal of selected cysteine residues in VDAC3 completely overturned channel activity, providing electrophysiological features similar to those of VDAC1 [15]. Likewise, Sodeoka and co-workers have reported that VDAC3 gating is activated by suppression of specific disulfide bonds within the pore [47].

4.3. The number of cysteine residues in VDAC isoforms increases during evolution: a possible explanation

The number of cysteine residues in VDAC raises from the unicellular eukaryotes (*S. cerevisiae* VDAC isoforms 1 and 2 have only two such

Table 5
Comparison of the absolute intensities of molecular ions of succinated peptides found in the analysis of rVDAC3 reduced with DTT, carboxyamidomethylated and digested in-solution.

Peptide	Position in the sequence	Measured monoisotopic *m/z*	Absolute intensity	Ratio succinat/norm
*C*STPTY**C**DLGK	2–12	701.7790 (2+)	$4.76 \cdot 10^5$	0.29
*C*STPTY***C***DLGK		672.2840 (2+)	$1.63 \cdot 10^6$	
TKS**C**SGVEFSTSGHAYTDTGK	33–53	760.3315 (3+)	$8.09 \cdot 10^4$	0.049
TKS***C***SGVEFSTSGHAYTDTGK		740.6678 (3+)	$1.65 \cdot 10^6$	
YRLD**C**R	225–230	417.2109 (2+)	$6.59 \cdot 10^4$	0.049
YRLD***C***R		441.7159 (2+)	$1.34 \cdot 10^6$	

* C: N-terminal acetylated; ***C***: cysteine carboxyamidomethylated; **C**: cysteine succinated.

Table 6
List of the mitochondrial membrane proteins present in the hydroxyapatite (HTP) eluate of Triton X-100 lysate that were identified by UHPLC/ESI-MS/MS. In the table the full name, the percentage of sequence coverage, the number of isoforms identified for each protein, the number of unique peptides, the total number of peptides, the molecular weight in KDa and the calculated isoelectric point are reported. Proteins identified by peptides containing cysteines are reported in bold.

Accession number	Description	Coverage	Proteins	Unique peptides	Peptides	MW [kDa]	Calc. pI
Q9Z2L0	Voltage-dependent anion-selective channel protein 1	95.41	1	32	33	30.7	8.54
P81155	Voltage-dependent anion-selective channel protein 2	64.41	1	14	17	31.7	7.49
P35171	Cytochrome c oxidase subunit 7A2	62.65	1	4	4	9.3	10.27
P62078	**Mitochondrial import inner membrane translocase subunit Tim8 B**	50.60	1	4	4	9.3	5.12
Q9R1Z0	Voltage-dependent anion-selective channel protein 3	45.23	1	8	10	30.8	8.70
Q9JJW3	Up-regulated during skeletal muscle growth protein 5	44.83	1	3	3	6.4	9.83
P26772	10 kDa heat shock protein	43.14	1	4	4	10,9	8,92
P11951	Cytochrome c oxidase subunit 6C-2	36.84	1	3	3	8.4	10.07
P00173	Cytochrome b5	31.34	1	3	3	15.3	4.98
Q9WVJ4	Synaptojanin-2-binding protein	26.90	1	4	4	15.8	6.80
P62898	Cytochrome c	22.86	1	3	3	11.6	9.58
Q9WVA1	**Mitochondrial import inner membrane translocase subunit Tim8 A**	22.68	1	2	2	11.0	5.16
P15999	ATP synthase subunit alpha	22.42	1	9	9	59.7	9.19
P13437	**3-ketoacyl-CoA thiolase**	20.15	1	4	4	41.8	7.94
P08011	**Microsomal glutathione S-transferase 1**	18.71	1	3	3	17.5	9.61
P35434	ATP synthase subunit delta	17.26	1	3	3	17.6	5.24
O88498	Bcl-2-like protein 11	12.76	1	2	2	22.0	6.54
P10719	ATP synthase subunit beta	10.78	1	4	4	56.3	5.34
P63039	60 kDa heat shock protein	8.73	1	4	4	60.9	6.18
Q66H15	Regulator of microtubule dynamics protein 3	7.86	1	3	3	52.3	5.02
P97521	Mitochondrial carnitine/acylcarnitine carrier protein	6.31	1	2	2	33.1	9.48
Q09073	ADP/ATP translocase 2	5.70	1	2	2	32.9	9.73
P22791	Hydroxymethylglutaryl-CoA synthase	5.31	1	3	3	56.9	8.68
Q5BJQ0	Atypical kinase ADCK3	4.31	1	2	2	72.2	6.46
P07756	Carbamoyl-phosphate synthase [ammonia]	3.53	1	4	4	164.5	6.77
Q64428	Trifunctional enzyme subunit alpha	3.28	1	2	2	82.6	9.06

residues) through less evolved animals (zebrafish has only one cysteine in the sequence of VDAC2) to mammalians, where there is the largest number of cysteines.

The functional relevance of cysteine oxidation remains untested in all but a few case: as with other posttranslational modifications, just because a cysteine is oxidized doesn't necessarily mean it plays a functional role. Sulfonic acid (RSO_3H) definitely represents a special issue. Due to resonance in the conjugate base, it can stabilize its negative charge and is comparable in strength to sulfuric acid. There are no known enzymes that can reverse this form back to any of the

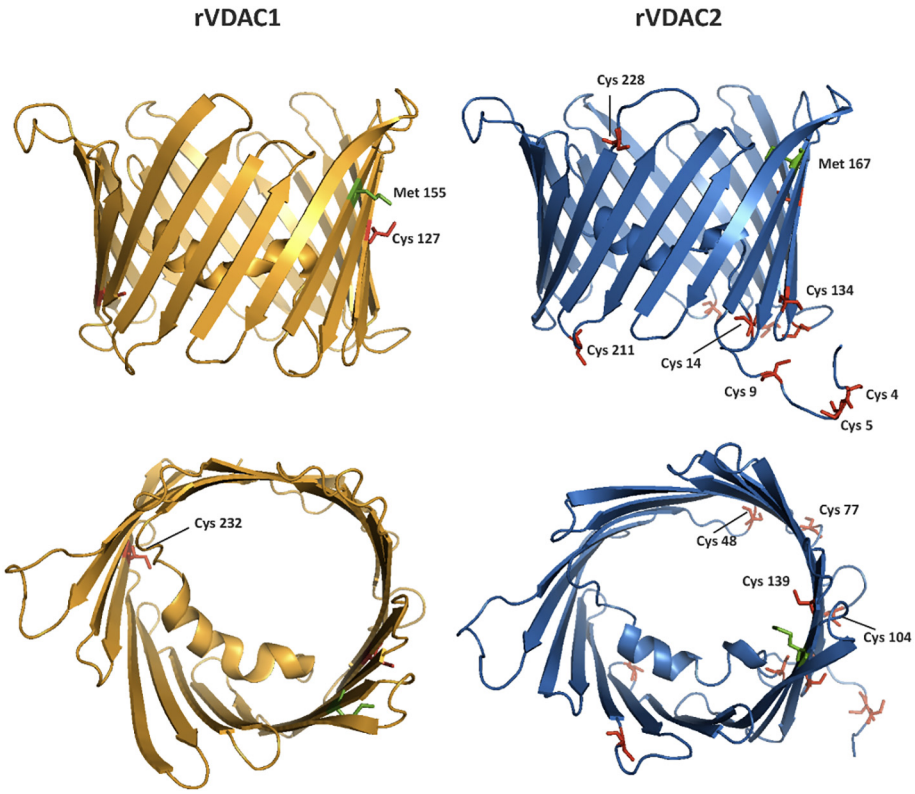

Fig. 6. Side and top views of rat VDAC1 and rat VDAC2 where the cysteine positions have been indicated. The structures are predicted by homology modelling, using mVDAC1 structure (pdb: 3EMN) as a template.

previous sulfur oxidative states (sulfenic and sulfinic forms) and it is suggested to play a role in either inhibiting proteins or targeting them for degradation [48]. In particular, the sulfonic acid group would act as a marker for ubiquitin-dependent protein degradation when formed on an N-terminal cysteine residue, such as in GTPase-activating proteins (the so-called "N-end rule pathway") [49]. In light of this, it is important to point out that in VDAC3, the N-terminal cysteine residue Cys 2 has always been found reduced, together with the nearby Cys 8 [32]. The same with regard to the N-terminal cysteines of the isoform 2 (residues Cys 4, 5, 9 and 14), always identified in the carboxyamidomethylated form. The over-oxidation to sulfonic acid observed, to varying degrees, for all the remaining residues of VDAC2 and VDAC3 and for the Cys 127 and 232 of VDAC1, should therefore assume a totally different meaning and have a presumable regulatory function.

4.4. Cysteine succination in VDAC

In this work it is also reported the identification of succinated cysteines in VDAC2 and VDAC3, but not in VDAC1. Succination is an irreversible post-translational modification that occurs when fumarate reacts with cysteine residues to generate S-(2-succino)-cysteine (2SC). Increased protein succination arises from elevated fumarate concentrations as a result of Krebs cycle inhibition, as observed in some mitochondrial diseases [50], cancer (with fumarate hydratase (FH)-deficiency) [51] and diabetes [52]. Interestingly, in the brainstem of a mouse model of Leigh syndrome, MS/MS analysis identified VDAC1 and VDAC2 as specific targets of succination: in particular, Cys77 and Cys48 were identified as endogenous sites of succination in VDAC2. Authors speculated that cysteine succination of VDAC decreases ATP synthesis in mitochondria, further worsening the already compromised mitochondrial function [50].

5. Conclusions

Our results demonstrate that the mitochondrial rVDAC1 and rVDAC2, in physiological state, contain methionines oxidized to methionine sulfoxide. Furthermore, cysteines 127 and 232 in rVDAC1, and 48, 77, 104, 211, and 228 in rVDAC2, respectively, are oxidized to sulfonic acid in relatively small amount respect to rVDAC3. The peculiar behavior of Met and Cys residues of VDACs may be related with the location of this proteins in a strongly oxidizing environment and may be connected with the regulation of the activity of these trans-membrane pore proteins. The structural features elucidated by the present work may be helpful for a better understanding of the functional role of VDACs 1 and 2.

Authors contributions

RS and MGGP produced the MS analysis; SR, MGGP, AM the biochemical experiments; VC analyzed the selenocysteine occurrence; VDP and SF designed the work and wrote the paper.

Conflict of interest

The authors declare that they have no conflicts of interest with the contents of this article.

Transparency document

The Transparency document associated with this article can be found, in the online version.

Acknowledgements

This work was supported by the Italian Ministero dell'Istruzione, dell'Università e della Ricerca, MIUR, (PRIN project 2015795S5W_005), by the FIR-UNICT 350 CD1 project 2017 to VDP and by a grant from PO FERS 2007/13 4.1.2.A, project "Piattaforma regionale di ricerca traslazionale per la salute". The authors gratefully acknowledge the Bionanotech Research and Innovation Tower (BRIT, PON project financed by the Italian Ministry for Education, University and Research, MIUR) for the availability of the Orbitrap Fusion mass spectrometer. A. Magrì has been recipient of an Umberto Veronesi fellowship. The authors thank dr. Stefano Conti Nibali for his valuable help in the analysis of structural features of VDAC isoforms.

Appendix A. Supplementary data

Supplementary data to this article can be found online at https://doi.org/10.1016/j.bbabio.2018.06.007.

References

[1] R. Benz, Permeation of hydrophilic solutes through mitochondrial outer membranes: review on mitochondrial porins, Biochim. Biophys. Acta 1197 (1994) 167–196.
[2] V. Shoshan-Barmatz, V. De Pinto, M. Zweckstetter, Z. Raviv, N. Keinan, N. Arbel, VDAC, a multi-functional mitochondrial protein regulating cell life and death, Mol. Asp. Med. 31 (2010) 227–285.
[3] V. Shoshan-Barmatz, M. Zakar, K. Rosenthal, S. Abu-Hamad, Key regions of VDAC1 functioning in apoptosis induction and regulation by hexokinase, Biochim. Biophys. Acta 1787 (2009) 421–430.
[4] E.N. Maldonado, K.L. Sheldon, D.N. DeHart, J. Patnaik, Y. Manevich, D.M. Townsend, S.M. Bezrukov, T.K. Rostovtseva, J.J. Lemasters, Voltage-dependent anion channels modulate mitochondrial metabolism in cancer cells: regulation by free tubulin and erastin, J. Biol. Chem. 288 (2013) 11920–11929.
[5] K.L. Sheldon, P.A. Gurnev, S.M. Bezrukov, D.L. Sackett, Tubulin tail sequences and post-translational modifications regulate closure of mitochondrial voltage-dependent anion channel (VDAC), J. Biol. Chem. 290 (2015) 26784–26789.
[6] C. Schwarzer, S. Barnikol-Watanabe, F.P. Thinnes, N. Hilschmann, Voltage-dependent anion-selective channel (VDAC) interacts with the dynein light chain Tctex1 and the heat-shock protein PBP74, Int. J. Biochem. Cell Biol. 34 (2002) 1059–1070.
[7] X. Xu, J.G. Forbes, M. Colombini, Actin modulates the gating of *Neurospora crassa* VDAC, J. Membr. Biol. 180 (2001) 73–81.
[8] T.K. Rostovtseva, P.A. Gurnev, O. Protchenko, D.P. Hoogerheide, T.L. Yap, C.C. Philpott, J.C. Lee, S.M. Bezrukov, α-Synuclein shows high affinity interaction with voltage-dependent anion channel, suggesting mechanisms of mitochondrial regulation and toxicity in Parkinson disease, J. Biol. Chem. 290 (2015) 18467–18477.
[9] A. Magrì, R. Belfiore, S. Reina, M.F. Tomasello, M.C. Di Rosa, F. Guarino, L. Leggio, V. De Pinto, A. Messina, Hexokinase I N-terminal based peptide prevents the VDAC1-SOD1 G93A interaction and re-establishes ALS cell viability, Sci. Rep. 6 (2016 Oct 10) 34802, , http://dx.doi.org/10.1038/srep34802.
[10] S. Shimizu, M. Narita, Y. Tsujimoto, Bcl-2 family proteins regulate the release of apoptogenic cytochrome c by the mitochondrial channel VDAC, Nature 399 (1999) 483–487.
[11] Y. Shi, J. Chen, C. Weng, R. Chen, Y. Zheng, Q. Chen, H. Tang, Identification of the protein-protein contact site and interaction mode of human VDAC1 EITH Bcl2 family proteins, Biochem. Biophys. Res. Commun. 305 (2003) 989–996.
[12] C.H. Wu, Y.W. Lin, T.F. Wu, J.L. Ko, P.H. Wang, Clinical implication of voltage-dependent anion channel 1 in uterine cervical cancer and its action on cervical cancer cells, Oncotarget 7 (2016) 4210–4225.
[13] E.H. Cheng, T.V. Sheiko, J.K. Fisher, W.J. Craigen, S.J. Korsmeyer, VDAC2 inhibits BAK activation and mitochondrial apoptosis, Science 301 (2003) 513–517.
[14] S. Reina, F. Guarino, A. Magrì, V. De Pinto, VDAC3 as a potential marker of mitochondrial status is involved in cancer and pathology, Front. Oncol. 6 (2016) 264.
[15] S. Reina, V. Checchetto, R. Saletti, A. Gupta, D. Chaturvedi, C. Guardiani, F. Guarino, M.A. Scorciapino, A. Magrì, S. Foti, M. Ceccarelli, A.A. Messina, R. Mahalakshmi, I. Szabo, V. De Pinto, VDAC3 as a sensor of oxidative state of the intermembrane space of mitochondria: the putative role of cysteine residue modifications, Oncotarget 7 (2016) 2249–2268.
[16] S. Hiller, R.G. Garces, T.J. Malia, V.Y. Orekhov, M. Colombini, G. Wagner, Solution structure of the integral human membrane protein VDAC-1 in detergent micelles, Science 321 (2008) 1206–1210.
[17] M. Bayrhuber, T. Meins, M. Habeck, S. Becker, K. Giller, S. Villinger, C. Vonrhein, C. Griesinger, M. Zweckstetter, K. Zeth, Structure of the human voltage-dependent anion channel, Proc. Natl. Acad. Sci. U. S. A. 105 (2008) 15370–15375.
[18] R. Ujwal, D. Cascio, J.P. Colletierc, S. Fahama, J. Zhanga, L. Toro, P. Ping, J. Abramson, The crystal structure of mouse VDAC1 at 2.3 A resolution reveals mechanistic insights into metabolite gating, Proc. Natl. Acad. Sci. U. S. A. 105 (2008) 17742–17747.
[19] M.F. Tomasello, F. Guarino, S. Reina, A. Messina, V. De Pinto, The voltage-dependent anion selective channel 1 (VDAC1) topography in the mitochondrial outer membrane as detected in intact cell, PLoS One 8 (2013) e81522.
[20] J. Schredelseker, A. Paz, C.J. López, C. Altenbach, C.S. Leung, M.K. Drexler, J.N. Chen, W.L. Hubbell, J. Abramson, High resolution structure and double

electron-electron resonance of the zebrafish voltage-dependent anion channel 2 reveal an oligomeric population, J. Biol. Chem. 289 (2014) 12566–12577.
[21] C. Martel, Z. Wang, C. Brenner, VDAC phosphorylation, a lipid sensor influencing the cell fate, Mitochondrion 19 (2014) 69–77.
[22] Yu, H., Diao, H., Wang, C., Lin, Y., Yu, F., Lu, H., Xu, W., Li, Z., Shi, H., Zhao, S., Zhou, Y., Zhang, Y. Acetylproteomic analysis reveals functional implications of lysine acetylation in human spermatozoa (sperm). Mol. Cell. Proteomics, 2015, 14, 1009–23. 2015.
[23] M. Yang, A.K. Camara, B.T. Wakim, Y. Zhou, A.K. Gadicherla, W.M. Kwok, D.F. Stowe, Tyrosine nitration of voltage-dependent anion channels in cardiac ischemia-reperfusion: reduction by peroxynitrite scavenging, Biochim Biophys Acta 1817 (2012) 2049–2059.
[24] R. Gupta, Phosphorylation of rat brain purified mitochondrial voltage-dependent anion channel by c-Jun N-terminal kinase-3 modifies open-channel noise, Biochem. Biophys. Res. Commun. 490 (2017) 1221–1225.
[25] Y. Chen, W.J. Craigen, D.J. Riley, Nek1 regulates cell death and mitochondrial membrane permeability through phosphorylation of VDAC1, Cell Cycle 8 (2009) 257–267.
[26] S. Yuan, Y. Fu, X. Wang, H. Shi, Y. Huang, X. Song, L. Li, N. Song, Y. Luo, Voltage-dependent anion channel 1 is involved in endostatin-induced endothelial cell apoptosis, FASEB J. 22 (2008) 2809–2820.
[27] J. Kerner, K. Lee, B. Tandler, C.L. Hoppel, VDAC proteomics: post-translation modifications, Biochim Biophys Acta 1818 (2012) 1520–1525.
[28] C. Martel, M. Allouche, D.D. Esposti, E. Fanelli, C. Boursier, C. Henry, J. Chopineau, G. Calamita, G. Kroemer, A. Lemoine, C. Brenner, Glycogen synthase kinase 3-mediated voltage-dependent anion channel phosphorylation controls outer mitochondrial membrane permeability during lipid accumulation, Hepatology 57 (2013) 93–102.
[29] L. Lefièvre, Y. Chen, S.J. Conner, J.L. Scott, S.J. Publicover, W.C. Ford, C.L. Barratt, Human spermatozoa contain multiple targets for protein S-nitrosylation: an alternative mechanism of the modulation of sperm function by nitric oxide? Proteomics 7 (2007) 3066–3084.
[30] A.H. Chang, H. Sancheti, J. Garcia, N. Kaplowitz, E. Cadenas, D. Han, Respiratory substrates regulate S-nitrosylation of mitochondrial proteins through a thiol-dependent pathway, Chem. Res. Toxicol. 27 (2014) 794–804.
[31] M. Schieber, N.S. Chandel, ROS function in redox signaling and oxidative stress, Curr. Biol. 24 (2014) 453–462.
[32] R. Saletti, S. Reina, M.G. Pittalà, R. Belfiore, V. Cunsolo, A. Messina, V. De Pinto, S. Foti, High resolution mass spectrometry characterization of the oxidation pattern of methionine and cysteine residues in rat liver mitochondria voltage-dependent anion selective channel 3 (VDAC3), Biochim. Biophys. Acta 1859 (2017) 301–311.
[33] V. De Pinto, G. Prezioso, F. Palmieri, A simple and rapid method for the purification of the mitochondrial porin from mammalian tissues, Biochim. Biophys. Acta 905 (1987) 499–502.
[34] D. Ben-Hail, V. Shoshan-Barmatz, Purification of VDAC1 from rat liver mitochondria, Cold Spring Harb Protoc 2014 (2014) 94–99.
[35] A.M. Distler, J. Kerner, S.M. Peterman, C.L. Hoppel, A targeted proteomic approach for the analysis of rat liver mitochondrial outer membrane proteins with extensive sequence coverage, Anal. Biochem. 356 (2006) 18–29.
[36] Z.Q. Guan, N.A. Yates, R. Bakhtiar, Detection and characterization of methionine oxidation in peptides by collision-induced dissociation and electron capture dissociation, J. Am. Soc. Mass Spectrom. 14 (2003) 605–613.
[37] R.J. Cremlyn, An Introduction to Organosulfur Chemistry, John Wiley & Sons, Inc, 1996.
[38] B. Grumbt, V. Stroobant, N. Terziyska, L. Israel, K. Hell, Functional characterization of Mia40p, the central component of the disulfide relay system of the mitochondrial intermembrane space, J. Biol. Chem. 282 (2007) 37461–37470.
[39] L. Banci, I. Bertini, C. Cefaro, S. Ciofi-Baffoni, A. Gallo, M. Martinelli, D.P. Sideris, N. Katrakili, K. Tokatlidis, MIA40 is an oxidoreductase that catalyzes oxidative protein folding in mitochondria, Nat. Struct. Mol. Biol. 16 (2009) 198–206.
[40] A. Chatzi, P. Manganas, K. Tokatlidis, Oxidative folding in the mitochondrial intermembrane space: A regulated process important for cell physiology and disease, Biochim. Biophys. Acta 2016 (1863) 1298–1306.
[41] F.N. Vögtle, J.M. Burkhart, S. Rao, C. Gerbeth, J. Hinrichs, J.C. Martinou, A. Chacinska, A. Sickmann, R.P. Zahedi, C. Meisinger, Intermembrane space proteome of yeast mitochondria, Mol. Cell. Proteomics 11 (2012) 1840–1852.
[42] K. Kojer, V. Peleh, G. Calabrese, J.M. Herrmann, J. Riemer, Kinetic control by limiting glutaredoxin amounts enables thiol oxidation in the reducing mitochondrial intermembrane space, Mol. Biol. Cell 26 (2015) 195–204.
[43] M. Cardenas-Rodriguez, K. Tokatlidis, Cytosolic redox components regulate protein homeostasis via additional localization in the mitochondrial intermembrane space, FEBS Lett. 591 (2017) 2661–2670.
[44] N. Fujiwara, M. Nakano, S. Kato, D. Yoshihara, T. Ookawara, H. Eguchi, N. Taniguchi, K. Suzuki, Oxidative modification to cysteine sulfonic acid of Cys111 in human copper-zinc superoxide dismutase, J. Biol. Chem. 282 (2007) 35933–35944.
[45] J.C. Lim, H.I. Choi, Y.S. Park, H.W. Nam, H.A. Woo, K.S. Kwon, Y.S. Kim, S.G. Rhee, K. Kim, H.Z. Chae, Irreversible oxidation of the active-site cysteine of peroxiredoxin to cysteine sulfonic acid for enhanced molecular chaperone activity, J. Biol. Chem. 283 (2008) 28873–28880.
[46] S. Galli, V.G. Antico Arciuch, C. Poderoso, D.P. Converso, Q. Zhou, E. Bal de Kier Joffé, E. Cadenas, J. Boczkowski, M.C. Carreras, J.J. Poderoso, Tumor cell phenotype is sustained by selective MAPK oxidation in mitochondria, PLoS One 3 (2008) e2379.
[47] M. Okazaki, K. Kurabayashi, M. Asanuma, Y. Saito, K. Dodo, M. Sodeoka, VDAC3 gating is activated by suppression of disulfide-bond formation between the N-terminal region and the bottom of the pore, Biochim. Biophys. Acta 1848 (2015) 3188–3196.
[48] K.G. Reddie, K.S. Carroll, Expanding the functional diversity of proteins through cysteine oxidation, Curr. Opin. Chem. Biol. 12 (2008) 746–754.
[49] T. Tasaki, Y.T. Kwon, The mammalian N-end rule pathway: new insights into its components and physiological roles, Trends Biochem. Sci. 32 (2007) 520–528.
[50] G.G. Piroli, A.M. Manuel, A.C. Clapper, M.D. Walla, J.E. Baatz, R.D. Palmiter, ... N. Frizzell, Succination is increased on select proteins in the brainstem of the NADH dehydrogenase (ubiquinone) Fe-S protein 4 (Ndufs4) knockout mouse, a model of Leigh syndrome, Mol. Cell. Proteomics 15 (2016) 445–461.
[51] P.J. Pollard, J.J. Briere, N.A. Alam, J. Barwell, E. Barclay, N.C. Wortham, T. Hunt, M. Mitchell, S. Olpin, S.J. Moat, I.P. Hargreaves, S.J. Heales, Y.L. Chung, J.R. Griffiths, A. Dalgleish, J.A. Mcgrath, M.J. Gleeson, S.V. Hodgson, R. Poulsom, P. Rustin, I.P.M. Tomlinson, Accumulation of Krebs cycle intermediates and over-expression of HIF1α in tumours which result from germline FH and SDH mutations, Hum. Mol. Genet. 14 (2005) 2231–2239.
[52] J.S. Isaacs, Y.J. Jung, D.R. Mole, S. Lee, C. Torres-Cabala, Y.L. Chung, M. Merino, J. Trepel, B. Zbar, J. Toro, P.J. Ratcliffe, W.M. Linehan, L. Neckers, HIF overexpression correlates with biallelic loss of fumarate hydratase in renal cancer: novel role of fumarate in regulation of HIF stability, Cancer Cell 8 (2005) 143–153.

Post-translational modifications of VDAC1 and VDAC2 cysteines from rat liver mitochondria.

Rosaria Saletti[a]*, Simona Reina[b,c]*, Maria G.G. Pittalà[c,d], Andrea Magrì[b,c,d], Vincenzo Cunsolo[a], Salvatore Foti[a#] and Vito De Pinto[c,d#]

[a]Department of Chemical Sciences, Organic Mass Spectrometry Laboratory, University of Catania, Viale A. Doria 6, 95125 Catania, Italy

[b]Department of Biological, Geological and Environmental Sciences, Section of Molecular Biology, University of Catania, Viale A. Doria 6, 95125 Catania, Italy

[c]National Institute for Biomembranes and Biosystems, Section of Catania, Viale A. Doria 6, 95125 Catania, Italy

[d]Department of Biomedicine and Biotechnology, Section of Biology and Genetics, Viale A. Doria 6, 95125 Catania, Italy

*These authors equally contributed to the article.

#Correspondence to:

Prof. Vito De Pinto, Department of Biomedicine and Biotechnology, Section of Biology and Genetics, University of Catania, Campus S. Sofia, Building 2, Viale A. Doria 6, 95125 Catania, Italy, Telephone: (+39)-095-7384244. E-mail: vdpbiofa@unict.it

Prof. Salvatore Foti, Department of Chemical Sciences, Organic Mass Spectrometry Laboratory, University of Catania, Campus S. Sofia, Building 1, Viale A. Doria 6, 95125 Catania, Italy, Telephone: (+39)-095-7385026. E-mail: sfoti@unict.it

SUPPLEMENTARY MATERIAL

Supplementary Table 1. Tryptic peptides found in rVDAC1 after DTT reduction and carboxyamidomethylation.

In the Table the respective retention time, experimentally measured and calculated monoisotopic m/z of the molecular ions, the position in the sequence and the peptide sequence of fragments present in the tryptic digest of reduced and carboxyamidomethylated rVDAC1 are reported. All sequences were confirmed by MS/MS. These sequences were used to build the sequence coverage scheme.

Frag. n.	Rt (min)	Monoisotopic m/z		Position in the sequence	Peptide sequence
		Measured	Calculated		
1	44.09	566.3058(+2)	566.3059	2-12	AVPPTYADLGK
2	59.60	1173.6154(+1)	1173.6150	2-12	*AVPPTYADLGK
3	50.56	744.3970(+2)	744.3963	2-15	*AVPPTYADLGKSAR
4	29.00	462.2513 (+2)	462.2509	13-20	SARDVFTK
5	80.89	586.9892(+3)	586.9894	13-28	SARDVFTKGYGFGLIK
6	62.64	482.2658 (+3)	482.2660	16-28	DVFTKGYGFGLIK
7	80.80	638.69708 (+3)	638.6960	16-32	DVFTKGYGFGLIKLDLK
8	56.57	427.7421 (+2)	427.7422	21-28	GYGFGLIK
9	73.14	662.3879 (+2)	662.3872	21-32	GYGFGLIKLDLK
10	36.29	730.3462(+3)	730.3450	33-53	TKSENGLEFTSSGSANTETTK
11	42.57	980.4434(+2)	980.4425	35-53	SENGLEFTSSGSANTETTK
12	43.84	930.1097 (+3)	930.1088	35-61	SENGLEFTSSGSANTETTKVNGSLETK
13	29.42	583.8123 (+2)	583.8118	54-63	VNGSLETKYR
14	67.99	565.2792 (+3)	565.2789	62-74	YRWTEYGLTFTEK
15	73.58	687.8337 (+2)	687.8324	64-74	WTEYGLTFTEK
16	60.13	1088.5308 (+2)	1088.5295	75-93	WNTDNTLGTEITVEDQLAR
17	59.02	849.9390 (+2)	849.9385	94-109	GLKLTFDSSFSPNTGK
18	60.44	913.9852 (+2)	913.9860	94-110	GLKLTFDSSFSPNTGKK
19	56.48	535.7902(+4)	535.7908	94-113	GLKLTFDSSFSPNTGKKNAK
20	51.20	700.8391 (+2)	700.8383	97-109	LTFDSSFSPNTGK
21	50.51	764.8865(+2)	764.8857	97-110	LTFDSSFSPNTGKK
22	21.68	433.2663 (+2)	433.2663	114-120	IKTGYKR
23	74.61	762.0449 (+3)	762.0428	120-139	REHINLG***C***DVDFDIAGPSIR
24	61.54	710.0099 (+3)	710.0091	121-139	EHINLG***C***DVDFDIAGPSIR
25	63.65	1055.5061(+2)	1055.5050	121-139	**E**HINLG***C***DVDFDIAGPSIR
26	68.53	1217.5914 (+2)	1217.5910	140-161	GALVLGYEGWLAGYQMNFETSK
27	40.15	486.2560 (+3)	486.2563	162-174	SRVTQSNFAVGYK
28	45.89	607.3146 (+2)	607.3142	164-174	VTQSNFAVGYK

29	59.02	867.4017(+3)	867.4015	175-197	TDEFQLHTNVNDGTEFGGSIYQK
30	61.73	763.0784 (+3)	763.0766	198-218	VNKKLETAVNLAWTAGNSNTR
31	58.10	973.5090 (+2)	973.5081	201-218	KLETAVNLAWTAGNSNTR
32	56.97	909.4614 (+2)	909.4607	202-218	LETAVNLAWTAGNSNTR
33	50.41	663.3255(+3)	663.3243	219-236	FGIAAKYQVDPDA***C***FSAK
34	45.58	700.8118(+2)	700.8112	225-236	YQVDPDA***C***FSAK
35	56.43	701.7319 (+3)	701.7318	237-256	VNNSSLIGLGYTQTLKPGIK
36	83.94	1038.9320 (+3)	1038.9306	237-266	VNNSSLIGLGYTQTLKPGIKLTLSALLDGK
37	62.22	1030.6118 (+1)	1030.6143	257-266	LTLSALLDGK
38	76.47	603.3404(+3)	603.3390	257-274	LTLSALLDGKNVNAGGHK
39	67.38	474.2636 (+2)	474.2635	275-283	LGLGLEFQA

*A: N-terminal acetylated; ***C***: cysteine carboxyamidomethylated; **E**: pyroglutamic acid form.

Supplementary Table 2. Sulfur-modified peptides found in rVDAC1 tryptic digest after DTT reduction and carboxyamidomethylation.

In the Table the respective retention time, experimentally measured and calculated monoisotopic m/z of the molecular ions, the position in the sequence and the peptide sequence of modified fragments present in the tryptic digest of reduced and carboxyamidomethylated rVDAC1 are reported. All sequences were confirmed by MS/MS.

Frag. n.	Rt (min)	Monoisotopic m/z		Position in the sequence	Peptide sequence
		Measured	Calculated		
1	62.69	1059.9929 (+2)	1059.9919	121-139	EHINLG**C**DVDFDIAGPSIR
2	64.44	1050.9885 (+2)	1050.9866	121-139	**E**HINLG**C**DVDFDIAGPSIR
3	67.55	1225.5898 (+2)	1225.5888	140-161	GALVLGYEGWLAGYQ**M**NFETSK
4	51.04	696.2938 (+2)	696.2931	225-236	YQVDPDA**C**FSAK

M: methionine sulfoxide; **C**: cysteine oxidized to sulfonic acid;**E**: pyroglutamic acid form.

Supplementary Table 3. Tryptic peptides found in rVDAC2 after DTT reduction and carboxyamidomethylation.

In the Table the respective retention time, experimentally measured and calculated monoisotopic m/z of the molecular ions, the position in the sequence and the peptide sequence of fragments present in the tryptic digest of reduced and carboxyamidomethylated rVDAC2 are reported. All sequences were confirmed by MS/MS. These sequences were used to build the sequence coverage scheme.

Frag. n.	Rt (min)	Monoisotopic m/z		Position in the sequence	Peptide sequence
		Measured	Calculated		
1	60.55	914.7682 (+3)	914.7672	2-24	*AE***CC**VPV***C***QRPI***C**IPPPYADLGK
2	54.76	580.6587 (+3)	580.6579	25-40	AARDIFNKGFGFGLVK
3	56.87	549.5637 (+4)	549.5642	25-44	AARDIFNKGFGFGLVKLDVK

4	63.94	721.3965 (+2)	721.3955	28-40	DIFNKGFGFGLVK
5	58.01	412.7366 (+2)	412.7369	33-40	GFGFGLVK
6	31.92	712.9837 (+3)	712.9832	45-65	TKS***C***SGVEFSTSGSSNTDTGK
7	41.45	954.4005 (+2)	954.3998	47-65	S***C***SGVEFSTSGSSNTDTGK
8	53.29	908.4147 (+3)	908.4153	47-73	S***C***SGVEFSTSGSSNTDTGKVSGTLETK
9	59.58	862.9038 (+2)	862.9031	74-86	YKW***C***EYGLTFTEK
10	57.74	717.3243 (+2)	717.3239	76-86	W***C***EYGLTFTEK
11	65.97	1260.1088 (+2)	1260.1078	87-108	WNTDNTLGTEIAIEDQI***C***QGLK
12	52.91	714.8546 (+2)	714.8539	109-121	LTFDTTFSPNTGK
13	51.55	778.9023(+2)	778.9014	109-122	LTFDTTFSPNTGKK
14	18.81	433.2663(+2)	433.2663	126-132	IKSAYKR
15	40.82	457.2299 (+2)	457.2300	179-186	SNFAVGYR
16	52.74	843.0677 (+3)	843.0665	187-209	TGDFQLHTNVNNGTEFGGSIYQK
17	60.13	1217.0264 (+2)	1217.0259	210-230	V***C***EDFDTSVNLAWTSGTN***C***TR
18	57.18	627.6761 (+3)	627.6754	231-248	FGIAAKYQLDPTASISAK
19	44.34	647.3381 (+2)	647.3379	237-248	YQLDPTASISAK
20	48.52	1052.0803 (+2)	1052.0815	249-268	VNNSSLIGVGYTQTLRPGVK
21	76.79	1034.2502 (+3)	1034.2503	249-278	VNNSSLIGVGYTQTLRPGVKLTLSALVDGK
22	60.95	605.6650 (+3)	605.6635	269-286	LTLSALVDGKSFNAGGHK
23	68.22	928.5361 (+1)	928.5350	287-295	LGLALELEA

*A: N-terminal acetylated; ***C***: cysteine carboxyamidomethylated.

Supplementary Table 4. Sulfur-modified peptides found in rVDAC2 tryptic digest after DTT reduction and carboxyamidomethylation.

In the Table the respective retention time, experimentally measured and calculated monoisotopic m/z of the molecular ions, the position in the sequence and the peptide sequence of modified fragments present in the tryptic digest of reduced and carboxyamidomethylated rVDAC2 are reported.

Frag. n.	**Rt (min)**	**Monoisotopic m/z**		**Position in the sequence**	**Peptide sequence**
		Measured	**Calculated**		
1	35.33	1064.4547 (+2)	1064.4530	45-65	TKS**C**SGVEFSTSGSSNTDTGK
2	43.32	949.8823 (+2)	949.8817	47-65	S**C**SGVEFSTSGSSNTDTGK
3	49.46	858.3899 (+2)	858.3850	74-86	YKW**C**EYGLTFTEK
4	45.81	712.8066 (+2)	712.8058	76-86	W**C**EYGLTFTEK
5	67.29	1255.5902 (+2)	1255.5897	87-108	WNTDNTLGTEIAIEDQI**C**QGLK
6	40.18	1207.9841 (+2)	1207.9894	210-230	V**C**EDFDTSVNLAWTSGTN**C**TR

C: cysteine oxidized to sulfonic acid.

Supplementary Table 5. Chymotryptic peptides found in rVDAC2 after DTT reduction and carboxyamidomethylation.

In the Table the respective retention time, experimentally measured and calculated monoisotopic m/z of the molecular ions, the position in the sequence and the peptide sequence of fragments present in the chymotryptic digest of reduced and carboxyamidomethylated rVDAC3 are reported. All sequences were confirmed by MS/MS except that indicated by an asterisk. These sequences were used to build the sequence coverage scheme.

Frag. n.	Rt (min)	Monoisotopic m/z		Position in the sequence	Peptide sequence
		Measured	Calculated		
1	52.52	678.8276 (+2)	678.8274	42-53	DVKTKS***C***SGVEF
2	40.50	707.3385 (+3)	707.3378	54-74	STSGSSNTDTGKVSGTLETKY
3	65.09	602.2791 (+2)	602.2793	75-83	KW***C***EYGLTF
4	60.25	491.2556 (+2)	491.2562	80-87	GLTFTEKW
5	68.55	1103.0220 (+2)	1103.0212	88-107	NTDNTLGTEIAIEDQI***C***QGL
6	63.09	773.8755 (+2)	773.8751	94-107	GTEIAIEDQI***C***QGL
7	51.34	508.3131 (+1)	508.3135	108-111	KLTF
8	59.71	486.7556 (+2)	486.7560	108-115	KLTFDTTF
9	38.63	677.3549(+3)	677.3572	112-130	DTTFSPNTGKKSGKIKSAY
10	45.88	644.8198 (+2)	644.8197	144-156	DFAGPAIHGSAVF
11	66.06	1015.4531 (+1)	1015.4525	157-165	GYEGWLAGY[a]
12	48.26	682.3234 (+1)	682.3234	162-167	LAGYQM[b]
13	49.66	619.8083 (+2)	619.8084	166-176	**Q**MTFDSAKSKL
14	62.49	451.9089 (+3)	451.9094	170-181	DSAKSKLTRSNF
15	63.60	906.4189 (+2)	906.4177	208-222	QKV***C***EDFDTSVNLAW
16	68.49	897.9058 (+2)	897.9044	208-222	**Q**KV***C***EDFDTSVNLAW
17	65.41	946.0960 (+3)	946.0942	208-231	QKV***C***EDFDTSVNLAWTSGTN***C***TRF
18	29.15	522.2324 (+2)	522.2324	223-231	TSGTN***C***TRF
19	61.95	872.9595 (+2)	872.9580	238-254	QLDPTASISAKVNNSSL
20	60.89	745.3923 (+3)	745.3936	238-259	QLDPTASISAKVNNSSLIGVGY
21	68.38	739.7190 (+3)	739.7186	238-259	**Q**LDPTASISAKVNNSSLIGVGY
22	41.55	556.8433 (+2)	556.8434	260-269	TQTLRPGVKL
23	63.35	663.9092 (+2)	663.9094	260-271	TQTLRPGVKLTL
24	58.46	569.3121 (+2)	569.3117	270-280	TLSALVDGKSF
25	62.35	815.4523 (+1)	815.4514	288-295	GLALELEA

C: cysteine carboxyamidomethylated; **Q**: pyroglutamic acid form; [a]sequence shared by rVDAC1 and 2; [b]sequence shared by rVDAC1, 2 and 3.

Supplementary Table 6. **Sulfur-modified peptides found in rVDAC2 chymotryptic digest after DTT reduction and carboxyamidomethylation.**

In the Table the respective retention time, experimentally measured and calculated monoisotopic m/z of the molecular ions, the position in the sequence and the peptide sequences of modified fragments present in the chymotryptic digest of reduced and carboxyamidomethylated rVDAC2 are reported. These sequences were used to build the sequence coverage scheme.

Frag. n.	Rt (min)	Monoisotopic m/z		Position in the sequence	Peptide sequence
		Measured	Calculated		
1	37.15	698.3186 (+1)	698.3183	162-167	LAGYQ**M**[a]
2	41.64	627.8057 (+2)	627.8059	166-176	**Q****M**TFDSAKSKL

M: methionine sulfoxide; **Q**: pyroglutamic acid form; [a]sequence shared by rVDAC 1, 2 and 3.

Supplementary Table 7. Succinated peptides found in rVDAC2 tryptic digest after DTT reduction and carboxyamidomethylation.

In the Table the respective retention time, experimentally measured and calculated monoisotopic m/z of the molecular ions, the position in the sequence and the peptide sequence of modified fragments present in the tryptic digest of reduced and carboxyamidomethylated rVDAC2 are reported. All sequences were confirmed by MS/MS.

Frag. n.	Rt (min)	Monoisotopic m/z		Position in the sequence	Peptide sequence
		Measured	Calculated		
1	35.11	732.6460(+3)	732.6468	45-65	TKS**C**SGVEFSTSGSSNTDTGK

C: cysteine succinated.

Supplementary Table 8. Succinated peptides found in rVDAC3 tryptic digest after DTT reduction and carboxyamidomethylation.

In the Table the respective retention time, experimentally measured and calculated monoisotopic m/z of the molecular ions, the position in the sequence and the peptide sequence of modified fragments present in the tryptic digest of reduced and carboxyamidomethylated rVDAC3 are reported. All sequences were confirmed by MS/MS.

Frag. n.	Rt (min)	Monoisotopic m/z		Position in the sequence	Peptide sequence
		Measured	Calculated		
1	49.90	701.7790 (2+)	701.7790	2-12	*_C_STPTY**C**DLGK
2	33.01	760.3315 (3+)	760.3309	33-53	TKS**C**SGVEFSTSGHAYTDTGK
3	32.34	417.2109 (2+)	471.2112	225-230	YRLD**C**R

*C: N-terminal acetylated; ***C***: cysteine carboxyamidomethylated; **C**: cysteine succinated.

Supplementary Figure 1. MS/MS spectrum of the doubly charged molecular ion at m/z 1173.6154 (calculated 1173.6150) of the N-terminal acetylated tryptic peptide of VDAC1 from *Rattus norvegicus*. The inset shows the full scan mass spectrum of molecular ion. Fragment ions originated from the neutral loss of H_2O are indicated by an asterisk. Fragment ions originated from the neutral loss of NH_3 are indicated by two asterisks.

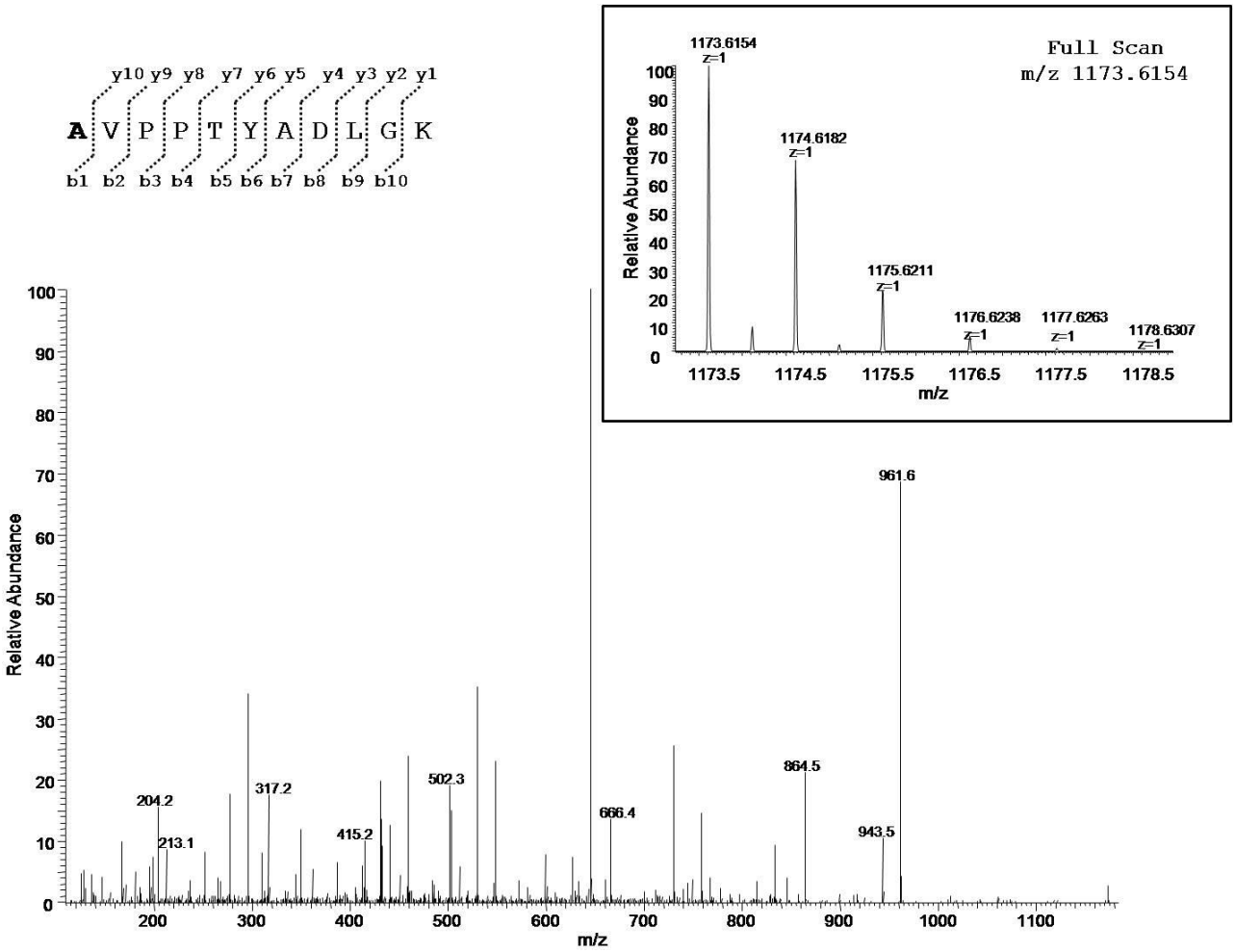

Supplementary Figure 2. MS/MS spectrum of the doubly charged molecular ion at m/z 1225.5898 (calculated 1225.5888) of the VDAC1 tryptic peptide from *Rattus norvegicus* containing methionine residue 155 in the oxidized form of methionine sulfoxide. The inset shows the full scan mass spectrum of molecular ion. Fragment ions originated from the neutral loss of NH_3 are indicated by two asterisks. Fragment ions originated from the neutral loss of methanesulfenic acid (CH_2SOH, 64 Da) are indicated by three asterisks.

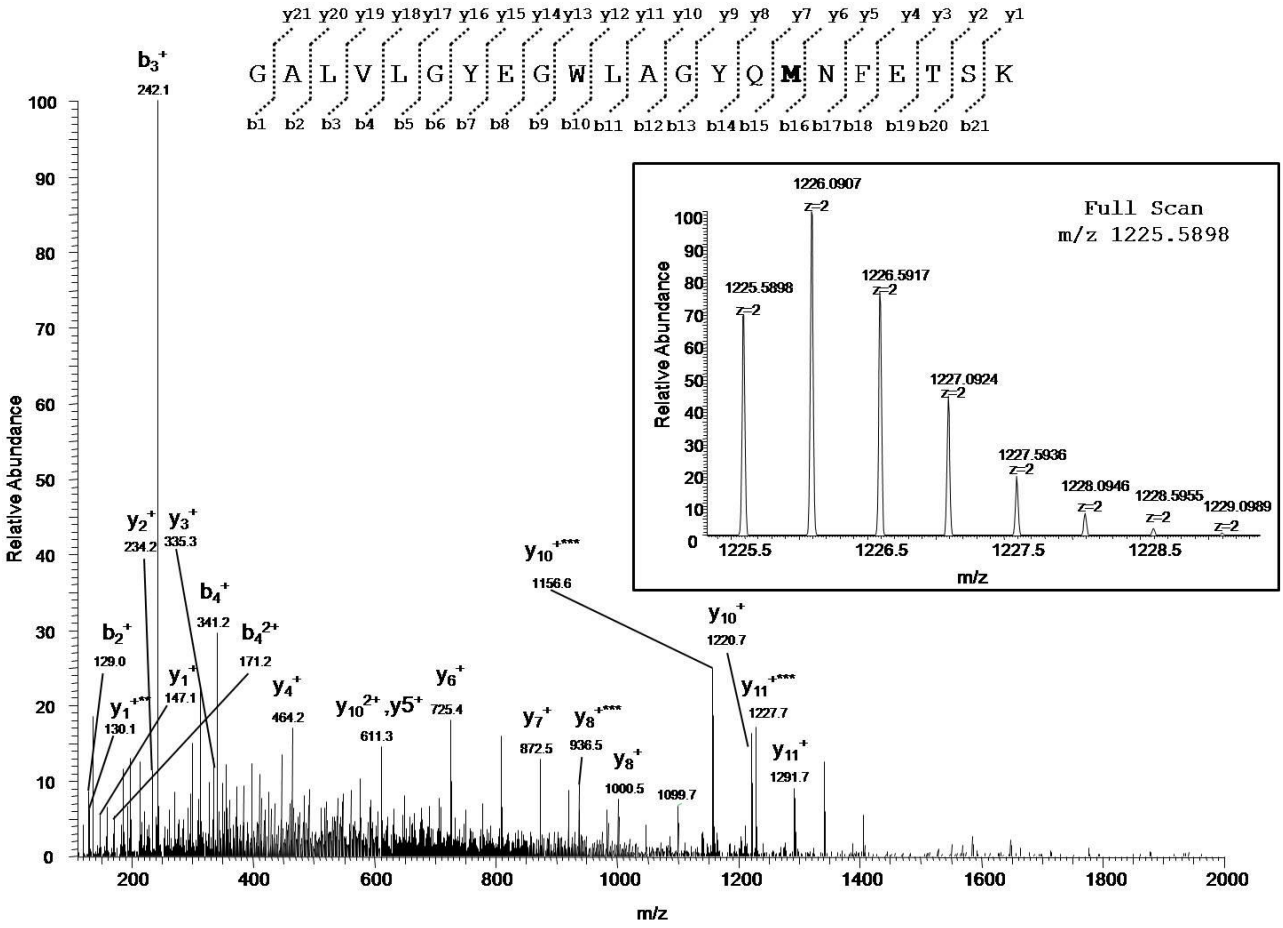

Supplementary Figure 3. MS/MS spectrum of the triply charged molecular ion at m/z 914.7682 (calculated 914.7672) of the N-terminal acetylated tryptic peptide of VDAC2 from *Rattus norvegicus.* The inset shows the full scan mass spectrum of molecular ion. Fragment ions originated from the neutral loss of H_2O are indicated by an asterisk.

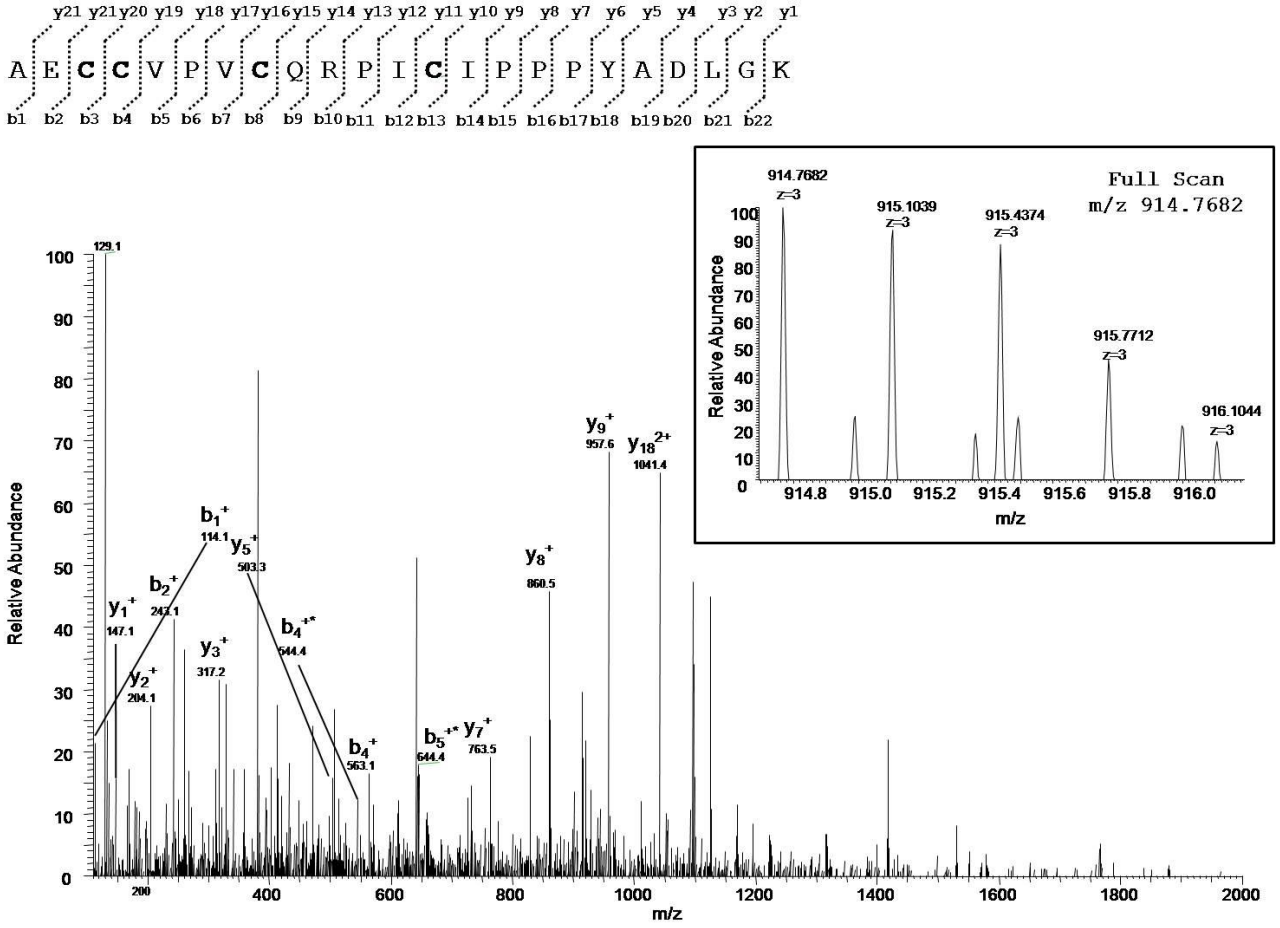

Supplementary Figure 4. Full scan mass spectrum of the doubly charged molecular ions at m/z 712.8066 (calculated 712.8058, peptide sequence W**C**EYGLTFTEK) and at m/z 858.3899 (calculated 858.3850, peptide sequence YKW**C**EYGLTFTEK) of the VDAC2 tryptic peptide from *Rattus norvegicus* containing cysteine residue 77 in the form of sulfonic acid. MS/MS spectrum not found.

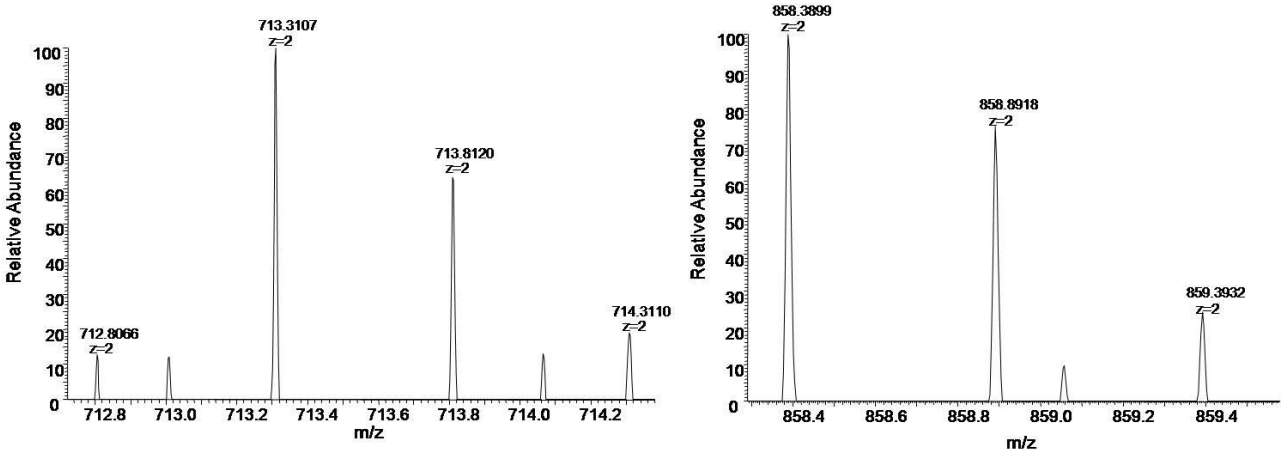

Supplementary Figure 5. Full scan mass spectrum of the doubly charged molecular ion at m/z 1255.5902 (calculated 1255.5897, peptide sequence WNTDNTLGTEIAIEDQI**C**QGLK) of the VDAC2 tryptic peptide from *Rattus norvegicus* containing cysteine residue 104 in the form of sulfonic acid. MS/MS spectrum not found.

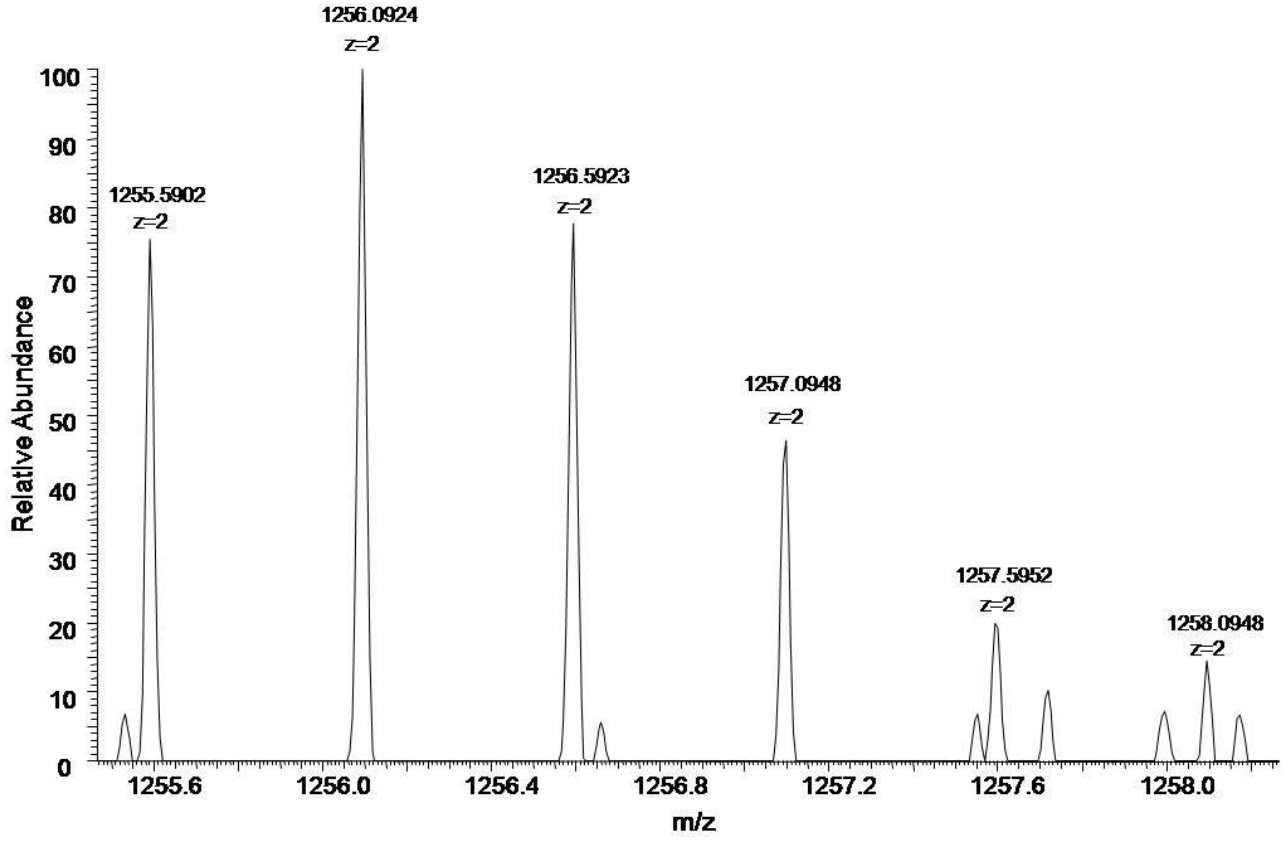

Supplementary Figure 6. Full scan mass spectrum of the doubly charged molecular ion at m/z 1207.9841 (calculated 1207.9894, peptide sequence V**C**EDFDTSVNLAWTSGTN**C**TR) of the VDAC2 tryptic peptide from *Rattus norvegicus* containing cysteine residues 211 and 228 in the form of sulfonic acid. MS/MS spectrum not found.

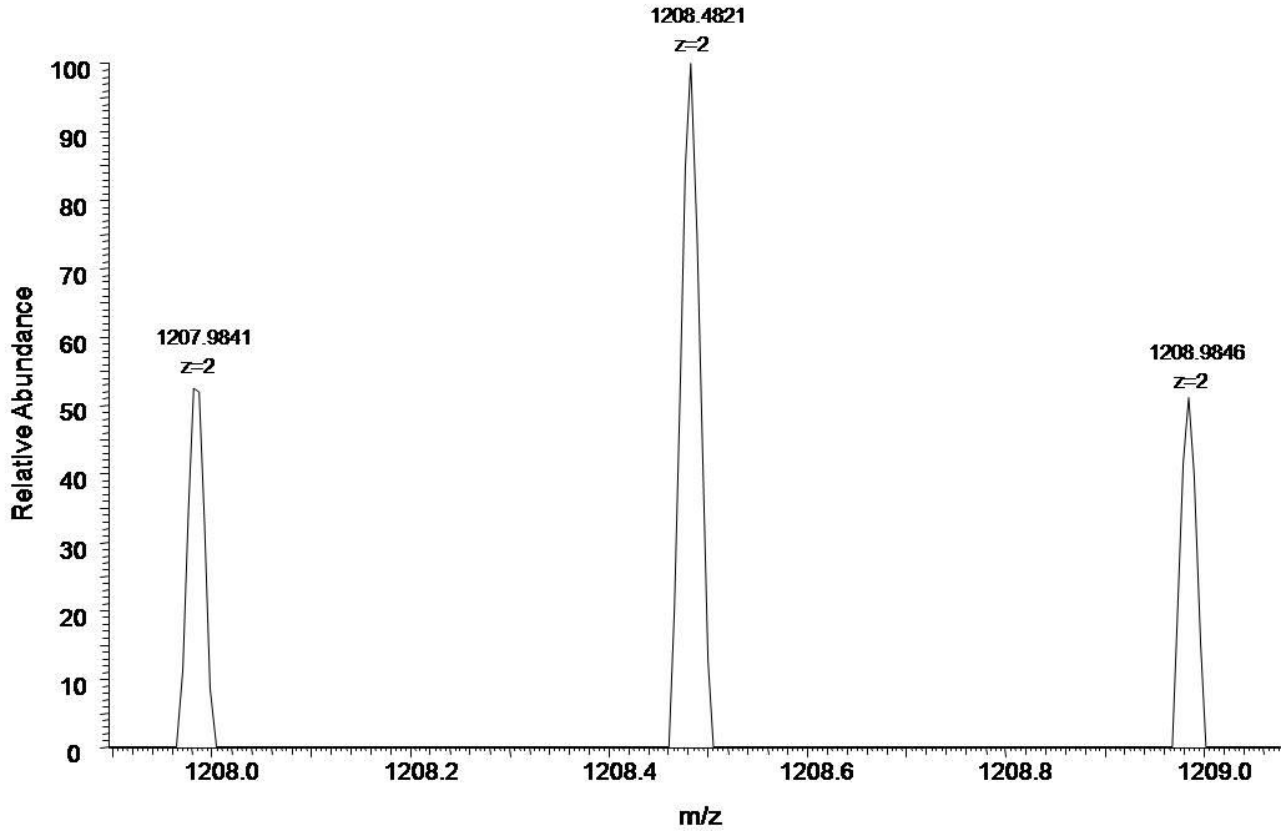

Supplementary Figure 7. Full scan mass spectrum of the single charged molecular ion at m/z 698.3186 (calculated 698.3183, peptide sequence LAGYQ**M**) and the doubly charged molecular ion at m/z 627.8057 (calculated 627.8059, peptide sequence **QM**TFDSAKSKL) of the VDAC2 chymotryptic peptides from *Rattus norvegicus* containing methionine residue 167 in the oxidized form of methionine sulfoxide. MS/MS spectrum not found.

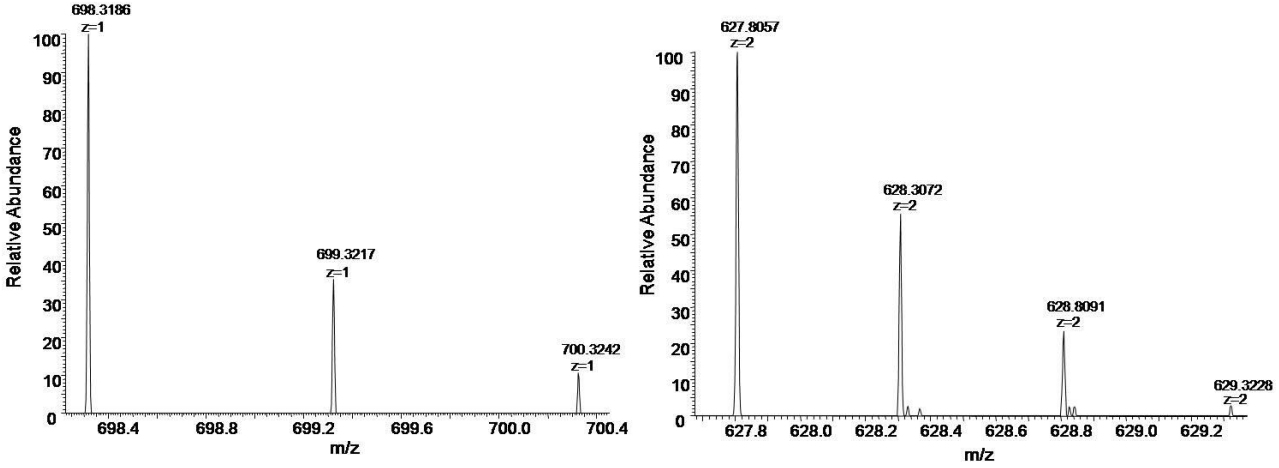

Supplementary Figure 8. MS/MS spectrum of the triply charged molecular ion at m/z 732.6460 (calculated732.6468) of the VDAC2 tryptic peptide from *Rattus norvegicus* containing cysteine residue 48 in the succinated form. The inset shows the full scan mass spectrum of molecular ion.

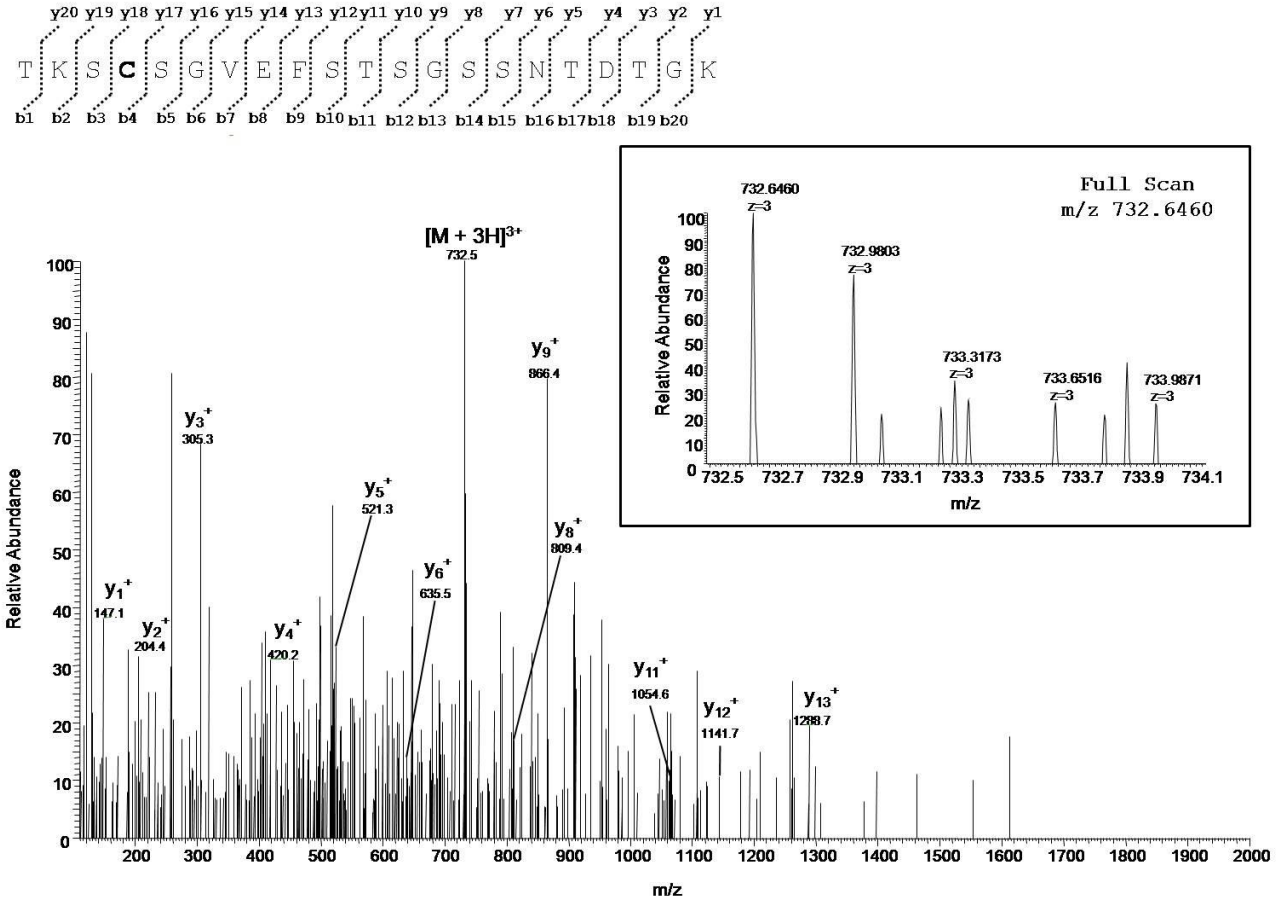

Supplementary Figure 9. MS/MS spectrum of the triply charged molecular ion at m/z 471.2109 (calculated471.2112) of the VDAC3 tryptic peptide from *Rattus norvegicus* containing cysteine residue 229 in the succinated form. The inset shows the full scan mass spectrum of molecular ion.

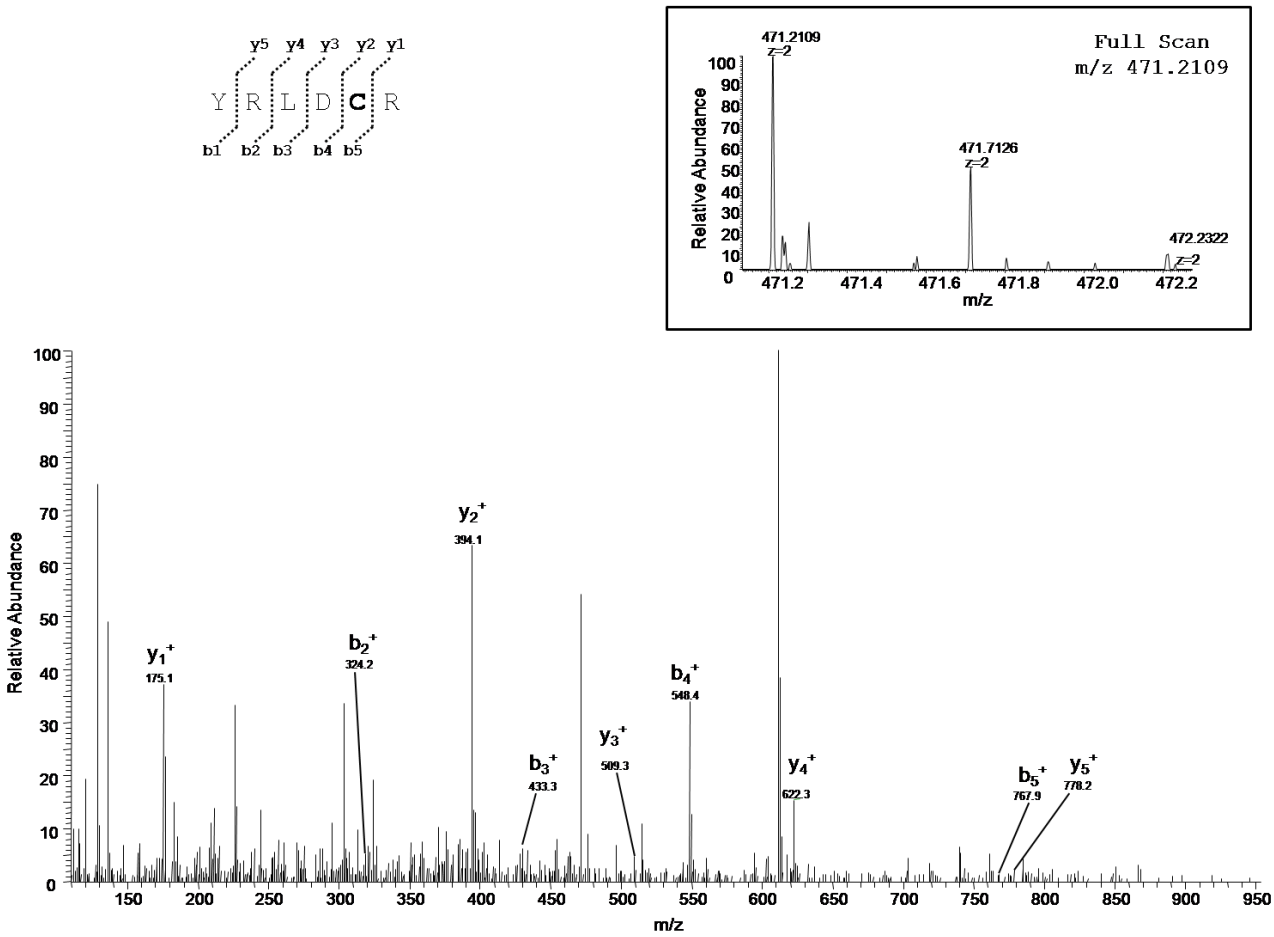

4. Article 2

A High Resolution Mass Spectrometry Study Reveals the Potential of Disulfide Formation in Human Mitochondrial Voltage-Dependent Anion Selective Channel Isoforms (hVDACs)

Maria G.G. Pittalà, Rosaria Saletti, Simona Reina, Vincenzo Cunsolo, Vito De Pinto and Salvatore Foti

Int. J. Mol. Sci. 2020, 21, 1468; doi:10.3390/ijms21041468

International Journal of
Molecular Sciences

MDPI

Article

A High Resolution Mass Spectrometry Study Reveals the Potential of Disulfide Formation in Human Mitochondrial Voltage-Dependent Anion Selective Channel Isoforms (hVDACs)

Maria G. G. Pittalà [1], Rosaria Saletti [2,*], Simona Reina [3], Vincenzo Cunsolo [2], Vito De Pinto [1,*] and Salvatore Foti [2]

1 Department of Biomedical and Biotechnological Sciences, University of Catania, Via S. Sofia 64, 95123 Catania, Italy; marinella.pitt@virgilio.it
2 Department of Chemical Sciences, Organic Mass Spectrometry Laboratory, University of Catania, Viale A. Doria 6, 95125 Catania, Italy; vcunsolo@unict.it (V.C.); sfoti@unict.it (S.F.)
3 Department of Biological, Geological and Environmental Sciences, Section of Molecular Biology, University of Catania, Viale A. Doria 6, 95125 Catania, Italy; simonareina@yahoo.it
* Correspondence: rsaletti@unict.it (R.S.); vdpbiofa@unict.it (V.D.P.); Tel.: +39-095-738-5026 (R.S.); +39-095-7384244 (V.D.P.)

Received: 19 December 2019; Accepted: 18 February 2020; Published: 21 February 2020

Abstract: The voltage-dependent anion-selective channels (VDACs), which are also known as eukaryotic porins, are pore-forming proteins, which allow for the passage of ions and small molecules across the outer mitochondrial membrane (OMM). They are involved in complex interactions that regulate organelle and cellular metabolism. We have recently reported the post-translational modifications (PTMs) of the three VDAC isoforms purified from rat liver mitochondria (rVDACs), showing, for the first time, the over-oxidation of the cysteine residues as an exclusive feature of VDACs. Noteworthy, this peculiar PTM is not detectable in other integral membrane mitochondrial proteins, as defined by their elution at low salt concentration by a hydroxyapatite column. In this study, the association of tryptic and chymotryptic proteolysis with UHPLC/High Resolution nESI-MS/MS, allowed for us to extend the investigation to the human VDACs. The over-oxidation of the cysteine residues, essentially irreversible in cell conditions, was as also certained in VDAC isoforms from human cells. In human VDAC2 and 3 isoforms the permanently reduced state of a cluster of close cysteines indicates the possibility that disulfide bridges are formed in the proteins. Importantly, the detailed oxidative PTMs that are found in human VDACs confirm and sustain our previous findings in rat tissues, claiming for a predictable characterization that has to be conveyed in the functional role of VDAC proteins within the cell. Data are available via ProteomeXchange with identifier PXD017482.

Keywords: Cysteine over-oxidation; mitochondria; Orbitrap Fusion Tribrid; hydroxyapatite; mitochondrial intermembrane space; outer mitochondrial membrane; post-translational modification

1. Introduction

The voltage-dependent anion selective channels (VDACs) are quantitatively relevant components of the mitochondrial proteome. Located in the outer mitochondrial membrane of all eukaryotes, VDACs form aqueous pores that govern ions and metabolites exchange across the organelle, thus contributing to cellular homeostasis maintenance. VDAC has emerged as a key player in cancer [1] and in neurodegenerative diseases, such as Alzheimer's disease (AD), Parkinson's disease (PD),

and Amyotrophic Lateral Sclerosis (ALS), because of its central role in metabolism and its interaction with several cytosolic enzymes and apoptotic factors [2]. In higher eukaryotes three VDAC isoforms, named VDAC1, VDAC2, and VDAC3, which are encoded by three separate genes located on different chromosomes, have been characterized [3]. VDAC1 is the most abundant and ubiquitously expressed of the three isoforms, while VDAC2 and VDAC3 have been estimated to be 10 and 100 times less expressed, respectively. The evolutionary history of VDACs suggests VDAC3 as the oldest isoform, while VDAC1/2 should derive from its duplication around 350 million years ago; VDAC1 is considered to be the youngest isoform since it diverged from VDAC2 300 million years ago. In mammals, VDAC1 and VDAC3 genes contain nine exons, while VDAC2 10: the additional exon encodes a 11 N-terminal amino acids extension with undetermined functional significance. VDAC isoforms display roughly 75% nucleotide sequence identity. Many mitochondrial porin sequences have been obtained by recombinant DNA technology [4–7]. VDAC2 from bovine spermatozoa and VDACs from rat liver mitochondria (rVDAC) have been partially characterized [8]. Interestingly, 90% sequence identity between the human and rat isoforms can be appreciated: in particular, the number and position of cysteine residues among VDACs of these mammal species are highly conserved. Rat and human VDAC2 and VDAC3, for example, both contain cysteines in the N-terminal α-helix, whereas VDAC1 has none. The evolutionary preservation of these residues could suggest a role of cysteine in the protein functionality. We were able to fully cover the rVDAC1 sequence, and extended the coverage of rVDAC2 and 3, by means of a newly established "in-solution" enzymatic proteolysis and UHPLC/High Resolution ESI MS/MS analysis in a previous work, which was performed on rat-derived mitochondria. This procedure enabled to avoid most of the possible technical biases in the protocol that could have modified the naturally occurring oxidation state of the oxidizable residues. We could then propose a detailed profile of the oxidation state of methionine and cysteine residues and the identification of other post-translational modifications for all three rat VDAC isoforms [9–11]. We also demonstrated that cysteine over-oxidation is peculiar to VDACs, since it was not observed in other highly hydrophobic transmembrane mitochondrial proteins analyzed. Here, the same experimental approach was applied to human VDACs that were purified from HAP1 cells mitochondria, producing the respective other post-translational modifications pattern. The results indicate that 1) the oxidative state of cysteine residues is conserved between rat and human; 2) there is a specific utilization of each specific cysteine, since some equivalent residues are always found in the reduced form (i.e., free thiol groups that are available to the oxidation to disulfide bridges), while others are constantly irreversibly over-oxidized as sulfonic acid. The consequences of these results are discussed.

2. Results

2.1. Mass Spectrometry Analysis of Human VDAC1

Reduction/alkylation of proteins was carried out before VDACs purification from the mitochondria that were obtained from HAP1 cells to exclude the possibility that any unspecific and/or undesired oxidation could happen during the purification protocol. Hydroxyapatite (HTP) eluates of Triton X-100 extract were in-solution digested by trypsin and hereinafter analyzed by mass spectrometry. In this experiment, every protein in the HTP eluate was digested, thus a very complex peptide mixture was produced. Table S1 reports hVDAC1 tryptic peptides that were identified in the analysis of mitochondria lysate incubated with dithiothreitol (DTT). UHPLC/High Resolution nESI-MS/MS of the tryptic digest allowed to almost completely cover the reported protein sequence (279 of 282 amino acid residues), with the exception of the tripeptide $N^{111}AK^{113}$ (Figure 1 and Tables S1 and S2). Although some predicted tryptic peptides of the hVDAC1 sequence are shared by two or three isoforms, unequivocal sequence coverage was obtained by the detection of unique peptides originated by missed cleavages whose sequences are boxed in Figure 1.

Figure 1. Sequence coverage map of hVDAC1 obtained by tryptic and chymotryptic digestion. The gray solid line indicates the sequence that was obtained with tryptic peptides; dotted lines the sequence obtained with chymotryptic peptides. The carboxyamidomethylated cysteine residue is highlighted in grey, the totally oxidized cysteine residue is highlighted in light blue and the partially oxidized methionine residues are highlighted in green. The acetyl group linked to the N-terminal alanine is shown in red. Unique tryptic peptides originated by missed-cleavages were used to distinguish and cover sequences shared by isoforms: they are indicated in the boxes. Sequences shared by more isoforms are reported in bold. Numbering of the sequence considered the starting methionine residue, actually deleted during protein maturation. Aspartic acid residue 73 shared by hVDAC1 and 2 is marked by an asterisk.

The results also confirmed that the N-terminal Met, as reported in the SwissProt database sequence (Acc. N. P21796), is missing in the mature protein and that the N-terminal Ala is acetylated (Figure 1, Figure S1, Table S1, molecular fragments 1, 2, and 3).

We particularly focused our investigations on the oxidation state of Met and Cys residues. The sequence of hVDAC1 contains two methionines in positions 129 and 155, and two cysteines in positions 127 and 232 (following the sequence numbering, including the starting Met^{1}, which is actually absent in the mature protein). Met^{129} and Met^{155} were detected in peptides in the normal form (Table S2, fragment 1, and Table S1, fragments 22 and 23), and also in the form of Met sulfoxide (Table S2, fragments 2 and 3). Figures 2 and 3, respectively, report the full scan and fragment ion mass spectra of the doubly charged molecular ion of the peptide E^{121}HINLGCDMDFDIAGPSIR^{139} with Met^{129} modified as methionine sulfoxide and Cys^{127} in the form of sulfonic acid, and of the peptide G^{140}ALVLGYEGWLAGYQMNFETAK^{161} with Met^{155} as methionine sulfoxide. The MS/MS spectra both show the typical neutral loss of 64 Da corresponding to the ejection of methanesulfenic acid from the side chain of MetO [12].

Although from these data a precise determination of the ratio between Met and Met sulfoxide cannot be obtained, a rough estimation of their relative abundance can be derived from the comparison of the absolute intensity of the multiply charged molecular ions of the respective peptides (Table 1). These calculations (Table 1) indicate approximately the same ratio of MetO/Met for the two methionines (1.5:1 for Met^{129}, and 0.8:1 MetO/Met for Met^{155}, respectively).

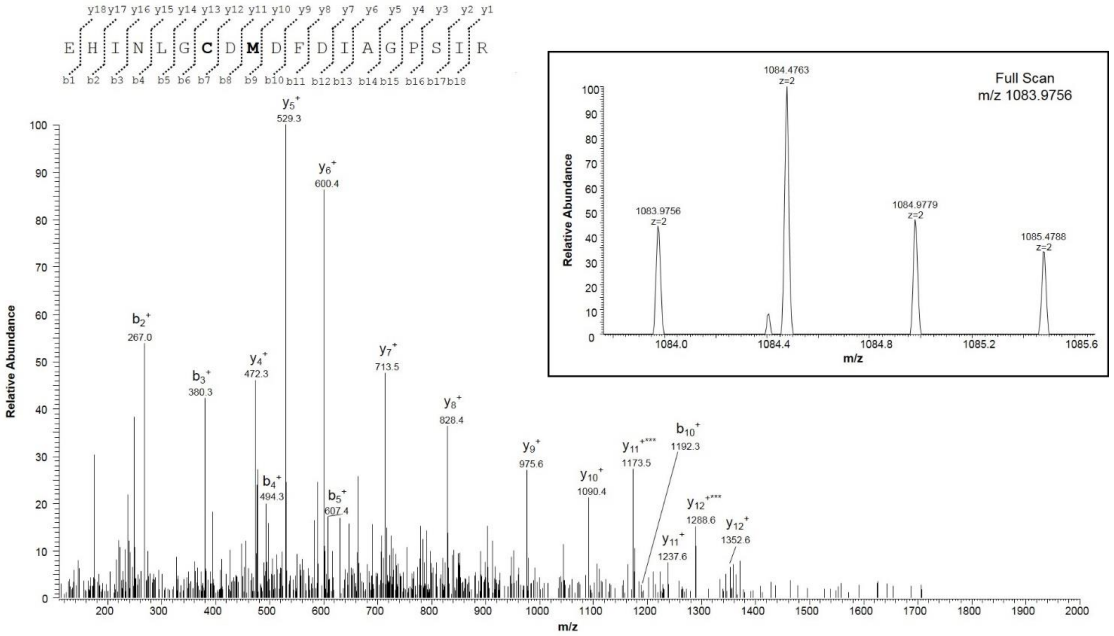

Figure 2. MS/MS spectrum of the doubly charged molecular ion at m/z 1083.9756 (calculated 1083.9754) of the VDAC1 tryptic peptide from HAP1 cells containing cysteine residue 127 in the form of sulfonic acid and methionine residue 129 in the oxidized form of methionine sulfoxide. The inset shows the full scan mass spectrum of molecular ion. Fragment ions originated from the neutral loss of methanesulfenic acid (CH_2SOH, 64 Da) are indicated by three asterisks.

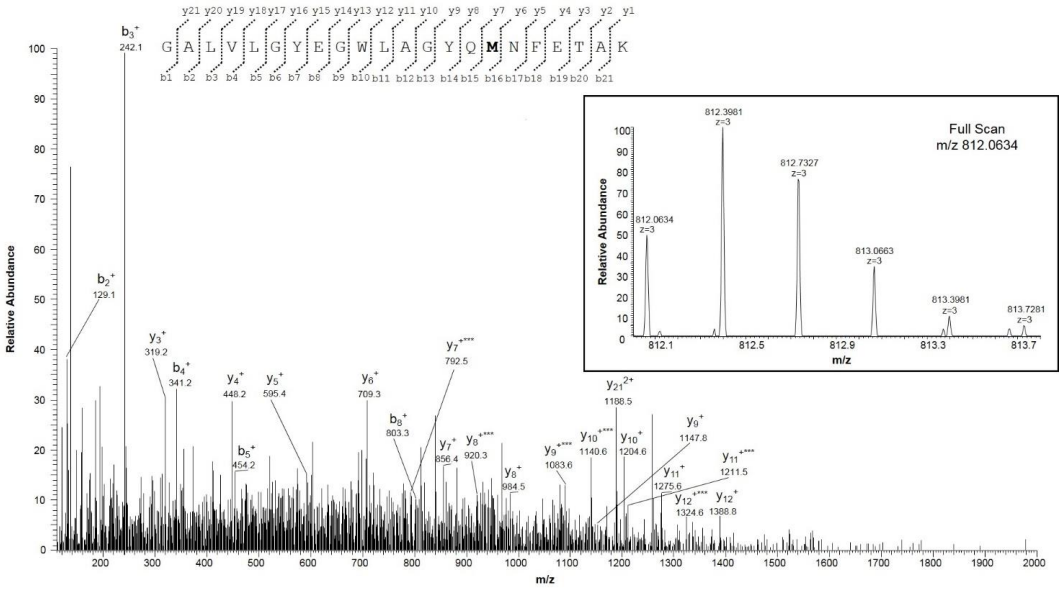

Figure 3. MS/MS spectrum of the triply charged molecular ion at m/z 812.0634 (calculated 812.0635) of the VDAC1 tryptic peptide from HAP1 cells containing methionine residue 155 in the oxidized form of methionine sulfoxide. The inset shows the full scan mass spectrum of molecular ion. Fragment ions originated from the neutral loss of methanesulfenic acid (CH_2SOH, 64 Da) are indicated by three asterisks.

Table 1. Comparison of the absolute intensities of molecular ions of selected sulfur containing tryptic peptides found in the analysis of hVDAC1 reduced with dithiothreitol (DTT), carboxyamidomethylated, and digested in-solution.

Peptide	Position in the Sequence	Measured Monoisotopic *m/z*	Absolute Intensity	Ratio Ox/Red
EHINLG**C**D**M**^{129}DFDIAGPSIR	121–139	1083.9756 (+2)	1.6×10^5	1.5
EHINLG**C**DMDFDIAGPSIR		1075.9784 (+2)	1.08×10^5	
GALVLGYEGWLAGYQ**M**^{155}NFETAK	140–161	812.0634 (+3)	6.4×10^5	0.8
GALVLGYEGWLAGYQMNFETAK		1209.5944 (+2)	8.5×10^5	

M: methionine sulfoxide; **C**: cysteine oxidized to sulfonic acid.

Analysis of the mass spectral data that were oriented to the determination of the oxidation state of cysteines showed that Cys^{232} was totally found in the carboxyamidomethylated form (Table S1, fragment 32), while Cys^{127} was exclusively detected in the oxidized form of sulfonic acid (Figure 2, Figure S2, and Table S2, fragments 1 and 2).

Chymotrypsin also digested hVDAC1. Complementary data obtained from the chymotryptic fragments resulted in the complete coverage of the sequence, including the stretch N^{111}AK^{113}, (Table S3, fragment 19). This analysis also confirmed the lack of Met^1, the acetylation of Ala^2 (Table S3, fragments 1 and 2), and the partial oxidation of Met^{129} to methionine sulfoxide (Table S4, fragments 1-3). In addition, Cys^{127} was only observed in trioxidized form (Table S4, fragments 1–3) and Cys^{232} exclusively in the carboxyamidomethylated form (Table S3, fragments 30 and 31), as found in the tryptic digest.

2.2. Mass Spectrometry Analysis of Human VDAC2

The peptides that were identified by tryptic digestion and UHPLC/High Resolution nESI-MS/MS of hVDAC2 covered 97.3% of the hVDAC2 sequence (285 of 293 amino acid residues) (Figure 4, Tables S5 and S6). Analogously to the hVDAC1 isoform, the N-terminal methionine, as reported in the SwissProt database sequence (Acc. N. P45880), is absent and the Ala^2 is in the acetylated form (Figure S3, and Table S5, fragment 1).

Figure 4. Sequence coverage map of hVDAC2 obtained by tryptic and chymotryptic digestion. Gray solid lines indicate the sequence obtained with tryptic peptides; dotted lines the sequence obtained with chymotryptic peptides. The carboxyamidomethylated cysteine residues are highlighted in grey, the partially oxidized cysteine residues are highlighted in orange, and the totally oxidized alanine residue is highlighted in light blue. The partially oxidized methionine residues are highlighted in green. The acetyl group linked to the N-terminal cysteine is shown in red. Unique tryptic peptides originated by missed-cleavages were used to distinguish and cover sequences shared by isoforms: they are indicated in the boxes. Sequences shared by isoforms are reported in bold. Numbering of the sequence considered the starting methionine residue, actually deleted during protein maturation. Aspartic acid residue 77 shared by hVDAC1 and 2 is marked by an asterisk.

Additionally, hVDAC2 shows tryptic peptides sequences that are shared by one or two other isoforms: unequivocal sequence coverage was obtained by detecting unique peptides originated by missed cleavages. Figure 4 boxes the sequences of these unique peptides.

In the hVDAC2 there are two internal methionines in position 12 and 166, and nine cysteines (sequence positions: 8, 13, 47, 76, 103, 133, 138, 210, and 227). Met^{12} and Met^{166} were identified both as normal Met (Table S5, fragment 2 and Table S6, fragment 6) and as Met sulfoxide (Figures S4 and S5, and Table S6, fragments 1, 2, and 7). The comparison of the absolute intensity of the doubly or triply charged molecular ions of the corresponding fragments indicates a ratio of approximately 10:1 and 1.5:1 MetO/Met for Met^{12} and Met^{166}, respectively (Table 2). Instead, the triply charged molecular ion of the tryptic peptide E^{132}-K^{172}, including two cysteines and Met^{166} was detected, but its corresponding MS/MS spectrum was not obtained: thus, Met^{166} was found either in the normal (Table S6, fragment 6) and oxidized form (Figure S5, Table S6, fragment 7), while it was not possible to determine which one of the two cysteines (Cys^{133} or Cys^{138}) was oxidized or reduced.

Table 2. Comparison of the absolute intensities of molecular ions of selected sulfur containing tryptic peptides found in the analysis of hVDAC2 reduced with DTT, carboxyamidomethylated, and digested in-solution.

Peptide	Position in the Sequence	Measured Monoisotopic *m/z*	Absolute Intensity	Ratio Ox/Red
P**M**C*C*IPPSYADLGK	11–23	732.8476 (+2)	8.79×10^5	9.8
PM*C*IPPSYADLGK		724.8497 (+2)	8.99×10^4	
S**C**SGVEFSTSGSSNTDTGK	46–64	949.8815 (+2)	1.80×10^4	0.01
S*C*SGVEFSTSGSSNTDTGK		954.4005 (+2)	1.59×10^6	
YKW**C**EYGLTFTEK	73–85	858.3821 (+2)	1.53×10^4	0.1
YKW*C*EYGLTFTEK		862.9037 (+2)	1.38×10^5	
WNTDNTLGTEIAIEDQI**C**QGLK	86–107	837.3958 (+3)	1.09×10^5	0.04
WNTDNTLGTEIAIEDQICQGLK		1260.1086 (+2)	2.98×10^6	
ECINLGCDVDFDFAGPAIHGSAVFGYEGW LAGYQ**M**TFDSAK[a]	132–172	1508.3225 (+3)	2.94×10^4	1.4
ECINLGCDVDFDFAGPAIHGSAVFGYEGW LAGYQMTFDSAK[a]		1502.9921 (+3)	2.12×10^4	
V**C**EDLDTSVNLAWTSGTN*C*TR	209–229	1195.5161 (+2)	4.40×10^4	0.1
V*C*EDLDTSVNLAWTSGTN*C*TR		800.3594 (+3)	4.40×10^5	

C: cysteine carboxyamidomethylated; **M**: methionine sulfoxide; **C**: cysteine oxidized to sulfonic acid. [a]One of the two cysteines of these peptides is trioxidized and one carboxyamidomethylated, but it was not possible to determine which one was modified because the MS/MS spectrum was not obtained.

Moreover, the partial oxidation of Cys^{47}, Cys^{76}, Cys^{103}, and Cys^{210} to sulfonic acid (Table S6, fragments 3, 4, 5, and 8, respectively, and Figure S6A–D), and the presence of the cysteines 8, 13, and 227 exclusively in the carboxyamidomethylated form were revealed (Table S5, fragments 1, 2, and 21). We could roughly estimate the relative abundance of the cysteines oxidized to sulfonic acid with respect to those in the carboxyamidomethylated form: this estimation is related with the ratio of the absolute intensity of the multiply charged molecular ions of the corresponding peptides, as reported in Table 2. In the evaluation of these results, it should be considered that the oxidation of cysteine to cysteine sulfonic acid introduces a strong negative charge in the peptide, thus hampering the formation of positive ions. However, even while taking these considerations into account, the data in Table 2 suggest that measurable amounts of Cys^{76} and Cys^{210} are oxidized to sulfonic acid (ratio ox/red 0.1), whereas Cys^{47} and Cys^{103} oxidized to sulfonic acid are only present in trace amounts (ratio ox/red 0.01 and 0.04, respectively).

Chymotryptic digestion of hVDAC2 was also performed to increase the sequence coverage. Combining the results that wereobtained in the tryptic and chymotryptic digestions, the coverage of

the sequence of hVDAC2 was extended to 98,3% (288 out of 293 amino acid residues) (Figure 3 and Table S7). The region that is still not covered corresponds to the sequence Ser^{173}-Arg^{177}.

Analysis of the chymotryptic digest confirmed the presence of cysteines 13, and 227 exclusively in the carboxyamidomethylated form (Table S7, fragments 1, 2, and 29), and of Cys^{210} in the normal and trioxidized form (Table S7, fragment 27, and Table S8, fragment 3).

Two fragments containing Cys^{133} and Cys^{138} were present in the chymotryptic mixture (Table S8, fragments 1 and 2). The MS/MS spectrum of the doubly charged molecular ion of fragment 1 (Figure S7) demonstrated that Cys^{133} was totally carboxyamidomethylated whereas Cys^{138} was completely in the form of sulfonic acid, thus allowing to characterize the oxidation state of these two cysteines that was not possible to determine in the analysis of the tryptic digest (see above). At the end, chymotryptic peptides, including methionines 12 and 166, were undetectable.

2.3. Mass Spectrometry Analysis of Human VDAC3

UHPLC/nESI-MS/MS of the in-solution tryptic digest of hVDAC3 resulted in a coverage of about 91% of the sequence (256 of 282 amino acid residues, Table S9 and Figure 5), thus extending the coverage that was obtained by other Authors from in-gel digestion and MALDI-ToF/ToF mass spectrometric analysis [13]. Although some predicted tryptic peptides of the hVDAC3 sequence are shared by other isoforms, unequivocal attribution for two of them was obtained by the detection of unique peptides originated by missed cleavages (Table S9, fragments 6 and 19, and Figure 5).

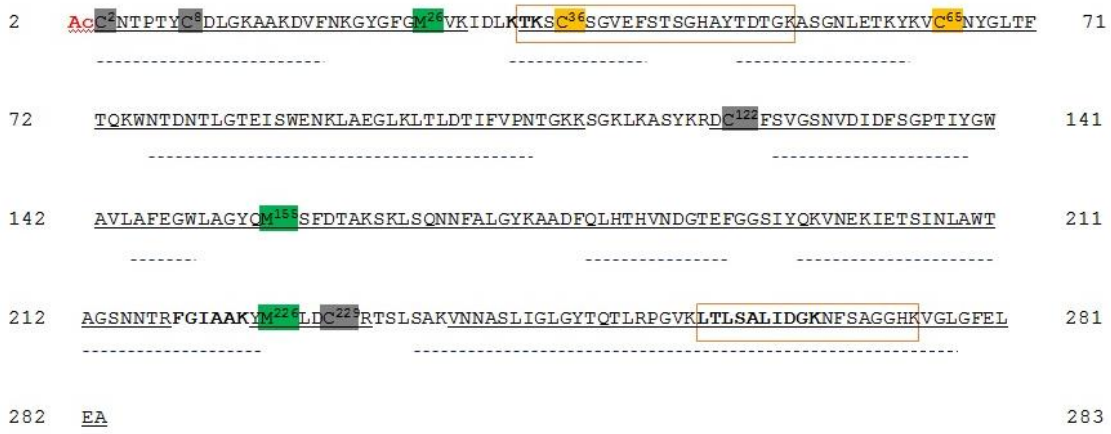

Figure 5. Sequence coverage map of hVDAC3 obtained by tryptic and chymotryptic digestion. The gray solid line indicates the sequence obtained with tryptic peptides; dotted lines the sequence obtained with chymotryptic peptides. The carboxyamidomethylated cysteine residues are highlighted in grey, and the partially oxidized cysteine residues are highlighted in orange. The partially oxidized methionine residues are highlighted in green. The acetyl group linked to the N-terminal cysteine is shown in red. Unique tryptic peptides originated by missed-cleavages were used to distinguish and cover sequences shared by isoforms: they are indicated in the boxes. Sequences that are shared by more isoforms are reported in bold. Numbering of the sequence considered the starting methionine residue, actually deleted during protein maturation

Similar to the other two isoforms, it was found that the N-terminal Met, as reported in the SwissProt database sequence (Acc. N. Q9Y277), is removed in the mature protein, and that the N-terminal Cys is present in the acetylated form (Figure S8 and Table S9, fragment 1).

hVDAC3 sequence includes three methionines in position 26, 155, and 226. For all of these three methionines, peptides containing residues in the normal state (Table S9, fragments 2, 4, 5, 12, and 17, respectively) and also oxidized to methionine sulfoxide were detected (Table S10, fragments 1, 4, and 5), with a ratio of about 0.1:1, 1:1, and 3:1 MetO/Met, respectively (Figure S9A–C and Table 3).

Table 3. Comparison of the absolute intensities of molecular ions of selected sulfur containing tryptic peptides found in the analysis of hVDAC3 reduced with DTT, carboxyamidomethylated, and digested in-solution.

Peptide	Position in the Sequence	Measured Monoisotopic *m/z*	Absolute Intensity	Ratio Ox/Red
GYGFG**M**VK	21–28	437.7098 (+2)	1.46×10^4	0.06
GYGFGMVK		429.7118 (+2)	2.51×10^5	
S**C**SGVEFSTSGHAYTDTGK	35–53	991.4069 (+2)	1.81×10^4	0.2
S*C*SGVEFSTSGHAYTDTGK		995.9267 (+2)	8.80×10^4	
YKV**C**NYGLTFTQK	62–74	806.8889 (+2)	1.01×10^4	0.05
YKV*C*NYGLTFTQK		811.4081 (+2)	1.97×10^5	
D*C*FSVGSNVDIDFSGPTIYGWAVLAFE GWLAGYQ**M**SFDTAK	121–161	1513.3688 (+3)	1.74×10^4	1.1
D*C*FSVGSNVDIDFSGPTIYGWAVLAFE GWLAGYQMSFDTAK		1508.0270 (+3)	1.59×10^4	
Y**M**LD*C*R	225–230	437.1832 (+2)	5.88×10^5	3.2
YMLD*C*R		429.1861 (+2)	1.86×10^5	

C: cysteine carboxyamidomethylated; **C**: cysteine oxidized to sulfonic acid; **M**: methionine sulfoxide.

In hVDAC3, there are six cysteines in position 2, 8, 36, 65, 122, and 229. Analysis of the mass spectral data showed that Cys^2 and Cys^8, of which the N-terminal Cys^2 was acetylated, were exclusively in the reduced and carboxyamidomethylated form (Figure S8 and Table S9, fragment 1). Also cysteines 122 and 229 (Table S9, fragments 12 and 17) were only identified in the reduced form. Cysteines 36 and 65 were found both in peptides containing these residues carboxyamidomethylated (Table S9, fragments 6, 7, and 9), and in peptides containing these residues in the form of sulfonic acid (Figures S10A,B and Table S10, fragments 2 and 3, respectively). From the comparison of the peak areas of the double charged molecular ions of the corresponding peptides, it was estimated that the ratio Ox/Red for these two cysteines is about 0.1–0.2 (Table 3).

The chymotryptic digestion of hVDAC3 was also performed. Although this analysis resulted in a low sequence coverage (63.5%, Table S11), the complementary data obtained allowed to extend the coverage to 94.3% (266 out of 282 amino acid residues). It should be noted that the peptide G^{220}IAAKY^{225} is common to all of the isoforms and, therefore, its attribution to the hVDAC3 sequence it is not univocal (Table S11, fragment 22). The regions not verified yet correspond to the sequences Ile^{29}-Leu^{31}, Ser^{111}-Arg^{120}, and Thr^{231}-Leu^{233} (Figure 5).

In addition, the data that were obtained confirmed the absence of Met^1, the acetylation of Cys^2, and the presence of Cys^2 and Cys^8 exclusively in the carboxyamidomethylated form (Table S11, fragments 1 and 2).

3. Discussion

The characterization of VDACs presents challenging issues due to extremely high hydrophobicity, the difficulty of isolating each single isoform, and of separating them from other mitochondrial proteins of similar hydrophobicity. Consequently, it is necessary to analyze them as components of a relatively complex mixture. Furthermore, SDS-electrophoretic separation, which could be used for a preliminary isolation, should desirably be avoided due to the potential danger of unwanted oxidation reactions, which could introduce artifacts in the proteins. For these reasons, we have developed an "in-solution" digestion procedure that can be directly applied to the enriched VDAC isoforms fraction obtained as eluate from hydroxyapatite chromatography. The resulting proteolytic mixture can be subsequently analyzed by UHLC/High-Resolution mass spectrometry. We applied this procedure to enriched protein extracts of rat liver mitochondria, with the aim of characterizing the VDAC isoforms PTMs of sulfur amino acids [10,11]. We obtained wide information about them (Table 4) with the surprising result of specific oxidations to sulfonic acid. In this work, we extended this analysis to human VDAC

isoforms that were obtained by enriched mitochondrial protein extracts from cultured cells. The aim was to extend our observation to the human proteins, to validate them, and verify their specificity. Using our "in-solution" protocol, in the present work we have been able to completely cover the sequence of hVDAC1, and almost completely the sequences of hVDAC2 and hVDAC3 (98.3% and 94.3%, respectively) from HAP1 cell mitochondria. It should be noted that the short regions not identified in hVDAC2 and hVDAC3 do not contain cysteines and methionines and they correspond to small tryptic or chymotryptic peptides or even to single amino acids, which cannot be detected in LC/MS analysis. In conclusion, the data obtained allowed for the determination of the oxidative states of all the cysteine and methionine residues present in the human isoforms.

Table 4. Comparison of the oxidation state of cysteines in rat and human VDAC isoforms. p. o.: partially oxidized; t.o.: totally oxidized; t.r.: totally reduced; rat: VDACs from rat liver; hu: VDACs from human HAP1 cells. Cysteine residues are aligned in the same rows according to their presumed homology.

Cysteine Position						Oxidative State					
VDAC1		**VDAC2**		**VDAC3**		**VDAC1**		**VDAC2**		**VDAC3**	
rat	***hu***	***rat***	***hu***	***rat***	***hu***	***rat***	***hu***	***rat***	***hu***	***rat***	***hu***
		4						t.r.			
		5						t.r.			
		9	8	2	2		-	t.r.	t.r.	t.r.	t.r.
		14	13	8	8		-	t.r.	t.r.	t.r.	t.r.
		48	47	36	36		-	p.o.	p.o.	p.o.	p.o.
		77	76	65	65		-	p.o.	p.o.	p.o.	p.o.
		104	103		-		-	p.o.	p.o.		-
		134	133	122	122		-	N.D.	t.r.	N.D.	t.r.
127	127	139	138		-	p.o.	t.o.	N.D.	t.o.		-
				165						p.o.	
		211	210		-		-	p.o.	p.o.		-
		228	227		-		-	p.o.	t.r.		-
				229	229		-		-	t.o.	t.r.
232	232				-	p.o.	t.r.		-		-

3.1. Oxidation States of Methionines in Human and Rat VDAC Isoforms

As previously found for the three rVDACs [10,11] also in the hVDAC isoforms methionines oxidized to sulfoxide and cysteines over-oxidized up to sulfonic acid were observed. Most internal methionines are conserved between rat and human notwithstanding the N-terminal methionines, usually cleaved up in every VDAC isoforms maturation process. In the sequence of rVDAC1 one methionine residue (Met^{155}) is conserved in hVDAC1. On the other hand, the rVDAC1 conserved Met^{155} is oxidized to MetO in a remarkable higher amount (Ox/Red ratio 65:1) than in the hVDAC1 (Ox/Red ratio 1:1). rVDAC2 shows only one internal Met (Met^{167}). The rat Met^{167} and the human conserved homologous Met^{166} are both oxidized to MetO in approximately equal amount (Ox/Red ratio 2:1 in hVDAC2 and 3:1 in rVDAC2). Met^{12}, exclusively found in hVDAC2, is mainly in the oxidized form (Ox/Red ratio 10:1). hVDAC3 sequence includes Met^{26}, Met^{155}, and Met^{226}. For all these three methionines, the ratio between oxidized (methionine sulfoxide)/normal was found to be approximately 0.1:1, 1:1, and 3:1. Met^{26} in hVDAC3 showed an oxidation state that was comparable to the analogous methionine in rVDAC3. In rVDAC3, the oxidation rate of Met^{155}, the latter conserved methionine, was not determined.

Methionine residues are highly susceptible to oxidation, even in mild conditions: reactive oxygen (ROS) and nitrogen species (NOS) generate in vivo methionine sulfoxide (MetO). MetO can be reduced

back to methionine *in vivo* by ubiquitous sulfoxide reductases [14]. Cyclic Met oxidation/MetO reduction leads to the consumption of ROS and it is considered as a scavenging system from oxidative damage [15,16]. On the other hand, MetO formation has little or no effect on protein susceptibility to proteolytic degradation [17,18].

3.2. Oxidation States of Cysteines in Human and Rat VDAC Isoforms

Cysteine oxidation has structural relevance for proteins, since it can support the disulfide bridge formation, a physiological protein cross-linking. An excess of oxidation, in contrast, can be irreversible and even harmful in the cell, producing a permanent modification to sulfone or sulfine with the fixation of permanent negative charges in the protein [19]. Thus, we examined with the highest attention the fate of cysteine residues in the human VDAC isoforms and compared their state with those of rat VDAC isoforms [10,11].

VDAC1 shows two cysteine residues that were conserved between rat and human (Table 4). In rat VDAC1 both cysteines are moderately oxidized, with a ratio Ox/Red in the range of 0.1–0.2 [11]. Instead in human VDAC1, Cys^{127}, which is embedded in the hydrophobic moiety of the outer mitochondrial membrane (OMM) (Figure 6/Figure S11), was found always and completely trioxidized, while Cys^{232}, facing the aqueous inside of the pore, was exclusively observed in the carboxyamidomethylated form, an indication that, in the native protein, it is available to reversible oxidation to form disulfide bridges.

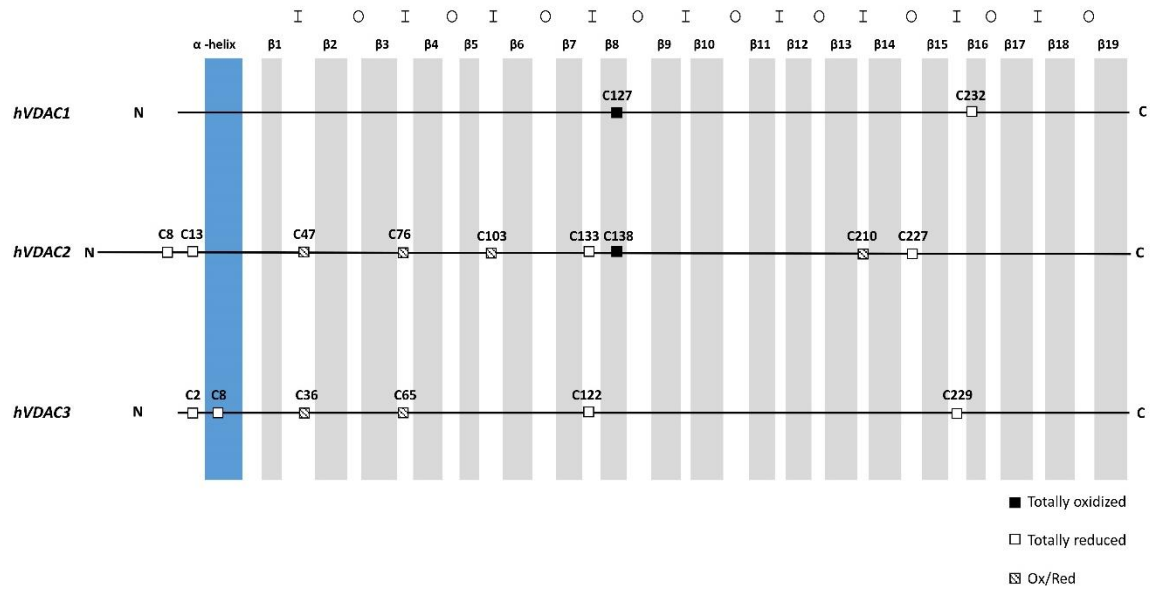

Figure 6. Scheme of the cysteine localization in the aligned sequences of human VDAC isoforms. N-terminal α-helix in blue, β-strands in gray. The internal loops, i.e., exposed to the inter membrane space, are indicated with I. The outer loops, i.e., exposed to the cytosol, are indicated with O.

VDAC2 is the longer isoform, with an N-terminal extension of 11 amino acids in mammals. It is also the richest in cysteines. In rat, VDAC2 shows 11 cysteines, while human VDAC2, only nine (Table 4). This difference is due to the presence in the rat N-terminal of two additional cysteines. Additionally, in hVDAC2, some Cys were found always completely reduced, as in rVDAC2, with no trace of over-oxidation. Other Cys were instead detected in both chemical states (Table 4). In particular, Cys^{8}, Cys^{13}, and Cys^{133} were exclusively found in the reduced form: these residues are exposed to the IMS and correspond to Cys^{9}, Cys^{14}, and Cys^{134} in rVDAC2 that have also been found to be reduced or not determined (Cys^{134}) [11]. Cys^{227}, which is also exposed to the cytosol, was found exclusively in the reduced form analogously to the Cys^{228} of rVDAC2, whose trioxidized form was detected in very low amount [11]. In rVDAC2, also the additional Cys^{4} and Cys^{5}, in the N-terminal moiety, are reduced; thus, VDAC2 has a cluster of cysteines exposed to the IMS that are available to reversible oxidation.

The oxidation state of the other positions is essentially conserved between rat and human. For hVDAC2, Cys^{138}, located in a position similar to Cys^{127} in hVDAC1, and therefore embedded in the hydrophobic phase of OMM, was totally found in the form of sulfonic acid (Figure 6/Figure S11). The sequence containing the corresponding residue in rVDAC2 (Cys^{139}) was not covered in our previous work and, consequently, its oxidation state could not be determined [11]. Assuming that, also in rat, this residue is over-oxidized, it is striking to notice that both VDAC1 and VDAC2 have an over-oxidized (and negatively charged) cysteine residue that is embedded in the hydrophobic milieu of the outer membrane. Such a peculiar, potentially destabilizing situation, lacks in the VDAC3, where this residue is absent, and could have a biological meaning that is possibly related to the different functions of the isoforms.

Cysteines in position 47, 76, 103, and 210 are in the ring region that is exposed to inter-membrane space (IMS). Among them, Cys^{76} was partially detected in the form of sulfonic acid with an Ox/Red ratio of about 0.1:1, similarly to the homologue Cys^{77} in rVDAC2 [11]. Cys^{47}, Cys^{103} and Cys^{210} are also found partially trioxidized but with a lower Ox/Red ratio (about 0.1:1 – 0.01:1), reproducing the trend observed for the homologous Cys^{48}, Cys^{104}, and Cys^{211} of rVDAC2 [11].

Among the six cysteines contained in the hVDAC3 sequence, Cys^{36} and Cys^{65} were detected trioxidized with an Ox/Red ratio of 0.2:1 and 0.1:1, respectively. Homologous Cys^{36} and Cys^{65} in rVDAC3 were found to be oxidized to a similar extend (Ox/Red ratio of 1.4 and 0.2, respectively). Cys^{2} and Cys^{122}, which are also facing the IMS (Figure 6/Figure S11), were found only in the reduced form, as Cys^{8}, which is inside the channel. The same result was obtained for the corresponding Cys^{2} and Cys^{8} of rVDAC3. The oxidation state of Cys^{122} of the rVDAC3 remained undetermined, because peptides containing this residue were not detectable, but, in analogy with what found for Cys^{122} in hVDAC3 and Cys^{133} in hVDAC2, it is presumably in the reduced form. By contrast, Cys^{229} in hVDAC3 was completely in the reduced form, whereas the same residue was totally trioxidized in rVDAC3.

3.3. Sulfur Oxidation State of VDAC Isoforms is Conserved Between Rat and Human, and Between Tissues and Cultured Cells

The comparison of the oxidation rate of methionines and cysteines among the human VDAC isoforms with the corresponding rat VDAC isoforms provides some interesting information. As a preliminary observation, it is important to underline that most of the data obtained for the oxidation states of cysteines in human VDACs are the same as those reported for the rat VDACs, thus demonstrating that they do not depend on the type of organism, at least in mammals, but they reflect a physiological condition. The peculiarity of the over-oxidation of these mitochondrial proteins has been reported in our previous works, where we analyzed several integral mitochondrial membrane proteins, but we did not discover a relevant amount of over-oxidized cysteines, if any, in other proteins [11]. Another validation of these data is that the application of the same methodologies to different kind of sources, living tissue from organism (rat liver), or cultivated cells (human HAP cell) resulted in remarkably similar results.

The pattern of cysteine oxidation of VDAC isoforms might foresee structural and functional consequences. We noticed that there are different classes of cysteines with respect to their location in the protein and to their oxidation state (Figure 6).

1. A first class of cysteines is those whose lateral residue protrudes and that are embedded in the hydrophobic moiety of the outer membrane. These are Cys^{127} in VDAC1 and Cys^{138} in VDAC2. Both were only found in the sulfonic, tri-oxidized state: the most hydrophilic, the most sterically bulk, the most improbable for a presence in a hydrophobic milieu. We have no idea about this particular position, but we notice that VDAC1 and VDAC2 also possess the well-known Glu^{73} residue (Figures 1 and 4), another hydrophilic residue that protrudes toward the hydrophobic part of the membrane, being involved in the binding of hexokinase to VDAC [20–22] and possibly in the oligomerization of the protein [23]. Interestingly, VDAC3 does not show any residue homologous to the $Cys^{127/138}$ or the

Glu[73]. This could mean that the isoform 1 and 2 have a different role in the stabilization/destabilization of the membrane or have relationships with different phospholipids.

2. A second class includes the abundant number of cysteines in the N-terminal sequence. There are two cysteines in the short sequences of the first amino acids in both VDAC2 and VDAC3 and they are even four in the homologous sequence of rat VDAC2. They were found always in the carboxymethylated form, suggesting that they are reduced in the cell or in a reversibly oxidized fashion. The most obvious of these states are disulfide bridges. We can also add Cys[122] in VDAC3 and Cys[133/134] in VDAC2 as members of this class, since they have also been found as stably carboxyamidomethylated, and they are in close proximity to the N-terminal cysteines, as shown in the structural model of VDAC2 and VDAC3 built upon the hVDAC1 available three-dimensional (3D) structure [22,24,25].

3. The third group of cysteines comprises a ring of residues predicted to be exposed to the IMS. These residues (Cys[47], Cys[76], Cys[103], and Cys[210] in hVDAC2 and Cys[36] and Cys[65] in hVDAC3) were found either in the oxidized or in the reduced (carboxyamidomethylated) forms, in variable ratios: they thus look to be residues subject to variable and possible reversible oxidations. These last residues would form the reservoir of the VDACs as a buffer against the oxidative action of ROS and other similar agents.

A less defined role has to be assigned to Cys[227/228] in VDAC2 and Cys[229] in VDAC3. The latter is present in a predicted turn that was exposed to the IMS. It was found always reduced in human, but always oxidized in rat: it is perhaps another member of the ring of cysteines proposed to buffer the oxidative potential of the IMS. Cys[227/228] of VDAC2 is, instead, the only cysteine predicted to be in a hydrophilic turn exposed to the cytosol. Its position is intriguing, also because it has been found always in reduced form in human, and almost completely reduced in rat. It is tempting to speculate that it can be involved in some kind of docking function of this protein.

4. Materials and Methods

4.1. Chemicals

All of the chemicals were of the highest purity commercially available and used without further purification. Ammonium bicarbonate, calcium chloride, phosphate buffered saline (PBS), Tris-HCl, Triton X-100, sucrose, mannitol, ethylene glycol tetraacetic acid (EGTA), ethylenediaminetetraacetic acid (EDTA), 4-(2-hydroxyethyl)-1-piperazineethanesulfonic acid (HEPES), formic acid (FA), dithiothreitol (DTT), iodoacetamide (IAA), and fetal bovine serum (FBS) were obtained from Sigma–Aldrich (Milan, Italy). IMDM (Iscove's Modified Dulbecco's Medium containing L-glutamine and 25 mM HEPES) was obtained from Gibco-Thermo Fisher Scientific. Human HAP1 cells were from Horizon Discovery (Cambridge, United Kingdom UK). Modified porcine trypsin and chymotrypsin were purchased from Promega (Milan, Italy). Water and acetonitrile (OPTIMA®LC/MS grade) for LC/MS analyses were provided from Fisher Scientific (Milan, Italy).

4.2. Extraction of Proteins from Human HAP1 Cell Culture Mitochondria Under Reducing Condition

Human HAP1 cells were cultured in monolayer (75 cm^2 tissue culture flask) until 75% confluence while using IMDM that was supplemented with 10% FBS and 1% penicillin/streptomycin (Invitrogen, Carlsbad, CA, USA). The cells were maintained in a humidified incubator at 37 °C with 5% CO_2. For mitochondria preparation, HAP1 cells were harvested by EDTA and washed with PBS three times before disruption. Every PBS wash was eliminated by centrifugation at 1500× *g* for five minutes at 4 °C [26].

The total cell pellet that was obtained was resuspended in 1 ml of hypotonic buffer (200 mM mannitol, 70 mM sucrose, 10 mM HEPES pH 7.5, 1 mM EGTA pH 8.0). The cells were incubated in ice for 10 min and then lysed. The lysate obtained was centrifuged (700× *g* for 25 min at 4 °C) to eliminate the non-lysed cells and the nuclei. To have a better yield, after recovering the supernatant, the pellet

containing the mitochondria, was again suspended in hypotonic buffer. Again, the suspension was first lysed and then centrifuged (700× *g* for 25 min at 4 °C).

The resulting supernatants from the two centrifugations were combined and then centrifuged at higher speed (7000× *g* for 15 min at 4 °C). The supernatant, containing the cytoplasmic fraction, was removed, while the pellet was washed with hypotonic buffer. The suspension was then centrifuged at high speed (7000× *g* for 15 min at 4 °C) and at the end, after removing the supernatant, the pellet containing the mitochondria was resuspended in 500 µL of hypotonic buffer and stored at 4 °C.

The total yield was determined by micro-Lowry method, resulting 3.65 g/L. The hypotonic buffer was then removed by centrifugation (10,000× *g* for 20 min at 4 °C). Reduction/alkylation was carried on before VDACs purification to avoid any possible artefact due to air exposure. 1.83 mg protein of intact mitochondria were incubated for 3 h at 4 °C in 1 ml of Tris-HCl 10 mM (pH 8.3) containing 0.037 mmol of DTT, which corresponds to an excess of 50:1 (mol/mol) over the estimated protein thiol groups. The temperature was kept at 4 °C to avoid possible reduction of methionine sulfoxide to methionine by methionine sulfoxide reductase. After centrifugation for 30 min at 10,000× *g* at 4 °C, alkylation was performed by addition of IAA at the 2:1M ratio over DTT for 1 h in the dark at 25 °C. The mixture was centrifuged for 30 min at 10,000× *g* at 4 °C and pellet was stored at −80 °C until further use.

The reduced and alkylated intact mitochondria were lysed in buffer A (10 mM Tris-HCl, 1 mM EDTA, 3% Triton X-100, pH 7.0) at a ratio 5:1 (mitochondria mg/buffer volume mL) [27] for 30 min. on ice and centrifuged at 17,400× *g* for 30 min. at 4 °C. The supernatant containing mitochondrial proteins was subsequently loaded onto a homemade glass column 5 × 80 mm, packed with 0.6 g of dry hydroxyapatite (Bio-Gel HTP, Biorad, Milan, Italy) [27]. The column was eluted with buffer A at 4 °C and fractions of 500 µL were collected and tested for protein content by a fluorometer assay (Invitrogen Qubit™ Protein Assay kit, ThermoFisher Scientific, Milan, Italy). Fractions containing proteins were pooled and dried under vacuum. The hydroxyapatite eluate was divided in two aliquots, which were reduced to less than 100 µL and then purified from non-protein contaminating molecules with the PlusOne 2-D Clean-Up kit (GE Healthcare Life Sciences, Milan, Italy), according to the manufacturer's instructions. The desalted protein pellet was suspended in 100 µL of 50 mM ammonium bicarbonate (pH 8.3) and incubated at 4 °C for 15 min. Next, 100 µL of 0.2% RapiGest SF (Waters, Milan, Italy) in 50 mM ammonium bicarbonate were added and the samples were kept at 4 °C for 30 min. Another aliquot of desalted protein pellet was suspended in 100 µL of 100 mM Tris-HCl, 10 mM calcium chloride (pH 8.0) and then incubated at 4 °C for 15 min. Next, 100 µL of 0.2% RapiGest SF in 100 mM Tris-HCl, 10 mM calcium chloride, were added and the samples were kept at 4 °C for 30 min. For each fraction, the recovered protein amount was determined in 40 µg by using a fluorometer assay. Reduced and alkylated proteins were then separately subjected to digestion while using modified porcine trypsin and chymotrypsin, respectively. Tryptic digestion was carried out at an enzyme-substrate ratio of 1:50 at 37 °C for 4 h; chymotryptic digestion was performed in Tris-HCl 100 mM, 10mM calcium chloride (pH 8.0) at an enzyme-substrate ratio of 1:20 overnight at 25 °C.

4.3. Liquid Chromatography and Tandem Mass Spectrometry (LC–MS/MS) Analysis

Mass spectrometry data were acquired on an Orbitrap Fusion Tribrid (Q-OT-qIT) mass spectrometer (ThermoFisher Scientific, Bremen, Germany) that was equipped with a ThermoFisher Scientific Dionex UltiMate 3000 RSLCnano system (Sunnyvale, CA, USA). Samples that were obtained by in-solution tryptic and chymotryptic digestion were reconstituted in 100 µL of 5% FA aqueous solution and 1 µL was loaded onto an Acclaim Trap® C18 column (100 µm i.d.×2 cm, 5 µm particle size, 100 Å). After washing the trapping column with solvent A (H_2O + 0.1% FA) for 3 min. at a flow rate of 7 µL/min., the peptides were eluted from the trapping column onto a PepMap®RSLC C18 EASYSpray, 75 µm × 50 cm, 2 µm, 100 Å column and were separated by elution at a flow rate of 0.250 µL/min., at 40 °C, with a linear gradient of solvent B (CH_3CN + 0.1% FA) in A from 5% to 20% in 32 min., followed by 20% to 40% in 30 min., and 40% to 60% in 20 min. The eluted peptides were ionized by a nanospray (Easy-spray ion source, Thermo Scientific) while using a spray voltage of 1.7 kV and

introduced into the mass spectrometer through a heated ion transfer tube (275 °C). The survey scans of peptide precursors in the m/z range 400–1600 were performed at resolution of 120,000 (@ 200 m/z) with a AGC target for Orbitrap survey of 4.0×10^5 and a maximum injection time of 50 ms. Tandem MS was performed by isolation at 1.6 Th with the quadrupole, and high energy collisional dissociation (HCD) was performed in the Ion Routing Multipole (IRM), while using a normalized collision energy of 35 and rapid scan MS analysis in the ion trap. Only those precursors with charge state 1–3 and intensity above the threshold of $5{\cdot}10^3$ were sampled for MS^2. The dynamic exclusion duration was set to 60 s with a 10 ppm tolerance around the selected precursor and its isotopes. Monoisotopic precursor selection was turned on. The AGC target and maximum injection time (ms) for MS/MS spectra were 1.0×10^4 and 100, respectively. The instrument was run in top speed mode with 3 s cycles, meaning that the instrument would continuously perform MS^2 events until the list of non-excluded precursors diminishes to zero or 3 s, whichever is shorter. MS/MS spectral quality was enhanced, enabling the parallelizable time option (i.e., by using all parallelizable time during full scan detection for MS/MS precursor injection and detection). Mass spectrometer calibration was performed while using the Pierce®LTQ Velos ESI Positive Ion Calibration Solution (Thermo Fisher Scientific). MS data acquisition was performed using the Xcalibur v. 3.0.63 software (Thermo Fisher Scientific).

4.4. Database Search

The LC–MS/MS data were processed by PEAKS software v. 8.5 (Bioinformatics Solutions Inc., Waterloo, ON, Canada). The data were searched against the 49,544 entries "Human" SwissProt database (release June 2019) Full tryptic or chymotrypsin peptides with a maximum of three missed cleavage sites were subjected to bioinformatic search. Cysteine carboxyamidomethylation was set as fixed modification, whereas the acetylation of protein N-terminal, trioxidation of cysteine, oxidation of methionine, and transformation of N-terminal glutamine and N-terminal glutamic acid residue in the pyroglutamic acid form were included as variable modifications. The precursor mass tolerance threshold was 10 ppm and the max fragment mass error was set to 0.6 Da. Finally, all of the protein hits obtained were processed by using the *inChorus* function of PEAKS. This tool combines the database search results of PEAKS software with those that were obtained by the Mascot search engine with the aim not only to increase the coverage, but also the confidence, since the engines using independent algorithms and, therefore, confirm each other's' results. Peptide spectral matches (PSM) were validated while using Target Decoy PSM Validator node based on q-values at a 0.1% False Discovery Rate (FDR).

The mass spectrometry proteomics data have been deposited to the ProteomeXchange Consortium (http://proteomecentral.proteomexchange.org) via the PRIDE partner repository [28] with the dataset identifier PXD017482.

5. Conclusions

The panoramic view of sulfur amino acids modification state of VDAC in mammals provides new, exciting perspectives for future researches aiming to unravel the role of each VDAC isoform in the control of OMM permeability, in the response to the ROS oxidative pressure on IMS, and, in general, on the mitochondrial quality control. From a technical point of view, the identification of disulfide bridge(s) is the next, highly challenging goal of our research.

Supplementary Materials: Supplementary materials can be found at http://www.mdpi.com/1422-0067/21/4/1468/s1.

Author Contributions: R.S., V.D.P. and S.F. conceived the project and prepared the original draft of the paper. M.G.G.P. and S.R. performed cells culture and sample isolation and preparation for proteomic analysis. R.S. and V.C. performed HPLC/MS experiments. M.G.G.P. and R.S. performed mass spectrometry data analysis by informatics software. All authors provided intellectual input to the study, reviewed, edited and approved the manuscript. All authors have read and agreed to the published version of the manuscript.

Funding: This research was partly supported by "Piano della Ricerca di Ateneo 2016-2018" of the University of Catania, Italy, and by MIUR (PRIN 2015795S5W_005 to VDP).

Acknowledgments: The authors gratefully acknowledge the Bio-Nanotech Research and Innovation Tower (BRIT; PON project financed by the Italian Ministry for Education, University and Research MIUR). The authors acknowledge Salvatore A.M. Cubisino for the structural images in Figure S11.

Conflicts of Interest: The authors declare no conflict of interest.

Abbreviations

PBS	phosphate buffered saline
EGTA	ethylene glycol tetraacetic acid
EDTA	ethylenediaminetetraacetic acid
FA	formic acid
HEPES	4-(2-hydroxyethyl)-1-piperazineethanesulfonic acid
DTT	dithiothreitol
IAA	iodoacetamide
FBS	fetal bovine serum
IMDM	Iscove's Modified Dulbecco's Medium

References

1. Reina, S.; De Pinto, V. Anti-cancer compounds targeted to VDAC: Potential and perspectives. *Curr. Med. Chem.* **2017**, *24*, 4447–4469. [CrossRef] [PubMed]
2. Magrì, A.; Belfiore, R.; Reina, S.; Tomasello, M.F.; Di Rosa, M.C.; Guarino, F.; Leggio, L.; De Pinto, V.; Messina, A. Hexokinase I N-terminal based peptide prevents the VDAC1-SOD1 G93A interaction and re-establishes ALS cell viability. *Sci. Rep.* **2016**, *6*, 1–14. [CrossRef]
3. Messina, A.; Reina, S.; Guarino, F.; De Pinto, V. VDAC isoforms in mammals. *Biochim. Biophys. Acta* **2012**, *1818*, 1466–1476. [CrossRef] [PubMed]
4. Blachly-Dyson, E.; Zambronicz, E.B.; Yu, W.H.; Adams, V.; McCabe, E.R.; Adelman, J.; Colombini, M.; Forte, M. Cloning and functional expression in yeast of two human isoforms of the outer mitochondrial membrane channel, the voltage-dependent anion channel. *J. Biol. Chem.* **1993**, *268*, 1835–1841. [PubMed]
5. Kleene, R.; Pfanner, N.; Pfaller, R.; Link, T.A.; Sebald, W.; Neupert, W.; Tropschug, M. Mitochondrial porin of Neurospora crassa: cDNA cloning, in vitro expression and import into mitochondria. *Embo J.* **1987**, *6*, 2627–2633. [CrossRef]
6. Messina, A.; Neri, M.; Perosa, F.; Caggese, C.; Marino, M.; Caizzi, R.; De Pinto, V. Cloning and chromosomal localization of a cDNA encoding a mitochondrial porin from Drosophila melanogaster. *FEBS Lett.* **1996**, *384*, 9–13. [CrossRef]
7. Troll, H.; Malchow, D.; Muller-Taubenberger, A.; Humbel, B.; Lottspeich, F.; Ecke, M.; Gerisch, G.; Schmid, A.; Benz, R. Purification, functional characterization, and cDNA sequencing of mitochondrial porin from Dictyostelium discoideum. *J. Biol. Chem.* **1992**, *267*, 21072–21079.
8. Menzel, V.A.; Cassarà, M.C.; Benz, R.; De Pinto, V.; Messina, A.; Cunsolo, V.; Saletti, R.; Hinsch, K.D.; Hinsch, E. Molecular and functional characterization of VDAC2 purified from mammal spermatozoa. *Biosci. Rep.* **2009**, *29*, 351–362. [CrossRef]
9. Reina, S.; Checchetto, V.; Saletti, R.; Gupta, A.; Chaturvedi, D.; Guardiani, C.; Guarino, F.; Scorciapino, M.A.; Magrì, A.; Foti, S.; et al. VDAC3 as a sensor of oxidative state of the intermembrane space of mitochondria: The putative role of cysteine residue modifications. *Oncotarget* **2016**, *7*, 2249–2268. [CrossRef]
10. Saletti, R.; Reina, S.; Pittalà, M.G.G.; Belfiore, R.; Cunsolo, V.; Messina, A.; De Pinto, V.; Foti, S. High resolution mass spectrometry characterization of the oxidation pattern of methionine and cysteine residues in rat liver mitochondria Voltage-Dependent Anion selective Channel 3 (VDAC3). *Biochim. Biophys. Acta Biomembr.* **2017**, *1859*, 301–311. [CrossRef]
11. Saletti, R.; Reina, S.; Pittalà, M.G.G.; Magrì, A.; Cunsolo, V.; Foti, S.; De Pinto, V. Post-translational modifications of VDAC1 and VDAC2 cysteines from rat liver mitochondria. *Biochim. Biophys. Acta Bioenerg.* **2018**, *1859*, 806–816. [CrossRef] [PubMed]
12. Guan, Z.Q.; Yates, N.A.; Bakhtiar, R. Detection and characterization of methionine oxidation in peptides by collision-induced dissociation and electron capture dissociation. *J. Am. Soc. Mass Spectrom.* **2003**, *14*, 605–613. [CrossRef]

13. Gupta, A.; Mahalakshmi, R. Helix–strand interaction regulates stability and aggregation of the human mitochondrial membrane protein channel VDAC3. *J. Gen. Physiol.* **2019**, *151*, 489–504. [CrossRef] [PubMed]
14. Stadtman, E.R.; Moskovitz, J.; Levine, R.L. Oxidation of methionine residues of proteins: Biological consequences. *Antioxid. Redox Signal.* **2003**, *5*, 577–582. [CrossRef] [PubMed]
15. Stadtman, E.R. Protein oxidation and aging. *Free Radic. Res.* **2006**, *40*, 1250–1258. [CrossRef] [PubMed]
16. Ugarte, N.; Petropoulos, I.; Friguet, B. Oxidized mitochondrial protein degradation and repair in aging and oxidative stress. *Antioxid. Redox Signal.* **2010**, *13*, 539–549. [CrossRef]
17. Levine, R.L.; Mosoni, L.; Berlett, B.S.; Stadtman, E.R. Methionine residues as endogenous antioxidants in proteins. *Proc. Natl. Acad. Sci. USA* **1996**, *93*, 15036–15040. [CrossRef]
18. Stadtman, E.R.; Moskovitz, J.; Berlett, B.S.; Levine, R.L. Cyclic oxidation and reduction of protein methionine residues is an important antioxidant mechanism. *Mol. Cell Biochem.* **2002**, *234*, 3–9. [CrossRef]
19. Bachi, A.; Dalle-Donne, I.; Scaloni, A. Redox proteomics: Chemical principles, methodological approaches and biological/biomedical promises. *Chem. Rev.* **2013**, *113*, 596–698. [CrossRef]
20. Zaid, H.; Abu-Hamad, S.; Israelson, A.; Nathan, I.; Shoshan-Barmatz, V. The voltage-dependent anion channel-1 modulates apoptotic cell death. *Cell Death Differ.* **2005**, *12*, 751–760. [CrossRef]
21. Abu-Hamad, S.; Zaid, H.; Israelson, A.; Nahon, E.; Shoshan-Barmatz, V. Hexokinase-I protection against apoptotic cell death is mediated via interaction with the voltage-dependent anion channel-1: Mapping the site of binding. *J. Biol. Chem.* **2008**, *283*, 13482–13490. [CrossRef] [PubMed]
22. Bayrhuber, M.; Meins, T.; Habeck, M.; Becker, S.; Giller, K.; Villinger, S.; Vonrhein, C.; Griesinger, C.; Zweckstetter, M.; Zeth, K. Structure of the human voltage-dependent anion channel. *Proc. Natl. Acad. Sci. USA* **2008**, *105*, 15370–15375. [CrossRef] [PubMed]
23. Mader, A.; Abu-Hamad, S.; Arbel, N.; Gutiérrez-Aguilar, M.; Shoshan-Barmatz, V. Dominant-negative VDAC1 mutants reveal oligomeric VDAC1 to be the active unit in mitochondria-mediated apoptosis. *Biochem. J.* **2010**, *429*, 147–155. [CrossRef] [PubMed]
24. Hiller, S.; Garces, R.G.; Malia, T.J.; Orekhov, V.Y.; Colombini, M.; Wagner, G. Solution structure of the integral human membrane protein VDAC-1 in detergent micelles. *Science* **2008**, *321*, 1206–1210. [CrossRef] [PubMed]
25. Ujwal, R.; Cascio, D.; Colletier, J.P.; Faham, S.; Zhang, J.; Toro, L.; Ping, P.; Abramson, J. The crystal structure of mouse VDAC1 at 2.3 angstrom resolution reveals mechanistic insights into metabolite gating. *Proc. Natl. Acad. Sci. USA* **2008**, *105*, 17742–17747. [CrossRef] [PubMed]
26. Schindler, A.; Foley, E. Hexokinase 1 blocks apoptotic signals at the mitochondria. *Cell. Signal.* **2013**, *25*, 2685–2692. [CrossRef]
27. De Pinto, V.; Benz, R.; Caggese, C.; Palmieri, F. Characterization of the mitochondrial porin from Drosophila melanogaster. *Biochim. Biophys. Acta* **1989**, *905*, 499–502. [CrossRef]
28. Bizcaino, J.A.; Cote, R.G.; Csordas, A.; Dianes, J.A.; Fabregat, A.; Foster, J.M.; Griss, J.; Alpi, E.; Birim, M.; Contell, J.; et al. The Proteomics Identifications (PRIDE) database and associated tools: Status in 2013. *Nucleic Acids Res.* **2013**, *41*, D1063–D1069. [CrossRef]

SUPPLEMENTARY MATERIALS TO:

A High Resolution Mass Spectrometry Study Reveals the Potential of Disulfide Formation in Human Mitochondrial Voltage-Dependent Anion Selective Channel Isoforms (hVDACs)

Maria G.G. Pittalà [1], Rosaria Saletti [2,*], Simona Reina [3], Vincenzo Cunsolo [2], Vito De Pinto [1,*] and Salvatore Foti [2]

[1] Department of Biomedical and Biotechnological Sciences, University of Catania, Via S. Sofia 64, 95123 Catania, Italy

[2] Department of Chemical Sciences, Organic Mass Spectrometry Laboratory, University of Catania, Viale A. Doria 6, 95125 Catania, Italy

[3] Department of Biological, Geological and Environmental Sciences, Section of Molecular Biology, University of Catania, Viale A. Doria 6, 95125 Catania, Italy

Keywords: Cysteine over-oxidation; Mitochondria; Orbitrap Fusion Tribrid; Hydroxyapatite; Mitochondrial intermembrane space; Outer mitochondrial membrane; Post-translational modification.

*Correspondence:

rsaletti@unict.it; Tel: +39 095 738 5026

vdpbiofa@unict.it; Tel: +39 095 7384244

Supplementary Fig.1

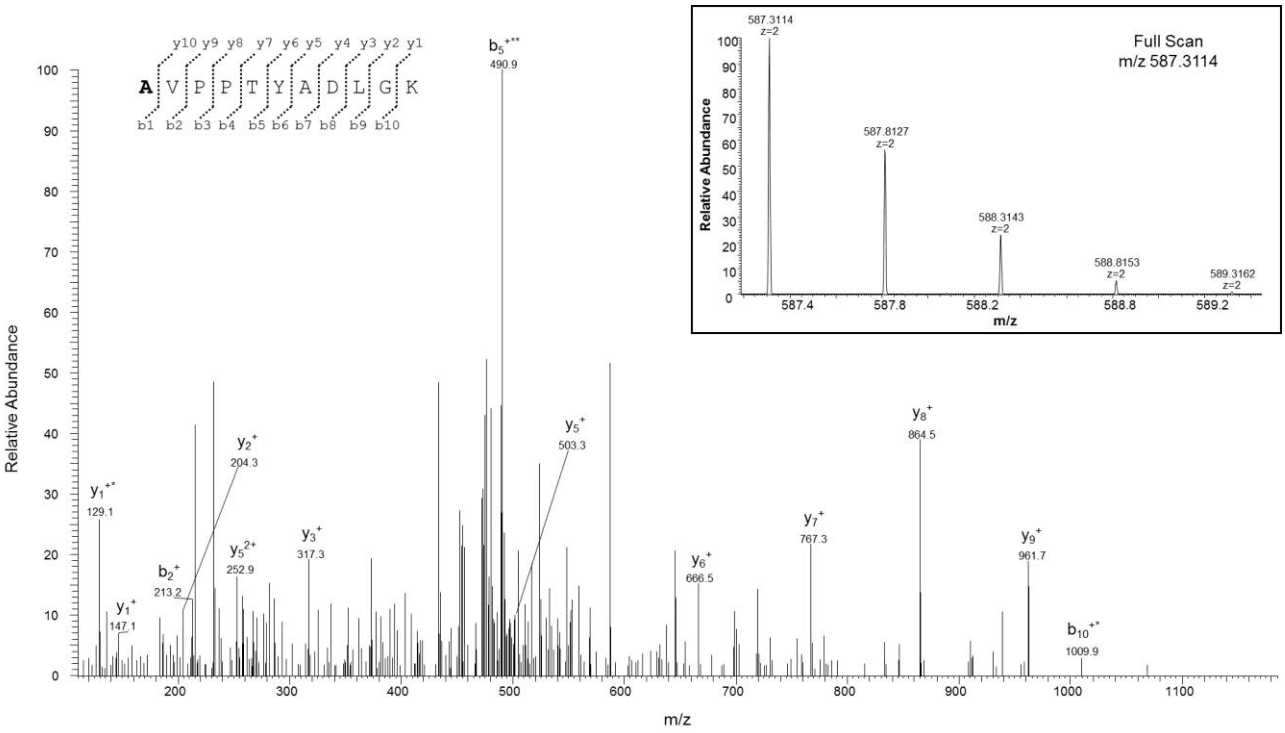

Supplementary Figure S1. MS/MS spectrum of the doubly charged molecular ion at m/z 587.3114 (calculated 587.3111) of the N-terminal acetylated tryptic peptide of VDAC1 from HAP1 cells. The inset shows the full scan mass spectrum of molecular ion. Fragment ions originated from the neutral loss of H_2O are indicated by an asterisk.

Supplementary Fig.2

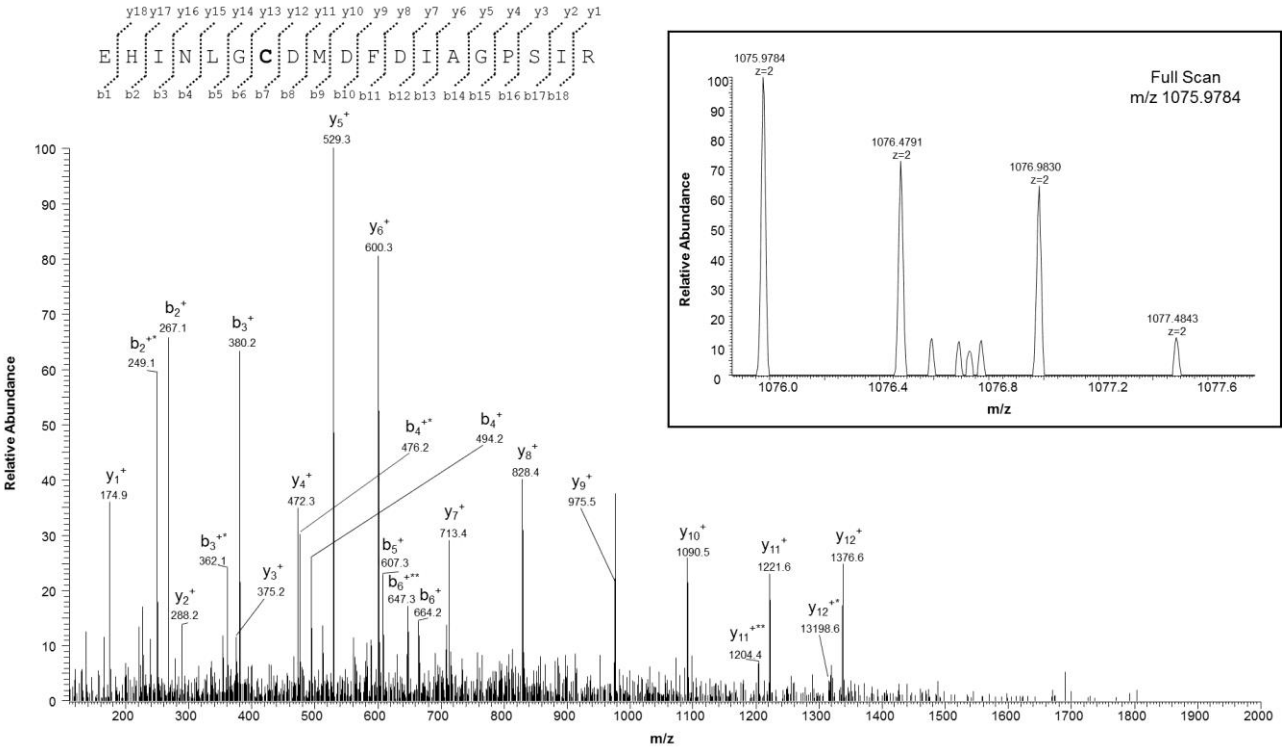

Supplementary Figure S2. MS/MS spectrum of the doubly charged molecular ion at m/z 1075.9784 (calculated 1075.9780) of the VDAC1 tryptic peptide from HAP1 cells containing cysteine residue 127 in the form of sulfonic acid. The inset shows the full scan mass spectrum of molecular ion. Fragment ions originated from the neutral loss of H_2O are indicated by an asterisk. Fragment ions originated from the neutral loss of NH_3 are indicated by two asterisks.

Supplementary Fig.3

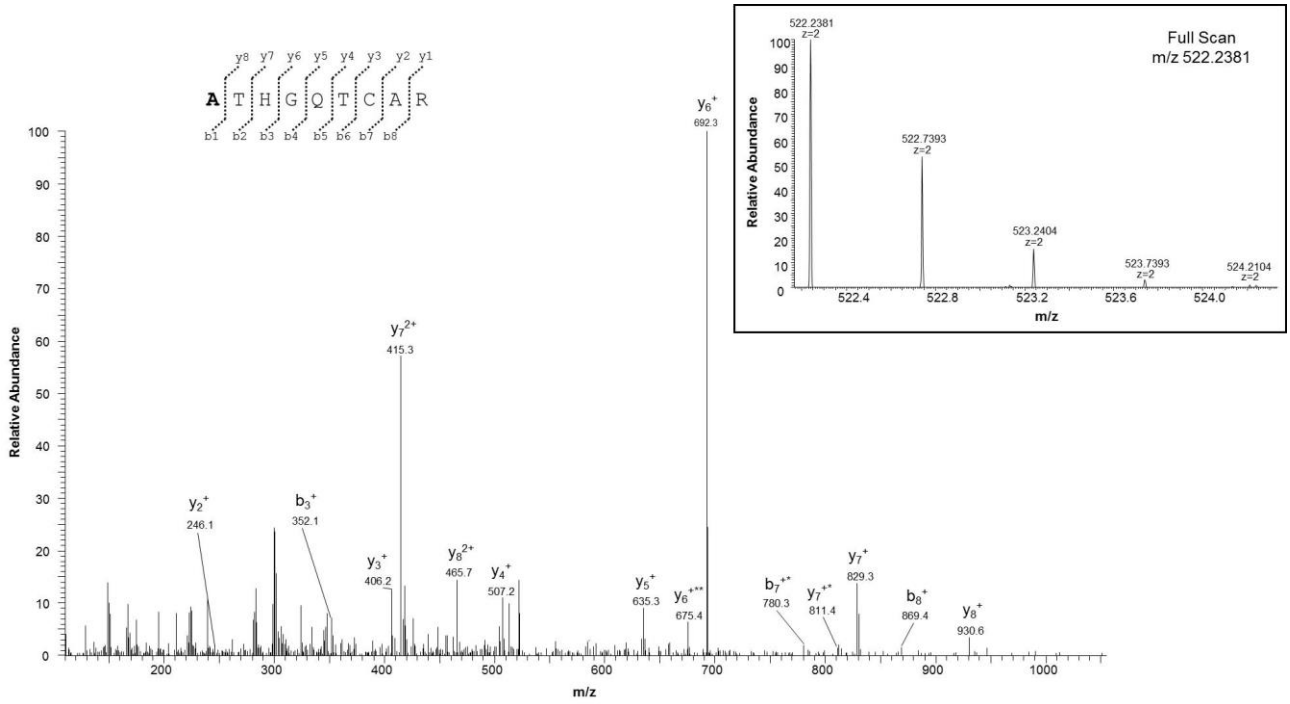

Supplementary Figure S3. MS/MS spectrum of the doubly charged molecular ion at m/z 522.2381 (calculated 522.2380) of the N-terminal acetylated tryptic peptide of VDAC2 from HAP1 cells. The inset shows the full scan mass spectrum of molecular ion. Fragment ions originated from the neutral loss of H_2O are indicated by an asterisk. Fragment ion originated from the neutral loss of NH_3 is indicated by two asterisks.

Supplementary Fig.4

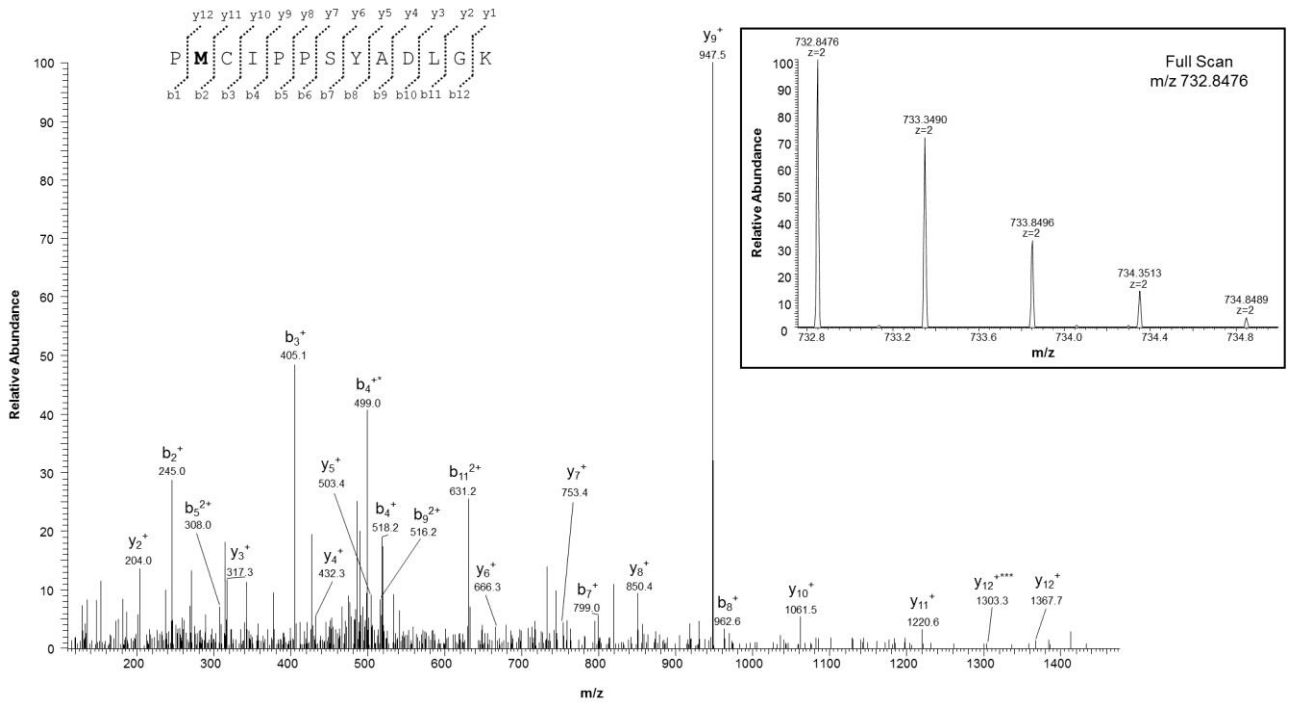

Supplementary Figure S4. MS/MS spectrum of the doubly charged molecular ion at m/z 732.8476 (calculated 732.8470) of the VDAC2 tryptic peptide from HAP1 cells containing methionine residue 12 in the oxidized form of methionine sulfoxide. The inset shows the full scan mass spectrum of molecular ion. Fragment ion originated from the neutral loss of H_2O is indicated by an asterisk. Fragment ion originated from the neutral loss of methanesulfenic acid (CH_2SOH, 64 Da) is indicated by three asterisks.

Supplementary Fig.5

E^{132} C I N L G C D V D F D F A G P A I H G S A V F G Y E G W L A G Y Q **M** T F D S A K^{172}

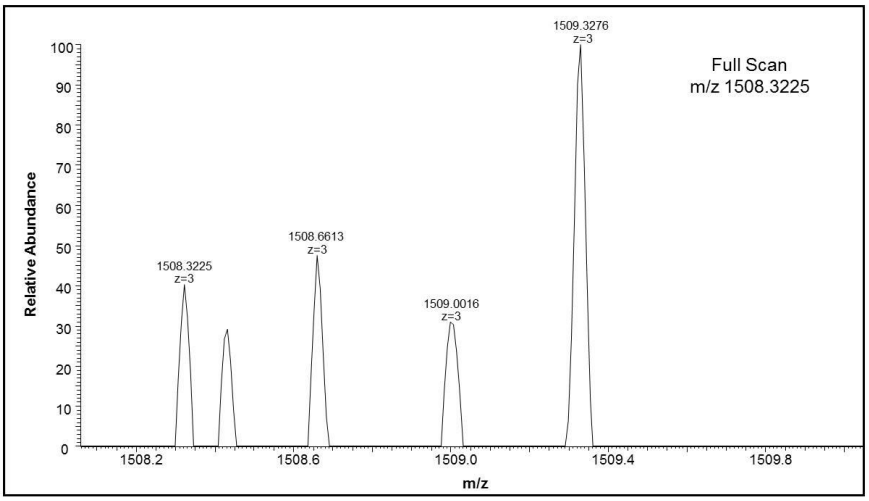

Supplementary Figure S5. Full scan mass spectrum of the triply charged molecular ion at m/z 1058.3225 (calculated 1058.3244) of the VDAC2 tryptic peptide from HAP1 cells containing methionine residue 166 in the oxidized form of methionine sulfoxide and one cysteine residue trioxidized.

Supplementary Fig.6A

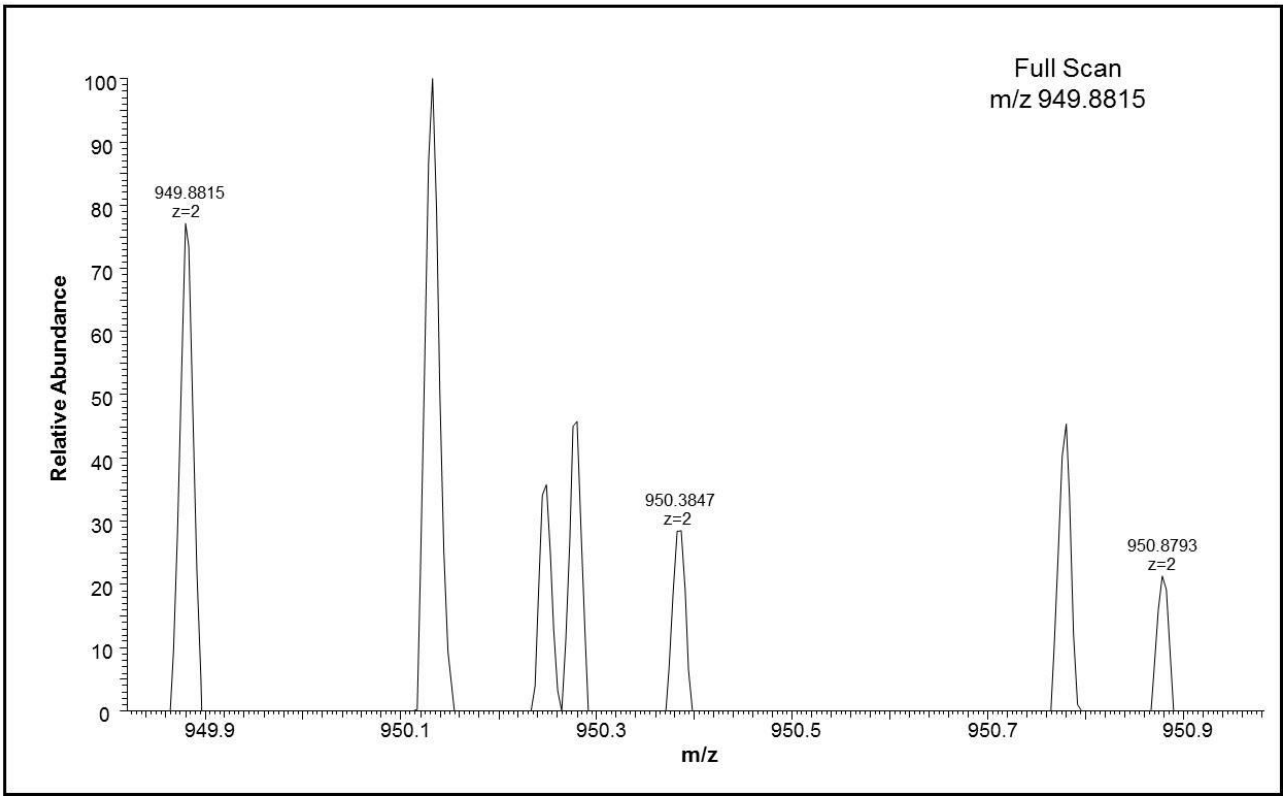

Supplementary Figure S6A. Full scan mass spectrum of the doubly charged molecular ion at m/z 949.8815 (calculated 949.8817) of the VDAC2 tryptic peptide from HAP1 cells containing cysteine residue 47 in the form of sulfonic acid.

Supplementary Fig.6B

B Y^{73} K W **C** E Y G L T F T E K^{85}

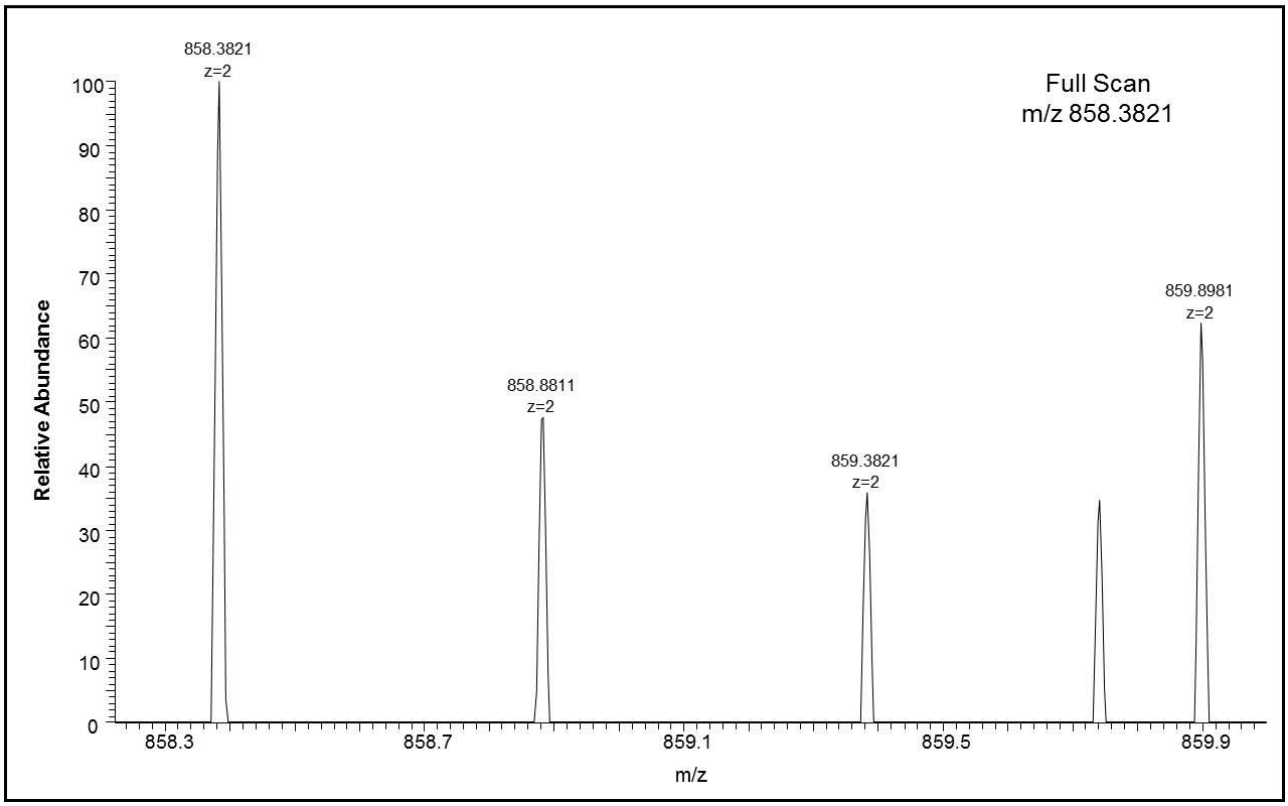

Supplementary Figure S6B. Full scan mass spectrum of the doubly charged molecular ion at m/z 858.3821 (calculated 858.3849) of the VDAC2 tryptic peptide from HAP1 cells containing cysteine residue 76 in the form of sulfonic acid.

Supplementary Fig.6C

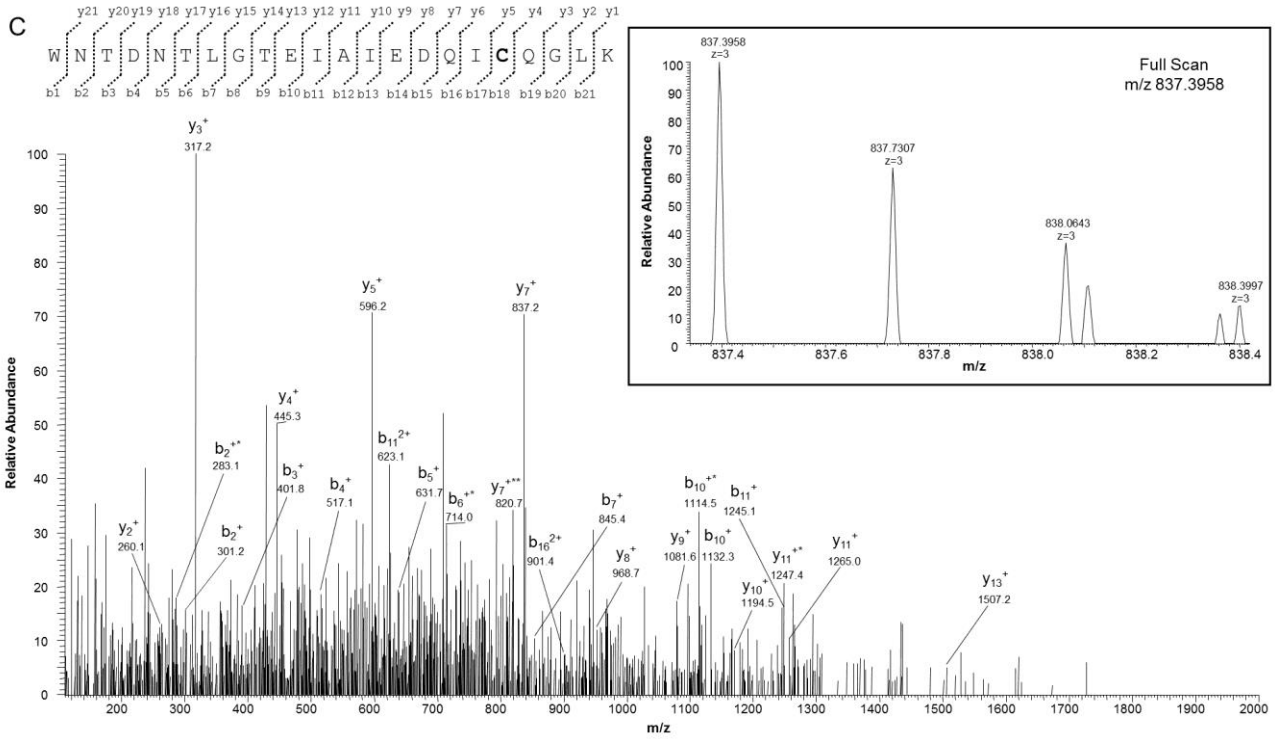

Supplementary Figure S6C. MS/MS spectrum of the triply charged molecular ion at m/z 837.3958 (calculated 837.3957) of the VDAC2 tryptic peptide from HAP1 cells containing cysteine residue 103 in the form of sulfonic acid. The inset shows the full scan mass spectrum of molecular ion. Fragment ions originated from the neutral loss of H_2O are indicated by an asterisk. Fragment ion originated from the neutral loss of NH_3 is indicated by two asterisks.

Supplementary Fig.6D

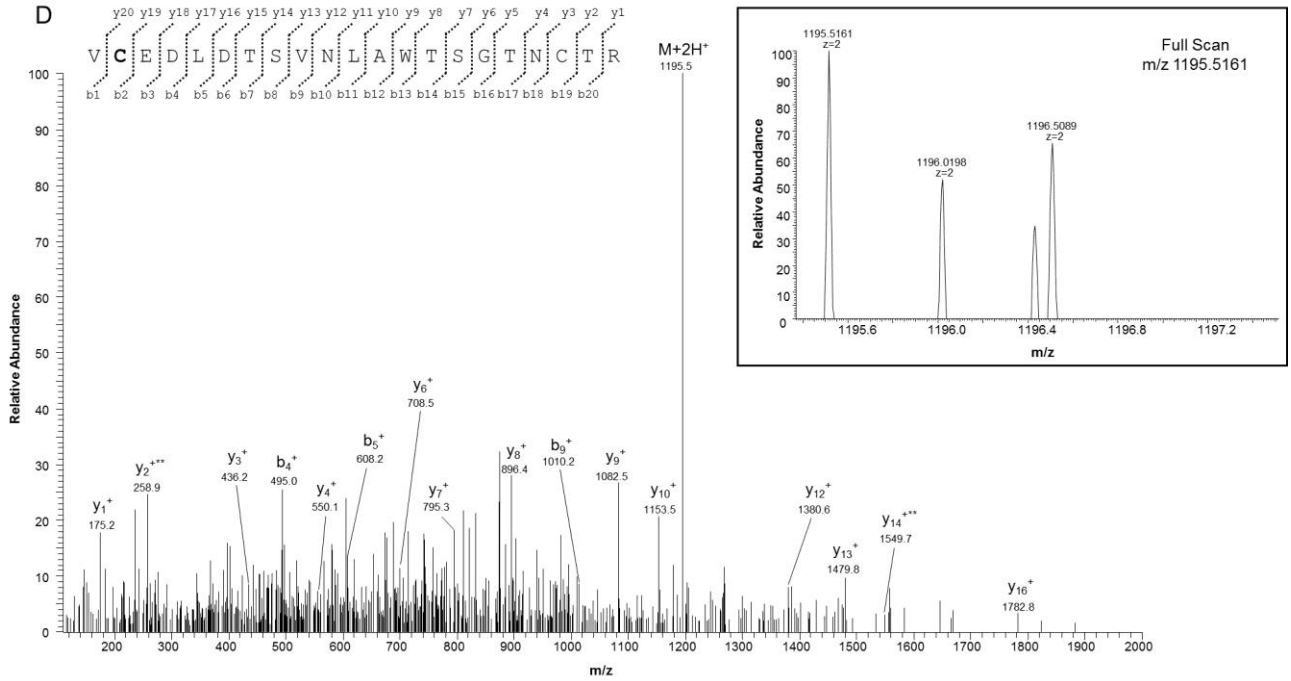

Supplementary Figure S6D. Full scan mass spectrum of the doubly charged molecular ion at m/z 1195.5161 (calculated 1195.5157) of the VDAC2 tryptic peptide from HAP1 cells containing cysteine residue 210 in the form of sulfonic acid. The inset shows the full scan mass spectrum of molecular ion. Fragments ions originated from the neutral loss of NH_3 are indicated by two asterisks.

Supplementary Fig.7

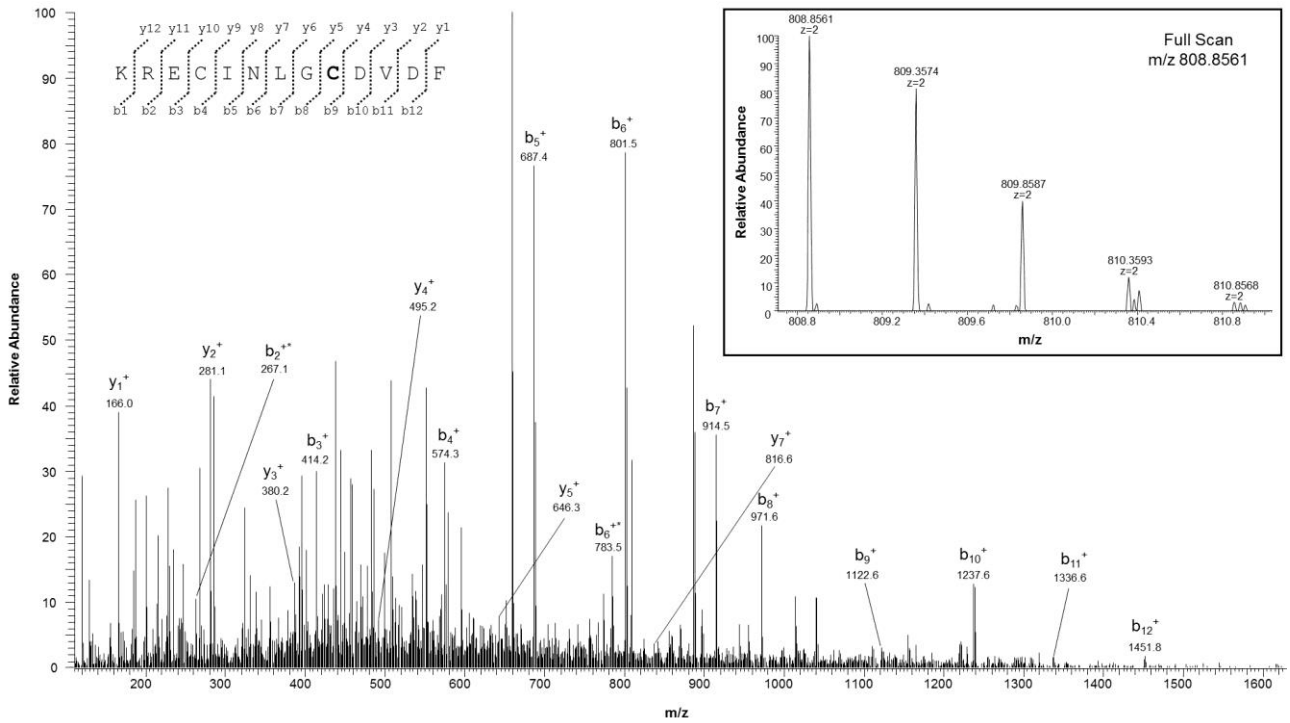

Supplementary Figure S7. MS/MS spectrum of the doubly charged molecular ion at m/z 808.8561 (calculated 808.8565) of the VDAC2 chymotryptic peptide from HAP1 cells containing cysteine residue 138 in the form of sulfonic acid. The inset shows the full scan mass spectrum of molecular ion. Fragment ions originated from the neutral loss of H_2O are indicated by an asterisk.

Supplementary Fig.8

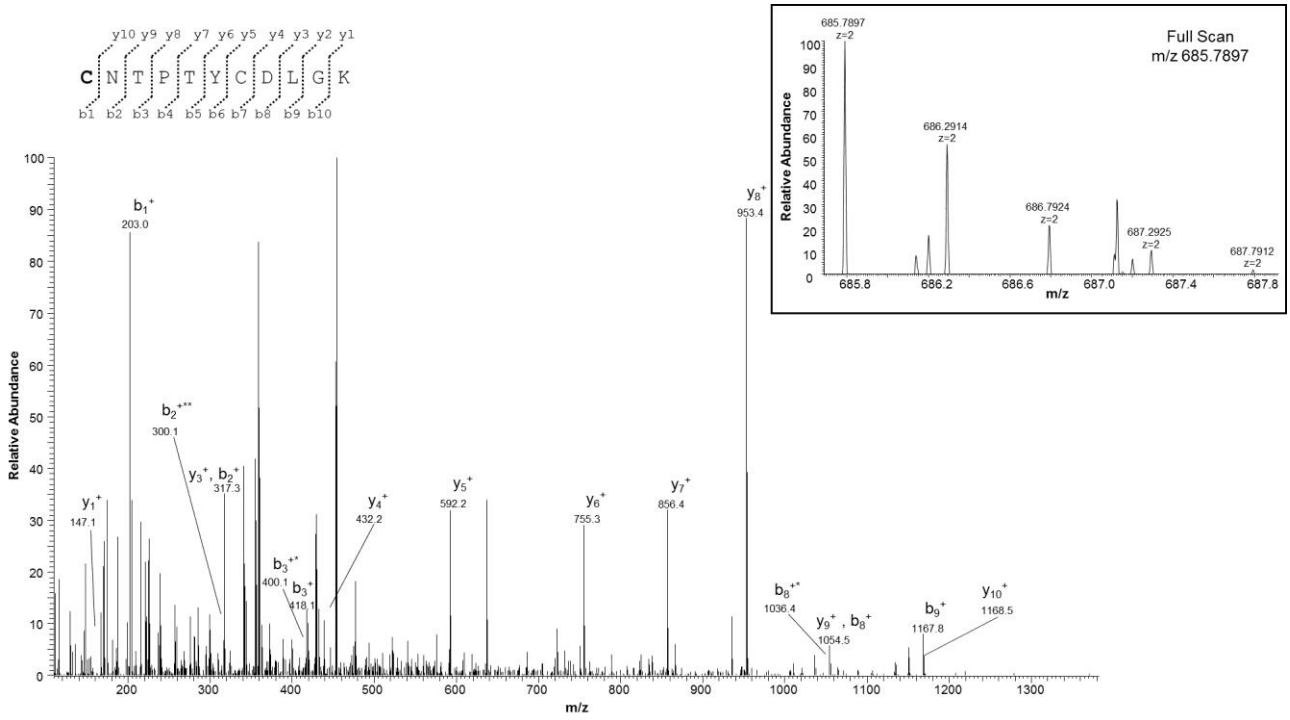

Supplementary Figure S8. MS/MS spectrum of the doubly charged molecular ion at m/z 685.7897 (calculated 685.7894) of the N-terminal acetylated tryptic peptide of VDAC3 from HAP1 cells with Cys^2 and Cys^8 in the carboxyamidomethylated form. The inset shows the full scan mass spectrum of molecular ion. Fragment ions originated from the neutral loss of H_2O are indicated by an asterisk. Fragment ion originated from the neutral loss of NH_3 is indicated by two asterisks.

Supplementary Fig.9A

A

G^{21} Y G F G **M** V K^{28}

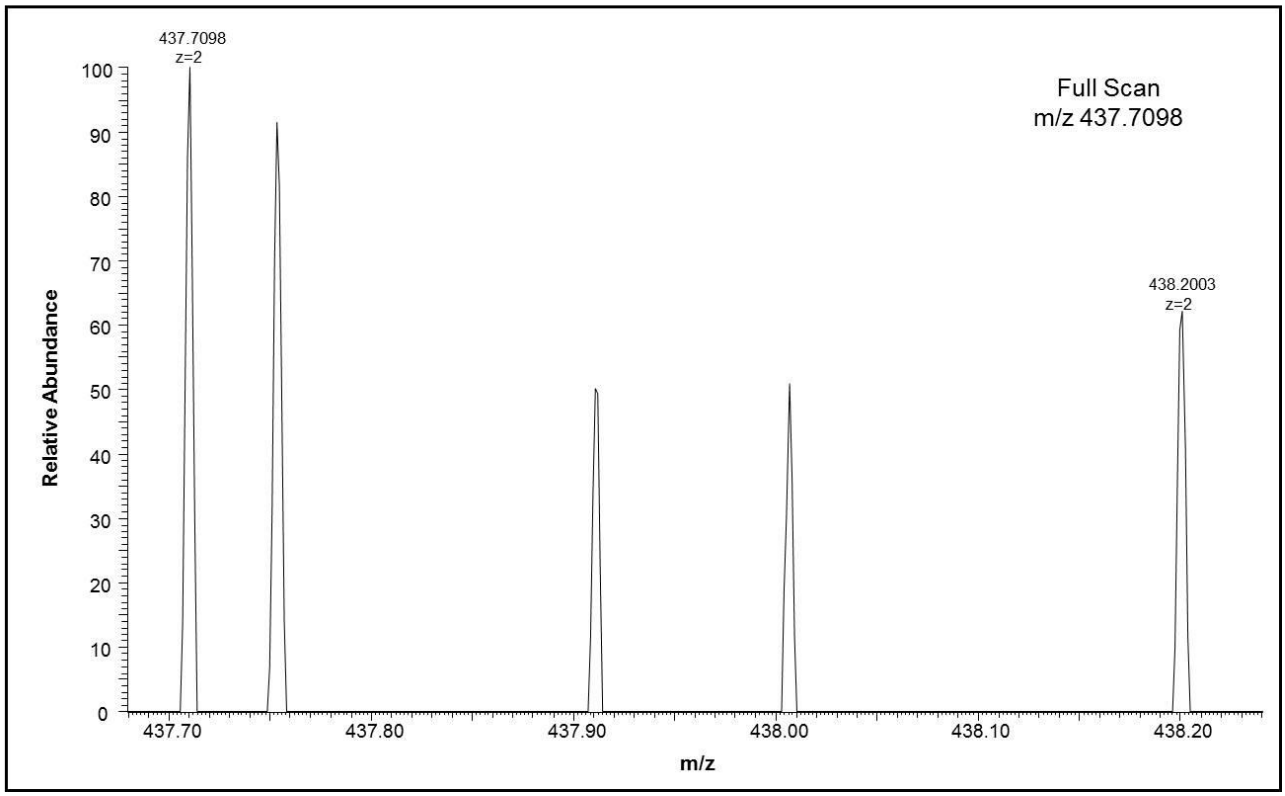

Supplementary Figure S9A. MS spectrum of the doubly charged molecular ion at m/z 437.7098 (calculated 437.7103) of the VDAC3 tryptic peptide from HAP1 cells containing methionine residue 26 in the oxidized form of methionine sulfoxide.

Supplementary Fig.9B

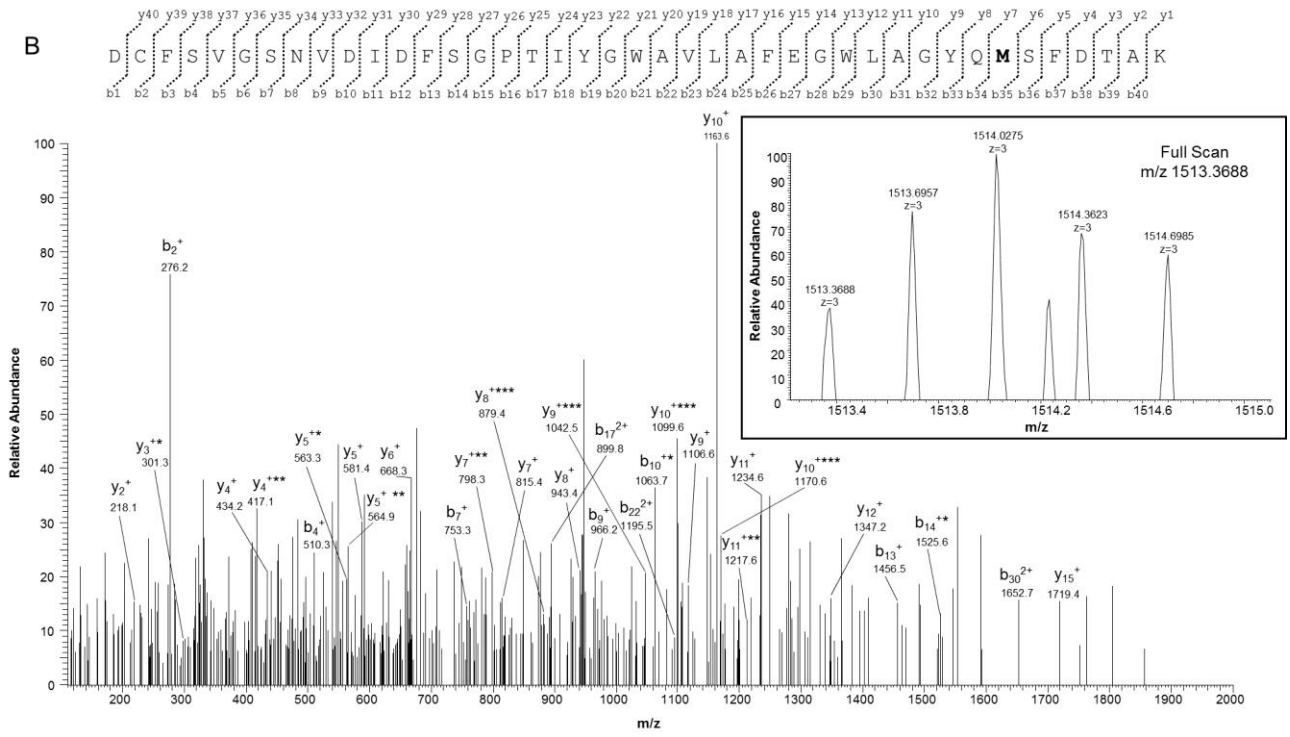

Supplementary Figure S9B. MS/MS spectrum of the triply charged molecular ion at m/z 1513.3688 (calculated 1513.3596) of the VDAC3 tryptic peptide from HAP1 cells containing methionine residue 155 in the oxidized form of methionine sulfoxide. The inset shows the full scan mass spectrum of molecular ion. Fragment ions originated from the neutral loss of H_2O are indicated by an asterisk. Fragment ions originated from the neutral loss of NH_3 are indicated by two asterisks. Fragment ions originated from the neutral loss of methanesulfenic acid (CH_2SOH, 64 Da) are indicated by three asterisks.

Supplementary Fig.9C

C

Y^{225} **M** L D C R^{230}

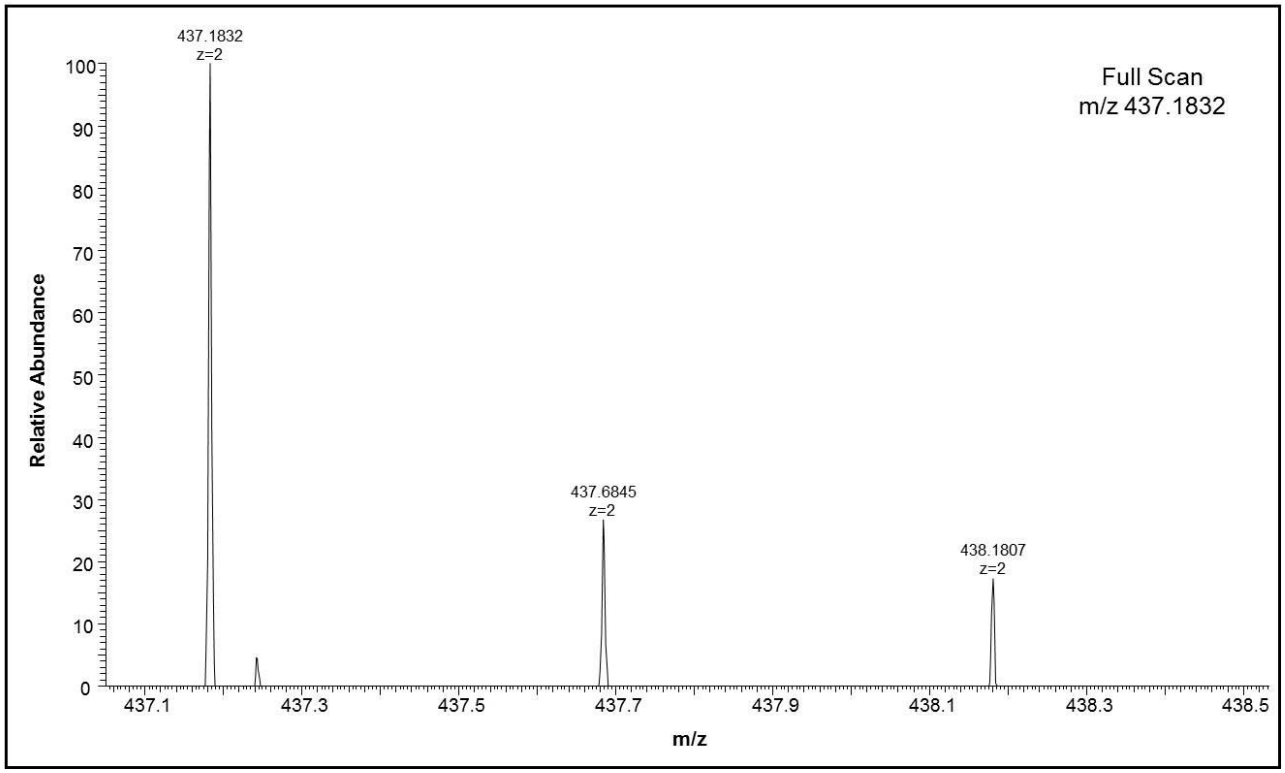

Supplementary Figure S9C. Full scan mass spectrum of the doubly charged molecular ion at m/z 437.1832 (calculated 437.1836) of the VDAC3 tryptic peptide from HAP1 cells containing methionine residue 226 in the oxidized form of methionine sulfoxide.

Supplementary Fig.10A

A S^{35} **C** S G V E F S T S G H A Y T D T G K^{53}

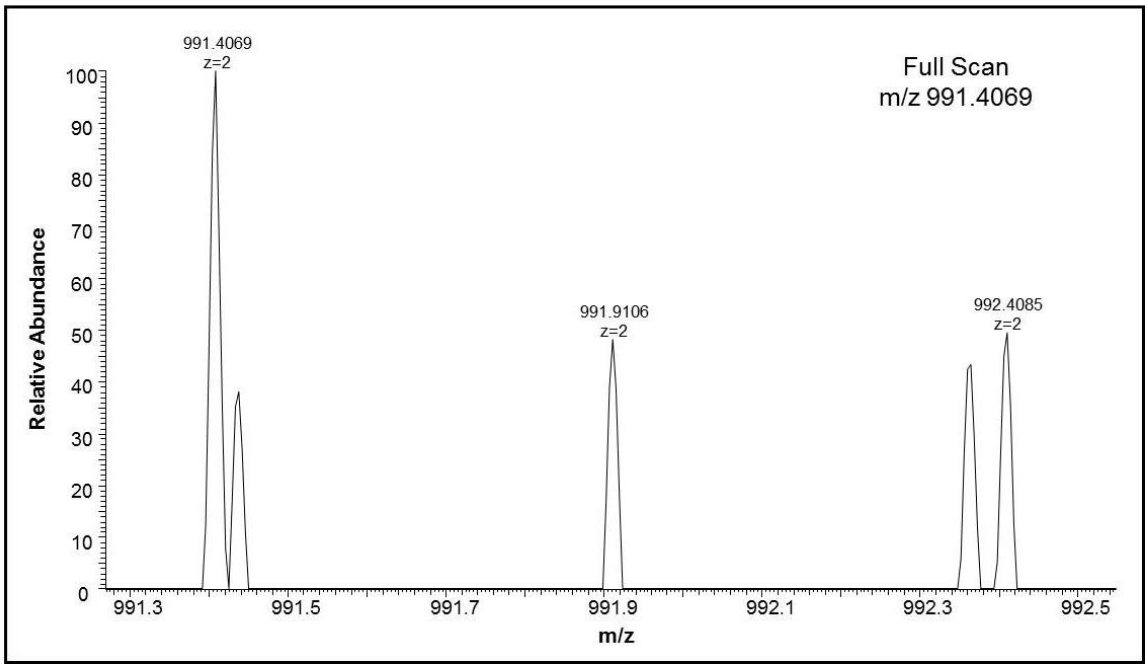

Supplementary Figure S10A. Full scan mass spectrum of the doubly charged molecular ion at m/z 991.4069 (calculated 991.4079) of the VDAC3 tryptic peptide from HAP1 cells containing cysteine residue 36 in the form of sulfonic acid.

Supplementary Fig.10B

B Y^{62} K V **C** N Y G L T F T Q K^{74}

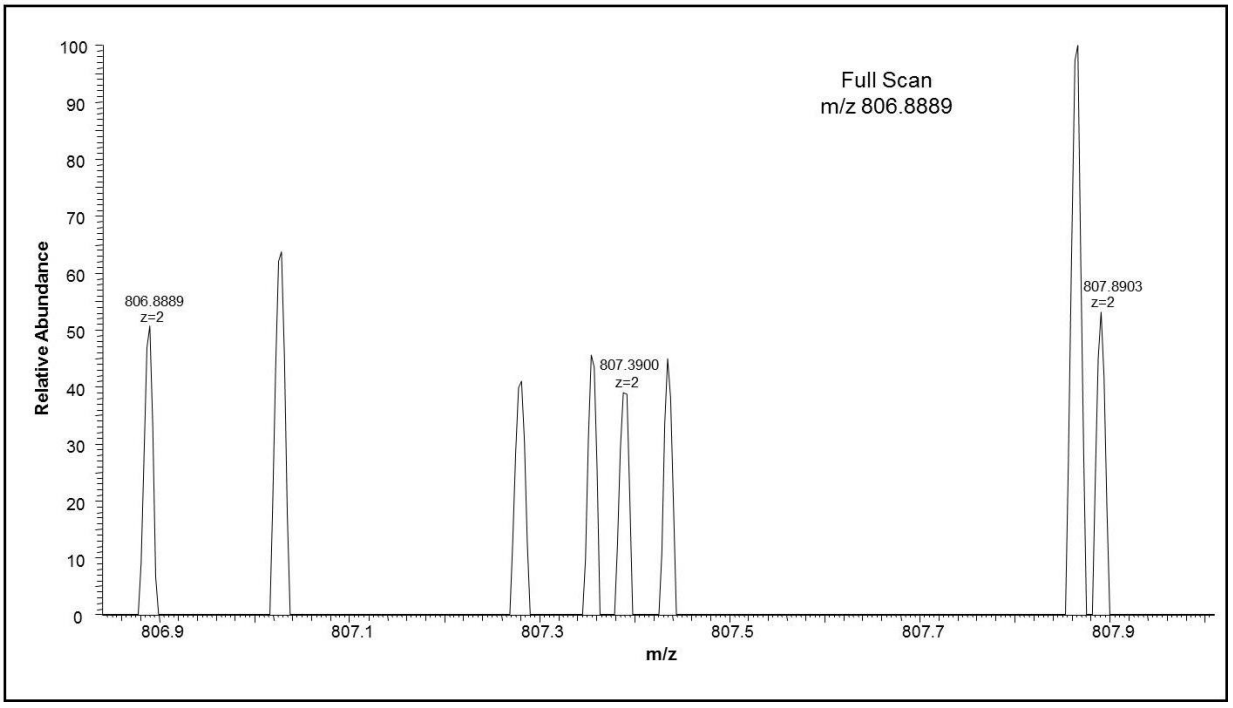

Supplementary Figure S10B. Full scan mass spectrum of the doubly charged molecular ion at m/z 806.8889 (calculated 806.8877) of the VDAC3 tryptic peptide from HAP1 cells containing cysteine residue 65 in the form of sulfonic acid.

Supplementary Fig.11

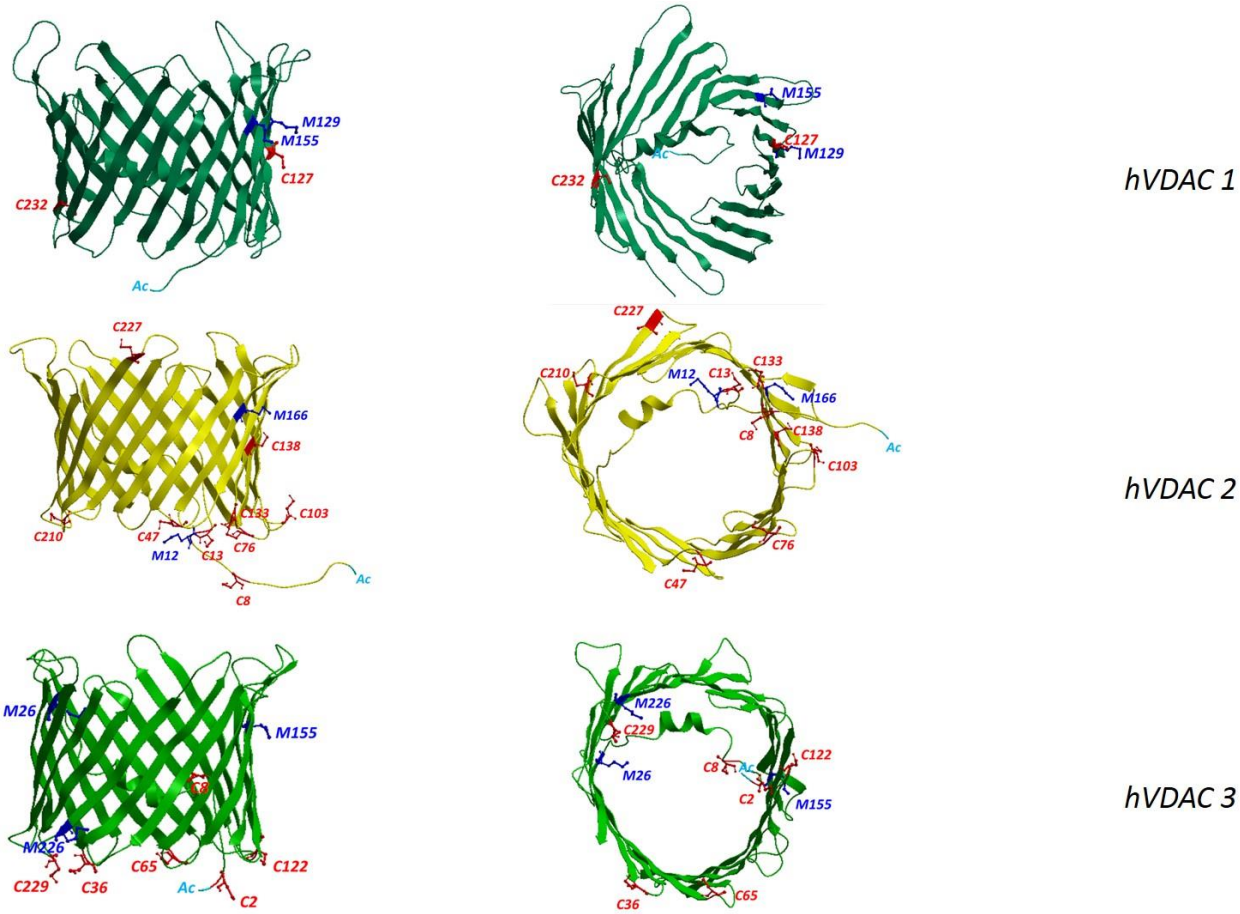

Supplementary Figure S11. Side and top views of human VDACs where the cysteine and methionine positions have been indicated. The structures are predicted by homology modelling, using hVDAC1 structure (pdb: 5XDO) as a template.

Supplementary Tables

Table S1. Tryptic peptides found in hVDAC1 after DTT reduction and carboxyamidomethylation.

Retention time, experimentally measured and calculated monoisotopic m/z of the molecular ions, position in the sequence and peptide sequence of fragments present in the tryptic digest of reduced and carboxyamidomethylated hVDAC1 are reported. All sequences were confirmed by MS/MS. These sequences were used to build the sequence coverage reported in Figure 1.

Frag. n.	Rt (min)	Monoisotopic m/z		Position in the sequence	Peptide sequence
		Measured	Calculated		
1	52.77	587.3114 (+2)	587.3111	2-12	*AVPPTYADLGK
2	77.18	744.3970 (+2)	744.3963	2-15	*AVPPTYADLGKSAR
3	80.15	693.3687 (+3)	693.3687	2-20	*AVPPTYADLGKSARDVFTK
4	79.64	462.2510 (+2)	462.2509	13-20	SARDVFTK
5	82.18	586.9897 (+3)	586.9894	13-28	SARDVFTKGYGFGLIK
6	82.96	743.4203 (+3)	743.4194	13-32	SARDVFTKGYGFGLIKLDLK
7	74.53	638.6965 (+3)	638.6960	16-32	DVFTKGYGFGLIKLDLK
8	71.47	427.7420 (+2)	427.7422	21-28	GYGFGLIK
9	74.08	662.3874 (+2)	662.3872	21-32	GYGFGLIKLDLK
10	69.86	730.3445 (+3)	730.3450	33-53	TKSENGLEFTSSGSANTETTK
11	71.43	1002.1581 (+3)	1002.1580	33-61	TKSENGLEFTSSGSANTETTKVTGSLETK
12	56.30	980.4427 (+2)	980.4425	35-53	SENGLEFTSSGSANTETTK
13	70.52	925.7787 (+3)	925.7771	35-61	SENGLEFTSSGSANTETTKVTGSLETK
14	53.90	417.7319 (+2)	417.7320	54-61	VTGSLETK
15	71.71	565.2792 (+3)	565.2789	62-74	YRWTEYGLTFTEK
16	71.28	687.8333 (+2)	687.8324	64-74	WTEYGLTFTEK
17	69.62	1088.5302 (+2)	1088.5295	75-93	WNTDNTLGTEITVEDQLAR
18	73.22	609.6602 (+3)	609.6597	94-110	GLKLTFDSSFSPNTGKK
19	62.89	700.8389 (+2)	700.8383	97-109	LTFDSSFSPNTGK
20	72.19	764.8867 (+2)	764.8857	97-110	LTFDSSFSPNTGKK
21	81.07	433.2663 (+2)	433.2663	114-120	IKTGYKR
22	74.14	1209.5944 (+2)	1209.5936	140-161	GALVLGYEGWLAGYQMNFETAK
23	62.22	887.7768 (+3)	887.7758	140-163	GALVLGYEGWLAGYQMNFETAKSR
24	79.64	728.8813 (+2)	728.8808	162-174	SRVTQSNFAVGYK
25	58.47	607.3146 (+2)	607.3142	164-174	VTQSNFAVGYK

26	72.70	867.4022 (+3)	867.4015	175-197	TDEFQLHTNVNDGTEFGGSIYQK
27	81.33	763.0762 (+3)	763.0766	198-218	VNKKLETAVNLAWTAGNSNTR
28	82.28	958.8586 (+3)	958.8577	198-224	VNKKLETAVNLAWTAGNSNTRFGIAAK
29	72.32	649.3425 (+3)	649.3412	201-218	KLETAVNLAWTAGNSNTR
30	81.60	845.1219 (+3)	845.1222	201-224	KLETAVNLAWTAGNSNTRFGIAAK
31	65.55	606.6434 (+3)	606.6429	202-218	LETAVNLAWTAGNSNTR
32	61.71	707.8189 (+2)	707.8190	225-236	YQIDPDA***C***FSAK
33	75.07	1038.9291 (+3)	1038.9306	237-266	VNNSSLIGLGYTQTLKPGIKLTLSALLDGK
34	71.82	603.3396 (+3)	603.3390	257-274	LTLSALLDGKNVNAGGHK
35	66.29	947.5201 (+1)	947.5197	275-283	LGLGLEFQA

*A: N-terminal acetylated; ***C***: cysteine carboxyamidomethylated.

Table S2. Sulfur-modified peptides found in hVDAC1 tryptic digest after DTT reduction and carboxyamidomethylation.

Retention time, experimentally measured and calculated monoisotopic m/z of the molecular ions, position in the sequence and peptide sequence of modified fragments present in the tryptic digest of reduced and carboxyamidomethylated hVDAC1 are reported. All sequences were confirmed by MS/MS. The sequence corresponding to the tryptic fragment 1 was used to build the sequence coverage reported in Figure 1.

Frag. n.	Rt (min)	Monoisotopic m/z		Position in the sequence	Peptide sequence
		Measured	Calculated		
1	70.86	1075.9784 (+2)	1075.9780	121-139	EHINLG**C**DMDFDIAGPSIR
2	66.31	1083.9756 (+2)	1083.9754	121-139	EHINLG**C**D**M**DFDIAGPSIR
3	73.63	812.0634 (+3)	812.0635	140-161	GALVLGYEGWLAGYQ**M**NFETAK

M: methionine sulfoxide; **C**: cysteine oxidized to sulfonic acid.

Table S3. Chymotryptic peptides found in hVDAC1 after DTT reduction and carboxyamidomethylation.

Retention time, experimentally measured and calculated monoisotopic m/z of the molecular ions, position in the sequence and peptide sequence of fragments present in the chymotryptic digest of reduced and carboxyamidomethylated hVDAC1 are reported. All sequences were confirmed by MS/MS. These sequences were used to build the sequence coverage reported in Figure 1.

Frag. n.	Rt (min)	Monoisotopic m/z		Position in the sequence	Peptide sequence
		Measured	Calculated		
1	59.35	689.3504 (+1)	689.3504	2-7	*AVPPTY
2	82.62	924.9778 (+2)	924.9782	2-18	*AVPPTYADLGKSARDVF
3	83.19	1178.6160 (+1)	1178.6164	8-18	ADLGKSARDVF
4	83.18	554.2932 (+2)	554.2938	9-18	DLGKSARDVF
5	83.23	440.2374 (+2)	440.2383	11-18	GKSARDVF
6	82.82	460.9050 (+3)	460.9056	30-41	DLKTKSENGLEF
7	53.38	795.3524 (+1)	795.3525	35-41	SENGLEF
8	66.64	820.9034 (+2)	820.9029	41-58	TSSGSANTETTKVTGSL
9	53.38	666.9990 (+3)	666.9996	41-61	TSSGSANTETTKVTGSLETK
10	82.47	1081.5264 (+2)	1081.5266	41-62	TSSGSANTETTKVTGSLETKY
11	80.66	499.2637 (+2)	499.2642	53-62	VTGSLETKY
12	82.61	754.3519 (+1)	754.3524	63-67	RWTEY
13	59.87	881.9216 (+2)	881.9213	76-91	NTDNTLGTEITVEDQL
14	78.55	995.4910 (+2)	995.4904	76-93	NTDNTLGTEITVEDQLAR
15	82.57	1080.5427 (+2)	1080.5431	76-95	NTDNTLGTEITVEDQLARGL
16	52.27	552.7734 (+2)	552.7751	82-91	GTEITVEDQL
17	76.55	666.3443 (+2)	666.3443	82-93	GTEITVEDQLAR
18	52.92	703.2937 (+1)	703.2939	98-103	TFDSSF
19	83.58	436.9262 (+3)	436.9265	107-118	TGKKNAKIKTGY
20	77.69	414.7321 (+2)	414.7329	132-139	DIAGPSIR
21	82.57	535.3035 (+2)	535.3042	132-142	DIAGPSIRGAL
22	82.68	666.3523 (+2)	666.3519	130-142	DFDIAGPSIRGAL
23	71.00	823.3994 (+1)	823.3990	143-149	VLGYEGW
24	83.04	814.9050 (+2)	814.9055	156-169	NFETAKSRVTQSNF
25	82.72	684.3497 (+2)	684.3499	158-169	ETAKSRVTQSNF
26	82.94	420.7684 (+2)	420.7692	196-202	**Q**KVNKKL

27	83.05	489.9556 (+3)	489.9564	196-208	**Q**KVNKKLETAVNL
28	84.04	508.3116 (+2)	508.3115	200-208	KKLETAVNL
29	79.79	484.2333 (+2)	484.2338	211-219	TAGNSNTRF
30	52.51	965.4039 (+1)	965.4038	226-233	QIDPDA***C***F
31	69.89	948.3775 (+1)	948.3773	226-233	**Q**IDPDA***C***F
32	76.02	460.2459 (+2)	460.2464	234-242	SAKVNNSSL
33	82.82	493.3060 (+2)	493.3062	248-256	TQTLKPGIK
34	83.18	549.8477 (+2)	549.8482	248-257	TQTLKPGIKL
35	83.32	435.2939 (+2)	435.2951	250-257	TLKPGIKL
36	83.18	605.3194 (+2)	605.3209	264-275	DGKNVNAGGHKL
37	77.04	635.3403 (+1)	635.3404	276-281	GLGLEF

*A: N-terminal acetylated; ***C***: cysteine carboxyamidomethylated.

Table S4. Sulfur-modified peptides found in hVDAC1chymotryptic digest after DTT reduction and carboxyamidomethylation.

Retention time, experimentally measured and calculated monoisotopic m/z of themolecular ions, position in the sequence and peptide sequence of modified fragments present in the tryptic digest of reduced and carboxyamidomethylated hVDAC1 are reported. All sequences were confirmed by MS/MS.

Frag. n.	Rt (min)	Monoisotopic m/z		Position in the sequence	Peptide sequence
		Measured	Calculated		
1	83.08	547.9050 (+3)	547.9052	119-131	KREHINLG**C**D**M**DF
2	83.37	817.7180 (+3)	817.7184	119-139	KREHINLG**C**D**M**DFDIAGPSIR
3	64.06	546.2050 (+2)	546.2051	123-131	INLG**C**D**M**DF

M: methionine sulfoxide; **C**: cysteine oxidized to sulfonic acid.

Table S5. Tryptic peptides found in hVDAC2 after DTT reduction and carboxyamidomethylation.

Retention time, experimentally measured and calculated monoisotopic m/z of the molecular ions, position in the sequence and peptide sequence of fragments identified in the tryptic digest of reduced and carboxyamidomethylated hVDAC2 are reported. All sequences were confirmed by MS/MS. These sequences were used to build the sequence coverage reported in Figure 4.

Frag. n.	Rt (min)	Monoisotopic m/z		Position in the sequence	Peptide sequence
		Measured	Calculated		
1	20.60	522.2381 (+2)	522.2380	2-10	*ATHGQT***C**AR
2	62.96	724.8497 (+2)	724.8493	11-23	PM**C**IPPSYADLGK
3	69.39	580.6580 (+3)	580.6579	24-39	AARDIFNKGFGFGLVK
4	52.32	636.3359 (+1)	636.3352	27-31	DIFNK
5	73.66	721.3983 (+2)	721.3955	27-39	DIFNKGFGFGLVK
6	73.41	633.0246 (+3)	633.0243	27-43	DIFNKGFGFGLVKLDVK
7	72.70	824.4675 (+1)	824.4665	32-39	GFGFGLVK
8	69.05	640.3745(+2)	640.3741	32-43	GFGFGLVKLDVK
9	76.34	989.4697 (+3)	989.4680	44-72	TKS**C**SGVEFSTSGSSNTDTGKVTGTLETK
10	50.57	954.4005 (+2)	954.3998	46-64	S**C**SGVEFSTSGSSNTDTGK
11	62.32	913.0883 (+3)	913.0871	46-72	S**C**SGVEFSTSGSSNTDTGKVTGTLETK
12	54.83	424.7398 (+2)	424.7398	65-72	VTGTLETK
13	70.28	862.9037 (+2)	862.9031	73-85	YKW**C**EYGLTFTEK
14	70.20	717.3246 (+2)	717.3239	75-85	W**C**EYGLTFTEK
15	70.08	1260.1086 (+2)	1260.1078	86-107	WNTDNTLGTEIAIEDQI**C**QGLK
16	63.73	714.8543 (+2)	714.8539	108-120	LTFDTTFSPNTGK
17	72.29	519.6038 (+3)	519.6034	108-121	LTFDTTFSPNTGKK
18	81.00	441.2637 (+2)	441.2638	125-131	IKSSYKR
19	60.36	470.7354 (+2)	470.7354	178-185	NNFAVGYR
20	73.51	843.3954 (+3)	843.3945	186-208	TGDFQLHTNVNDGTEFGGSIYQK
21	64.20	800.3594 (+3)	800.3583	209-229	V**C**EDLDTSVNLAWTSGTN**C**TR
22	67.28	627.6754 (+3)	627.6754	230-247	FGIAAKYQLDPTASISAK
23	60.48	647.3386 (+2)	647.3379	236-247	YQLDPTASISAK
24	72.52	1052.0819 (+2)	1052.0815	248-267	VNNSSLIGVGYTQTLRPGVK
25	63.77	861.4634 (+2)	861.4627	248-263	VNNSSLIGVGYTQTLR
26	70.64	508.8031 (+2)	508.8030	268-277	LTLSALVDGK
27	73.06	560.3090 (+3)	560.3089	278-294	SINAGGHKVGLALELEA

28	86.17	914.5200 (+1)	914.5193	286-294	VGLALELEA

C: cysteine carboxyamidomethylated.

Table S6. Sulfur-modified peptides found in hVDAC2 tryptic digest after DTT reduction and carboxyamidomethylation.

Retention time, experimentally measured and calculated monoisotopic m/z of the molecular ions, position in the sequence and peptide sequence of modified fragments present in the tryptic digest of reduced and carboxyamidomethylated hVDAC2 are reported. The sequence corresponding to the tryptic fragment 6 was used to build the sequence coverage reported in Figure 4.

Frag. n.	Rt (min)	Monoisotopic m/z		Position in the sequence	Peptide sequence
		Measured	Calculated		
1	70.99	830.3859 (+3)	830.3842	2-23	*ATHGQT***C**ARP**M****C**IPPSYADLGK
2	58.95	732.8476 (+2)	732.8470	11-23	P**M****C**IPPSYADLGK
3	34.88	949.8815 (+2)	949.8817	46-64	S**C**SGVEFSTSGSSNTDTGK
4	50.32	858.3821 (+2)	858.3849	73-85	YKW**C**EYGLTFTEK
5	64.20	837.3958 (+3)	837.3957	86-107	WNTDNTLGTEIAIEDQI**C**QGLK
6	75.00	1502.9921 (+3)	1502.9928	132-172	ECINLGCDVDFDFAGPAIHGSAVF GYEGWLAGYQMTFDSAK[a]
7	74.86	1508.3225 (+3)	1508.3244	132-172	ECINLGCDVDFDFAGPAIHGSAVF GYEGWLAGYQ**M**TFDSAK[a]
8	58.38	1195.5161 (+2)	1195.5157	209-229	V**C**EDLDTSVNLAWTSGTNCTR

*A: N-terminal acetylated; ***C***: cysteine carboxyamidomethylated;**M**: methionine sulfoxide; **C**: cysteine oxidized to sulfonic acid. [a]One of the two cysteines of these peptides is trioxidized and one carboxyamidomethylated, but it was not possible to determine which one because the MS/MS spectrum was not obtained.

Table S7. Chymotryptic peptides found in hVDAC2 after DTT reduction and carboxyamidomethylation.

Retention time, experimentally measured and calculated monoisotopic m/z of the molecular ions, position in the sequence and peptide sequence of fragments present in the chymotryptic digest of reduced and carboxyamidomethylated hVDAC2 are reported. All sequences were confirmed by MS/MS. These sequences were used to build the sequence coverage reported in Figure 4.

Frag. n.	Rt (min)	Monoisotopic m/z		Position in the sequence	Peptide sequence
		Measured	Calculated		
1	39.04	736.3335 (+1)	736.3340	13-18	***C***IPPSY
2	83.27	947.4795 (+2)	947.4806	13-29	***C***IPPSYADLGKAARDIF
3	83.33	588.8218 (+2)	588.8228	19-29	ADLGKAARDIF
4	83.32	439.2476 (+2)	439.2487	22-29	GKAARDIF
5	82.56	678.8268 (+2)	678.8274	41-52	DVKTKS***C***SGVEF
6	66.10	806.8889 (+2)	806.8872	53-69	STSGSSNTDTGKVTGTL
7	82.43	657.6551 (+3)	657.6558	53-72	STSGSSNTDTGKVTGTLETK
8	82.44	1067.5112 (+2)	1067.5115	53-73	STSGSSNTDTGKVTGTLETKY
9	82.56	785.3288 (+1)	785.3292	74-78	KW***C***EY
10	84.62	491.2559 (+2)	491.2556	79-86	GLTFTEKW
11	60.42	1017.9684 (+2)	1017.9684	87-104	NTDNTLGTEIAIEDQI***C***Q
12	69.36	1103.0211 (+2)	1103.0212	87-106	NTDNTLGTEIAIEDQI***C***QGL
13	62.59	773.8753 (+2)	773.8751	93-106	GTEIAIEDQI***C***QGL
14	57.02	731.3260 (+1)	731.3252	109-114	TFDTTF
15	83.55	527.9586 (+3)	527.9586	115-129	SPNTGKKSGKIKSSY
16	83.58	428.5822 (+3)	428.5827	118-129	TGKKSGKIKSSY
17	82.90	435.2398 (+2)	435.2405	122-129	SGKIKSSY
18	80.60	414.2059 (+2)	414.2065	143-150	DFAGPAIH
19	81.97	571.2858 (+2)	571.2860	143-154	DFAGPAIHGSAV
20	82.62	644.8198 (+2)	644.8202	143-155	DFAGPAIHGSAVF
21	82.90	487.2461 (+2)	487.2467	185-192	RTGDFQLH
22	83.04	650.9693 (+3)	650.9700	185-201	RTGDFQLHTNVNDGTEF
23	41.50	874.3983 (+1)	874.3981	207-213	**Q**KV***C***EDL
24	42.96	695.8116 (+2)	695.8120	207-218	**Q**KV***C***EDLDTSVN
25	66.97	704.3253 (+2)	704.3252	207-218	QKV***C***EDLDTSVN
26	56.51	752.3541 (+2)	752.3539	207-219	**Q**KV***C***EDLDTSVNL
27	82.63	889.4253 (+2)	889.4255	207-221	QKV***C***EDLDTSVNLAW

28	42.36	648.3202 (+1)	648.3204	214-219	DTSVNL
29	80.21	522.2326 (+2)	522.2329	222-230	TSGTN***C***TRF
30	68.37	827.4156 (+1)	827.4151	237-244	**Q**LDPTASI
31	48.45	844.4415 (+1)	844.4416	237-244	QLDPTASI
32	43.57	931.4734 (+1)	931.4736	237-245	QLDPTASIS
33	49.63	557.2931 (+2)	557.2935	237-247	**Q**LDPTASISAK
34	69.78	565.8065 (+2)	565.8068	237-247	QLDPTASISAK
35	70.92	672.3620 (+2)	672.3624	237-249	QLDPTASISAKVN
36	78.57	872.9585 (+2)	872.9580	237-253	QLDPTASISAKVNNSSL
37	66.80	1109.0743 (+2)	1109.0740	237-258	**Q**LDPTASISAKVNNSSLIGVGY
38	83.37	1117.5881 (+2)	1117.5873	237-258	QLDPTASISAKVNNSSLIGVGY
39	84.81	556.8430 (+2)	556.8429	259-268	TQTLRPGVKL
40	91.33	903.5153 (+1)	903.5151	269-277	TLSALVDGK
41	89.01	609.3410 (+2)	609.3409	269-280	TLSALVDGKSIN
42	82.52	663.3441 (+2)	663.3446	271-284	SALVDGKSINAGGH
43	83.37	861.9788 (+2)	861.9790	271-288	SALVDGKSINAGGHKVGL
44	83.32	484.6031 (+3)	484.6042	274-288	VDGKSINAGGHKVGL
45	83.13	526.7957 (+2)	526.7965	278-288	SINAGGHKVGL
46	47.91	645.3458 (+1)	645.3459	289-294	ALELEA

*A: N-terminal acetylated; ***C***: cysteine carboxyamidomethylated; **Q**: pyroglutamic acid form.

Table S8. Sulfur-modified peptides found in hVDAC2 chymotryptic digest after DTT reduction and carboxyamidomethylation.

Retention time, experimentally measured and calculated monoisotopic m/z of the molecular ions, position in the sequence and peptide sequence of modified fragments present in the tryptic digest of reduced and carboxyamidomethylated hVDAC2 are reported. All sequences were confirmed by MS/MS.

Frag. n.	Rt (min)	Monoisotopic m/z		Position in the sequence	Peptide sequence
		Measured	Calculated		
1	82.51	808.8561 (+2)	808.8565	130-142	KRE**C**INLG**C**DVDF
2	83.32	962.7771 (+3)	962.7781	130-155	KRE**C**INLG**C**DVDFDFAGPAIHGSAVF
3	64.28	747.8359 (+2)	747.8355	207-219	**Q**KV**C**EDLDTSVNL

M: methionine sulfoxide; **C**: cysteine oxidized to sulfonic acid; **Q**: pyroglutamic acid form.

Table S9. Tryptic peptides found in hVDAC3 after DTT reduction and carboxyamidomethylation.

Respective retention time, experimentally measured and calculated monoisotopic m/z of the molecular ions, position in the sequence and peptide sequence of fragments present in the tryptic digest of reduced and carboxyamidomethylated hVDAC3 are reported. All sequences were confirmed by MS/MS. These sequences were used to build the sequence coverage reported in Figure 5.

Frag. n.	Rt (min)	Monoisotopic m/z		Position in the sequence	Peptide sequence
		Measured	Calculated		
1	42.66	685.7897 (+2)	685.7894	2-12	*_C_NTPTY_C_DLGK
2	67.96	577.9682 (+3)	577.9677	13-28	AAKDVFNKGYGFGMVK
3	56.97	622.3202 (+1)	622.3195	16-20	DVFNK
4	70.33	487.9118 (+3)	487.9114	16-28	DVFNKGYGFGMVK
5	65.19	429.7118 (+2)	429.7126	21-28	GYGFGMVK
6	76.51	740.6682 (+3)	740.6673	33-53	TKS_C_SGVEFSTSGHAYTDTGK
7	65.94	995.9267 (+2)	995.9260	35-53	S_C_SGVEFSTSGHAYTDTGK
8	55.12	410.2136 (+2)	410.2140	54-61	ASGNLETK
9	69.57	811.4081 (+2)	811.4058	62-74	YKV_C_NYGLTFTQK
10	67.11	954.4420 (+2)	954.4421	75-90	WNTDNTLGTEISWENK
11	72.64	720.0880 (+3)	720.0876	91-110	LAEGLKLTLDTIFVPNTGKK
12	88.90	1508.0270 (+3)	1508.0276	121-161	D_C_FSVGSNVDIDFSGPTIYGWAVLAFE GWLAGYQMSFDTAK
13	69.46	490.5965 (+3)	490.5964	162-174	SKLSQNNFALGYK
14	62.54	627.8281 (+2)	627.8275	164-174	LSQNNFALGYK
15	72.74	845.7346 (+3)	845.7348	175-197	AADFQLHTHVNDGTEFGGSIYQK
16	72.25	733.3964 (+3)	733.3960	198-218	VNEKIETSINLAWTAGSNNTR
17	58.53	429.1861 (+2)	429.1859	225-230	YMLD_C_R
18	71.98	701.0652 (+3)	701.0637	237-256	VNNASLIGLGYTQTLRPGVK
19	68.52	610.3358 (+3)	610.3354	257-274	LTLSALIDGKNFSAGGHK
20	66.67	409.2012 (+2)	409.2012	267-274	NFSAGGHK
21	63.61	934.4893 (+1)	934.4880	275-283	VGLGFELEA

*_C_: N-terminal acetylated; _C_: cysteine carboxyamidomethylated.

Table S10. Sulfur-modified peptides found in hVDAC3 tryptic digest after DTT reduction and carboxyamidomethylation.

Retention time, experimentally measured and calculated monoisotopic m/z of the molecular ions, position in the sequence and peptide sequence of modified fragments present in the tryptic digest of reduced and carboxyamidomethylated hVDAC3 are reported.

Frag. n.	Rt (min)	Monoisotopic m/z		Position in the sequence	Peptide sequence
		Measured	Calculated		
1	60.77	437.7098 (+2)	437.7103	21-28	GYGFG**M**VK
2	52.53	991.4069 (+2)	991.4079	35-53	S**C**SGVEFSTSGHAYTDTGK
3	60.39	806.8889 (+2)	806.8877	62-74	YKV**C**NYGLTFTQK
4	87.68	1513.3688 (+3)	1513.3596	121-161	D***C***FSVGSNVDIDFSGPTIYGWAV LAFEGWLAGYQ**M**SFDTAK
5	54.24	437.1832(+2)	437.1836	225-230	Y**M**LD***C***R

C: cysteine carboxyamidomethylated;**C**: cysteine oxidized to sulfonic acid; **M**: methionine sulfoxide.

Table S11. Chymotryptic peptides found in hVDAC3 after DTT reduction and carboxyamidomethylation.

Retention time, experimentally measured and calculated monoisotopic m/z of the molecular ions, position in the sequence and peptide sequence of fragments present in the chymotryptic digest of reduced and carboxyamidomethylated hVDAC3 are reported. These sequences were used to build the sequence coverage reported in Figure 5.

Frag. n.	Rt (min)	Monoisotopic m/z		Position in the sequence	Peptide sequence
		Measured	Calculated		
1	46.14	797.3140 (+1)	797.3134	2-7	*CNTPTY
2	82.39	1001.4583 (+2)	1001.4559	2-18	*CNTPTYCDLGKAAKDVF
3	83.09	532.2928 (+2)	532.2933	9-18	DLGKAAKDVF
4	84.76	571.7789 (+2)	571.7792	32-41	KTKSCSGVEF
5	82.52	742.8654 (+2)	742.8656	49-62	TDTGKASGNLETKY
6	63.49	675.8124 (+2)	675.8128	76-87	NTDNTLGTEISW
7	54.92	692.3252 (+1)	692.3255	82-87	GTEISW
8	91.59	873.4681 (+1)	873.4682	88-95	ENKLAEGL
9	83.47	475.7809 (+2)	475.7820	96-103	KLTLDTIF
10	70.83	709.3773 (+1)	709.3772	98-103	TLDTIF
11	63.46	1019.5420 (+1)	1019.5413	98-106	TLDTIFVPN
12	59.81	526.7488 (+2)	526.7489	124-133	SVGSNVDIDF
13	65.20	835.8998 (+2)	835.8996	124-139	SVGSNVDIDFSGPTIY
14	65.35	609.2670 (+1)	609.2673	145-149	AFEGW
15	88.40	690.8130 (+2)	690.8130	179-190	**Q**LHTHVNDGTEF
16	83.08	466.5529 (+3)	466.5535	179-190	QLHTHVNDGTEF
17	82.30	510.2252 (+2)	510.2256	182-190	THVNDGTEF
18	82.21	749.9092 (+2)	749.9098	196-208	**Q**KVNEKIETSINL
19	83.08	758.4230 (+2)	758.4230	196-208	QKVNEKIETSINL
20	92.01	878.4682 (+2)	878.4679	196-210	**Q**KVNEKIETSINLAW
21	82.55	484.2334 (+2)	484.2337	211-219	TAGSNNTRF
22	84.26	622.3562 (+1)	622.3559	220-225	GIAAKY[a]
23	76.39	452.2487 (+2)	452.2489	234-242	SAKVNNASL
24	91.90	703.8864 (+2)	703.8860	234-247	SAKVNNASLIGLGY
25	83.13	556.8425 (+2)	556.8429	248-257	TQTLRPGVKL
26	92.28	589.8251 (+2)	589.8249	258-268	TLSALIDGKNF
27	82.52	482.7581 (+2)	482.7591	260-268	SALIDGKNF

28	83.18	413.2320 (+2)	413.2331	269-277	SAGGHKVGL

*C: N-terminal acetylated; ***C***: cysteine carboxyamidomethylated. [a]This peptideis common to all the isoforms and therefore its attribution to the hVDAC3 sequence it is not univocal.

5. Article 3

High resolution mass spectrometry characterization of the oxidation pattern of methionine and cysteine residues in rat liver mitochondria voltage-dependent anion selective channel 3 (VDAC3)

Rosaria Saletti, Simona Reina, Maria G.G. Pittalà, Ramona Belfiore, Vincenzo Cunsolo, Angela Messina, Vito De Pinto and Salvatore Foti

BBA-Biomembranes 1859 (2017) 301-311

Biochimica et Biophysica Acta 1859 (2017) 301–311

Contents lists available at ScienceDirect

Biochimica et Biophysica Acta

journal homepage: www.elsevier.com/locate/bbamem

High resolution mass spectrometry characterization of the oxidation pattern of methionine and cysteine residues in rat liver mitochondria voltage-dependent anion selective channel 3 (VDAC3)

Rosaria Saletti [a,*], Simona Reina [b,c], Maria G.G. Pittalà [a,d], Ramona Belfiore [c,d], Vincenzo Cunsolo [a], Angela Messina [b,c], Vito De Pinto [c,d], Salvatore Foti [a]

[a] Department of Chemical Sciences, Organic Mass Spectrometry Laboratory, University of Catania, Viale A. Doria 6, 95125 Catania, Italy
[b] Department of Biological, Geological and Environmental Sciences, Section of Molecular Biology, University of Catania, Viale A. Doria 6, 95125 Catania, Italy
[c] National Institute for Biomembranes and Biosystems, Section of Catania, Viale A. Doria 6, 95125 Catania, Italy
[d] Department of Biomedicine and Biotechnology, Section of Biology and Genetics, Viale A. Doria 6, 95125 Catania, Italy

ARTICLE INFO

Article history:
Received 3 August 2016
Received in revised form 18 November 2016
Accepted 14 December 2016
Available online 16 December 2016

Keywords:
Voltage dependent anion selective channel isoform 3 (VDAC3)
Amino acid redox state
Cysteine
Mitochondrial outer membrane
Mitochondrial intermembrane space
Orbitrap tribrid mass spectrometer

ABSTRACT

Voltage-dependent anion selective channels (VDACs) are integral membrane proteins found in the mitochondrial outer membrane. In comparison with the most abundant isoform VDAC1, there is little knowledge about the functional role of VDAC3. Unlikely VDAC1, cysteine residues are particularly abundant in VDAC3. Since the mitochondrial intermembrane space (IMS) has an oxidative potential we questioned whether the redox state of VDAC3 can be modified. By means of SDS-PAGE separation, tryptic and chymotryptic proteolysis and UHPLC/High Resolution ESI-MS/MS analysis we investigated the oxidation state of cysteine and methionine residues of rat liver VDAC3. Our results demonstrate that the mitochondrial VDAC3, in physiological state, contains methionines oxidized to methionine sulfoxide. Furthermore, cysteine residues 36, 65, and 165 are oxidized to a remarkable extend to sulfonic acid. Cysteines 2 and 8 are observed exclusively in the carboxyamidomethylated form. Cys^{229} is detected exclusively in the oxidized form of sulfonic acid, whereas the oxidation state of Cys^{122} could not be determined because peptides containing this residue were not detected. Control experiments ruled out the possibility that over-oxidation of cysteines might be due to artefactual reasons. The peculiar behavior of Met and Cys residues of VDAC3 may be related with the accessibility of the protein to a strongly oxidizing environment and may be connected with the regulation of the activity of this trans-membrane pore protein.

1. Introduction

Voltage-dependent anion selective channels (VDACs), also known as mitochondrial porins, are the most abundant integral membrane proteins found in the outer membrane, separating the intermembrane space from the cytosol [1,2]. They are pore-forming proteins (30–35 kDa) originally identified in mitochondria of eukaryotic cells [1]. Functional characterization of VDAC isoforms, named VDAC1, VDAC2 and VDAC3, in the chronological order of their discovery, has been mainly achieved by reconstitution into planar bilayer membranes [3,4]. It was shown that while VDAC1 and VDAC2 isoforms are able to form pores in lipid bilayers, VDAC3 had no evident pore-forming ability [3]. Recently, more extensive experiments discovered a reduced but clear pore-forming ability also for VDAC3 [5]. This finding suggests a distinct function for each VDAC isoform. An increasing body of evidence, indeed, indicates that VDAC plays a major role in the metabolite flow in and out of mitochondria, resulting in the regulation of mitochondrial functions [6]. The whole exchange of metabolites, cations and information between mitochondria and the cell occurs through the outer membrane. This membrane creates a diffusion barrier for small molecules (adenine nucleotides, phosphocreatine, creatine, etc.) causing rate-dependent concentration gradients as a prerequisite for the action of ADP shuttles via creatine kinases or adenylate kinases. This means that VDAC isoforms may act as a "governor" of the mitochondrial bioenergetics [7].

In comparison with the most abundant isoform VDAC1, there is little knowledge about the functional role of the other isoforms VDAC2 and VDAC3. In addition, the existing information derives mainly from recombinant proteins expressed in yeast or *E. coli* and from mutant mice and cells [8]. VDAC2 has been partially purified and characterized in bovine spermatozoa [9], but no specific purification protocol has been

* Corresponding author at: Department of Chemical Sciences, Organic Mass Spectrometry Laboratory, University of Catania, Campus S. Sofia, Building 1, Viale A. Doria 6, 95125 Catania, Italy.
E-mail addresses: rsaletti@unict.it (R. Saletti), simonareina@yahoo.it (S. Reina), marinella.pitt@virgilio.it (M.G.G. Pittalà), belfi88@hotmail.it (R. Belfiore), vcunsolo@unict.it (V. Cunsolo), mess@unict.it (A. Messina), vdpbiofa@unict.it (V. De Pinto), sfoti@unict.it (S. Foti).

http://dx.doi.org/10.1016/j.bbamem.2016.12.003
0005-2736/

assessed, neither a clear picture of its specific function has been determined [4,10]. There are even less data about VDAC3, partially characterized as cytoskeletal-associated structure [11–13].

From the structural point of view, all three isoforms show sequence homology and are expected to share several structural elements. The structure of human VDAC1 has been determined using different techniques (both NMR [14], X-ray crystallography [15] and a mix of these two [16]), leading to a strong, coherent model in terms of secondary structure architecture. According to Ujwal and colleagues, the α-helix of the N-terminal segment is oriented against the interior wall, causing a partial narrowing at the center of the pore, and thus possibly regulating the conductance of ions and metabolites passing through the VDAC pore. The topography of VDAC1 in the mitochondrial outer membrane has been determined in intact cells [17], revealing that the N-terminus is located versus the cytosol. Recently the structure of zebrafish VDAC2 has been determined at 2.8 Å resolution, confirming the general organization of the pore [18]. The modeling of the human VDAC3 structure based upon the VDAC1 crystal structure [15], and the assignment of a transmembrane sidedness based on recent advances [17] shows that, similarly to VDAC1, its transmembrane domain should consist of up-and-down β-barrels, but leaves unsolved the problem of the N-terminal domain and of the loop arrangement [19]. It also shows that the VDAC3 cysteine residues protrude toward the mitochondrial intermembrane space (IMS), an oxidizing space of the cell (Fig. 1). Overall, structural similarities between the three isoforms suggest a pore-forming ability for all of them, although the properties of these pores might well be different.

Unlikely VDAC1, cysteine residues are particularly abundant in VDAC2 and in VDAC3, the least known isoform. Since the IMS has an oxidative potential, we questioned whether it could modify the redox state of these proteins. This work is thus aimed to the investigation of the oxidation state of cysteine and methionine residues of VDAC3 by means of SDS-PAGE separation and UHPLC/High Resolution ESI-MS/MS analysis. To this purpose the native VDAC3 from rat liver mitochondria was studied.

2. Materials and methods

2.1. Chemicals

All chemicals were of the highest purity commercially available and were used without further purification. Ammonium bicarbonate, Tris HCl, Triton X-100, EDTA, glycerol, bromophenol blue, sodium dodecyl sulfate (SDS), acetic acid (AA), formic acid (FA), dithiothreitol (DTT), iodoacetamide (IAA), chymotrypsin and chicken lysozyme were obtained from Sigma-Aldrich (Milan, Italy). Modified porcine trypsin was purchased from Promega (Madison, WI, USA). Water and acetonitrile (OPTIMA® LC/MS grade) for LC/MS analyses were provided from Fisher Scientific (Milan, Italy).

2.2. Preparation of VDAC3 enriched fractions from rat liver mitochondria

Rat liver mitochondria were prepared by standard procedures [20]. 25 mg of rat liver mitochondria were solubilized for 30 min on ice with 5 mL of buffer A (10 mM Tris HCl, 1 mM EDTA pH 7.0) including 3% Triton X-100 and then centrifuged at 17,400 ×*g* for 30 min at 4 °C. The supernatant was loaded onto 5 g of dry hydroxyapatite (Bio-Gel HTP, Biorad) packed in a glass Econo-column 2.5 × 30 cm (Biorad) [20,21]. The column was eluted at 4 °C with buffer A and five fraction of 0.6 mL were collected. Protein fractions were precipitated with 9 volumes of cold acetone for 30 min. Pellets were solubilized in SDS sample buffer to control the protein content by SDS-PAGE.

2.3. Electrophoretic analysis

After precipitation with 9 volumes of cold acetone, the protein pellet was solubilized in SDS sample buffer without reducing agents (4% SDS, 20% glycerol, 0.004% bromophenol blue, 0.125 M Tris HCl, pH 6.8) and loaded on a 12% polyacrylamide gel with a ratio acrylamide-bis acrylamide of 30:0.8. To get a higher resolution of polypeptides of Mr close to 30 kDa a 17% polyacrylamide gel with a ratio acrylamide/bis acrylamide of 150 was performed [21].

2.4. In-gel digestion of 1D-SDS-PAGE bands

After SDS-PAGE separation of the proteins, the bands were manually cut in small pieces, transferred to 1.5 mL microcentrifuge tubes, washed three times with 50 μL of H_2O and 50 μL of CH_3CN alternatively, shrunk in CH_3CN and dried under vacuum. Then, proteins were reduced by incubation in 10 mM DTT in 50 μL of ammonium bicarbonate (pH 8.3; 0.1 M) for 30 min at 56 °C. Subsequently, alkylation was performed by addition of 50 μL of 55 mM iodoacetamide in ammonium bicarbonate (pH 8.3; 0.1 M) and the reaction was carried out for 30 min in the dark at room temperature. Gel pieces were shrunk in CH_3CN and dried

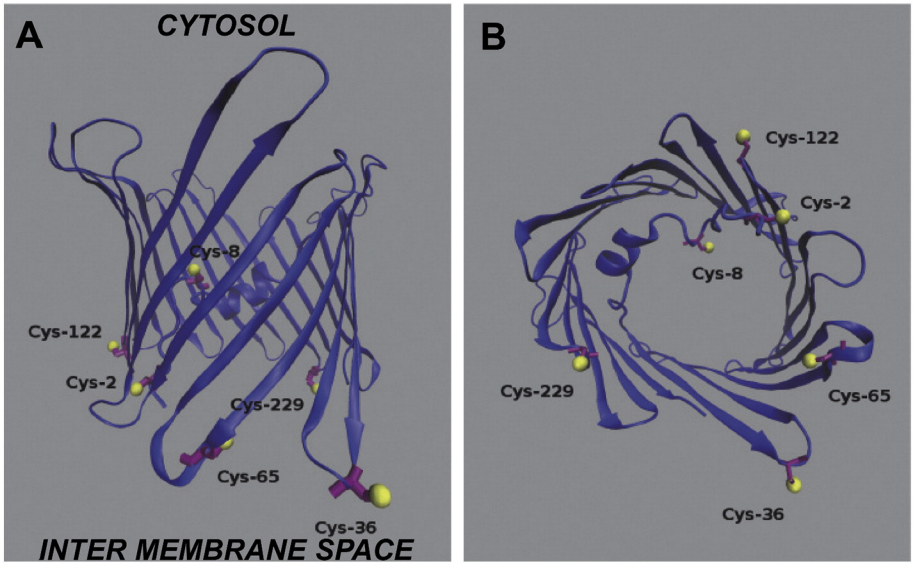

Fig. 1. A predicted structural model of human VDAC3 embedded in the mitochondrial outer membrane, showing the localization of cysteine residues. A) side view of the pore. B) a view of the pore from the intermembrane mitochondrial space. The authors are indebted to Carlo Guardiani (Cagliari, Warwick) for the figure drawing.

under vacuum. Finally, alkylated proteins were subjected to in-gel digestion using modified porcine trypsin or chymotrypsin. 30 μL of 10 ng/μL trypsin in ammonium bicarbonate (pH 8.3; 50 mM) were added to the dry gel pieces. For the chymotryptic digestion, 50 μL of 10 ng/μL of chymotrypsin were added. After soaking trypsin or chymotrypsin into the gel pieces, the supernatant containing an excess of enzyme was discarded and the gel pieces were covered with 50 μL of ammonium bicarbonate (pH 8.3; 50 mM). Digestion was allowed to proceed overnight at 37 °C. After in-gel digestion, the supernatant solution was transferred into a clean 1.5 mL tube. The peptides were extracted from gel pieces with 50 μL of 5% aqueous FA and subsequently with 50 μL of CH_3CN. This extraction procedure was repeated three times. The total extracts were pooled with the first supernatant and lyophilized.

2.5. Control experiments using chicken lysozyme

Two different experimental procedures were performed.

In the first, 10 μg of lysozyme, was loaded on a polyacrylamide gel and the corresponding band was subjected to reduction with DTT, alkylation with IAA and in-gel trypsin digestion using the same conditions described above for the 1D-SDS-PAGE bands of the hydroxyapatite eluate.

In the second experiment, lysozyme was solubilized in 50 mM ammonium bicarbonate, pH 8.3, at a concentration of 1 μg/μL. 10-fold molar excess of DTT over the thiol groups concentration, dissolved in the same buffer, was added and the reduction was carried out for 3 h in the dark at 25 °C. Alkylation was performed by addition of iodoacetamide at the same molar ratio over total thiol groups for 1 h in the dark at 25 °C. Trypsin, at an enzyme/substrate ratio of 1:50 (mol/mol), was added and the solution was incubated at 37 °C for 4 h.

Finally, the two tryptic digests were analyzed by nano UHPLC/High Resolution nano ESI-MS/MS.

2.6. In-solution digestion of the hydroxyapatite eluate

The hydroxyapatite eluate was purified from non-protein contaminating molecules with the PlusOne 2-D Clean-Up Kit (GE Healthcare Life Sciences, Milan, Italy) according to the manufacturer's recommendations. The desalted protein pellet obtained was suspended in 100 μL of 50 mM ammonium bicarbonate (pH 8.3) and incubate in ice for 15 min. After, 100 μL of 0.2% RapiGest SF (Waters, Milan, Italy) in 50 mM ammonium bicarbonate were added and the sample was put in ice for 30 min. Protein amount, determined using Fluorometer Assay Kit, resulted 1 μg. The reduction was carried out by adding 2.6 μg of DTT dissolved in the same buffer for 3 h in the dark at 25 °C. Subsequently, alkylation was performed by addition of iodoacetamide at the same molar ratio over total thiol groups and the reaction allowed to proceed for 1 h in the dark at 25 °C. Finally, reduced and alkylated proteins were subjected to digestion using modified porcine trypsin or chymotrypsin in ammonium bicarbonate (pH 8.3) at an enzyme-substrate ratio of 1:50 and 1:25, respectively, at 37 °C for 4 h. The protein digests were then dried under vacuum, redissolved in 20 μL of 5% FA and analyzed by nano UHPLC/High Resolution nano ESI-MS/MS.

2.7. Reduction and alkylation of intact mitochondria

5 mg of intact mitochondria were incubated in 1 mL of 1 M DTT, 10 mM Tris HCl, 3% Triton X-100 pH 8.3 for 30′ at 4 °C. The supernatant was isolated from the insolubilized material by centrifugation at 17,400 × *g* for 30 min at 4 °C. Alkylation was performed by addition of iodoacetamide at the 2:1 molar ratio over DTT for 1 h in the dark at 25 °C. Purification and in-solution digestion of the hydroxyapatite eluate were performed as described above.

2.8. Liquid chromatography and tandem mass spectrometry (LC–MS/MS) analysis

Mass spectrometry data were acquired on an Orbitrap Fusion Tribrid (Q-OT-qIT) mass spectrometer (ThermoFisher Scientific, Bremen, Germany) equipped with a ThermoFisher Scientific Dionex UltiMate 3000 RSLCnano system (Sunnyvale, CA). Samples obtained by in-gel digestion were reconstituted in 20 μL of 5% FA aqueous solution and 1 μL was loaded onto an Acclaim®Nano Trap C18 column (100 μm i.d. × 2 cm, 5 μm particle size, 100 Å). After washing the trapping column with solvent A (H_2O/CH_3CN, 98/2 + 0.1% FA) for 3 min at a flow rate of 7 μL/min, the peptides were eluted from the trapping column onto an PepMap® RSLC C18 Easy-spray column (75 μm i.d. × 15 cm, 3 μm particle size, 100 Å). Peptides were separated at a flow rate of 300 nL/min at 40 °C with a linear gradient of solvent B (CH_3CN + 0.1% FA) in A from 1% to 60% over 30 min. For the analysis of the tryptic digest of the lysate of mitochondria incubated with DTT, a linear gradient of solvent B in A from 1% to 60% over 60 min was used. Eluted peptides were ionized by a nanospray (Easy-spray ion source, Thermo Scientific) using a spray voltage of 1.7 kV and introduced into the mass spectrometer through a heated ion transfer tube (250 °C). Survey scans of peptide precursors in the *m/z* range 400–1600 were performed at resolution of 120,000 (@ 200 *m/z*) with a AGC target for Orbitrap survey of 2.0×10^5 and a maximum injection time of 50 ms. Tandem MS was performed by isolation at 1.6 Th with the quadrupole, and high energy collisional dissociation (HCD) was performed in the Ion Routing Multipole (IRM), using a normalized collision energy of 35 and rapid scan MS analysis in the ion trap. Only those precursors with charge state 1–3 and an

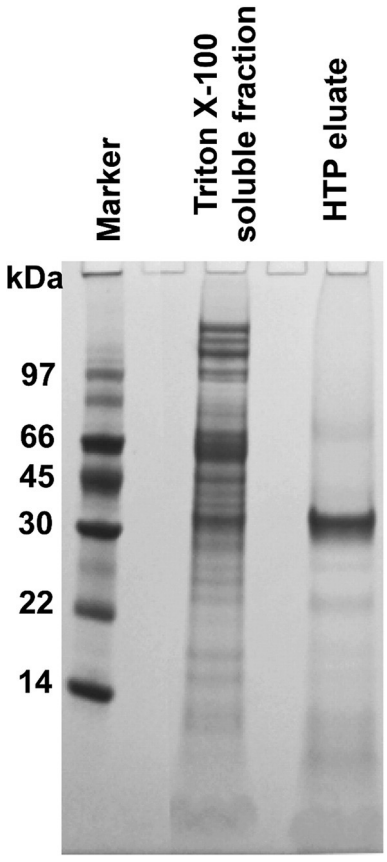

Fig. 2. Electrophoretic pattern of the rVDAC3 HTP eluate. Rat liver mitochondria were solubilized with Triton X-100. The solubilized material was loaded onto a HTP chromatographic column as in Refs. [20] and [21]. An aliquot of the Triton X-100 solubilized proteins (lane 2) and of the HTP eluate were run on a 17.5% (30:0.8 acrylamide:bis acrylamide) SDS-PAGE in not reducing conditions.

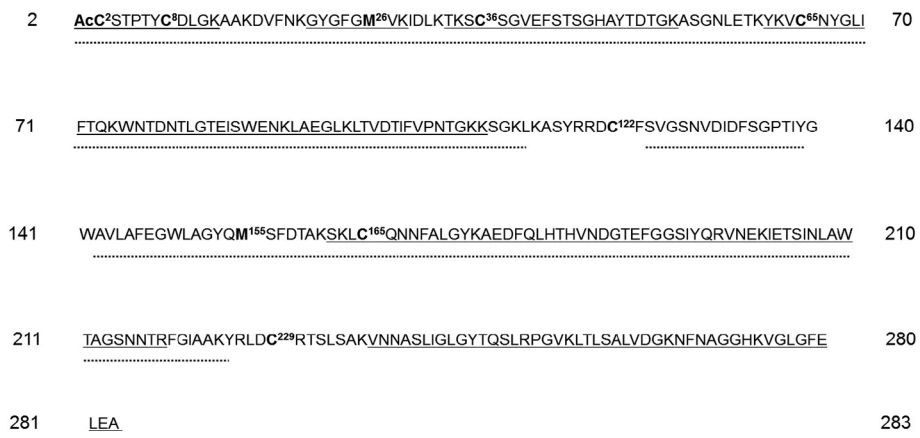

Fig. 3. Sequence coverage map of rVDAC3 obtained by enzymatic in-gel digestion. Solid lines indicate the coverage obtained with tryptic peptides; dotted lines the coverage obtained with chymotryptic peptides. The asterisk (*) indicates the substitution Lys → Asn[128] with respect to the sequence reported in SwissProt Acc. N. Q9R1Z0.

intensity above the threshold of $5 \cdot 10^3$ were sampled for MS^2. The dynamic exclusion duration was set to 25 s with a 10 ppm tolerance around the selected precursor and its isotopes. Monoisotopic precursor selection was turned on. AGC target and maximum injection time (ms) for MS/MS spectra were 1.0×10^4 and 300, respectively. The instrument was run in top speed mode with 3 s cycles, meaning the instrument would continuously perform MS^2 events until the list of non-excluded precursors diminishes to zero or 3 s, whichever is shorter. MS/MS spectral quality was enhanced enabling the parallelizable time option (i.e. by using all parallelizable time during full scan detection for MS/MS precursor injection and detection).

Samples obtained by in-solution digestion were analyzed by loading 1 μL of the reconstituted 5% FA aqueous solution onto the Acclaim®Nano Trap C18 column, as described before. Peptides were eluted from the trapping column onto a PepMap® RSLC C18 EASY-Spray, 75 μm × 50 cm, 2 μm, 100 Å column and were separated by elution at a flow rate of 0.3 μL/min, at 40 °C, with a linear gradient of solvent B in A from 5% to 20% in 32 min, followed by 20% to 40% in 30 min, and 40% to 60% in 20 min.

Eluted peptides were ionized by a nanospray (Easy-spray ion source, Thermo Scientific) using the same conditions as above, with the following modifications: ion transfer tube, 275 °C; AGC target for Orbitrap survey of 4.0×10^5; precursors with charge state 1–4 and an intensity above the threshold of $5 \cdot 10^3$ were sampled for MS^2; the dynamic exclusion duration was set to 60 s with a 10 ppm tolerance around the selected precursor and its isotopes. AGC target and maximum injection time (ms) for MS/MS spectra were 1.0×10^4 and 100, respectively.

Mass spectrometer calibration was performed using the Pierce® LTQ Velos ESI Positive Ion Calibration Solution (Thermo Fisher Scientific). MS data acquisition was performed using the *Xcalibur* v. 3.0.63 software (Thermo Fisher Scientific).

2.9. Database search

LC–MS/MS data were processed using Proteome Discoverer v. 1.4.1.14 (Thermo Scientific). Data were searched against the SwissProt database (release July 2016, containing 550,552 entries) using the MASCOT algorithm (Matrix Science, London, UK, version 2.5.1). The search

Table 1
Tryptic peptides found in rVDAC3 after DTT reduction and carboxyamidomethylation.
In the table the respective retention time, experimentally measured and calculated monoisotopic *m/z* of the molecular ions, the position in the sequence and the peptide sequence of fragments present in the tryptic digest of reduced and carboxyamidomethylated rVDAC3 are reported. All sequences were confirmed by MS/MS. These sequences were used to build the sequence coverage scheme shown in Fig. 3.

Frag. n.	Rt (min)	Monoisotopic *m/z*		Position in the sequence	Peptide sequence
		Measured	Calculated		
1	18.47	672.2839 (2+)	672.2839	2–12	[a]**C**STPTY**C**DLGK
2	18.38	429.7128 (2+)	429.7126	21–28	GYGFGMVK
3	15.15	740.6678 (3+)	740.6673	33–53	TKS**C**SGVEFSTSGHAYTDTGK
4	17.31	664.2868 (3+)	664.2864	35–53	S**C**SGVEFSTSGHAYTDTGK
5	19.35	545.2855 (3+)	545.2851	62–74	YKV**C**NYGLIFTQK
6	20.20	671.8466 (2+)	671.8448	64–74	V**C**NYGLIFTQK
7	21.28	954.4443 (2+)	954.4421	75–90	WNTDNTLGTEISWENK
8	22.72	840.4176 (3+)	840.4186	75–96	WNTDNTLGTEISWENKLAEGLK
9	20.95	702.8905 (2+)	702.8903	97–109	LTVDTIFVPNTGK
10	19.26	766.9389 (2+)	766.9378	97–110	LTVDTIFVPNTGKK
11	17.07	514.9289 (3+)	514.9293	162–174	SKL**C**QNNFALGYK
12	18.34	664.3278 (2+)	664.3268	164–174	L**C**QNNFALGYK
13	18.60	874.4052 (3+)	874.4054	175–197	AEDFQLHTHVNDGTEFGGSIYQR
14	21.03	773.3964 (3+)	773.3960	198–218	VNEKIETSINLAWTAGSNNTR
15	20.98	924.4673 (2+)	924.4659	202–218	IETSINLAWTAGSNNTR
16	19.73	1044.0853 (2+)	1044.0840	237–256	VNNASLIGLGYTQSLRPGVK
17	20.62	1016.5982 (1+)	1016.5986	257–266	LTLSALVDGK
18	19.06	614.6669 (3+)	614.6671	257–274	LTLSALVDGKNFNAGGHK
19	27.91	934.4882 (1+)	934.4880	275–283	VGLGFELEA

[a] C: N-terminal acetylated; **C**: cysteine carboxyamidomethylated.

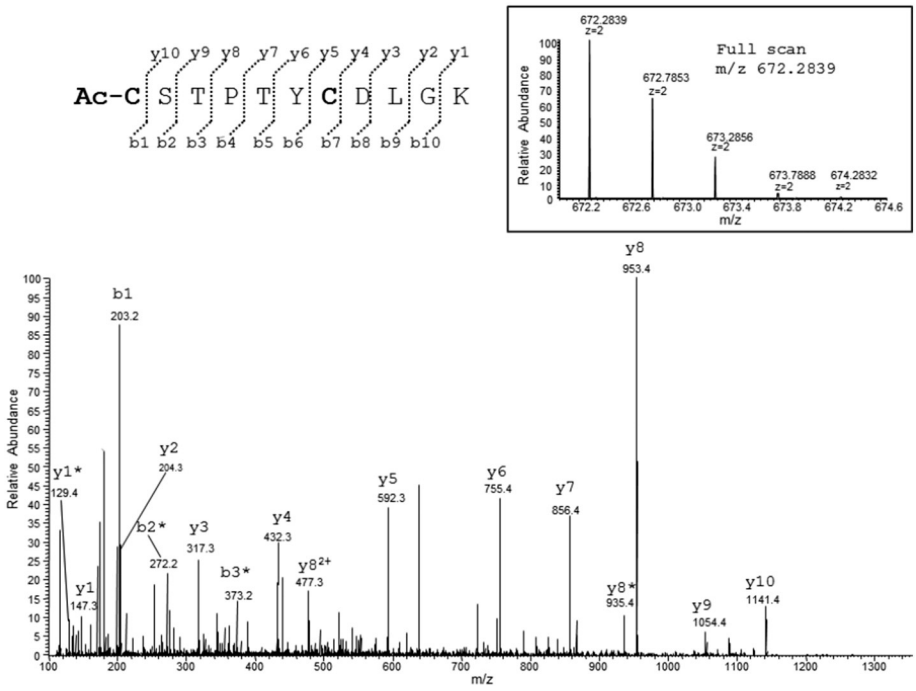

Fig. 4. MS/MS mass spectrum of the doubly charged molecular ion at *m/z* 672.2839 (calculated 672.2839) of the N-terminal acetylated tryptic peptide of rVDAC3 containing cysteine residues 2 and 8 carboxyamidomethylated. Fragment ions originated from the neutral loss of H_2O are indicated by an asterisk. The full scan mass spectrum of the molecular ions is shown in the inset.

was performed against *Rattus* sequences database (7961 sequences). Full tryptic or chymotrypsin peptides with a maximum of 3 missed cleavage sites were subjected to bioinformatic search. Cysteine carboxyamidomethylation was set as fixed modification, whereas acetylation of protein N-terminal, trioxidation of cysteine, oxidation of methionine, and transformation of N-terminal glutamine and N-terminal glutamic acid residue in the pyroglutamic acid form were included as variable modifications. The precursor mass tolerance threshold was 10 ppm and the max fragment mass error was set to 0.6 Da. Peptide spectral matches (PSM) were validated using Target Decoy PSM Validator node based on q-values at a 1% FDR.

3. Results

3.1. Mass spectrometric analysis of VDAC3 from rat liver mitochondria

3.1.1. Tryptic digestion

The primary structure of VDAC3 from *Rattus norvegicus* (rVDAC3) has been investigated by tryptic and proteinase K digestion, and MALDI and ESI-MS/MS mass spectrometric analysis [22]. When combining the coverage obtained in all the experiments, a total coverage of 82% (231 of 282 amino acids) was achieved. The N-terminal methionine was never found, indicating it is removed during protein maturation. The protein stretches not covered in this analysis included the sequences Ser^{111}-Phe^{157} and Val^{198}-Glu^{200}. In our work rVDAC3 was enriched in the hydroxyapatite (HTP) eluate of Triton X-100 solubilized rat liver mitochondria. The eluate mainly contained electrophoretic bands in the range of 30–35 kDa (Fig. 2), which were excised and digested by trypsin, with prior reduction of the disulfide bridges and blocking by iodoacetamide of the thiol groups.

UHPLC/ESI-MS/MS of the tryptic peptides of the reduced and carboxyamidomethylated protein showed that rVDAC3 was spread in all the region between 30–35 kDa, together with other proteins, mainly VDAC1, VDAC2 and several other mitochondrial proteins from *Rattus norvegicus*. The peptides identified covered 70% of the rVDAC3 sequence (Fig. 3, Table 1).

The results also confirmed that the N-terminal Met, reported in the SwissProt database sequence (Acc. N. Q9R1Z0), is absent in the mature protein and that the N-terminal Cys is present in the acetylated form (Fig. 4, Table 1, fragment 1).

Table 2
Sulfur-modified peptides found in rVDAC3 tryptic digest after DTT reduction and carboxyamidomethylation.
In the table the respective retention time, experimentally measured and calculated monoisotopic *m/z* of the molecular ions, the position in the sequence and the peptide sequence of modified fragments present in the tryptic digest of reduced and carboxyamidomethylated rVDAC3 are reported. All sequences were confirmed by MS/MS.

Frag. n.	Rt (min)	Monoisotopic *m/z*		Position in the sequence	Peptide sequence
		Measured	Calculated		
1	18.47	493.2430 (3+)	493.2433	16–28	DVFNKGYGFG**M**VK
2	16.66	874.4123 (1+)	874.4127	21–28	GYGFG**M**VK
3	15.84	737.6550 (3+)	737.6554	33–53	TKS**C**SGVEFSTSGHAYTDTGK
4	17.11	991.4084 (2+)	991.4079	35–53	S**C**SGVEFSTSGHAYTDTGK
5	20.79	812.9068 (2+)	812.9058	62–74	YKV**C**NYGLIFTQK
6	18.38	767.3725 (2+)	767.3722	162–174	SKL**C**QNNFALGYK
7	20.15	659.8099 (2+)	659.8087	164–174	L**C**QNNFALGYK

M: methionine sulfoxide; **C**: cysteine oxidized to sulfonic acid.

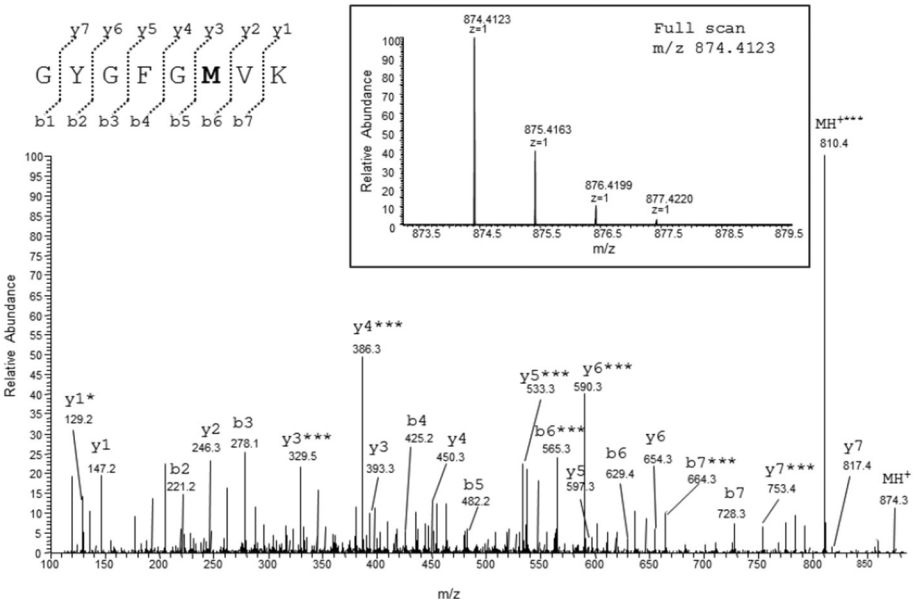

Fig. 5. MS/MS mass spectrum of the single charged molecular ion at *m/z* 874.4123 (calculated 874.4127) of the tryptic peptide of reduced and carboxyamidomethylated rVDAC3 containing methionine residue 26 in the oxidized form of methionine sulfoxide. Fragment ion originated from the neutral loss of H_2O is indicated by an asterisk. Fragment ions originated from the neutral loss of methanesulfenic acid (CH_3SOH, 64 Da) are indicated by three asterisks. The full scan mass spectrum of the molecular ion is shown in the inset.

Data analysis was particularly focused on the investigation of the oxidation state of Met and Cys residues. The sequence of rat VDAC3 includes two methionines in position 26 and 155. It should be noted that the numeration adopted in the discussion starts from Met[1], which, actually, has been shown to be absent.

Among the peptides identified, besides fragments containing Met[26] in the normal form (Table 1, fragment 2), peptides containing this residue in the form of methionine sulfoxide were also detected (Table 2, fragments 1 and 2). The full scan and fragment ion mass spectrum of the molecular ion of the peptide G[21]YGFGMVK[28] containing Met[26] as methionine sulfoxide are reported in Fig. 5. The MS/MS spectrum shows the characteristic neutral loss of 64 Da corresponding to the ejection of methanesulfenic acid from the side chain of MetO [23]. The oxidation state of Met[155] was not determined because this residue is present in a peptide not detected.

The sequence of rVDAC3 includes seven cysteines in position 2, 8, 36, 65, 122, 165, and 229. Again, the numeration adopted starts from Met[1], which, actually, has been shown to be absent. Analysis of the mass spectral data oriented to the determination of oxidation state of cysteines showed that Cys[2] and Cys[8], which are in the same N-terminal tryptic peptide with Cys[2] acetylated, are identified exclusively in the reduced and carboxyamidomethylated form (Fig. 4, Table 1, fragment 1). For cysteines 36, 65 and 165, besides the peptides containing these residues carboxyamidomethylated (Table 1, fragments 3, 4, 5, 6, 11, and 12), peptides containing these residues in the form of sulfonic acid are also detected (Fig. 6A, B, and C, and Table 2, fragments 3, 4, 5, 6 and 7).

The oxidation state of cysteines 122 and 229 could not be determined because these residues were not contained in the identified tryptic peptides.

3.1.2. Chymotryptic digestion

To increase the sequence coverage, chymotryptic digestion was also performed. When combining the coverage obtained in the tryptic and chymotryptic digestions, the coverage of the sequence of rVDAC3 was extended to 96% (271 out of 282 amino acids) (Fig. 3, Tables 3 and 4).

The regions still not covered correspond to the sequence Lys[115]-Phe[123] and Gly[140]-Trp[141], stretches that resulted also not determined in a previous work [22]. Noticeable, the mass spectral data showed that there is a point substitution Lys → Asn[128] with respect to the reported sequence (SwissProt Acc. N. Q9R1Z0). This substitution is consistent with the sequence reported in SwissProt Acc. N. AAF80117.

Mass spectral analysis confirmed the absence of Met[1], the acetylation of Cys[2] (Table 3, fragment 1) and the oxidation of Met[26] to methionine sulfoxide (Table 4, fragment 1). In addition, Met[155] was detected both as normal methionine (Table 3, fragment 12) and as methionine sulfoxide (Table 4, fragment 3). The results also confirmed the presence of Cys[2] and Cys[8] exclusively in the carboxyamidomethylated form (Table 3, fragment 1), and the partial oxidation of Cys[65] and Cys[165] to sulfonic acid (Table 4, fragments 2 and 4). Cys[36] was found in the carboxyamidomethylated form (Table 4, fragment 1), whereas Cys[229], whose oxidation state could not be determined in the analysis of the tryptic peptides, was detected exclusively in the form of sulfonic acid (Table 4, fragment 5). Peptides containing Cys[122] were not detected.

3.2. Control experiments using chicken lysozyme as model protein show that the SDS-PAGE run does not cause unspecific oxidation of cysteines

It has been reported that methionines and cysteines may undergo artefactual oxidation under the conditions employed for the sodium dodecyl sulfate-gel electrophoresis [24,25]. In order to exclude the possibility that the oxidation of cysteine and methionine residues of rVDAC3 is due to the conditions used in the electrophoretic run, chicken lysozyme, as model protein, was electrophoresed on polyacrylamide gel and subjected to trypsin in-gel digestion followed by peptide analysis by mass spectrometry, adopting the same experimental conditions used for the analysis of VDACs. Moreover, the investigation was repeated using an in-solution digestion procedure, thus avoiding the

Fig. 6. (A) MS/MS mass spectrum of the triply charged molecular ion at *m/z* 737.6550 (calculated 737.6554) of the tryptic peptide of reduced and carboxyamidomethylated rVDAC3 containing cysteine residue 36 in the form of sulfonic acid. (B) MS/MS mass spectrum of the doubly charged molecular ion at *m/z* 812.9068 (calculated 812.9058) of the tryptic peptide of reduced and carboxyamidomethylated rVDAC3 containing cysteine residue 65 in the form of sulfonic acid. (C) MS/MS mass spectrum of the doubly charged molecular ion at *m/z* 659.8099 (calculated 659.8087) of the tryptic peptide of reduced and carboxyamidomethylated rVDAC3 containing cysteine residue 165 in the form of sulfonic acid. Fragment ions originated from the neutral loss of H_2O are indicated by an asterisk. Fragment ions originated from the neutral loss of NH_3 are indicated by two asterisks. The full scan mass spectrum of the molecular ion is shown in the inset.

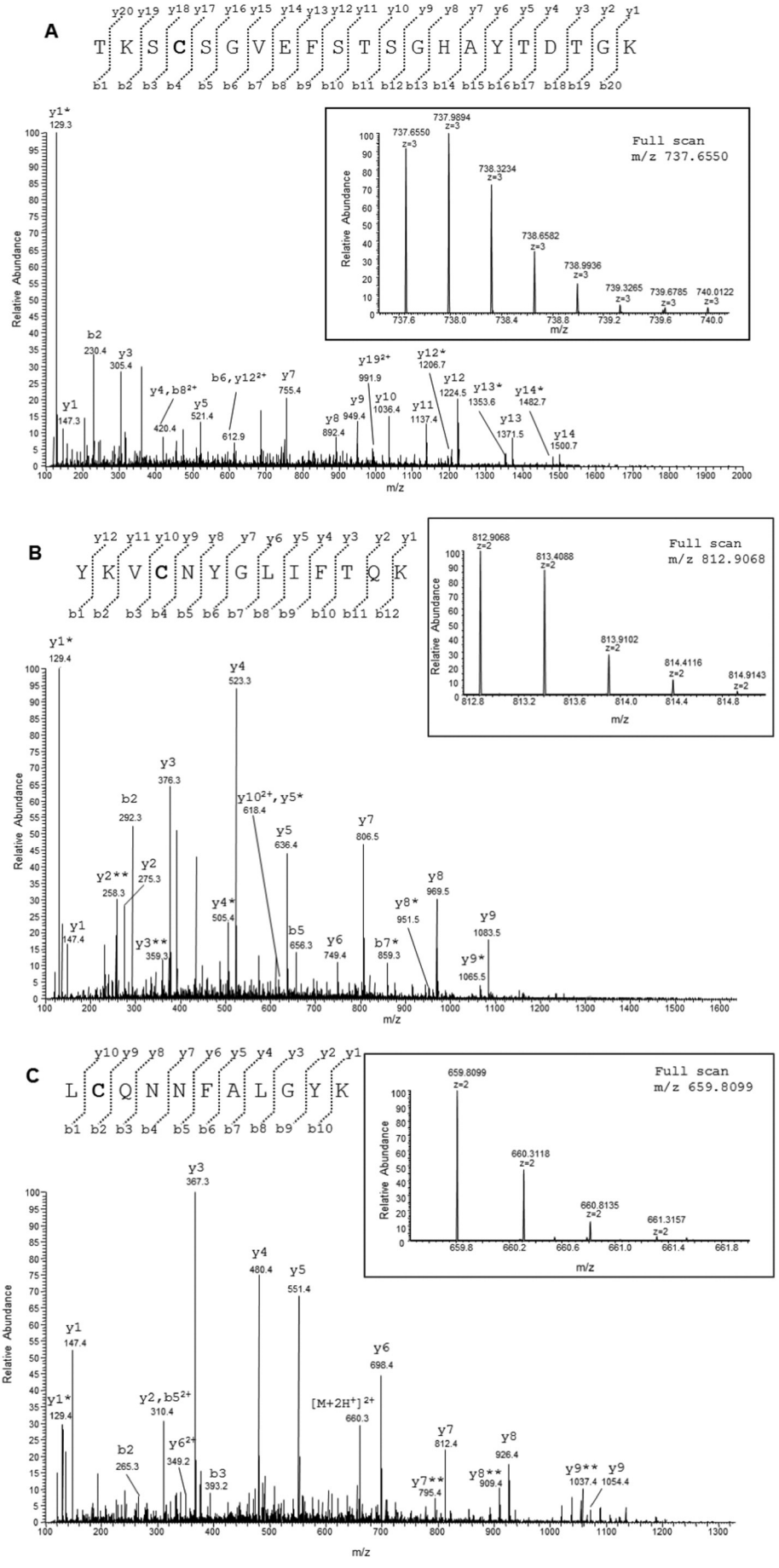
A
T K S C S G V E F S T S G H A Y T D T G K
Full scan
m/z 737.6550
B
Y K V C N Y G L I F T Q K
Full scan
m/z 812.9068
C
L C Q N N F A L G Y K
Full scan
m/z 659.8099
Relative Abundance
m/z

Table 3
Chymotryptic peptides found in rVDAC3 after DTT reduction and carboxyamidomethylation.
In the table the respective retention time, experimentally measured and calculated monoisotopic *m/z* of the molecular ions, the position in the sequence and the peptide sequence of fragments present in the chymotryptic digest of reduced and carboxyamidomethylated rVDAC3 are reported. All sequences were confirmed by MS/MS except that indicated by an asterisk. These sequences were used to build the sequence coverage scheme shown in Fig. 3.

Frag. n.	Rt (min)	Monoisotopic *m/z*		Position in the sequence	Peptide sequence
		Measured	Calculated		
1	19.85	813.0436 (3+)	813.0436	2–22	[a]**C**STPTY**C**DLGKAAKDVFNKGY
2	11.20	730.0095 (3+)	730.0099	42–62	STSGHAYTDTGKASGNLETKY
3	11.00	742.8646 (2+)	742.8650	49–62	TDTGKASGNLETKY
4	14.29	717.0124 (3+)	717.0125	49–67	TDTGKASGNLETKYKV**C**NY
5	19.98	496.7817 (2+)	496.7818	68–75	GLIFTQKW
6	22.02	1103.0367 (2+)	1103.0371	76–95	NTDNTLGTEISWENKLAEGL
7	18.08	557.8269 (2+)	557.8270	88–97	ENKLAEGLKL
8	16.88	602.3438 (3+)	602.3438	98–114	TVDTIFVPNTGKKSGKL
9	23.48	835.8995 (2+)	835.8990	124–139	SVGS**N**VDIDFSGPTIY[b]
10	24.81	892.4570 (1+)	892.4563	142–149	AVLAFEGW
11	23.33	1013.4730 (1+)	1013.4727	144–153	AFEGWLAGY
12	16.22	419.2166 (3+)	419.2169	154–164	QMSFDTAKSKL[a]
13	11.87	713.3426 (2+)	713.3432	158–169	DTAKSKL**C**QNNF
14	17.96	507.2504 (2+)	507.2506	170–178	ALGYKAEDF
15	17.73	822.3831 (3+)	822.3838	174–195	KAEDFQLHTHVNDGTEFGGSIY
16	16.39	772.4260 (2+)	772.4256	196–208	QRVNEKIETSINL
17	18.89	600.9917 (3+)	600.9916	196–210	QRVNEKIETSINLAW
18	15.82	612.7915 (2+)	612.7914	209–219	AWTAGSNNTRF
19	17.02	914.4604 (2+)	914.4605	209–225	AWTAGSNNTRFGIAAKY
20	15.14	785.9022 (2+)	785.9023	211–225	TAGSNNTRFGIAAKY
21	18.59	703.8857 (2+)	703.8855	234–247	SAKVNNASLIGLGY
22	14.34	549.8351 (2+)	549.8351	248–257	TQSLRPGVKL
23	16.85	656.9010 (2+)	656.9010	248–259	TQSLRPGVKLTL
24	18.80	1164.6257 (1+)	1164.6259	258–268	TLSALVDGKNF
25	15.82	475.7508 (2+)	475.7507	260–268	SALVDGKNF
26	14.67	528.7828 (2+)	528.7829	269–279	NAGGHKVGLGF
27	17.60	749.8857 (2+)	749.8861	269–283	NAGGHKVGLGFELEA

[b] Peptide carrying the substitutions Lys → Asn^{128}.
[a] C: N-terminal acetylated; **C**: cysteine carboxyamidomethylated.

electrophoretic step. Chicken lysozyme contains two methionines and eight cysteine residues. Tryptic digestion is expected to originate 18 fragments (Supplementary Table 1). Methionine residues are contained in the tryptic fragments 3 and 13. Fragment 3 resulted undetectable under our chromatographic conditions, probably because to the occurrence of missed cleavages. Therefore, peptide 13 was selected as marker for possible methionine oxidation induced by electrophoresis. Cysteine residues are contained in the tryptic peptides 3, 6, 9, 11, 15 and 17. Fragment 11 comprises three cysteine residues. Fragments 3, 15 and 17 were not detected under our chromatographic conditions, probably for the same reason above noted or because of their small size. Therefore, fragments 6, 9 and 11 were selected as markers of possible cysteine oxidation induced by electrophoresis.

The relative abundance of peptides containing methionine oxide and cysteine residues oxidized to sulfonic acid and "normal" (containing methionine and carboxyamidomethylated cysteines) peptides was estimated from the ratio of the absolute intensities of the respective multiply charged molecular ions. These results are summarized in Supplementary Table 2a and b.

Results in Supplementary Table 2a and b show that when the protein is reduced, blocked and digested after the electrophoretic step, the amount of methionine oxide increases by one order of magnitude with respect to the protein reduced, blocked and digested in solution. Therefore, it appears that methionine residues are to some extent susceptible to oxidation under the electrophoretic run conditions.

Results in Supplementary Table 2a and b also show that the three cysteine residues contained in the peptides 6, 9 and 11 are not found or found in trace amount in the form of sulfonic acid, with no significant differences between the two samples, indicating that cysteine residues oxidation is not affected by the electrophoresis. In conclusion, the analysis of the tryptic digests of lysozyme demonstrates that the oxidation of methionine residues is affected to some extent by the electrophoresis, whereas cysteine residues are totally not susceptible to oxidation to sulfonic acid both under the electrophoretic run and in-solution digestion conditions.

3.3. Direct digestion of HTP eluates shows that cysteine over-oxidation precedes the electrophoretic separation

To further validate these results, the hydroxyapatite eluate of Triton X-100 solubilized rat liver mitochondria was directly digested in-solution by trypsin or chymotrypsin, thus avoiding the electrophoretic run, and the resulting peptide mixtures analyzed by UHPLC/High Resolution ESI-MS/MS. In this experiment every protein present in the hydroxyapatite eluate was digested. Therefore, due to the high complexity of the resulting peptide mixture, the sequence coverage of VDAC3 obtained combining the peptides identified in the tryptic and chymotryptic digestions was slightly less extended with respect to the in-gel analysis (80%, 225 out of 282 amino acids, Supplementary Tables 3 and 5, Supplementary Fig. 1).

However, the presence of Met^{26} oxidized to methionine sulfoxide was confirmed (Supplementary Table 4, fragments 1–5). Although from these data a precise determination of the amount of methionine and methionine sulfoxide respectively present in the digestion mixture cannot be obtained, a rough estimation of their relative abundance can be derived from the comparison of the absolute intensities of the multiply charged molecular ions of the respective peptides. These calculations for the doubly charged molecular ion of the peptide

G^{21}YGFGMVK^{28}, detected in the tryptic digest, indicate a ratio of about 0.6:1 MetO/Met (Table 5).

However, the oxidation of cysteines 36, 65, 165 (Supplementary Table 4, fragments 6, 7, 8, 9 and 10), and 229 (Supplementary Table 6, fragment 1) to sulfonic acid, and the presence of Cys^2 and Cys^8

Table 4
Sulfur-modified peptides found in rVDAC3 chymotryptic digest after DTT reduction and carboxyamidomethylation.
In the table the respective retention time, experimentally measured and calculated monoisotopic *m/z* of the molecular ions, the position in the sequence and the peptide sequences of modified fragments present in the chymotryptic digest of reduced and carboxyamidomethylated rVDAC3 are reported. All sequences were confirmed by MS/MS. These sequences were used to build the sequence coverage scheme shown in Fig. 3.

Frag. n.	Rt (min)	Monoisotopic *m/z*		Position in the sequence	Peptide sequence
		Measured	Calculated		
1	17.97	707.0237 (3+)	707.0240	23–41	GFG**M**VKIDLKTKS***C***SGVEF
2	22.35	552.7733 (2+)	552.7736	63–71	KV**C**NYGLIF
3	17.13	627.8052 (2+)	627.8057	154–164	**Q****M**SFDTAKSKL
4	14.59	708.8251 (2+)	708.8251	158–169	DTAKSKL**C**QNNF
5	12.06	506.2480 (2+)	506.2482	226–233	RLD**C**RTSL

M: methionine sulfoxide; **C**: cysteine oxidized to sulfonic acid; ***C***: cysteine carboxyamidomethylated; **Q**: pyroglutamic acid form.

exclusively in the carboxyamidomethylated form was confirmed (Supplementary Table 3, fragment 1).

Again, a rough estimation of the relative abundance of the cysteines oxidized to sulfonic acid with respect to the Cys detected in the carboxyamidomethylated form can be derived from the ratio of the absolute intensities of the multiply charged molecular ions of the respective peptides. From these comparisons (Table 5), a ratio Cys-oxidized-to-sulfonic-acid/Cys-carboxyamidomethylated ranging from about 0.2:1 to 2:1 is observed. In the evaluation of these results it should be considered that the oxidation of cysteine to cysteine sulfonic acid introduces a strong negative charge in the peptide, thus hampering the formation of positive ions. On the other hand, in the presence of the strong negatively charged sulfonic group, the susceptibility to tryptic cleavage of proximal Arg or Lys sites may be reduced, thus favoring the formation of peptides containing missed cleavages. However, even taking into account these considerations, the data in Table 5 suggest that a considerable amount of cysteines is oxidized to sulfonic acid. Cys^{229} was detected exclusively in the form of sulfonic acid (Supplementary Table 6, fragment 1).

3.4. Pre-incubation of mitochondria with DTT shows that over-oxidations preexist to the chromatographic separation

To exclude the possibility that any unspecific and undesired oxidation could happen during the purification protocol, we added DTT to the buffer used to suspend the mitochondria and in the purification steps, as described in the Experimental Section. In-solution tryptic digestion of the hydroxyapatite eluate and mass spectrometry analysis was then performed using the same procedure adopted for the in-solution digestion of the hydroxyapatite eluate obtained under non reducing conditions (described above). rVDAC3 peptides found in the analysis of the lysate of mitochondria incubated with DTT are reported in Supplementary Table 7. In particular, sulfur-modified peptides 1–6 (Supplementary Table 8 and Supplementary Fig. 2A, B and C) were detected. As reported in the Supplementary Table 9, no difference was observed in the ratio MetO/Met and Cys-oxidized-to-sulfonic-acid/Cys-carboxyamidomethylated with respect to the data shown in Table 5, thus confirming that the oxidation state of sulfur containing peptides is not influenced by the analytical experimental procedures employed.

4. Discussion

Investigation of membrane proteins is generally difficult due to their low solubility. Analysis of rVDAC3 was complicated by the impossibility to separate the protein from the other VDAC isoforms and from the other proteins present in the hydroxyapatite eluate. However, high resolution mass spectrometry provided a powerful tool to overcome this difficulty.

Converging evidences, provided by all the experiments, clearly indicate that in rVDAC3 Met^1 is absent and that Cys^2 is acetylated. Although N-terminal acetylation is widespread in eukaryotes, the biological relevance of this modification is only known for a few substrates [26,27]. Unlike ε-lysine modification, N-terminal acetylation, catalyzed by N-terminal acetyltransferases, is irreversible and occurs co-translationally (for reviews see [28,29]). It has been suggested that co-translational N-acetylation modifies protein–protein interaction [30], affects accumulation of the mature protein(s) in target organelles [31], and confers metabolic stability on the protein by providing general protection from peptidases and the ubiquitin-mediated pathway of protein degradation [32]. In the present case the structural significance of N-acetylation is unclear.

The results also demonstrate that methionines 26 and 155 in rVDAC3 are present both in the normal form and in considerable amount in the form of methionine sulfoxide. Methionine residues are highly susceptible to oxidation mediated by reactive oxygen (ROS) and nitrogen species (NOS) [33]. Mild oxidizing conditions determine in vivo generation of methionine sulfoxide (MetO), which can be further oxidized to methionine sulfone ($MetO_2$) under stronger oxidizing conditions. MetO exists as a mixture of S and R diastereomers and its production is tightly regulated in vivo by ubiquitous sulfoxide reductases, which catalyze the thioredoxin-dependent reduction of MetO into methionine [34]. MetO diastereomers necessitate separate enzymes: MsrA and MsrB for Met-S-SO and Met-R-SO, respectively. Conversely, $MetO_2$ cannot be reduced in vivo. Cyclic Met oxidation/MetO reduction leads to consumption of ROS and thereby acts as a scavenging

Table 5
Comparison of the absolute intensities of molecular ions of selected sulfur containing tryptic peptides found in the analysis of rVDAC3 reduced with DTT, carboxyamidomethylated and digested in-solution.

Peptide	Position in the sequence	Measured monoisotopic *m/z*	Absolute intensity	Ratio Ox/Red
GYGFG**M**VK	21–28	437.7099 (2+)	$3.33 \cdot 10^6$	0.55
GYGFG**M**VK		429.7122 (2+)	$6.10 \cdot 10^6$	
TKS***C***SGVEFSTSGHAYTDTGK	33–53	737.6556 (3+)	$2.35 \cdot 10^6$	1.42
TKS***C***SGVEFSTSGHAYTDTGK		740.6678 (3+)	$1.65 \cdot 10^6$	
YKV**C**NYGLIFTQK	62–74	812.9064 (2+)	$4.87 \cdot 10^4$	0.18
YKV**C**NYGLIFTQK		817.4260 (2+)	$2.67 \cdot 10^5$	
SKL**C**QNNFALGYK	162–174	767.3719 (2+)	$1.47 \cdot 10^6$	1.87
SKL***C***QNNFALGYK		771.8906 (2+)	$7.85 \cdot 10^5$	

M: methionine sulfoxide; ***C***: cysteine carboxyamidomethylated; **C**: cysteine oxidized to sulfonic acid.

system to protect proteins from oxidative damage [35,36]. This hypothesis is consistent with the observation that, unlike other modifications, MetO formation has little or no effect on protein susceptibility to proteolytic degradation [37,38]. Numerous studies reported that MetO levels in proteins increase during aging and in certain diseases, in particular the neurodegenerative ones [39]. Evidence for an additional role of certain methionines as oxidation sensors in the redox regulation of enzyme activity is accumulating [40–42].

VDAC3 isoforms are particularly rich in cysteines. The predictive homology modelling of hVDAC3 indicates that cysteine residues, in the native state, populate loop segment located in the ring region oriented towards the inter-membrane space (Fig. 1). The structural model also suggests that, upon adopting a 19-stranded form, some cysteines are unlikely to be spatially proximal for disulfide bond formation [43]. Therefore, the structural and, conversely, the functional role of cysteines remained unclear. Our results unequivocally demonstrate that the cysteines in rVDAC3 have differentiated roles. Concordant evidences, provided by all the experiments performed, lead to the conclusion that cysteines 36, 65 and 165 are oxidized to a remarkable extend to sulfonic acid. Cysteines 2 and 8 are observed exclusively in the carboxyamidomethylated form, suggesting that in the native protein they are present either in the reduced form as free thiol groups or oxidized to disulfide. Cys^{229} is detected exclusively in the oxidized form of sulfonic acid, whereas the oxidation state of Cys^{122} could not be determined because peptides containing this residue were not detected. It is well known that cysteine thiol groups are susceptible to several oxidative modifications. In particular, cysteine thiol groups are oxidized by ROS to generate sulfenic (—SOH) groups. Once formed, —SOH can further undergo oxidation to —SO_2H and —SO_3H or additional reactions with other thiol groups to generate disulfide bonds. —SO_2H and —SO_3H derivatives are generally considered in vivo to be irreversible oxidation products, with the only exception of the catalytic cysteine in 2-Cys peroxiredoxins, which in vivo can be reduced back to —SH by sulfiredoxin or sestrin, protein-specific sulfinic acid reductase [44]. Being an irreversible modification, cysteine oxidation to sulfonic acid cannot be envisaged as a mechanism for dynamic regulation of protein activity. Therefore, the presence of cysteines 36, 65 and 165 as sulfonic acid in rVDAC3 may derive from protein aging or, conversely, these residues may have a functional role in such oxidation state for the activity of these trans-membrane pore proteins. Irreversible oxidation of cysteines, also termed over-oxidation, introducing distinct negative charges, can result in changes in protein structure or at least can modify the electrostatic surface of the protein accessible to water. Over-oxidation can also be required to target a protein to degradation. In particular, in the N-end rule pathway, the presence of an oxidated N-terminal cysteine in certain mammalian proteins, such as GTPase-activating proteins (RGS), is required for arginylation by ATE1 R-transferases and subsequent ubiquitin-dependent degradation [45,46]. In VDAC3, Cys^2 becomes the N-terminal end after post-translational modifications. In our work we have never detected the oxidated form of Cys^2: this can mean that the potentially Cys^2-oxidated, if existing, is a marker used to remove the protein from the membrane for degradation.

The three VDAC isoforms differ in the number and distribution in the sequence of the cysteines. Most of the cysteine residues of VDAC3 (cysteines 2, 36, 65, 122 and 229) are exposed towards the IMS, as visualized in the protein model [19]. The IMS has oxidizing properties that can impact on cysteines. In a previous report [47] we showed preliminary mass spectrometry data, which confirmed that cysteines in VDAC3 can exist in different oxidation states. As a consequence, in experiments where cysteines 2, 8 and 122 were removed in different combinations, the range of VDAC3 oxidation was reduced and the mutants regained the ability to complement the lack of the homologous porin1 in yeast cells [47]. Almost simultaneously, another group came to similar conclusions about cysteines in VDAC3 [48]. They produced also other cysteine mutants and claimed that the decreased channel gating observed for VDAC3 was due to fixation of the N-terminal domain to the bottom of the pore. The hypothesis that such gating function could be exerted by the disulfide bridge 2-122 did not find confirmations in our mass spectrometry analysis. The bioinformatic simulation of disulfide bridges in VDAC3 interestingly showed that the candidate S—S bridges are not really able to fully occlude the pore [43]. It was instead proposed that the formation of disulfide bridge(s) may change the exposition of residues in the N-terminal sequence, thus changing the presentation and the docking state of VDAC3 [49].

5. Conclusions

Our results demonstrate that the mitochondrial rVDAC3, in physiological state, contains methionines oxidized to methionine sulfoxide. Furthermore, cysteines 36, 65, 165 and 229 are oxidized to sulfonic acid in considerable amount. The peculiar behavior of Met and Cys residues of VDAC3 may be related with the location of this proteins in a strongly oxidizing environment and may be connected with the regulation of the activity of these trans-membrane pore proteins. The structural features elucidated by the present work may be helpful for a better understanding of the functional role of VDAC3.

Supplementary data to this article can be found online at http://dx.doi.org/10.1016/j.bbamem.2016.12.003.

Conflict of interest

The authors declare that they have no conflicts of interest with the contents of this article.

Transparency document

The Transparency document associated with this article can be found, in online version.

Acknowledgements

This work was supported by the Italian Ministero dell'Istruzione, dell'Università e della Ricerca, MIUR, (PRIN project 2015795S5W_005), by the FIR-UNICT project 2014 to AAM, RS and VDP and by a grant from PO FERS 2007/13 4.1.2.A, project "Piattaforma regionale di ricerca traslazionale per la salute".

References

[1] S.J. Schein, M. Colombini, A. Finkelstein, Reconstitution in planar lipid bilayers of a voltage-dependent anion-selective channel obtained from paramecium mitochondria, J. Membr. Biol. 30 (1976) 99–120.
[2] R. Benz, Permeation of hydrophilic solutes through mitochondrial outer membranes — review on mitochondrial porins, Biochim. Biophys. Acta 1197 (1994) 167–196.
[3] X. Xu, W. Decker, M.J. Sampson, W.J. Craigen, M. Colombini, Mouse VDAC isoforms expressed in yeast: channel properties and their roles in mitochondrial outer membrane permeability, J. Membr. Biol. 170 (1999) 89–102.
[4] A. Messina, S. Reina, F. Guarino, V. De Pinto, VDAC isoforms in mammals, Biochim. Biophys. Acta, Biomembr. 1818 (2012) 1466–1476.
[5] V. Checchetto, S. Reina, A. Magrì, I. Szabo, V. De Pinto, Recombinant human voltage dependent anion selective channel isoform 3 (hVDAC3) forms pores with a very small conductance, Cell Physiol. Biochem. 34 (2014) 842–853.
[6] V. Shoshan-Barmatz, V. De Pinto, M. Zweckstetter, Z. Raviv, N. Keinan, N. Arbel, VDAC, a multi-functional mitochondrial protein regulating cell life and death, Mol. Asp. Med. 31 (2010) 227–285.
[7] J.J. Lemasters, Modulation of mitochondrial membrane permeability in pathogenesis, autophagy and control of metabolism, J. Gastroenterol. Hepatol. 22 (2007) S31–S37.
[8] K. Anflous, W.J. Craigen, Mitochondrial porins in mammals: insights into functional roles from mutant mice and cells, in: R. Benz (Ed.), Bacterial and Eukaryotic Porins: Structure, Function, Mechanism, Wiley-VCH, Weinheim 2004, pp. 285–305.
[9] V.A. Menzel, M.C. Cassarà, R. Benz, V. De Pinto, A. Messina, V. Cunsolo, R. Saletti, K.D. Hinsch, E. Hinsch, Molecular and functional characterization of VDAC2 purified from mammal spermatozoa, Biosci. Rep. 29 (2009) 351–362.
[10] V. De Pinto, F. Guarino, A. Guarnera, A. Messina, S. Reina, F.M. Tomasello, V. Palermo, C. Mazzoni, Characterization of human VDAC isoforms: A peculiar function for VDAC3? Biochim. Biophys. Acta, Bioenerg. 1797 (2010) (66-66).
[11] K.D. Hinsch, V. De Pinto, V.A. Aires, X. Schneider, A. Messina, E. Hinsch, Voltage-dependent anion-selective channels VDAC2 and VDAC3 are abundant proteins in

bovine outer dense fibers, a cytoskeletal component of the sperm flagellum, J. Biol. Chem. 279 (2004) 15281–15288.
[12] M.J. Sampson, W.K. Decker, A.L. Beaudet, W. Ruitenbeek, D. Armstrong, M.J. Hicks, W.J. Craigen, Immotile sperm and infertility in mice lacking mitochondrial voltage-dependent anion channel type 3, J. Biol. Chem. 276 (2001) 39206–39212.
[13] S. Majumder, H.A. Fisk, VDAC3 and Mps1 negatively regulate ciliogenesis, Cell Cycle 12 (2013) 849–858.
[14] S. Hiller, R.G. Garces, T.J. Malia, V.Y. Orekhov, M. Colombini, G. Wagner, Solution structure of the integral human membrane protein VDAC-1 in detergent micelles, Science 321 (2008) 1206–1210.
[15] R. Ujwal, D. Cascio, J.P. Colletier, S. Faham, J. Zhang, L. Toro, P. Ping, J. Abramson, The crystal structure of mouse VDAC1 at 2.3 angstrom resolution reveals mechanistic insights into metabolite gating, Proc. Natl. Acad. Sci. U. S. A. 105 (2008) 17742–17747.
[16] M. Bayrhuber, T. Meins, M. Habeck, S. Becker, K. Giller, S. Villinger, C. Vonrhein, C. Griesinger, M. Zweckstetter, K. Zeth, Structure of the human voltage-dependent anion channel, Proc. Natl. Acad. Sci. U. S. A. 105 (2008) 15370–15375.
[17] M.F. Tomasello, F. Guarino, S. Reina, A. Messina, V. De Pinto, The voltage-dependent anion selective channel 1 (VDAC1) topography in the mitochondrial outer membrane as detected in intact cell, PLoS One 8 (2013), e81522. .
[18] J. Schredelseker, A. Paz, C.J. Lopez, C. Altenbach, C.S. Leung, M.K. Drexler, J.N. Chen, W.L. Hubbell, J. Abramson, High resolution structure and double electron–electron resonance of the zebrafish voltage-dependent anion channel 2 reveal an oligomeric population, J. Biol. Chem. 289 (2014) 12566–12577.
[19] G.F. Amodeo, M.A. Scorciapino, A. Messina, V. De Pinto, M. Ceccarelli, Charged residues distribution modulates selectivity of the open state of human isoforms of the voltage dependent anion-selective channel, PLoS One 9 (2014), e103879. .
[20] V. De Pinto, G. Prezioso, F. Palmieri, A simple and rapid method for the purification of the mitochondrial porin from mammalian tissues, Biochim. Biophys. Acta 905 (1987) 499–502.
[21] V. De Pinto, R. Benz, C. Caggese, F. Palmieri, Characterization of the mitochondrial porin from *Drosophila melanogaster*, Biochim. Biophys. Acta 987 (1989) 1–7.
[22] A.M. Distler, J. Kerner, S.M. Peterman, C.L. Hoppel, A targeted proteomic approach for the analysis of rat liver mitochondrial outer membrane proteins with extensive sequence coverage, Anal. Biochem. 356 (2006) 18–29.
[23] Z.Q. Guan, N.A. Yates, R. Bakhtiar, Detection and characterization of methionine oxidation in peptides by collision-induced dissociation and electron capture dissociation, J. Am. Soc. Mass Spectrom. 14 (2003) 605–613.
[24] G. Sun, V.E. Anderson, Prevention of artifactual protein oxidation generated during sodium dodecil sulfate-gel electrophoresis, Electrophoresis 25 (2004) 959–965.
[25] K. Klarskov, D. Roecklin, B. Bouchon, J. Sabatie, A. Van Dorsselaer, R. Bishoff, Analysis of recombinant schistosoma-mansoni antigen RSMP 28 by online liquid-chromatography mass-spectrometry combined with sodium dodecyl-sulfate polyacrylamide-gel electrophoresis, Anal. Biochem. 216 (1994) 127–134.
[26] R. Caesar, J. Warringer, A. Blomberg, Physiological importance and identification of novel targets for the N-terminal acetyltransferase NatB, Eukaryot. Cell 5 (2006) 368–378.
[27] B. Polevoda, J. Norbeck, H. Takakura, A. Blomberg, F. Sherman, Identification and specificities of N-terminal acetyltransferases from *Saccharomyces cerevisiae*, EMBO J. 18 (1999) 6155–6168.
[28] B. Polevoda, F. Sherman, N alpha-terminal acetylation of eukaryotic proteins, J. Biol. Chem. 275 (2000) 36479–36482.
[29] B. Polevoda, F. Sherman, N-terminal acetyltransferases and sequence requirements for N-terminal acetylation of eukaryotic proteins, J. Mol. Biol. 325 (2003) 595–622.
[30] L.R. Manning, J.M. Manning, The acetylation state of human fetal hemoglobin modulates the strength of its subunit interactions: Long-range effects and implications for histone interactions in the nucleosome, Biochemistry 40 (2001) 1635–1639.
[31] P. Pesaresi, N.A. Gardner, S. Masiero, A. Dietzmann, L. Eichacker, R. Wickner, F. Salamini, D. Leister, Cytoplasmic N-terminal protein acetylation is required for efficient photosynthesis in *Arabidopsis*, Plant Cell 15 (2003) 1817–1832.
[32] A. Hershko, H. Heller, E. Eytan, G. Kaklij, I.A. Rose, Role of the alpha-amino group of protein in ubiquitin-mediated protein breakdown, Proc. Natl. Acad. Sci. U. S. A. 81 (1984) 7021–7025.
[33] R.L. Levine, J. Moskovitz, E.R. Stadtman, Oxidation of methionine in proteins: roles in antioxidant defense and cellular regulation, IUBMB Life 50 (2000) 301–307.
[34] E.R. Stadtman, J. Moskovitz, R.L. Levine, Oxidation of methionine residues of proteins: biological consequences, Antioxid. Redox Signal. 5 (2003) 577–582.
[35] E.R. Stadtman, Protein oxidation and aging, Free Radic. Res. 40 (2006) 1250–1258.
[36] N. Ugarte, I. Petropoulos, B. Friguet, Oxidized mitochondrial protein degradation and repair in aging and oxidative stress, Antioxid. Redox Signal. 13 (2010) 539–549.
[37] R.L. Levine, L. Mosoni, B.S. Berlett, E.R. Stadtman, Methionine residues as endogenous antioxidants in proteins, Proc. Natl. Acad. Sci. U. S. A. 93 (1996) 15036–15040.
[38] E.R. Stadtman, J. Moskovitz, B.S. Berlett, R.L. Levine, Cyclic oxidation and reduction of protein methionine residues is an important antioxidant mechanism, Mol. Cell Biochem. 234–235 (2002) 3–9.
[39] E.R. Stadtman, H. Van Remmen, A. Richardson, N.B. Wehr, R.L. Levine, Methionine oxidation and aging, Biochim. Biophys. Acta 1703 (2005) 135–140.
[40] R.K. Bartlett, R.J.B. Urbauer, A. Anbanandam, H.S. Smallwood, J.L. Urbauer, T.C. Squier, Oxidation of Met(144) and Met(145) in calmodulin blocks calmodulin dependent activation of the plasma membrane Ca-ATPase, Biochemistry 42 (2003) 3231–3238.
[41] D.J. Bigelow, T.C. Squier, Redox modulation of cellular signaling and metabolism through reversible oxidation of methionine sensors in calcium regulatory proteins, Biochim. Biophys. Acta 1703 (2005) 121–134.
[42] J.R. Erickson, M.L. Joiner, X. Guan, W. Kutschke, J. Yang, C.V. Oddis, R.K. Bartlett, J.S. Lowe, S.E. O'Donnell, N. Aykin-Burns, M.C. Zimmerman, K. Zimmerman, A.J.L. Ham, R.M. Weiss, D.R. Spitz, M.A. Shea, R.J. Colbran, P.J. Mohler, M.E. Anderson, A dynamic pathway for calcium-independent activation of CaMKII by methionine oxidation, Cell 133 (2008) 462–474.
[43] C. Guardiani, L. Leggio, M.A. Scorciapino, V. De Pinto, M. Ceccarelli, A computational study of ion current modulation in hVDAC3 induced by disulfide bonds, Biochim. Biophys. Acta 1858 (2016) 813–823.
[44] A. Bachi, I. Dalle-Donne, A. Scaloni, Redox proteomics: chemical principles, methodological approaches and biological/biomedical promises, Chem. Rev. 113 (2013) 596–698.
[45] K.G. Reddie, K.S. Carroll, Expanding the functional diversity of proteins through cysteine oxidation, Curr. Opin. Chem. Biol. 12 (2008) 746–754.
[46] T. Tasaki, Y.T. Kwon, The mammalian N-end rule pathway: new insights into its components and physiological roles, Trends Biochem. Sci. 32 (2007) 520–528.
[47] S. Reina, V. Checchetto, R. Saletti, A. Gupta, D. Chaturvedi, C. Guardiani, F. Guarino, M.A. Scorciapino, A. Magrì, S. Foti, M. Ceccarelli, A.A. Messina, R. Mahalakshmi, I. Szabo, V. De Pinto, VDAC3 as a sensor of oxidative state of the intermembrane space of mitochondria: the putative role of cysteine residue modifications, Oncotarget 7 (2016) 2249–2268.
[48] M. Okazaki, K. Kurabayashi, M. Asanuma, Y. Saito, K. Dodo, M. Sodeoka, VDAC3 gating is activated by suppression of disulfide-bond formation between the N-terminal region and the bottom of the pore, Biochim. Biophys. Acta 1848 (2015) 3188–3196.
[49] V. De Pinto, S. Reina, A. Gupta, A. Messina, R. Mahalakshmi, Role of cysteines in mammalian VDAC isoforms' function, Biochim. Biophys. Acta 1857 (2016) 1219–1227.

Supplementary Table 1. Expected tryptic peptides of reduced and carboxyamidomethylated chicken lysozyme.

In the Table the calculated monoisotopic m/z of the mono and multiply charged molecular ions, the position in the sequence and the peptide sequence of the fragments expected in tryptic digest of reduced and carboxyamidomethylated chicken lysozyme are reported.

Frag. n.	Calculated monoisotopic m/z			Position in the sequence	Peptide sequence
	MH^+	$M2H^+$	$M3H^+$		
1	147.1128	74.0600	49.7091	1	K
2	478.2772	239.6423	160.0973	2–5	VFGR
3	893.4219	447.2146	298.4788	6– 13	***C***ELAAAMK
4	175.1190	88.0631	59.0445	14	R
5	874.4166	437.7119	292.1437	15–21	HGLDNYR
6	1325.6307	663.3190	442.5484	22–33	GYSLGNWV***C***AAK
7	1428.6502	714.8288	476.8883	34–45	FESNFNTQATNR
8	1753.8351	877.4212	585.2832	46–61	NTDGSTDYGILQINSR
9	993.3996	497.2034	331.8047	62–68	WW***C***NDGR
10	517.2729	259.1401	173.0958	69-73	TPGSR
11	2508.1891	1254.5982	836.7346	74–96	NL***C***NIP***C***SALLSSDITASVN***C***AK
12	147.1128	74.0600	49.7091	97	K
13	1675.8009	838.4041	559.2718	98-112	IVSDGNGMNAWVAWR
14	289.1619	145.0846	97.0588	113–114	NR
15	307.1435	154.0754	103.0527	115–116	***C***K
16	1045.5425	523.2749	349.1857	117–125	GTDVQAWIR
17	392.1711	196.5892	131.3952	126–128	G***C***R
18	132.1019	66.5546	44.7055	129	L

C: cysteine carboxyamidomethylated.

Supplementary Table 2a. Comparison of the absolute intensities of molecular ions of selected sulfur containing peptides found in the analysis of tryptic digest of chicken lysozyme reduced and carboxyamidomethylated after SDS-PAGE.

Frag. n.	Chicken lysozyme tryptic peptide	Position in the sequence	Measured monoisotopic *m/z*	Absolute intensity	Ratio Ox/Red
13	IVSDGNG**M**NAWVAWR	98-112	846.4017 (2+)	$1.31 \cdot 10^{7}$	0.27
	IVSDGNGMNAWVAWR		838.4059 (2+)	$4.77 \cdot 10^{7}$	
6	GYSLGNWV**C**AAK	22-33	658.8009 (2+)	$1.50 \cdot 10^{5}$	$5.62 \cdot 10^{-4}$
	GYSLGNWV***C***AAK		663.3211 (2+)	$2.67 \cdot 10^{8}$	
9	WW**C**NDGR	62-68	492.6847 (2+)	$1.54 \cdot 10^{5}$	$1.31 \cdot 10^{-3}$
	WW***C***NDGR		497.2057 (2+)	$1.18 \cdot 10^{8}$	
11	NL**C**NIP**C**SALLSSDITASVN**C**AK	74-96	Notfound	-	
	NL***C***NIP***C***SALLSSDITASVN***C***AK		1254.5989 (+2)	$2.65 \cdot 10^{6}$	

M: methionine sulfoxide; ***C***: cysteine carboxyamidomethylated; **C**: cysteine oxidized to sulfonic acid.

Supplementary Table 2b. Comparison of the absolute intensities of molecular ions of selected sulfur containing peptides found in the analysis of in-solution tryptic digest of reduced and carboxyamidomethylated chicken lysozyme.

Frag. n.	Peptide	Position in the sequence	Measured monoisotopic *m/z*	Absolute intensity	Ratio Ox/Red
13	IVSDGNG**M**NAWVAWR	98-112	846.4012 (2+)	$6.31 \cdot 10^{6}$	$2.20 \cdot 10^{-2}$
	IVSDGNGMNAWVAWR		838.4059 (2+)	$2.87 \cdot 10^{8}$	
6	GYSLGNWV**C**AAK	22-33	658.8004 (2+)	$1.35 \cdot 10^{5}$	$1.34 \cdot 10^{-4}$
	GYSLGNWV***C***AAK		663.3210 (2+)	$1.01 \cdot 10^{9}$	
9	WW**C**NDGR	62-68	492.6853 (2+)	$6.08 \cdot 10^{4}$	$0.97 \cdot 10^{-4}$
	WW***C***NDGR		497.2052 (2+)	$6.26 \cdot 10^{8}$	
11	NL**C**NIP**C**SALLSSDITASVN**C**AK	74-96	Not found	-	
	NL***C***NIP***C***SALLSSDITASVN***C***AK		1254.5994 (+2)	$1.79 \cdot 10^{7}$	

M: methionine sulfoxide; ***C***: cysteine carboxyamidomethylated; **C**: cysteine oxidized to sulfonic acid.

Supplementary Table 3. Tryptic peptides found in the analysis of rVDAC3 reduced with DTT, carboxyamidomethylated and digested in-solution.

In the Table the respective retention time, experimentally measured and calculated monoisotopic m/z of the molecular ions, the position in the sequence and the peptide sequence of fragments present in the tryptic digest of reduced and carboxyamidomethylated rVDAC3 are reported. All sequences were confirmed by MS/MS. These sequences were used to build the sequence coverage scheme shown in Supplementary Fig. 1.

Frag. n.	Rt (min)	Monoisotopic m/z		Position in the sequence	Peptide sequence
		Measured	Calculated		
1	45.91	672.2836 (2+)	672.2839	2-12	*CSTPTYCDLGK
2	42.57	433.7278 (4+)	433.7280	13-28	AAKDVFNKGYGFGMVK
3	50.16	734.3997 (3+)	734.3978	13-32	AAKDVFNKGYGFGMVKIDLK
4	49.85	731.3638 (2+)	731.3634	16-28	DVFNKGYGFGMVK
5	55.17	644.3425 (3+)	644.3414	16-32	DVFNKGYGFGMVKIDLK
6	51.41	540.7935 (4+)	540.7939	16-34	DVFNKGYGFGMVKIDLKTK
7	43.83	429.7122 (2+)	429.7126	21-28	GYGFGMVK
8	30.22	740.6678 (3+)	740.6673	33-53	TKSCSGVEFSTSGHAYTDTGK
9	31.90	755.8530 (4+)	755.8534	33-61	TKSCSGVEFSTSGHAYTDTGKASGNLETK
10	34.99	995.9261 (2+)	995.9260	35-53	SCSGVEFSTSGHAYTDTGK
11	35.09	931.0883 (3+)	931.0874	35-61	SCSGVEFSTSGHAYTDTGKASGNLETK
12	48.26	817.4260 (2+)	817.4240	62-74	YKVCNYGLIFTQK
13	51.97	671.8449 (2+)	671.8448	64-74	VCNYGLIFTQK
14	54.52	954.4418 (2+)	954.4421	75-90	WNTDNTLGTEISWENK
15	59.02	840.4190 (3+)	840.4186	75-96	WNTDNTLGTEISWENKLAEGLK
16	57.81	672.7180 (3+)	672.7174	91-109	LAEGLKLTVDTIFVPNTGK
17	53.67	715.4160 (3+)	715.4157	91-110	LAEGLKLTVDTIFVPNTGKK
18	55.05	702.8909 (2+)	702.8903	97-109	LTVDTIFVPNTGK
19	47.87	766.9381 (2+)	766.9378	97-110	LTVDTIFVPNTGKK
20	38.43	771.8906 (2+)	771.8903	162-174	SKLCQNNFALGYK
21	43.85	664.3254 (2+)	664.3268	164-174	LCQNNFALGYK
22	51.86	983.2153 (4+)	983.2134	164-197	LCQNNFALGYKAEDFQLHTHVNDGTEFGGSIYQR
23	46.27	874.4056 (3+)	874.4054	175-197	AEDFQLHTHVNDGTEFGGSIYQR
24	49.88	1159.5886 (2+)	1159.5904	198-218	VNEKIETSINLAWTAGSNNTR
25	53.50	924.4669 (2+)	924.4659	202-218	IETSINLAWTAGSNNTR
26	49.77	892.1684 (3+)	892.1677	231-256	TSLSAKVNNASLIGLGYTQSLRPGVK
27	49.92	1044.0846 (2+)	1044.0840	237-256	VNNASLIGLGYTQSLRPGVK
28	59.42	1028.9182 (3+)	1028.9187	237-266	VNNASLIGLGYTQSLRPGVKLTLSALVDGK
29	56.09	978.2887 (4+)	978.2883	237-274	VNNASLIGLGYTQSLRPGVKLTLSALVDGKNFNAGGHK
30	51.91	508.8030 (2+)	508.8030	257-266	LTLSALVDGK
31	46.42	461.2522 (4+)	461.2526	257-274	LTLSALVDGKNFNAGGHK

32	50.32	587.2972 (3+)	587.2969	267-283	NFNAGGHKVGLGFELEA

*C: N-terminal acetylated; ***C***: cysteine carboxyamidomethylated.

Supplementary Table 4. Sulfur-modified tryptic peptides found in the analysis of rVDAC3 reduced with DTT, carboxyamidomethylated and digested in-solution.

In the Table the respective retention time, experimentally measured and calculated monoisotopic m/z of the molecular ions, the position in the sequence and the peptide sequence of modified fragments present in the tryptic digest of reduced and carboxyamidomethylated rVDAC3 are reported. All sequences were confirmed by MS/MS except that indicated by an asterisk.

Frag. n.	Rt (min)	Monoisotopic m/z		Position in the sequence	Peptide sequence
		Measured	Calculated		
1	38.37	583.2997 (3+)	583.2998	13-28	AAKDVFNKGYGFG**M**VK
2	46.60	555.0479 (4+)	555.0493	13-32	AAKDVFNKGYGFG**M**VKIDLK
3	44.70	739.3613 (2+)	739.3611	16-28	DVFNKGYGFG**M**VK
4	52.14	649.6737 (3+)	649.6734	16-32	DVFNKGYGFG**M**VKIDLK
5	36.70	437.7099 (2+)	437.7103	21-28	GYGFG**M**VK
6	33.23	737.6556 (3+)	737.6554	33-53	TKS**C**SGVEFSTSGHAYTDTGK
7	34.18	1004.4578 (3+)	1004.4564	33-61	TKS**C**SGVEFSTSGHAYTDTGKAS GNLETK
8	38.72	991.4080 (2+)	991.4079	35-53	S**C**SGVEFSTSGHAYTDTGK
9	52.38	812.9064 (2+)	812.9058	62-74	YKV**C**NYGLIFTQK *
10	44.59	767.3719 (2+)	767.3722	162-174	SKL**C**QNNFALGYK

M: methionine sulfoxide; **C**: cysteine oxidized to sulfonic acid.

Supplementary Table 5. Chymotryptic peptides found in the analysis of rVDAC3 reduced with DTT, carboxyamidomethylated and digested in-solution.

In the Table the respective retention time, experimentally measured and calculated monoisotopic m/z of the molecular ions, the position in the sequence and the peptide sequence of fragments present in the chymotryptic digest of reduced and carboxyamidomethylated rVDAC3 are reported. All sequences were confirmed by MS/MS. These sequences were used to build the sequence coverage scheme shown in Supplementary Fig. 1.

Frag. n.	Rt (min)	Monoisotopic m/z		Position in the sequence	Peptide sequence
		Measured	Calculated		
1	65.35	494.2481 (2+)	494.2484	174-181	KAEDFQLH
2	50.15	763.9103 (2+)	763.9126	196-208	**Q**RVNEKIETSINL
3	23.50	484.2328 (2+)	484.2332	211-219	TAGSNNTRF
4	65.68	703.8848 (2+)	703.8855	234-247	SAKVNNASLIGLGY
5	49.96	818.4384 (2+)	818.4387	234-249	SAKVNNASLIGLGYTQ
6	51.97	582.8156 (2+)	582.8166	258-268	TLSALVDGKNF
7	40.18	475.7510 (2+)	475.7507	260-268	SALVDGKNF
8	73.14	749.8854 (2+)	749.8861	269-283	NAGGHKVGLGFELEA

Q: pyroglutamic acid form.

Supplementary Table 6. Sulfur-modified chymotryptic peptide found in the analysis of rVDAC3 reduced with DTT, carboxyamidomethylated and digested in-solution.

In the Table the respective retention time, experimentally measured and calculated monoisotopic m/z of the molecular ion, the position in the sequence and the peptide sequence of the modified fragment present in the chymotryptic digest of reduced and carboxyamidomethylated rVDAC3 is reported. The sequence was confirmed by MS/MS.

Frag. n.	Rt (min)	Monoisotopic m/z		Position in the sequence	Peptide sequence
		Measured	Calculated		
1	31.88	506.2480 (2+)	506.2483	226-233	RLD**C**RTSL

C: cysteine oxidized to sulfonic acid.

Supplementary Table 7. rVDAC3 peptides found in the analysis of the tryptic digest of the lysate of mitochondria incubated with DTT, carboxyamidomethylated and digested in-solution.

In the Table the respective retention time, experimentally measured and calculated monoisotopic m/z of the molecular ions, the position in the sequence and the peptide sequence of fragments present in tryptic digestof the lysate of mitochondria incubated with DTT, carboxyamidomethylated and digested in-solution are reported. All sequences were confirmed by MS/MS.

Frag. n.	Rt (min)	Monoisotopic m/z		Position in the sequence	Peptide sequence
		Measured	Calculated		
1	24.76	672.2839 (2+)	672.2839	2-12	**C*STPTY*C*DLGK
2	50.75	734.3994 (3+)	734.3978	13-32	AAKDVFNKGYGFGMVKIDLK
3	47.12	487.9114 (3+)	487.9114	16-28	DVFNKGYGFGMVK
4	24.35	429.7125 (2+)	429.7126	21-28	GYGFGMVK
5	19.29	740.6673 (3+)	740.6673	33-53	TKS*C*SGVEFSTSGHAYTDTGK
6	42.43	995.9271 (2+)	995.9260	35-53	S*C*SGVEFSTSGHAYTDTGK
7	46.36	931.0880 (3+)	931.0874	35-61	S*C*SGVEFSTSGHAYTDTGKASGNLETK
8	41.14	954.4432 (2+)	954.4421	75-90	WNTDNTLGTEISWENK
9	48.18	840.4174 (3+)	840.4186	75-96	WNTDNTLGTEISWENKLAEGLK
10	49.99	715.4169 (3+)	715.4157	91-110	LAEGLKLTVDTIFVPNTGKK
11	46.59	511.6275 (3+)	511.6276	97-110	LTVDTIFVPNTGKK
12	22.67	771.8902 (2+)	771.8903	162-174	SKL*C*QNNFALGYK
13	24.58	664.3268 (2+)	664.3268	164-174	L*C*QNNFALGYK
14	48.26	874.4064 (3+)	874.4054	175-197	AEDFQLHTHVNDGTEFGGSIYQR
15	45.10	1159.5949 (2+)	1159.5904	198-218	VNEKIETSINLAWTAGSNNTR
16	40.78	924.4670 (2+)	924.4659	202-218	IETSINLAWTAGSNNTR
17	48.95	892.1683 (3+)	892.1677	231-256	TSLSAKVNNASLIGLGYTQSLRPGVK
18	46.72	1044.0845 (2+)	1044.0840	237-256	VNNASLIGLGYTQSLRPGVK
19	42.53	422.7067 (2+)	422.7067	267-274	NFNAGGHK
20	28.53	1016.5993 (1+)	1016.5986	257-266	LTLSALVDGK
21	49.19	614.6661 (3+)	614.6671	257-274	LTLSALVDGKNFNAGGHK
22	48.43	880.4431 (2+)	880.4417	267-283	NFNAGGHKVGLGFELEA

*C: N-terminal acetylated; ***C***: cysteine carboxyamidomethylated.

Supplementary Table 8. rVDAC3 sulfur-modified peptides found in the analysis of the tryptic digest of the lysate of mitochondria incubated with DTT, carboxyamidomethylated and digested in-solution.

In the Table the respective retention time, experimentally measured and calculated monoisotopic m/z of the molecular ions, the position in the sequence and the peptide sequence of modified fragments present in tryptic digest of the lysate of mitochondria incubated with DTT, carboxyamidomethylated and digested in-solution are reported. All sequences were confirmed by MS/MS.

Frag. n.	Rt (min)	Monoisotopic m/z		Position in the sequence	Peptide sequence
		Measured	Calculated		
1	48.54	583.2983 (3+)	583.2998	13-28	AAKDVFNKGYGFG**M**VK
2	50.33	739.7283 (3+)	739.7298	13-32	AAKDVFNKGYGFG**M**VKIDLK
3	45.50	493.2433 (3+)	493.2434	16-28	DVFNKGYGFG**M**VK
4	20.44	737.6547 (3+)	737.6554	33-53	TKS**C**SGVEFSTSGHAYTDTGK
5	34.06	991.4085 (2+)	991.4079	35-53	S**C**SGVEFSTSGHAYTDTGK
6	24.92	767.3721 (2+)	767.3722	162-174	SKL**C**QNNFALGYK

M: methionine sulfoxide; **C**: cysteine oxidized to sulfonic acid.

Supplementary Table 9. Comparison of the absolute intensities of molecular ions of selected sulfur containing peptides found in the analysis of the tryptic digest of the lysate of mitochondria incubated with DTT, carboxyamidomethylated and digested in-solution.

Peptide	Position in the sequence	Measured monoisotopic *m/z*	Absolute intensity	Ratio Ox/Red
DVFNKGYGFG**M**VK	16-28	493.2433 (3+)	$1.71 \cdot 10^6$	0.63
DVFNKGYGFGMVK		487.9114 (3+)	$2.73 \cdot 10^6$	
TKS**C**SGVEFSTSGHAYTDTGK	33-53	737.6547 (3+)	$8.30 \cdot 10^5$	3,56
TKS***C***SGVEFSTSGHAYTDTGK		740.6673 (3+)	$2.33 \cdot 10^5$	
SKL**C**QNNFALGYK	162-174	767.3721 (2+)	$2.71 \cdot 10^5$	2.53
SKL***C***QNNFALGYK		771.8902 (2+)	$1.07 \cdot 10^5$	

M: methionine sulfoxide; ***C***: cysteine carboxyamidomethylated; **C**: cysteine oxidized to sulfonic acid

6. Article 4

Cysteine oxidations in mitochondrial membrane proteins: the case of VDAC isoforms in mammals

Simona Reina, Maria Gaetana Giovanna Pittalà, Francesca Guarino, Angela Messina, Vito De Pinto, Salvatore Foti, Rosaria Saletti

Submitted to Frontiers in Cell and Developmental Biology (11-02-2020)

Manuscript ID: 534133

Accepted 29-04-2020

frontiers in Cell and Developmental Biology

MINI REVIEW
published: 04 June 2020
doi: 10.3389/fcell.2020.00397

Cysteine Oxidations in Mitochondrial Membrane Proteins: The Case of VDAC Isoforms in Mammals

Simona Reina[1], Maria Gaetana Giovanna Pittalà[2], Francesca Guarino[2], Angela Messina[1], Vito De Pinto[2], Salvatore Foti[3] and Rosaria Saletti[3]*

[1] Section of Molecular Biology, Department of Biological, Geological and Environmental Sciences, University of Catania, Catania, Italy, [2] Section of Biology and Genetics, Department of Biomedical and Biotechnological Sciences, University of Catania, Catania, Italy, [3] Organic Mass Spectrometry Laboratory, Department of Chemical Sciences, University of Catania, Catania, Italy

Cysteine residues are reactive amino acids that can undergo several modifications driven by redox reagents. Mitochondria are the source of an abundant production of radical species, and it is surprising that such a large availability of highly reactive chemicals is compatible with viable and active organelles, needed for the cell functions. In this work, we review the results highlighting the modifications of cysteines in the most abundant proteins of the outer mitochondrial membrane (OMM), that is, the voltage-dependent anion selective channel (VDAC) isoforms. This interesting protein family carries several cysteines exposed to the oxidative intermembrane space (IMS). Through mass spectrometry (MS) analysis, cysteine posttranslational modifications (PTMs) were precisely determined, and it was discovered that such cysteines can be subject to several oxidization degrees, ranging from the disulfide bridge to the most oxidized, the sulfonic acid, one. The large spectra of VDAC cysteine oxidations, which is unique for OMM proteins, indicate that they have both a regulative function and a buffering capacity able to counteract excess of mitochondrial reactive oxygen species (ROS) load. The consequence of these peculiar cysteine PTMs is discussed.

Keywords: cysteine overoxidation, outer mitochondrial membrane, voltage-dependent anion selective channel isoforms, Orbitrap Fusion Tribrid, posttranslational modification, ROS

OPEN ACCESS

Edited by:
Pablo M. Garcia-Roves, University of Barcelona, Spain

Reviewed by:
Johannes M. Herrmann, University of Kaiserslautern, Germany
Catherine Brenner, Délégation Paris-Villejuif-01 (CNRS), France
Esther Imperlini, Institute of Research and Medical Care (IRCCS) SDN, Italy

****Correspondence:***
Simona Reina
simonareina@yahoo.it

Specialty section:
This article was submitted to Cell Death and Survival, a section of the journal Frontiers in Cell and Developmental Biology

Received: *11 February 2020*
Accepted: *29 April 2020*
Published: *04 June 2020*

Citation:
Reina S, Pittalà MGG, Guarino F, Messina A, De Pinto V, Foti S and Saletti R (2020) Cysteine Oxidations in Mitochondrial Membrane Proteins: The Case of VDAC Isoforms in Mammals. Front. Cell Dev. Biol. 8:397. doi: 10.3389/fcell.2020.00397

GENOME–PROTEOME DISCORDANCE: AN OVERVIEW ON PROTEIN POSTTRANSLATIONAL MODIFICATIONS

The mammalian proteome is vastly more complex than the related genome: an imbalance between one million different proteins against approximately 25,000 genes is estimated in humans (International Human Genome Sequencing Consortium, 2004; Clamp et al., 2007). The reasons for this inconsistency reside both in the molecular mechanisms that allow a single gene to encode for numerous proteins (i.e., alternative splicing, genomic recombination, alternative promoters, and termination sites) and in the posttranslational modifications (PTMs) which represent a wide range of chemical changes that proteins may undergo after synthesis. They include the specific cleavage of protein precursors, the covalent addition or removal of low-molecular groups, and the formation of disulfide bonds or other redox modifications (Wang et al., 2014; Duan and Walther, 2015). PTMs are crucial for several cellular processes such as protein turnover and

signaling and are commonly mediated by enzymatic activity. Many of them have been extensively characterized, and phosphorylation is perhaps the most known example. Conversely, only in the last two decades have reactive oxygen species (ROS)/reactive nitrogen species (RNS) been identified as physiological regulators of intracellular signaling pathways through the covalent modification of specific cysteine residues within redox-sensitive proteins (Chung et al., 2013). Although the "oxidative posttranslational modifications" (Ox-PTMs) still represent a little explored field, the increasing number of tools aimed at identifying and quantifying them [e.g., high-throughput mass spectrometry (MS) analysis] continues to broaden the knowledge of redox regulation (Spickett and Pitt, 2012; Shakir et al., 2017; Anjo et al., 2019).

Peculiarity of Cysteine Ox-PTMs and Their Correlation With Pathological Conditions

Because of their redox-reactive thiol (–SH) side chain, cysteine residues are likely subjected to various Ox-PTMs including *S*-nitrosylation (or *S*-nitrosation, SNO), sulfhydration (SSH), *S*-acylation, *S*-glutathionylation, disulfide bonds (RS-SR), sulfenylation (SOH), sulfinic acid (SO_2H), and sulfonic acid (SO_3H) (Forrester and Stamler, 2007; Murray and Van Eyk, 2012; Alcock et al., 2018). Except for sulfonic acid, all the reported Ox-PTMs are readily reversible and ruled by specific enzymatic activities. Sulfiredoxin (Srx1), for example, acts on oxidative states up to sulfinic acid by reducing them back to thiol in an ATP-dependent manner (Biteau et al., 2003; Chang et al., 2004). The biological significance of most of these reversible modifications has been amply investigated under physiological and non-physiological conditions (Bechtel and Weerapana, 2017). On the contrary, knowledge about the impact of irreversible Ox-PTMs on cell physiology is quite restricted.

Reversible Thiol Modification: Addition of Groups to Cysteine

S-nitrosylation, the covalent attachment of a nitrous (NO) moiety to –SH functional groups, protects proteins against further cellular oxidative and nitrosative stress. Specific enzymes, called nitrosylases, are responsible for NO group transfer in either metal-to-cysteine or cysteine-to-cysteine mechanisms (Anand and Stamler, 2012). Treatments of mouse hearts with NO donors to increase *S*-nitrosylation, especially in mitochondria, prior to an ischemic insult, reduce indeed infarct size by avoiding critical cysteine irreversible oxidation (Duranski et al., 2005). Under physiological conditions, it represents an important modulator of signal transduction pathways: mitochondrial SNO proteins inhibit respiratory complex I (CI) to modulate mitochondrial ROS production, promote the selective import of mitochondrial protein, enhance mitochondrial fission, and affect the mitochondrial permeability transition pore (MPTP) opening (Piantadosi, 2011; Fernando et al., 2019). However, aging or environmental toxins that increase NO production lead to aberrant *S*-nitrosylation reactions that contribute to neurodegenerative diseases, including Alzheimer's disease (AD) and Parkinson's disease (PD) (Nakamura et al., 2013).

Sulfhydration (SSH) has lately been acknowledged as a PTM analogous to nitrosylation that consists in the conversion of a –SH group to a –SSH or a persulfide group. Hydrogen sulfide (H_2S) represents a ubiquitous gaseous signaling molecule with important physiological vasorelaxant properties (Iciek et al., 2015; Zhang et al., 2017) that, in mammals, is enzymatically generated by three enzymes: cystathionine β-synthase (CBS), cystathionine γ-lyase (CTH or CSE), and 3-mercaptopyruvate sulfurtransferase (3MST) (Rose et al., 2017). The reason that proteins undergo this type of modification is not known, although they have been identified by LC–MS/MS. Recently, Tonks et al. suggested that H_2S, produced by CSE consequently to endoplasmic reticulum (ER) stress, sulfhydrates protein tyrosine phosphatase 1B (PTP1B) (Krishnan et al., 2011). This event, in turn, causes the ER kinase PERK activation during the response to ER stress. Interestingly, anomalous sulfhydration has been linked to several pathological conditions ranging from heart diseases to neurodegeneration (i.e., PD) (Paul and Snyder, 2018).

S-acylation is a highly conserved PTM that takes place in all eukaryotic organisms and is regulated by the same enzyme families from yeast to humans. It consists in the covalent attachment of an acyl chain to a cysteine residue and is the only fully reversible posttranslational lipid modification of proteins. Because of the weak nature of the thioester bonds within the intracellular environment, most *S*-acylated proteins rapidly undergo *S*-acylation and deacylation cycles (Chamberlain and Shipston, 2015; Feldman et al., 2015; Pedro et al., 2017). *S*-acylation increases protein hydrophobicity that, in turn, can affect several properties ranging from structure to assembly, maturation, and function. Although the major lipid incorporated into endogenous proteins is palmitate (C 16:0), fatty acids such as oleate (C 18:1) and stearate (C 18:0) can also be added. In particular, *S*-acylation is detected in transmembrane proteins where it is required for stable membrane binding. In this regard, the blockage in the *S*-acylation of specific residues increases protein ubiquitination and degradation (Valdez Taubas and Pelham, 2005). The recent development of *S*-acylation proteomic profiling together with the identification of enzymes that regulate protein *S*-acylation and deacylation has brought new interest into the physiological function of this peculiar Ox-PTM. To date, 47 acylated proteins have been detected in the yeast *Saccharomyces cerevisiae* (Roth et al., 2006) whereas mammalian cells contain hundreds of these modified proteins (Wan et al., 2007; Yang et al., 2010). Interestingly, there is no evidence for *S*-acylation occurrence in prokaryotes. On the contrary, *S*-acylation of many viral proteins is catalyzed by the host cell machinery (Kordyukova et al., 2010).

S-glutathionylation (SSG) consists in the addition of the tripeptide glutathione (GSH), the main low-molecular-weight antioxidant of both prokaryotes and eukaryotes, to protein cysteine residues through the establishment of a covalent linkage (Dalle-Donne et al., 2009). This reversible thiol modification is promoted by oxidative and/or nitrosative stress and acts as a repository for reduced glutathione, since the oxidized form (GSSG) is either rapidly excreted from the cells or reduced back

to GSH via NADPH-dependent glutathione reductase (Lushchak, 2012). Anyhow, *S*-glutathionylation also occurs under unstressed conditions (Dalle-Donne et al., 2009). Not all cysteines can undergo *S*-glutathionylation: it has been proposed that low pK_a values and, possibly, the three-dimensional proximity to His, Lys, and Arg residues are key factors that make specific Cys appropriate targets for such PTMs (Grek et al., 2013). Numerous molecular mechanisms have been suggested to explain protein *S*-glutathionylation, ranging from the direct thiol–disulfide exchange reaction of a cysteinyl residue with GSSG to the activation of a thiol group to reactive sulfur intermediates (sulfenyl amide, sulfenic acid, or *S*-nitrosyl) which then react with GSH (Allen and Mieyal, 2012). The enzymes responsible for GSH conjugation are called glutathione *S*-transferases, while the reverse reaction is catalyzed by glutaredoxins (Grxs). Certainly, the main role of *S*-glutathionylation is to prevent thiol irreversible oxidation, though it can affect protein function by altering charge and molecular mass, by inducing conformational changes, or by sterically blocking catalytic sites (Grek et al., 2013). The synergy between *S*-glutathionylation and *S*-deglutathionylation thus contributes to the regulation of redox homeostasis, cytoskeletal assembly, protein folding, and stability. Moreover, several evidences have reported their involvement in the control of cell signaling pathways associated with viral infections and apoptosis induced by tumor necrosis factor (Dalle-Donne et al., 2009). Mitochondria contain several *S*-glutathionylation targets thanks to the thiol transferase glutaredoxin 2 (Grx2), which is considered an important redox sensor within the organelle (Xiong et al., 2011).

Reversible Thiol Modification: Redox Modification of Cysteine Sulfur

Disulfide bonds (RS-SR) are essential PTMs involved in protein folding and in the stabilization of their tertiary and quaternary structures. Disulfide formation depends on the spatial proximity to another cysteine and can also occur through a reaction with sulfenic acid in the presence of high concentrations of ROS. They indeed convert SOH groups into thiol radicals (RS·) which, in turn, react with other thiolates to form a disulfide bond (reviewed in Summa et al., 2007; Depuydt et al., 2011; Herrmann and Riemer, 2012). In eukaryotic cells, specific enzymes catalyze disulfide exchange within the ER and the mitochondrial intermembrane space (IMS). In yeast, for example, the ER contains the sulfhydryl oxidase endoplasmic oxidoreductin 1 (Ero1) that transfers oxidizing equivalents first to the disulfide isomerase (PDI) and then to secretory proteins. Disulfide formation in the IMS of mitochondria is entrusted, instead, to the MIA system, which will be described in depth in the following sections (Stojanovski et al., 2008). Noteworthy is that some RS-SR are dynamic and modulate protein signaling: that is, in mammalian cells, the stress sensor NPGPx transmits oxidative stress signals through its Cys57–Cys86 disulfide bond. Once oxidized, NPGPx binds to GRP78 (glucose-regulated protein), giving rise to covalent intermediates between NPGPx-Cys86 and GRP78-Cys41/Cys420 that culminate in the enhancement of the GRP78 chaperone activity. The knockout (KO) of NPGPx gene increases the intracellular ROS content and impairs GRP78 chaperone activity, leading to the accumulation of misfolded proteins (Wei et al., 2012). An involvement of S–S bridges in neurodegenerative disorders has been recently proposed. Some evidence suggests that intermolecular disulfide bonds in mutant superoxide dismutase 1 (SOD1) may have a role in its aggregation, a hallmark of some familial amyotrophic lateral sclerosis (ALS) variants (Furukawa et al., 2006). Moreover, intramolecular and intermolecular disulfide bonds seem to be involved in the pathological Tau isoforms typical of AD and other neurodegenerative disorders (Walker et al., 2012; Kim et al., 2015).

Sulfenylation (RSOH) is the first step of cysteinyl thiol oxidation. Because of their high reactivity and instability, sulfenic acids (–SOH) have been reputed for a long time as intermediates to additional cysteine modifications (Lo Conte and Carroll, 2013). They can be generated following the condensation of a thiol with a hydroxyl radical, the hydrolysis of *S*-nitrosothiols, and the reaction of a thiol or a thiolate anion with a high concentration of hydrogen peroxide and with thiosulfinates (Hall et al., 2010). Moreover, sulfenic acids can result from the reaction of a thiol or thiolate anion with hypochlorous acid, which represents a powerful bactericidal compound generated within neutrophils during inflammation. The reactivity of the thiol side chain is modulated by the surrounding protein environment that drives the fate of sulfenic acid to an irreversible chemical modification or to a "protective" disulfide bond (Ferrer-Sueta et al., 2011; Roos and Messens, 2011). Accumulating evidence proposes cysteine *S*-sulfenylation as a redox-based signal transduction mechanism in living cells, which is also involved in transcription regulation (Poole and Nelson, 2008; Roos and Messens, 2011; Heppner et al., 2018). The functional domains of several protein phosphatases, acetyltransferases, kinases, deubiquitinases, and deacetylases contain *S*-sulfenylated sites, suggesting the existence of a regulatory cross-talk between *S*-sulfenylation and other major PTM events. Tandem MS revealed –SOH modification also in the catalytic cycle of many enzymes as well as peroxiredoxin (Prx) and NADH peroxidase (Poole et al., 2004; Portillo et al., 2017). Dysregulated protein sulfenylation has been associated with several human pathologies including hypertension (Camargo et al., 2018) and aggressive cancer phenotypes (Truong et al., 2016).

Sulfinic acid (RSO_2H) is the further oxidized step of –SOH achieved in the presence of excess oxidants (Griesser et al., 2018; Urmey and Zondlo, 2020). The biological function of sulfinic acid has been largely debated, due to the general belief that this Ox-PTM could be an artifact triggered by protein isolation procedures. However, this idea was totally discredited after the discovery that the catalytic cysteine of human Prx1 is selectively oxidized to Cys-SO_2H but not to Cys-SO_3H, as sulfinic acid is re-reduced to Cys-SH by sulfiredoxin (SRX). In mammals, intracellular sulfinic acid levels depend upon cysteine dioxygenase (CDO), a metabolic enzyme that regulates cysteine homeostasis according to the dietary intakes of sulfur amino acids (Stipanuk et al., 2009). In the last decade, a functional role for $-SO_2H$ modification has been reported for a growing list of proteins (Lo Conte and Carroll, 2013), including the

copper–zinc SOD1, the PD protein DJ-1, and the D-amino acid oxidase (DAO) (Blackinton et al., 2009). Sulfinic acid modulates indeed protein metal binding features: in matrix metalloproteases, the oxidation of a cysteine residue to $–SO_2H$ activates protease function and is essential for catalytic activity. Despite its association with diseases linked to oxidative stress, including cancer and neurodegenerative disorders, the rationale of sulfinic acid is essentially unknown because of the difficulties of its detection (Neumann et al., 2003; Canet-Avilés et al., 2004). Antibodies against sulfinic acid have limited affinity and specificity. Moreover, MS analysis struggles with the existence of other modifications with the same nominal mass shift, like *S*-sulfhydration (–SSH) (Akter et al., 2018).

Irreversible Thiol Modification: A Way With No Return

Sulfonic acid (RSO_3H) results from the oxidation of $–SO_2H$ by strong oxidizers such as ONOOH, H_2O_2, or HOX, and it is considered a dead-end product since no biological pathway has been discovered for $–SO_3H$ reduction. Due to their relative stability compared to the reversible thiol modifications, they can be detected directly by MS, although with some difficulties. Sulfinic and sulfonic acid fragmentations are indeed nearly indistinguishable from the fragmentation patterns of other PTMs and necessitate high-resolution MS instruments to differentiate them (Gaillot et al., 2020). To date, the role of cysteine sulfonic acid in protein function/conformation is still controversial since it is not completely clarified if Cys-SO_3H can be counted as an oxidative damage or a signaling modification. Literature contains just a few examples in this regard. Lim et al. (2008) proposed that the sulfonic acid formation of yeast Prx1 cysteine in an active site enhances the protein chaperone activity, representing a marker of the cumulative oxidative stress in cells. Lately, Wu et al. (2017) refined this concept, concluding that the two indispensable cysteines of human Prx1, cysteine in the active site (C_P), responsible for peroxide reduction, and resolving cysteine (C_R), which deals with C_P regeneration, exhibit different propensities to sulfonation. Accordingly, the most frequent overoxidation of human Prx1 hits C_R: sulfonation of Prx1 fosters its activity as a chaperone, preventing proteins from unfolding and irreversible aggregation (Wu et al., 2017). The existence of cysteine residues susceptible to sulfonation appears as an exclusive evolutionary feature of eukaryotic Prxs involved in cell survival during oxidative stress and argues in favor of Cys-SO_3H as a signaling PTM rather than a simple oxidative damage (Delaunay et al., 2002; Jang et al., 2004; Jarvis et al., 2012; Sobotta et al., 2015). Interestingly, overoxidation of Prxs cysteines follows a precise circadian rhythm in human blood cells that has been identified as a transcription-independent marker (O'Neill and Reddy, 2011; Edgar et al., 2012). The Cys149 residue of the active site of GAPDH is also rapidly overoxidized to sulfonic acid by H_2O_2, and this modification is associated with glycolysis inhibition and with numerous side activities including the induction of apoptosis (Colussi et al., 2000). Cys149 irreversible oxidation is regulated by *S*-glutathionylation and disulfide bond formation with the residue Cys154 (Muronetz et al., 2020). In human mutant SOD1, the peroxidation of Cys111 to sulfonic acid has been implied in the pathology of the degeneration/death of familial ALS motor neurons. Immunohistochemical analysis proved indeed the accumulation of mutant SOD1 with overoxidized Cys111 residue in the Lewy body-like hyaline inclusions and vacuole rims of the spinal cord of familial ALS-transgenic mice (Fujiwara et al., 2007). A pathophysiological relevance of sulfonation has been observed also in PD: an increase in the level of sulfonated parkin correlates with its insolubility in human PD brains (Chakraborty et al., 2017). In endocrinology, sulfonation represents a particularly explored biological phenomenon (Wallace et al., 2010). Cys-SO_3H modification of neuroendocrine peptides strongly affects their receptor binding (Wallace et al., 2010). The oxidation of an N-terminal cysteine residue to sulfonic acid, such as the Cys2 residue of GTPase-activating proteins, has been described as a marker for ubiquitin-dependent protein degradation (Arg/N–degron pathway) (Barros and McStay, 2020). The acetylation of the N-terminal amino group also represents a protective mechanism against irreversible oxidation and seems to act as a degradation signal in the Ac/N–degron pathway. Sulfonic acid is present in mammalian cells as taurine, a low-molecular-weight antioxidant, also an osmoregulator and participant in calcium signaling pathways. Taurine is particularly abundant in the heart, skeletal muscle tissue, retinas, and central nervous system.

MITOCHONDRIAL PROTEINS PTMs INVOLVING CYSTEINE OXIDATION

Cysteine residues constitute only 2% of the total amino acid content, but the mitochondrial proteome is rich in protein thiols. Mitochondria are dynamic organelles responsible for maintaining redox cellular homeostasis thanks to the continuous generation and wasting of ROS/RNS. The production of ATP and the formation of the proton gradient are, however, imperfect, as the premature leak of electrons from complexes I and III leads to the formation of $O_2^{\bullet -}$. MnSOD rapidly dismutates $O_2^{\bullet -}$ to hydrogen peroxide more stably than other ROSs. The electron transport chain, in addition to the nitrite reductase activity, has been proposed as responsible for the NO· generation within mitochondria: the existence of a mitochondrial nitric oxide synthase (mtNOS) is, indeed, still debated. H_2O_2 is the most relevant radical species in redox signaling that reversibly oxidizes protein cysteine thiols (–SH) to sulfenic acid (–SOH) through a mechanism called "redox switch" (Spadaro et al., 2010). However, $O_2^{\bullet -}$ also exerts a signaling role by disassembling Fe–S clusters in several enzymes of the TCA cycle and in respiratory complexes (Mailloux et al., 2014). At high concentrations, $O_2^{\bullet -}$ and H_2O_2 can lead to oxidative stress due to the production of the hydroxyl radical (·OH), the ROS that is most reactive. In addition, $O_2^{\bullet -}$ can combine with nitric oxide (NO) to form the powerful oxidant peroxynitrite ($ONOO^-$) (Fridovich, 1995; Radi, 2013). Under physiological conditions, ROS/RNS generated in mitochondria mainly regulate mitochondrial protein interactions, localization, and activity (Ray et al., 2012; Mailloux et al., 2014) through the oxidative modification of redox-sensitive cysteine residues.

It has been reported that the sulfenylation of the Cys253 residue of uncoupling protein 1 (UCP1) within the brown adipose mitochondria of mammalian cells participates in the thermogenic regulation of energy expenditure (Chouchani et al., 2016). *In vivo* in mice, the selective *S*-nitrosation of the Cys39 residue on the ND3 subunit of CI was instead proposed to be cardioprotective (Chouchani et al., 2013). If unregulated, ROS can oxidatively damage biomolecules (proteins, DNA, and lipids), ultimately leading to neurological disorders, metabolic diseases, aging (Bulteau et al., 2006), and other pathologies. Hence, the control of the cellular ROS balance mainly relies on two redox regulatory systems: the reduced/oxidized thioredoxin and the glutathione (GSH)/glutathione disulfide (GSSG) (Holmgren et al., 2005; Jones, 2006).

Mitochondrial Compartments Possess Different Redox Potentials

The outer mitochondrial membrane (OMM), non-specifically permeable to low-molecular-weight solutes, and the inner mitochondrial membrane (IMM), selectively permeable, define two distinct aqueous compartments within the organelle: the matrix and the IMS. The mitochondrial matrix, that is, the innermost compartment, exhibits a pH of about 8.0 (Llopis et al., 1998) and is the site of numerous enzymatic reactions including organellar DNA replication, transcription, and protein biosynthesis. Components of the mitochondrial IMS are involved, instead, in several processes ranging from the transport of proteins, metal ions, or electrons to the inner membrane proteins assembling up to cellular respiration. The IMS also sequesters several apoptotic components released into the cytosol to trigger programmed cell death. The IMS pH value is about 0.8 units more acidic than the matrix: this asymmetry creates an electrochemical gradient across the inner membrane, exploited in ATP synthesis (Holoubek et al., 2007). Interestingly, the pH of the matrix and IMS differently affects their redox potentials. ROS production is strongly influenced by pH (Shu et al., 1997): in hepatocytes, the extracellular pH controls hydroxyl radical (·OH) and NO production (Shu et al., 1997). Likewise, the more acidic pH of the mitochondrial IMS makes it a strong oxidizing environment (Hu et al., 2008; Kojer et al., 2012, 2015). Besides, the IMS of eukaryotic cells contains a dedicated machinery, called the MIA/CHCHD4 complex or disulfide relay-dependent import machinery, responsible for the import and oxidative folding of substrates with conserved cysteine motifs (CX_3C and CX_9C). The oxidoreductase Mia40 and the FAD-dependent sulfhydryl oxidase essential for respiration and viability 1 (Erv1) are the crucial components of the MIA complex in yeast. Initially, Mia40 forms a transient intermolecular disulfide bond with imported precursor proteins. Afterward, the isomerization of this disulfide bond causes the introduction of an intramolecular S–S bridge within the imported precursor protein. Following oxidation of the substrate, Mia40 is reoxidized by Erv1 (Lee et al., 2000; Dabir et al., 2007; Banci et al., 2009; Tienson et al., 2009; Bien et al., 2010). A stepwise evolution of the MIA pathway has been proposed in Allen et al. (2008). Accordingly, the ancestral IMS import pathway only included an Erv1 protein, as nowadays in *Leishmania* and *Trypanosoma*. At this stage, Erv1 can still work alone, suggesting that Mia40 behaves as a kind of import chaperone. In fungi, Erv1 necessarily required Mia40 to oxidize substrate proteins because of its inability to do it by itself. The metazoan homolog of yeast Mia40 is the CHCHD4 protein, with the same role as the core component of the disulfide relay-dependent import machinery. They share the same ability to oxidize pairs of reduced cysteines to disulfide bridges, provided that they are present in the motif CX_3C or CX_9C. While the yeast Mia40 is a transmembrane protein, metazoan CHCHD4 is smaller, soluble, and moving inside the IMS. Since Mia/CHCHD4 are involved in the proper folding of Cys-containing proteins, they are also considered key components of the quality control system that impacts the IMS targeted proteins (Chatzi and Tokatlidis, 2013). To date, several IMS proteins have been detected with structural disulfide bridges, and the list is constantly increasing (Cavallaro, 2010; Gross et al., 2011; Vögtle et al., 2012). A few examples are the intermitochondrial space Atp23 protein, which is a strongly oxidized protease associated with the IMM (Weckbecker et al., 2012); the protein anamorsin, implicated in Fe/S cluster assembly (Banci et al., 2011); and the Ca^{2+} uniporters MICU1 and MICU2 (Petrungaro et al., 2015). Disulfide bonds within IMS proteins have also lately been considered as part of a quality control system: Longen et al. (2014) proposed that the presence of these Ox-PTMs in the eukaryotic mitochondrial ribosomal Mrp10 protein is sufficient to avoid its proteolytic degradation in the IMS before moving to the mitochondrial matrix. Nevertheless, the presence of special reductases (i.e., thioredoxin and glutaredoxin; Holmgren, 2000) within the IMS causes the reduction of cysteine residues in many proteins and protein domains contained therein. Most of these cysteines are coordination sites for metal ions (Sco1, Sco2, Cox2, Cox11, and Cox17), heme cofactors (cytochrome *c* and cytochrome c_1), and iron–sulfur clusters (Rieske Fe/S protein Rip1). The mitochondrial matrix possesses several redox repair systems: reduced/oxidized thioredoxin and the GSH/GSSG are both involved in disulfide bonds or sulfenic acid reduction (Santo-Domingo et al., 2015).

Redox Modification of OMM Proteins: The VDAC Case

In spite of plenty of reports about the redox modifications of the mitochondrial matrix, IMS, and inner membrane proteins, very little is known about the outer membrane proteins. This is possibly due to underrepresentation of membrane proteins in proteome profiles (protein heterogeneity, hydrophobicity, limited solubility, restricted enzyme accessibility, and low abundance are responsible for it) that downsizes their detection and identification. In order to overcome these restrictions, numerous strategies have been developed to increase the enrichment, solubilization, separation, and cleavage of membrane proteins (Schmitt et al., 2006; Niemann et al., 2013; Bak et al., 2017). Voltage-dependent anion selective channels (VDACs) are surely the most represented proteins of the OMM involved in cellular processes that range from metabolism regulation to cell death control (Benz, 1994;

Colombini et al., 1996). Alterations of VDAC expression and activity correlate with several pathologies such as cancer and neurodegenerative disorders (Shoshan-Barmatz et al., 2010; Magrì et al., 2016, 2018; Reina and De Pinto, 2017). In higher eukaryotes, VDAC exists in three different isoforms called VDAC1, VDAC2, and VDAC3 according to the chronological order of their uncovering. Evolutionary analyses suggest that VDAC3 is the oldest protein and VDAC1 is the most recent mitochondrial porin (Young et al., 2007; Messina et al., 2012). Structurally, VDAC forms an aqueous channel arranged in a transmembrane β-barrel linked to an α-helix moiety at the N-terminus (Bayrhuber et al., 2008; Hiller et al., 2008; Ujwal et al., 2008; Schredelseker et al., 2014). In each β-strand, hydrophilic and hydrophobic residues alternate regularly: the former point to the lumen of the pore while the latter interact with the membrane environment. Interestingly, all β-strands follow a steady array of antiparallel units with the exception of β-strands 1 and 19 that, running parallel, make both the N-terminus and the C-terminus point toward the IMS (Tomasello et al., 2013). The amphipathic α-helix tail seems to be placed inside the pore, but, to date, the exact position and local structure of this segment are still debated (De Pinto et al., 2007). However, although the general organization of the three isoforms is similar, different molecular weights and amino acid compositions may be associated to distinct roles in the cell. In particular, VDAC isoforms differ in the number and distribution of cysteines so that they have been the subject of specific investigations to unravel a peculiar role for these residues in protein activities (De Pinto et al., 2016; Reina et al., 2016). In humans, VDAC1, VDAC2, and VDAC3 have two, nine, and six cysteines, respectively. Considering VDAC3 is the oldest isoform, it is tempting to speculate that evolution has decreased cysteine number in VDAC1, according to an ubiquitous expression and proapoptotic function, while increasing cysteine content in VDAC2, possibly to favor its involvement as an antiapoptotic protein (De Pinto et al., 2016). VDACs are exposed to both cytosol and IMS (**Figure 1**). Interestingly, many of the cysteine residues are located in protein loops exposed to IMS and its oxidative potential. In addition, VDAC has been proposed as the only escape route from the mitochondria of the unreacted superoxide radical ($O^{2-\bullet}$), a by-product of complex III of the respiratory chain (Han et al., 2003). At a variance from hydrogen peroxide (H_2O_2), $O^{2-\bullet}$ is very active but has a short life and cannot freely diffuse trough the membrane (Bleier et al., 2015). Our research group was the first to report a detailed profile of the oxidative state of VDAC cysteines and methionines (Saletti et al., 2017, 2018) by affinity chromatography purification and UHLC/high-resolution *n*-ESI-MS/MS. What we noticed is that a cysteine redox modification pattern is conserved during evolution. In both human (Pittalà et al., 2020) and rat VDACs (Saletti et al., 2017, 2018), indeed, residues are in the reduced form (i.e., free thiol groups available to disulfide bond formation), while others are constantly and irreversibly overoxidized to sulfonic acid. We thus hypothesized that a specific modification of each cysteine may correlate to a specific structural or functional role. Very recently, a "shot-gun" cysteine-targeted MS analysis that identified ∼1500 reactive cysteine residues on ∼450 mitochondrial proteins in HEK293T cells was able to detect cysteines highly sensitive to *S*-nitrosoglutathione (GSNO) also in VDAC proteins (Bak et al., 2017).

Cysteine Residues in VDAC Isoforms

VDAC1

VDAC1 is the best-characterized VDAC isoform. It provided the first description of typical voltage dependence and ion selectivity features that are the fingerprint of these pores. VDAC1 has been thoroughly characterized by electrophysiological studies (Blachly-Dyson et al., 1993; Xu et al., 1999) and is considered one of the main actors of bioenergetic metabolism and cell death regulation (Maldonado et al., 2010; Camara et al., 2011; Maldonado and Lemasters, 2012). Its 3D structure was elucidated (Bayrhuber et al., 2008; Hiller et al., 2008; Ujwal et al., 2008). A large number of reports describe VDAC1 as a docking site for proapoptotic (Bax, Bak, and Bim) and antiapoptotic (Bcl2 and Bcl-xL) factors (Shimizu et al., 2001; Vander Heiden et al., 2001; Arbel et al., 2012; Huang et al., 2013; Liu et al., 2015), as well as for cytosolic enzymes [hexokinases (HK) I and II] (Fiek et al., 1982; Abu-Hamad et al., 2008). The interaction with HK makes VDAC1 a key player in cancer and other pathologies, including neurodegenerative diseases (Maldonado and Lemasters, 2012; Leanza et al., 2014; Reina and De Pinto, 2017; Magrì et al., 2018), that share mitochondrial dysfunction and oxidative stress. VDAC1 contains only two cysteines (Cys127 and Cys232). Cys127 residue (β-strand 8) protrudes in phospholipidic hydrophobic milieu, while Cys232 is located in β-strand 16 and faces the water-accessible side of the channel (Bayrhuber et al., 2008; Hiller et al., 2008; Ujwal et al., 2008). Still, there is no evidence that oxidation can rule VDAC1 activity through the Ox-PTMs of its sulfhydryl groups. Nevertheless, already in De Pinto et al. (1991), the authors established that the two conserved cysteine residues of VDAC1 from bovine heart mitochondria are sensitive to oxidation. Both the oxidized and reduced forms of VDAC1, however, showed the same biophysical properties into artificial lipid membranes, disclaiming any redox regulation of channel activity (De Pinto et al., 1991). Later, Aram et al. (2010) confirmed that the pore is not affected by VDAC1 cysteine deletion and observed that ROS-producing agents such as selenite, As_2O_3, or H_2O_2 do not change apoptosis in human cells overexpressing rat VDAC1. Moreover, cross-linking experiments let them conclude that VDAC1 cysteines are not involved in intermolecular S–S bridge and thus do not take part in oligomerization (Aram et al., 2010). Overall, reports available so far agree that cysteine residues have no functional role in VDAC1 (Teijido et al., 2012). Recent findings revealed a conserved pattern in oxidative status, conserved among human and rat VDAC1: Cys127 was always detected in the trioxidized form of $-SO_3H$ and Cys232 exclusively in the reduced and carboxyamidomethylated form (Pittalà et al., 2020).

VDAC2

Analogous to isoform 1, VDAC2 participates in several cellular processes, from metabolite exchange through the OMM (Maurya and Mahalakshmi, 2016; Naghdi and Hajnóczky, 2016) to calcium homeostasis regulation (Subedi et al., 2011; Shimizu et al., 2015).

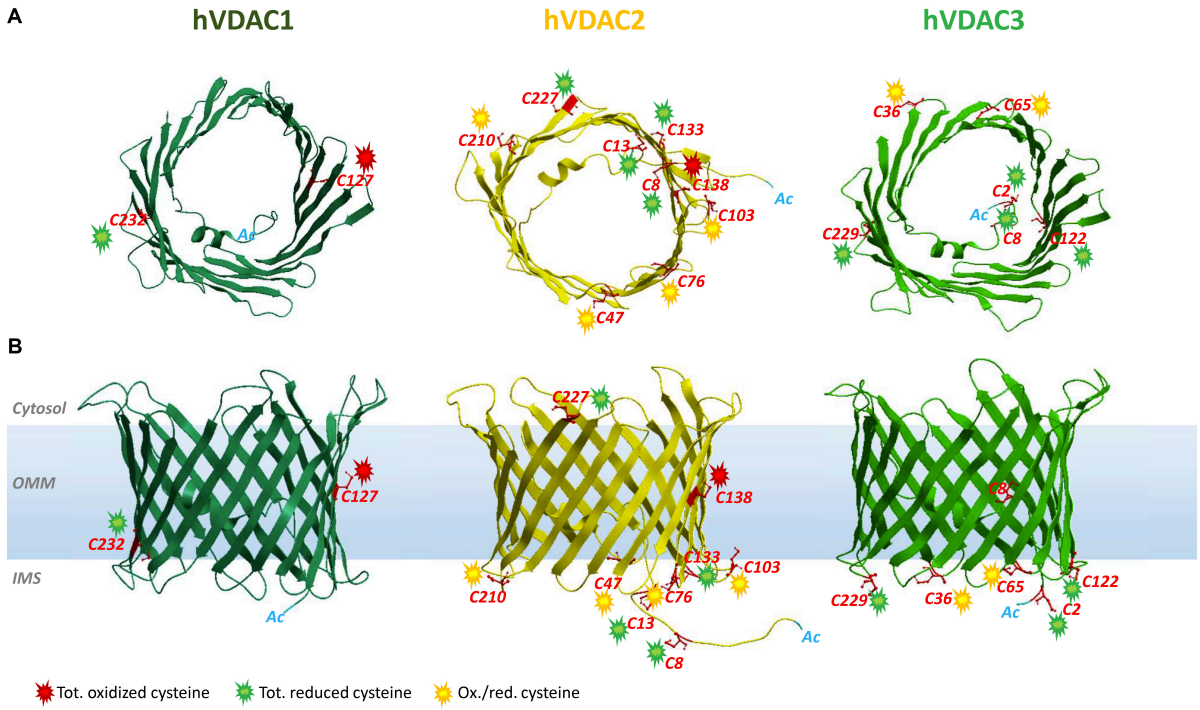

FIGURE 1 | Structure of human VDAC isoforms highlighting cysteine residues and their preferred oxidation states. The structures of hVDAC2 (yellow) and hVDAC3 (light green) β-barrels were modeled using the structure of hVDAC1 [dark green (PDB ID: 2JH4)] as a template. **(A)** Top view of hVDACs with the N-terminal α-helix folded within the pore. **(B)** Side view of the β-barrels embedded in the OMM. The cysteine residues are highlighted (in red), and their oxidative state is indicated by colored sparks: green (totally reduced), red (totally oxidized), or yellow (red/ox, i.e., partially oxidized). There are no VDAC cysteines in the outer face of the membrane, exposed toward the cytosol.

Although ubiquitous, it is predominantly expressed in the heart and testes and, at the same time, poorly represented in the liver (Yamamoto et al., 2006; Calvo et al., 2016). The N-terminal region, which contains the voltage sensor of the channel, carries an extension of 11 additional residues only in VDAC2. The only available crystal structure is zebrafish VDAC2 (zfVDAC2), whose sequence is only about 90% similar to mammalian VDAC2 (Schredelseker et al., 2014), and confirms substantial analogy with the published structures of mouse and human VDAC1. Mouse, human, zebrafish, and bovine isoform 2 easily insert into bilayer membranes as canonical VDAC pores with similar single-channel conductance, voltage gating, and anion selectivity (Blachly-Dyson et al., 1993; Xu et al., 1999; Komarov et al., 2005; Menzel et al., 2009; Maurya and Mahalakshmi, 2015). VDAC2 is considered antiapoptotic, a distinction from VDAC1 and VDAC3: VDAC2 complexes with the proapoptotic factors BAK (Cheng et al., 2003) and BAX (Chin et al., 2018), thereby hampering programmed cell death. Accordingly, VDAC2 KO is lethal *in utero* (Cheng et al., 2003), and conditional KO animals display severe dysfunction in the apoptotic pathways (Ren et al., 2009). VDAC isoform 2 also possesses the highest cysteine content (nine in humans and 11 in rats, **Figure 2**). This intriguing hallmark has prompted numerous studies aimed at identifying the role of such residues in protein structure and function. Maurya and Mahalakshmi (2013, 2014, 2015) demonstrated that VDAC2 cysteines strengthen β-barrel association to OMM, while lowering structure stability. Moreover, it has been reported that deletion (Majumder and Fisk, 2013) or modification (Piroli et al., 2016) of human VDAC2 cysteine residues can impair channel function. For instance, VDAC2 Cys47 and Cys76 succination has been linked to reduced ATP synthesis within mitochondria of the Leigh syndrome mouse model (Piroli et al., 2016). In Naghdi et al. (2015), cysteines are considered unessential for VDAC2-mediated Bak recruitment and tBid—induced cytochrome *c* release. A role for cysteines in ROS regulation has also been speculated (Maurya and Mahalakshmi, 2015), although no experimental evidence has yet proven it. Saletti et al. (2018) and Pittalà et al. (2020) first supplied a detailed profile of VDAC2 Cys Ox-PTMs that reveals a precise and evolutively conserved scheme in thiol oxidation. The N-terminal cysteine residues 8 and 13, together with the unique thiol group located in a loop exposed toward the cytosol (i.e., Cys 227 in **Figure 1**), were reported as totally reduced. Cysteines 47, 76, 103, and 210, all located in IMS loops, were instead identified as partially oxidated to $-SO_3H$. Surprisingly, VDAC2 Cys138, which faces the lipid environment of the OMM (**Figure 1**), was found fully trioxidized to sulfonic acid as the homologous residue in VDAC1 (Cys127, **Figures 1**, **2**).

VDAC3

VDAC3 is the least known isoform. Its 3D structure has not yet been experimentally resolved, albeit several homology

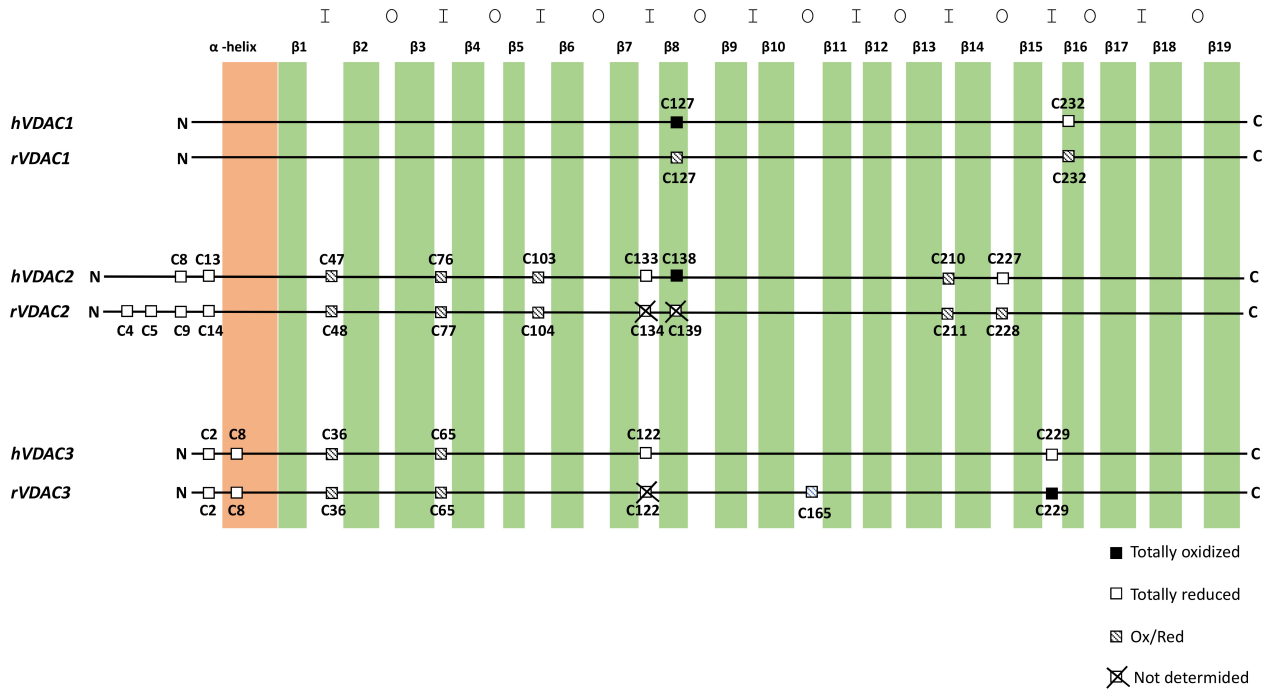

FIGURE 2 | Cysteine localization in the aligned sequences of human and rat VDAC isoforms. The N-terminal α-helix is shown in light orange, and β-strands are in green. The internal loops, that is, exposed to the intermembrane space, are indicated with I. The outer loops, that is, exposed to the cytosol, are indicated with O.

modeling predictions have confirmed a β-barrel organization almost identical to VDAC1 and VDAC2 (Bayrhuber et al., 2008; Hiller et al., 2008; Ujwal et al., 2008; De Pinto et al., 2010; Schredelseker et al., 2014). Unlike VDAC1 and VDAC2, ubiquitously expressed in all eukaryotes, VDAC3 prevails in the cerebral cortex, liver, heart, testes, and spermatozoa (Sampson et al., 2001). Herein, it participates in sperm mobility since VDAC3-null mice show a single microtubule doublet loss within the epididymal axoneme (Sampson et al., 2001) and in disassembly of cilia during the cell cycle by targeting Mps1 protein kinase to centrosomes (Majumder and Fisk, 2013). *S. cerevisiae* cells devoid of endogenous porin (Δ*por1*) have been extensively exploited for functional studies on VDAC proteins: as reported, the heterologous expressions of VDAC1 and VDAC2 fully complement the growth defect associated with gene loss, while that of VDAC3 only partially did so (Sampson et al., 1997; Reina et al., 2010). VDAC3 pore-forming activity was more difficult to be detected and did not show the homogeneous activity usually found with VDAC1 and VDAC2. Recombinant VDAC3 resulted in poor insertion in bilayers and hectic pore formation (Xu et al., 1999; Checchetto et al., 2014). In Checchetto et al. (2014), we demonstrated that, under non-reducing conditions, the majority of inserted VDAC3 forms very small pores with a lower conductance compared to the other isoforms. The modified activity pattern of VDAC3 pushed to look for differences between the VDAC3 structure and, in particular, VDAC1. The most striking was the cysteine content (De Pinto et al., 2016). Human VDAC3 contains indeed six cysteines (residues 2, 8, 36, 65, 122, and 229; Cys2 is the actual N-terminal residue, since Met1 is removed after biosynthesis) (Saletti et al., 2017, 2018; Pittalà et al., 2020). Except for Cys8, located within the pore, all cysteine residues protrude toward the IMS. The first clue about the relevance of VDAC3 cysteines goes back to the year 2010, when "swapping" experiments of the VDAC3 N-terminus (containing two cysteines) with the corresponding region of VDAC1 (lacking cysteines) totally changed isoform 3 pore activity (Reina et al., 2010). Next, electrophysiological data reported VDAC3 as able to form typical voltage-dependent pores (although with a remarkable lower insertion rate compared to VDAC1 and VDAC2), when refolded under highly reducing conditions (Queralt-Martín et al., 2020). Deletion of cysteines in engineered human VDAC3 molecules strongly affected both electrophysiological parameters and its ability to revert the mutant phenotype of Δpor1 yeast (Okazaki et al., 2015; Reina et al., 2016). The most relevant residue(s) for protein function appears to be 2, 8, and 122 in human VDAC3, since their mutation always restored formation of large pores and Δpor1 growth (Reina et al., 2016). Furthermore, the simultaneous mutation of any VDAC3 cysteines to alanine had a similar effect (Queralt-Martín et al., 2020). From MS analysis (Saletti et al., 2018; Pittalà et al., 2020) the preferred redox state of cysteines is conserved between rat and human VDAC3 analyzed. Accordingly, Cys2, Cys8, Cys122, and Cys229 were entirely identified in the reduced form, with the N-terminal Cys2 found acetylated. Cys36

and Cys65 were detected in a reduced form and trioxidized to sulfonic acid.

CONCLUSION

Hypotheses About the Role of Cys Ox-PTMs in VDAC Isoforms

Based on MS data reported for VDAC1, VDAC2, and VDAC3 in humans and rats, we found that the oxidation state of each specific residue is the same (Saletti et al., 2018; Pittalà et al., 2020). Thus, we speculated about the relationships between location of residue and oxidation state. In **Figure 1**, the position of the cysteines with respect to the water/phospholipidic phases is shown. **Figure 2**, instead, exhibits, on an analytical scheme, the oxidative modifications borne by the residues with respect to their location in structural elements of the pore. We thus noticed that cysteines whose lateral residue is embedded in the hydrophobic moiety of the membrane are trioxidized to $-SO_3H$. This finding is very surprising, since the charged modified sulfur residues protrude into the most hydrophobic part of the membrane bilayer, an apparent oddity, if it has no reason to be, unless it has a function as a spot for a structure intended to dock the OMM. These residues are present only in VDAC1 and VDAC2.

Cysteines in the N-terminal domain sequence steadily emerge as totally reduced. To be detected in MS as carboxymethylated sulfur, they indeed have to be protected *in vivo* by irreversible oxidation events. VDAC2 and VDAC3 alone have cysteines in the N-terminus. This group of totally reduced cysteines, exposed to IMS or residing inside the channel, could form disulfide bonds in VDACs as proposed in Okazaki et al. (2015) and Reina et al. (2016) and with the aim of changing pore useful diameter for modulating water-soluble molecule flow. It is not known how the formation of these hypothetical disulfide bridges may happen. It is tempting to speculate that the MIA/CHCHD4 complex could be involved. Although VDACs cannot be the subject or component of this specific quality control system because of a different import pathway, it is suggested to imagine that in metazoans CHCHD4 might interact with the VDAC2 and VDAC3 cysteines protruding toward IMS in reduced form (Pittalà et al., 2020). VDAC2 shows a motif CX_4C and VDAC3 a motif CX_5C in the N-terminal end. The possibility that CHCHD4 can oxidize cysteine pairs in a non-conventional motif has been highlighted for mitochondrial p53, which contains CX_5C and CX_1C motifs (Zhuang et al., 2013; Park et al., 2016), and it is true also for Erv1, containing a $CX_{16}C$ motif (Terziyska et al., 2007). CHCHD4, indeed, could represent a direct link of VDAC with apoptosis-inducing factor (AIF) (reviewed in Reinhardt et al., 2020): CHCHD4 is the first AIF mitochondrial interactor that was discovered. A CHCHD4 cysteine pair is reoxidized by ALR and docked to AIF-NADH. Another intriguing connection between VDACs and AIF could be found in the essential role of AIF in import and folding of CI subunits (Vahsen et al., 2004): it is known that CI is the most important ROS producer within the IMS, and these ROS are candidate to oxidize VDAC cysteines.

A ring of residues exposed or predicted to be exposed to the IMS is the third group of cysteines with distinct modifications as found by MS spectra: it turns out that they are in either oxidized or carboxyamidomethylated form, thus inclined to variable and possible reversible oxidations. This girdle of cysteine residues located in the turns connecting the β-strands and exposed to IMS can thus work as an oxidation buffer located on the inner surface of the OMM with the function of counteracting excess of ROS produced by the OXPHOS (Reina et al., 2016).

Our interpretation of such differences, experimentally determined by MS, is that types of cysteine residues may have specific roles in the operation of VDAC isoforms.

Thus, the pattern of cysteine oxidation could also be the key to understanding the evolution of the three VDAC isoforms: VDAC1 has only two, one of them in sulfonic state and exposed to the hydrophobic layer of the OMM; VDAC2 has 9–11 cysteines, in the three categories we described above; thus, it has also the overoxidized one; VDAC3 has again six to seven cysteines but lacks the category of overoxidized one.

Okazaki et al. (2015) proposed that the transient formation of a S–S bridge between VDAC3 residues placed in the protein N-terminus with those at the bottom of the pore could change its permeability, albeit the nature of such conductance hindrance is not clear yet. Molecular dynamic simulations have shown that disulfide formation between the nearest cysteines available did not affect the channel diameter but rather changed the electrical charge disposition on the protein surface (Amodeo et al., 2014; Guardiani et al., 2016). There are only indications of experimentally determined disulfide bridges in VDAC (Reina et al., 2016). Interestingly, the insertion of negative charges by $-SO_3H$ formation can modify the protein conformation by electric repulsions inside the chain or toward phospholipids. Some authors suggested that these conformational changes can initiate protein incorporation into mitochondria-derived vesicles (MDVs), later targeted to lysosomes. MDVs, whose production is induced by mitochondrial stress (Sugiura et al., 2014), contain numerous oxidized proteins derived mainly from the OMM. VDAC1 appears among these proteins (Soubannier et al., 2012), whereas no evidence about the VDAC3 cysteine status or its presence within MDVs has been reported.

Posttranslational removal of N-terminal methionine leaves VDAC3 Cys2 as the first amino acid. All proteomic analysis revealed this residue as completely acetylated, a PTM that, beside significantly influencing protein stability, activity, folding, and localization, triggers specific protein degradation by the Ac/N–degron pathway. This peculiar branch of the N-rule pathway controls several aspects of protein quality control (Eldeeb and Fahlman, 2016). Any dysregulation of N-terminal acetylation, which protects cysteine against irreversible oxidation, leads to serious pathological conditions including neurodegenerative diseases, cancers, hypertension, and X-linked genetic disorders (Rope et al., 2011; Aksnes et al., 2015, 2016).

Possible Pathological Implications of Redox Cysteine Modifications in VDACs

Despite VDAC being involved in several mitochondria-associated pathologies such as hypertension (Alvira et al., 2012; Zhu et al., 2019), diabetes (Sasaki et al., 2012; Zhang et al., 2019), cancer (Maldonado and Lemasters, 2012; Reina and De Pinto, 2017; Magrì et al., 2018), cardiovascular diseases (Karachitos et al., 2017), and neurodegenerative disorders, such as ALS (Magrì et al., 2016), PD (Rostovtseva et al., 2015), and AD (Manczak and Reddy, 2012), very little is known about the correlation of its Cys-Ox-PTMs with the aforementioned diseases. This is undoubtedly attributable to the few data available on these VDAC modifications, whose identification and analysis results are challenging. To quote some examples, Zahid et al. reported alterations in the *S*-nitrosylation pattern of VDAC2 in AD (Zhao et al., 2015); in Lam et al. (2010), the authors listed VDAC1, VDAC2, and VDAC3 among the *S*-nitrosylated targets in the prostate epithelial cell line.

The role of VDAC cysteine disulfide bridges or of its oxidation to sulfonic acid has yet to be discovered. It is suggested that the degree of VDAC oxidation on the mitochondrial surface could function as a signal of ROS load within the mitochondrial network, even if much more needs to be done to truly understand their biological meaning.

AUTHOR CONTRIBUTIONS

SR conceived the review organization and wrote most of it. MP selected the references and contributed to the oxidized cysteine discovery. FG, AM, and VD wrote the discussion section. SF and RS reviewed and revised the text and the Mass Spectroscopy analysis.

FUNDING

This research was partly supported by a grant from "Piano della Ricerca di Ateneo 2016–2018" of the University of Catania, Italy, to all the participants and by a MIUR PNR "Proof of Concept 2018" grant (codex: PEPSLA) to AM.

ACKNOWLEDGMENTS

The authors gratefully acknowledge the Bio-Nanotech Research and Innovation Tower (BRIT; PON project financed by the Italian Ministry for Education, University and Research MIUR) and Dr. Salvatore A.M. Cubisino (University of Catania) for modeling human VDAC structures.

REFERENCES

Abu-Hamad, S., Zaid, H., Israelson, A., Nahon, E., and Shoshan-Barmatz, V. (2008). Hexokinase-I protection against apoptotic cell death is mediated via interaction with the voltage-dependent anion channel-1: mapping the site of binding. *J. Biol. Chem.* 283, 13482–13490. doi: 10.1074/jbc.M708216200

Aksnes, H., Drazic, A., and Arnesen, T. (2015). (Hyper)tension release by N-terminal acetylation. *Trends Biochem. Sci.* 40, 422–424. doi: 10.1016/j.tibs.2015.05.003

Aksnes, H., Drazic, A., Marie, M., and Arnesen, T. (2016). First things first: vital protein marks by N-terminal acetyltransferases. *Trends Biochem. Sci.* 41, 746–760. doi: 10.1016/j.tibs.2016.07.005

Akter, S., Fu, L., Jung, Y., Lo Conte, M., Lawson, J. R., Lowther, W. T., et al. (2018). Chemical proteomics reveals new targets of cysteine sulfinic acid reductase. *Nat. Chem. Biol.* 14, 995–1004. doi: 10.1038/s41589-018-0116-2

Alcock, L. J., Perkins, M. V., and Chalker, J. M. (2018). Chemical methods for mapping cysteine oxidation. *Chem. Soc. Rev.* 47, 231–268. doi: 10.1039/c7cs00607a

Allen, E. M., and Mieyal, J. J. (2012). Protein-thiol oxidation and cell death: regulatory role of glutaredoxins. *Antioxid. Redox Signal.* 17, 1748–1763. doi: 10.1089/ars.2012.4644

Allen, J. W., Ferguson, S. J., and Ginger, M. L. (2008). Distinctive biochemistry in the trypanosome mitochondrial intermembrane space suggests a model for stepwise evolution of the MIA pathway for import of cysteine-rich proteins. *FEBS Lett.* 582, 2817–2825. doi: 10.1016/j.febslet.2008.07.015

Alvira, C. M., Umesh, A., Husted, C., Ying, L., Hou, Y., Lyu, S. C., et al. (2012). Voltage-dependent anion channel-2 interaction with nitric oxide synthase enhances pulmonary artery endothelial cell nitric oxide production. *Am. J. Respir. Cell Mol.* 47, 669–678. doi: 10.1165/rcmb.2011-0436OC

Amodeo, G. F., Scorciapino, M. A., Messina, A., De Pinto, V., and Ceccarelli, M. (2014). Charged residues distribution modulates selectivity of the open state of human isoforms of the voltage dependent anion-selective channel. *PLoS One* 9:e103879. doi: 10.1371/journal.pone.0103879

Anand, P., and Stamler, J. S. (2012). Enzymatic mechanisms regulating protein S-nitrosylation: implications in health and disease. *J. Mol. Med.* 90, 233–244. doi: 10.1007/s00109-012-0878-z

Anjo, S. I., Melo, M. N., Loureiro, L. R., Sabala, L., Castanheira, P., Grãos, M., et al. (2019). oxSWATH: An integrative method for a comprehensive redox-centered analysis combined with a generic differential proteomics screening. *Redox Biol.* 22:101130. doi: 10.1016/j.redox.2019.101130

Aram, L., Geula, S., Arbel, N., and Shoshan-Barmatz, V. (2010). VDAC1 cysteine residues: topology and function in channel activity and apoptosis. *Biochem. J.* 427, 445–454. doi: 10.1042/BJ20091690

Arbel, N., Ben-Hail, D., and Shoshan-Barmatz, V. (2012). Mediation of the antiapoptotic activity of Bcl-xL protein upon interaction with VDAC1 protein. *J. Biol. Chem.* 287, 23152–23161. doi: 10.1074/jbc.M112.345918

Bak, D. W., Pizzagalli, M. D., and Weerapana, E. (2017). Identifying functional cysteine residues in the mitochondria. *ACS Chem. Biol.* 12, 947–957. doi: 10.1021/acschembio.6b01074

Banci, L., Bertini, I., Cefaro, C., Ciofi-Baffoni, S., Gallo, A., Martinelli, M., et al. (2009). MIA40 is an oxidoreductase that catalyzes oxidative protein folding in mitochondria. *Nat. Struct. Mol. Biol.* 16, 198–206. doi: 10.1038/nsmb.1553

Banci, L., Bertini, I., Ciofi-Baffoni, S., Boscaro, F., Chatzi, A., Mikolajczyk, M., et al. (2011). Anamorsin is a [2Fe-2S] cluster-containing substrate of the Mia40-dependent mitochondrial protein trapping machinery. *Chem. Biol.* 18, 794–804. doi: 10.1016/j.chembiol.2011.03.015

Barros, M. H., and McStay, G. P. (2020). Modular biogenesis of mitochondrial respiratory complexes. *Mitochondrion* 50, 94–114. doi: 10.1016/j.mito.2019.10.008

Bayrhuber, M., Meins, T., Habeck, M., Becker, S., Giller, K., Villinger, S., et al. (2008). Structure of the human voltage-dependent anion channel. *Proc. Natl. Acad. Sci. U.S.A.* 105, 15370–15375. doi: 10.1073/pnas.0808115105

Bechtel, T. J., and Weerapana, E. (2017). From structure to redox: the diverse functional roles of disulfides and implications in disease. *Proteomics* 17:10.1002/pmic.201600391. doi: 10.1002/pmic.201600391

Benz, R. (1994). Permeation of hydrophilic solutes through mitochondrial outer membranes: review on mitochondrial porins. *Biochim. Biophys. Acta* 1197, 167–196. doi: 10.1016/0304-4157(94)90004-3

Bien, M., Longen, S., Wagener, N., Chwalla, I., Herrmann, J. M., and Riemer, J. (2010). Mitochondrial disulfide bond formation is driven by intersubunit electron transfer in Erv1 and proofread by glutathione. *Mol. Cell* 37, 516–528. doi: 10.1016/j.molcel.2010.01.017

Biteau, B., Labarre, J., and Toledano, M. B. (2003). ATP-dependent reduction of cysteine-sulphinic acid by *S. cerevisiae* sulphiredoxin. *Nature* 425, 980–984. doi: 10.1038/nature02075

Blachly-Dyson, E., Zambronicz, E. B., Yu, W. H., Adams, V., McCabe, E. R., Adelman, J., et al. (1993). Cloning and functional expression in yeast of two human isoforms of the outer mitochondrial membrane channel, the voltage-dependent anion channel. *J. Biol. Chem.* 268, 1835–1841.

Blackinton, J., Lakshminarasimhan, M., Thomas, K. J., Ahmad, R., Greggio, E., Raza, A. S., et al. (2009). Formation of a stabilized cysteine sulfinic acid is critical for the mitochondrial function of the parkinsonism protein DJ-1. *J. Biol. Chem.* 284, 6476–6485. doi: 10.1074/jbc.M806599200

Bleier, L., Wittig, I., Heide, H., Steger, M., Brandt, U., and Dröse, S. (2015). Generator-specific targets of mitochondrial reactive oxygen species. *Free Radic. Biol. Med.* 78, 1–10. doi: 10.1016/j.freeradbiomed.2014.10.511

Bulteau, A. L., Szweda, L. I., and Friguet, B. (2006). Mitochondrial protein oxidation and degradation in response to oxidative stress and aging. *Exp. Gerontol.* 41, 653–657. doi: 10.1016/j.exger.2006.03.013

Calvo, S. E., Clauser, K. R., and Mootha, V. K. (2016). MitoCarta2.0: an updated inventory of mammalian mitochondrial proteins. *Nucleic Acids Res.* 44, 1251–1257. doi: 10.1093/nar/gkv1003

Camara, A. K., Bienengraeber, M., and Stowe, D. F. (2011). Mitochondrial approaches to protect against cardiac ischemia and reperfusion injury. *Front. Physiol.* 2:13. doi: 10.3389/fphys.2011.00013

Camargo, L. L., Harvey, A. P., Rios, F. J., Tsiropoulou, S., Da Silva, R. N. O., Cao, Z., et al. (2018). Vascular Nox (NADPH Oxidase) compartmentalization, protein hyperoxidation, and endoplasmic reticulum stress response in hypertension. *Hypertension* 72, 235–246. doi: 10.1161/HYPERTENSIONAHA.118.10824

Canet-Avilés, R. M., Wilson, M. A., Miller, D. W., Ahmad, R., McLendon, C., Bandyopadhyay, S., et al. (2004). The Parkinson's disease protein DJ-1 is neuroprotective due to cysteine-sulfinic acid-driven mitochondrial localization. *Proc. Natl. Acad. Sci. U.S.A.* 101, 9103–9108. doi: 10.1073/pnas.0402959101

Cavallaro, G. (2010). Genome-wide analysis of eukaryotic twin CX9C proteins. *Mol. Biosyst.* 6, 2459–2470. doi: 10.1039/c0mb00058b

Chakraborty, J., Basso, V., and Ziviani, E. (2017). Post translational modification of Parkin. *Biol. Direct* 12:6. doi: 10.1186/s13062-017-0176-3

Chamberlain, L. H., and Shipston, M. J. (2015). The physiology of protein S-acylation. *Physiol. Rev.* 95, 341–376. doi: 10.1152/physrev.00032.2014

Chang, T. S., Jeong, W., Woo, H. A., Lee, S. M., Park, S., and Rhee, S. G. (2004). Characterization of mammalian sulfiredoxin and its reactivation of hyperoxidized peroxiredoxin through reduction of cysteine sulfinic acid in the active site to cysteine. *J. Biol. Chem.* 279, 50994–51001. doi: 10.1074/jbc.m409482200

Chatzi, A., and Tokatlidis, K. (2013). The mitochondrial intermembrane space: a hub for oxidative folding linked to protein biogenesis. *Antioxid. Redox Signal.* 19, 54–62. doi: 10.1089/ars.2012.4855

Checchetto, V., Reina, S., Magrì, A., Szabo, I., and De Pinto, V. (2014). Recombinant human voltage dependent anion selective channel isoform 3 (hVDAC3) forms pores with a very small conductance. *Cell. Physiol. Biochem.* 34, 842–853. doi: 10.1159/000363047

Cheng, E. H., Sheiko, T. V., Fisher, J. K., Craigen, W. J., and Korsmeyer, S. J. (2003). VDAC2 inhibits BAK activation and mitochondrial apoptosis. *Science* 301, 513–517. doi: 10.1126/science.1083995

Chin, H. S., Li, M. X., Tan, I. K. L., Ninni, S. R. L., and Dewson, G. (2018). VDAC2 enables BAX to mediate apoptosis and limit tumor development. *Nat. Commun.* 9:4976. doi: 10.1038/s41467-018-07309-4

Chouchani, E. T., Kazak, L., Jedrychowski, M. P., Lu, G. Z., Erickson, B. K., Szpyt, J., et al. (2016). Mitochondrial ROS regulate thermogenic energy expenditure and sulfenylation of UCP1. *Nature* 532, 112–116. doi: 10.1038/nature17399

Chouchani, E. T., Methner, C., Nadtochiy, S. M., Logan, A., Pell, V. R., Ding, S., et al. (2013). Cardioprotection by S-nitrosation of a cysteine switch on mitochondrial complex I. *Nat. Med.* 19, 753–759. doi: 10.1038/nm.3212

Chung, H. S., Wang, S. B., Venkatraman, V., Murray, C. I., and Van Eyk, J. E. (2013). Cysteine oxidative post translational modifications: emerging regulation in the cardiovascular system. *Circ. Res.* 112, 382–392. doi: 10.1161/CIRCRESAHA.112.268680

Clamp, M., Fry, B., Kamal, M., Xie, X., Cuff, J., Lin, M. F., et al. (2007). Distinguishing protein-coding and noncoding genes in the human genome. *Proc. Natl. Acad. Sci. U.S.A.* 104, 19428–19433. doi: 10.1073/pnas.0709013104

Colombini, M., Blachly-Dyson, E., and Forte, M. (1996). VDAC, a channel in the outer mitochondrial membrane. *Ion Channels* 4, 169–202. doi: 10.1007/978-1-4899-1775-1_5

Colussi, C., Albertini, M. C., Coppola, S., Rovidati, S., Galli, F., and Ghibelli, L. (2000). H_2O_2-induced block of glycolysis as an active ADP-ribosylation reaction protecting cells from apoptosis. *FASEB J.* 14, 2266–2276. doi: 10.1096/fj.00-0074com

Dabir, D. V., Leverich, E. P., Kim, S. K., Tsai, F. D., Hirasawa, M., Knaff, D. B., et al. (2007). A role for cytochrome *c* and cytochrome *c* peroxidase in electron shuttling from Erv1. *EMBO J.* 26, 4801–4811. doi: 10.1038/sj.emboj.7601909

Dalle-Donne, I., Rossi, R., Colombo, G., Giustarini, D., and Milzani, A. (2009). Protein S-Glutathionylation: a regulatory device from bacteria to humans. *Trends Biochem. Sci.* 34, 85–96. doi: 10.1016/j.tibs.2008.11.002

De Pinto, V., Al Jamal, J. A., Benz, R., Genchi, G., and Palmieri, F. (1991). Characterization of SH groups in porin of bovine heart mitochondria. Porin cysteines are localized in the channel walls. *Eur. J. Biochem.* 202, 903–911. doi: 10.1111/j.1432-1033.1991.tb16450.x

De Pinto, V., Guarino, F., Guarnera, A., Messina, A., Reina, S., Tomasello, F. M., et al. (2010). Characterization of human VDAC isoforms: a peculiar function for VDAC3? *Biochim. Biophys. Acta* 1797, 1268–1275. doi: 10.1016/j.bbabio.2010.01.031

De Pinto, V., Reina, S., Gupta, A., Messina, A., and Mahalakshmi, R. (2016). Role of cysteines in mammalian VDAC isoforms' function. *Biochim. Biophys. Acta* 1857, 1219–1227. doi: 10.1016/j.bbabio.2016.02.020

De Pinto, V., Tomasello, F., Messina, A., Guarino, F., Benz, R., La Mendola, D., et al. (2007). Determination of the conformation of the human VDAC1 N-terminal peptide, a protein moiety essential for the functional properties of the pore. *Chem. Biochem.* 8, 744–756. doi: 10.1002/cbic.200700009

Delaunay, A., Pflieger, D., Barrault, M. B., Vinh, J., and Toledano, M. B. (2002). A thiol peroxidase is an H_2O_2 receptor and redoxtransducer in gene activation. *Cell* 111, 471–481. doi: 10.1016/s0092-8674(02)01048-6

Depuydt, M., Messens, J., and Collet, J. F. (2011). How proteins form disulfide bonds. *Antioxid. Redox Signal.* 15, 49–66. doi: 10.1089/ars.2010.3575

Duan, G., and Walther, D. (2015). The roles of post-translational modifications in the context of protein interaction networks. *PLoS Comput. Biol.* 11:e1004049. doi: 10.1371/journal.pcbi.1004049

Duranski, M. R., Greer, J. J., Dejam, A., Jaganmohan, S., Hogg, N., Langston, W., et al. (2005). Cytoprotective effects of nitrite during in vivo ischemia-reperfusion of the heart and liver. *J. Clin. Invest.* 115, 1232–1240. doi: 10.1172/jci22493

Edgar, R. S., Green, E. W., Zhao, Y., van Ooijen, G., Olmedo, M., Qin, X., et al. (2012). Peroxiredoxins are conserved markers of circadian rhythms. *Nature* 485, 459–464. doi: 10.1038/nature11088

Eldeeb, M., and Fahlman, R. (2016). The-N-end rule: the beginning determines the end. *Protein Pept. Lett.* 23, 343–348. doi: 10.2174/0929866523666160108115809

Feldman, J. L., Dittenhafer-Reed, K. E., Kudo, N., Thelen, J. N., Ito, A., Yoshida, M., et al. (2015). Kinetic and structural basis for Acyl-group selectivity and NAD (+) dependence in sirtuin-catalyzed deacylation. *Biochemistry* 54, 3037–3050. doi: 10.1021/acs.biochem.5b00150

Fernando, V., Zheng, X., Walia, Y., Sharma, V., Letson, J., and Furuta, S. (2019). S-Nitrosylation: an emerging paradigm of redox signaling. *Antioxidants* 8:E404. doi: 10.3390/antiox8090404

Ferrer-Sueta, G., Manta, B., Botti, H., Radi, R., Trujillo, M., and Denicola, A. (2011). Factors affecting protein thiol reactivity and specificity in peroxide reduction. *Chem. Res. Toxicol.* 24, 434–450. doi: 10.1021/tx100413v

Fiek, C., Benz, R., Roos, N., and Brdiczka, D. (1982). Evidence for identity between the hexokinase-binding protein and the mitochondrial porin in the outer membrane of rat liver mitochondria. *Biochim. Biophys. Acta* 688, 429–440. doi: 10.1016/0005-2736(82)90354-6

Forrester, M. T., and Stamler, J. S. (2007). A classification scheme for redox-based modifications of proteins. *Am. J. Respir. Cell Mol. Biol.* 36, 135–137. doi: 10.1165/rcmb.2006-001ed

Fridovich, I. (1995). Superoxide radical and superoxide dismutases. *Annu. Rev. Biochem.* 64, 97–112. doi: 10.1146/annurev.bi.64.070195.000525

Fujiwara, N., Nakano, M., Kato, S., Yoshihara, D., Ookawara, T., Eguchi, H., et al. (2007). Oxidative modification to cysteine sulfonic acid of Cys111 in human copper-zinc superoxide dismutase. *J. Biol. Chem.* 282, 35933–35944. doi: 10.1074/jbc.m702941200

Furukawa, Y., Fu, R., Deng, H. X., Siddique, T., and O'Halloran, T. V. (2006). Disulfide cross-linked protein represents a significant fraction of ALS-associated Cu, Zn-superoxide dismutase aggregates in spinal cords of model mice. *Proc. Natl. Acad. Sci. U.S.A.* 103, 7148–7153. doi: 10.1073/pnas.0602048103

Gaillot, C., Delolme, F., Fabre, L., Charreyre, M. T., Ladavière, C., and Favier, A. (2020). Taking advantage of oxidation to characterize thiol-containing polymer chains by MALDI-TOF mass spectrometry. *Anal. Chem.* 92, 3804–3809. doi: 10.1021/acs.analchem.9b05207

Grek, C. L., Zhang, J., Manevich, Y., Townsend, D. M., and Tew, K. D. (2013). Causes and consequences of cysteine S-Glutathionylation. *J. Biol. Chem.* 288, 26497–26504. doi: 10.1074/jbc.R113.461368

Griesser, M., Chauvin, J. R., and Pratt, D. A. (2018). The hydrogen atom transfer reactivity of sulfinic acids. *Chem. Sci.* 9, 7218–7229. doi: 10.1039/c8sc02400f

Gross, D. P., Burgard, C. A., Reddehase, S., Leitch, J. M., Culotta, V. C., and Hell, K. (2011). Mitochondrial Ccs1 contains a structural disulfide bond crucial for the import of this unconventional substrate by the disulfide relay system. *Mol. Biol. Cell* 22, 3758–3767. doi: 10.1091/mbc.E11-04-0296

Guardiani, C., Leggio, L., Scorciapino, M. A., De Pinto, V., and Ceccarelli, M. (2016). A computational study of ion current modulation in hVDAC3 induced by disulfide bonds. *Biochim. Biophys. Acta* 1858:813823. doi: 10.1016/j.bbamem.2016.01.013

Hall, A., Parsonage, D., Poole, L. B., and Karplus, P. A. (2010). Structural evidence that peroxiredoxin catalytic power is based on transition-state stabilization. *J. Mol. Biol.* 402, 194–209. doi: 10.1016/j.jmb.2010.07.022

Han, D., Antunes, F., Canali, R., Rettori, D., and Cadenas, E. (2003). Voltage-dependent anion channels control the release of the superoxide anion from mitochondria to cytosol. *J. Biol. Chem.* 278, 5557–5563. doi: 10.1074/jbc.m210269200

Heppner, D. E., Dustin, C. M., Liao, C., Hristova, M., Veith, C., Little, A. C., et al. (2018). Direct cysteine sulfenylation drives activation of the Src kinase. *Nat. Commun.* 9:4522. doi: 10.1038/s41467-018-06790-1

Herrmann, J. M., and Riemer, J. (2012). Mitochondrial disulfide relay: redox-regulated protein import into the intermembrane space. *J. Biol. Chem.* 287, 4426–4433. doi: 10.1074/jbc.R111.270678

Hiller, S., Garces, R. G., Malia, T. J., Orekhov, V. Y., Colombini, M., and Wagner, G. (2008). Solution structure of the integral human membrane protein VDAC-1 in detergent micelles. *Science* 321, 1206–1210. doi: 10.1126/science.1161302

Holmgren, A. (2000). Antioxidant function of thioredoxin and glutaredoxin systems. *Antioxid. Redox Signal.* 2, 811–820. doi: 10.1089/ars.2000.2.4-811

Holmgren, A., Johansson, C., Berndt, C., Lönn, M. E., Hudemann, C., and Lillig, C. H. (2005). Thiol redox control via thioredoxin and glutaredoxin systems. *Biochem. Soc. Trans.* 33, 1375–1377. doi: 10.1042/bst0331375

Holoubek, A., Večeř, J., and Sigler, K. (2007). Monitoring of the proton electrochemical gradient in reconstituted vesicles: quantitative measurements of both transmembrane potential and intravesicular pH by ratiometric fluorescent probes. *J. Fluoresc.* 17, 201–213. doi: 10.1007/s10895-007-0159-3

Hu, J., Dong, L., and Outten, C. E. (2008). The redox environment in the mitochondrial intermembrane space is maintained separately from the cytosol and matrix. *J Biol. Chem.* 283, 29126–29134. doi: 10.1074/jbc.M803028200

Huang, H., Hu, X., Eno, C. O., Zhao, G., Li, C., and White, C. (2013). An interaction between Bcl-xL and the voltage-dependent anion channel (VDAC)promotes mitochondrial Ca^{2+} uptake. *J. Biol. Chem.* 288, 19870–19881. doi: 10.1074/jbc.M112.448290

Iciek, M., Kowalczyk-Pachel, D., Bilska-Wilkosz, A., Kwiecień, I., Górny, M., and Włodek, L. (2015). S-sulfhydration as a cellular redox regulation. *Biosci. Rep.* 36:e00304. doi: 10.1042/BSR20150147

International Human Genome Sequencing Consortium. (2004). Finishing the euchromatic sequence of the human genome. *Nature* 431, 931–945. doi: 10.1038/nature03001

Jang, H. H., Lee, K. O., Chi, Y. H., Jung, B. G., Park, S. K., Park, J. H., et al. (2004). Two enzymes in one; two yeast peroxiredoxins display oxidative stress-dependent switching from a peroxidase to a molecular chaperone function. *Cell* 117, 625–635.

Jarvis, R. M., Hughes, S. M., and Ledgerwood, E. C. (2012). Peroxiredoxin 1 functions as a signal peroxidase to receive, transduce, and transmit peroxide signals in mammalian cells. *Free Radic. Biol. Med.* 53, 1522–1530. doi: 10.1016/j.freeradbiomed.2012.08.001

Jones, D. P. (2006). Redefining oxidative stress. *Antioxid. Redox Signal.* 8, 1865–1879. doi: 10.1089/ars.2006.8.1865

Karachitos, A., Jordan, J., and Kmita, H. (2017). VDAC-targeted drugs affecting cytoprotection and mitochondrial physiology in cerebrovascular and cardiovascular diseases. *Curr. Med. Chem.* 24, 4419–4434. doi: 10.2174/0929867324666170530073238

Kim, D., Lim, S., Haque, M., Ryoo, N., Hong, H. S., Rhim, H., et al. (2015). Identification of disulfide cross-linked tau dimer responsible for tau propagation. *Sci. Rep.* 5:15231. doi: 10.1038/srep15231

Kojer, K., Bien, M., Gangel, H., Morgan, B., Dick, T. P., and Riemer, J. (2012). Glutathione redox potential in the mitochondrial intermembrane space is linked to the cytosol and impacts the Mia40 redox state. *EMBO J.* 31, 3169–3182. doi: 10.1038/emboj.2012.165

Kojer, K., Peleh, V., Calabrese, G., Herrmann, J. M., and Riemer, J. (2015). Kinetic control by limiting glutaredoxin amounts enables thiol oxidation in the reducing mitochondrial intermembrane space. *Mol. Biol. Cell* 26, 195–204. doi: 10.1091/mbc.E14-10-1422

Komarov, A. G., Deng, D., Craigen, W. J., and Colombini, M. (2005). New insights into the mechanism of permeation through large channels. *Biophys. J.* 89, 3950–3959. doi: 10.1529/biophysj.105.070037

Kordyukova, L. V., Serebryakova, M. V., Baratova, L. A., and Veit, M. (2010). Site-specific attachment of palmitate or stearate to cytoplasmic versus transmembrane cysteines is a common feature of viral spike proteins. *Virology* 398, 49–56. doi: 10.1016/j.virol.2009.11.039

Krishnan, N., Fu, C., Pappin, D. J., and Tonks, N. K. (2011). H2S-Induced sulfhydration of the phosphatase PTP1B and its role in the endoplasmic reticulum stress response. *Sci. Signal.* 4:ra86. doi: 10.1126/scisignal.2002329

Lam, Y. W., Yuan, Y., Isaac, J., Babu, C. V., Meller, J., and Ho, S. M. (2010). Comprehensive identification and modified-site mapping of S-nitrosylated targets in prostate epithelial cells. *PLoS One* 5:e9075. doi: 10.1371/journal.pone.0009075

Leanza, L., Zoratti, M., Gulbins, E., and Szabò, I. (2014). Mitochondrial ion channels as oncological targets. *Oncogene* 33, 5569–5581. doi: 10.1038/onc.2013.578

Lee, J., Hofhaus, G., and Lisowsky, T. (2000). Erv1p from *Saccharomyces cerevisiae* is a FAD-linked sulfhydryl oxidase. *FEBS Lett.* 477, 62–66. doi: 10.1016/s0014-5793(00)01767-1

Lim, J. C., Choi, H. I., Park, Y. S., Nam, H. W., Woo, H. A., Kwon, K. S., et al. (2008). Irreversible oxidation of the active-site cysteine of peroxiredoxin to cysteine sulfonic acid for enhanced molecular chaperone activity. *J. Biol. Chem.* 283, 28873–28880. doi: 10.1074/jbc.M804087200

Liu, Z., Luo, Q., and Guo, C. (2015). Bim and VDAC1 are hierarchically essential for mitochondrial ATF2 mediated cell death. *Cancer Cell Int.* 15:34. doi: 10.1186/s12935-015-0188-y

Llopis, J., McCaffery, J. M., Miyawaki, A., Farquhar, M. G., and Tsien, R. Y. (1998). Measurement of cytosolic, mitochondrial, and Golgi pH in single living cells with green fluorescent proteins. *Proc. Natl. Acad. Sci. U.S.A.* 95, 6803–6808. doi: 10.1073/pnas.95.12.6803

Lo Conte, M., and Carroll, K. S. (2013). The redox biochemistry of protein sulfenylation and sulfinylation. *J. Biol. Chem.* 288, 26480–26488. doi: 10.1074/jbc.R113.467738

Longen, S., Woellhaf, M. W., Petrungaro, C., Riemer, J., and Herrmann, J. M. (2014). The disulfide relay of the intermembrane space oxidizes the ribosomal subunit mrp10 on its transit into the mitochondrial matrix. *Dev. Cell* 28, 30–42. doi: 10.1016/j.devcel.2013.11.007

Lushchak, V. I. (2012). Glutathione homeostasis and functions: potential targets for medical interventions. *J. Amino Acids* 2012:736837. doi: 10.1155/2012/736837

Magrì, A., Belfiore, R., Reina, S., Tomasello, M. F., Di Rosa, M. C., Guarino, F., et al. (2016). Hexokinase I N-terminal based peptide prevents the VDAC1-SOD1 G93A interaction and re-establishes ALS cell viability. *Sci Rep.* 6:34802. doi: 10.1038/srep34802

Magrì, A., Reina, S., and De Pinto, V. (2018). VDAC1 as pharmacological target in cancer and neurodegeneration: focus on its role in apoptosis. *Front. Chem.* 6:108. doi: 10.3389/fchem.2018.00108

Mailloux, R. J., Jin, X., and Willmore, W. G. (2014). Redox regulation of mitochondrial function with emphasis on cysteine oxidation reactions. *Redox Biol.* 2, 123–139. doi: 10.1016/j.redox.2013.12.011

Majumder, S., and Fisk, H. A. (2013). VDAC3 and Mps1 negatively regulate ciliogenesis. *Cell Cycle* 12, 849–858. doi: 10.4161/cc.23824

Maldonado, E. N., and Lemasters, J. J. (2012). Warburg revisited: regulation of mitochondrial metabolism by voltage-dependent anion channels in cancer cells. *J. Pharmacol. Exp. Ther.* 342, 637–641. doi: 10.1124/jpet.112.192153

Maldonado, E. N., Patnaik, J., Mullins, M. R., and Lemasters, J. J. (2010). Free tubulin modulates mitochondrial membrane potential in cancer cells. *Cancer Res.* 70, 10192–10201. doi: 10.1158/0008-5472.CAN-10-2429

Manczak, M., and Reddy, P. H. (2012). Abnormal interaction of VDAC1 with amyloid beta and phosphorylated tau causes mitochondrial dysfunction in Alzheimer's disease. *Hum. Mol. Genet.* 21, 5131–5146. doi: 10.1093/hmg/dds360

Maurya, S. R., and Mahalakshmi, R. (2013). Modulation of human mitochondrial voltage-dependent anion channel 2 (hVDAC-2) structural stability by cysteine-assisted barrel-lipid interactions. *J. Biol. Chem.* 288, 25584–25592. doi: 10.1074/jbc.M113.493692

Maurya, S. R., and Mahalakshmi, R. (2014). Influence of protein – micelle ratios and cysteine residues on the kinetic stability and unfolding rates of human mitochondrial VDAC-2. *PLoS One* 9:e87701. doi: 10.1371/journal.pone.0087701

Maurya, S. R., and Mahalakshmi, R. (2015). N-helix and cysteines inter-regulate human mitochondrial VDAC-2 function and biochemistry. *J. Biol. Chem.* 290, 30240–30252. doi: 10.1074/jbc.M115.693978

Maurya, S. R., and Mahalakshmi, R. (2016). VDAC-2: Mitochondrial outer membrane regulator masquerading as a channel? *FEBS J.* 283, 1831–1836. doi: 10.1111/febs.13637

Menzel, V. A., Cassará, M. C., Benz, R., De Pinto, V., Messina, A., Cunsolo, V., et al. (2009). Molecular and functional characterization of VDAC2 purified from mammal spermatozoa. *Biosci. Rep.* 29, 351–362. doi: 10.1042/BSR20080123

Messina, A., Reina, S., Guarino, F., and De Pinto, V. (2012). VDAC isoforms in mammals. *Biochim. Biophys. Acta* 1818, 1466–1476. doi: 10.1016/j.bbamem.2011.10.005

Muronetz, V. I., Melnikova, A. K., Saso, L., and Schmalhausen, E. V. (2020). Influence of oxidative stress on catalytic and non-glycolytic functions of glyceraldehyde-3-phosphate dehydrogenase. *Curr. Med. Chem.* 27, 2040–2058. doi: 10.2174/0929867325666180530101057

Murray, C. I., and Van Eyk, J. E. (2012). Chasing cysteine oxidative modifications: proteomic tools for characterizing cysteine redox status. *Circ. Cardiovasc. Genet.* 5:591. doi: 10.1161/circgenetics.111.961425

Naghdi, S., and Hajnóczky, G. (2016). VDAC2-specific cellular functions and the underlying structure. *Biochim. Biophys. Acta* 1863, 2503–2514. doi: 10.1016/j.bbamcr.2016.04.020

Naghdi, S., Várnai, P., and Hajnóczky, G. (2015). Motifs of VDAC2 required for mitochondrial Bak import and tBid-induced apoptosis. *Proc. Natl. Acad. Sci. U.S.A.* 112, E5590–E5599. doi: 10.1073/pnas.1510574112

Nakamura, T., Tu, S., Akhtar, M. W., Sunico, C. R., Okamoto, S., and Lipton, S. A. (2013). Aberrant protein s-nitrosylation in neurodegenerative diseases. *Neuron* 78, 596–614. doi: 10.1016/j.neuron.2013.05.005

Neumann, C. A., Krause, D. S., Carman, C. V., Das, S., Dubey, D. P., Abraham, J. L., et al. (2003). Essential role for the peroxiredoxin Prdx1 in erythrocyte antioxidant defence and tumour suppression. *Nature* 424, 561–565. doi: 10.1038/nature01819

Niemann, M., Wiese, S., Mani, J., Chanfon, A., Jackson, C., Meisinger, C., et al. (2013). Mitochondrial outer membrane proteome of Trypanosoma brucei reveals novel factors required to maintain mitochondrial morphology. *Mol. Cell. Proteomics* 12, 515–528. doi: 10.1074/mcp.M112.023093

Okazaki, M., Kurabayashi, K., Asanuma, M., Saito, Y., Dodo, K., and Sodeoka, M. (2015). VDAC3 gating is activated by suppression of disulfide-bond formation between the N-terminal region and the bottom of the pore. *Biochim. Biophys. Acta* 1848, 3188–3196. doi: 10.1016/j.bbamem.2015.09.017

O'Neill, J. S., and Reddy, A. B. (2011). Circadian clocks in human red blood cells. *Nature* 469, 498–503. doi: 10.1038/nature09702

Park, J. H., Zhuang, J., Li, J., and Hwang, P. M. (2016). p53 as guardian of the mitochondrial genome. *FEBS Lett.* 590, 924–934. doi: 10.1002/1873-3468.12061

Paul, B. D., and Snyder, S. H. (2018). Gasotransmitter hydrogen sulfide signaling in neuronal health and disease. *Biochem. Pharmacol.* 149, 101–109. doi: 10.1016/j.bcp.2017.11.019

Pedro, M. P., Vilcaes, A. A., Gomez, G. A., and Daniotti, J. L. (2017). Individual S-acylated cysteines differentially contribute to H-Ras endomembrane trafficking and acylation/deacylation cycles. *Mol. Biol. Cell* 28, 962–974. doi: 10.1091/mbc.E16-08-0603

Petrungaro, C., Zimmermann, K. M., Küttner, V., Fischer, M., Dengjel, J., Bogeski, I., et al. (2015). The Ca^{2+}-dependent release of the Mia40-Induced MICU1-MICU2 dimer from MCU regulates mitochondrial Ca^{2+} uptake. *Cell Metab.* 22, 721–733. doi: 10.1016/j.cmet.2015.08.019

Piantadosi, C. (2011). Regulation of mitochondrial processes by protein S-nitrosylation. *Biochim. Biophys. Acta* 1820, 712–721. doi: 10.1016/j.bbagen.2011.03.008

Piroli, G. G., Manuel, A. M., Clapper, A. C., Walla, M. D., Baatz, J. E., Palmiter, R. D., et al. (2016). Succination is Increased on Select Proteins in the Brainstem of the NADH dehydrogenase (ubiquinone) Fe-S protein 4 (Ndufs4) Knockout Mouse, a Model of Leigh Syndrome. *Mol. Cell. Proteomics* 15, 445–461. doi: 10.1074/mcp.M115.051516

Pittalà, M. G. G., Saletti, R., Reina, S., Cunsolo, V., De Pinto, V., and Foti, S. (2020). A high resolution mass spectrometry study reveals the potential of disulfide formation in human mitochondrial voltage-dependent anion selective channel isoforms (hVDACs). *Int. J. Mol. Sci.* 21:E1468. doi: 10.3390/ijms21041468

Poole, L. B., Karplus, P. A., and Claiborne, A. (2004). Protein sulfenic acids in redox signaling. *Annu. Rev. Pharmacol. Toxicol.* 44, 325–347.

Poole, L. B., and Nelson, K. J. (2008). Discovering mechanisms of signaling-mediated cysteine oxidation. *Curr. Opin. Chem. Biol.* 12, 18–24. doi: 10.1016/j.cbpa.2008.01.021

Portillo, S. D., Ferrer-Sueta, G., and Coitiño, L. (2017). Insights into the mechanism of peroxiredoxin 6 sulfenic acid reduction by ascorbate. *Free Radic. Biol. Med.* 112:31. doi: 10.1016/j.freeradbiomed.2017.10.036

Queralt-Martín, M., Bergdoll, L., Teijido, O., Munshi, N., Jacobs, D., Kuszak, A. J., et al. (2020). A lower affinity to cytosolic proteins reveals VDAC3 isoform-specific role in mitochondrial biology. *J. Gen. Physiol.* 152:e201912501. doi: 10.1085/jgp.201912501

Radi, R. (2013). Peroxynitrite, a stealthy biological oxidant. *J. Biol. Chem.* 288, 26464–26472. doi: 10.1074/jbc.R113.472936

Ray, P. D., Huang, B. W., and Tsuji, Y. (2012). Reactive oxygen species (ROS) homeostasis and redox regulation in cellular signaling. *Cell Signal.* 24, 981–990. doi: 10.1016/j.cellsig.2012.01.008

Reina, S., Checchetto, V., Saletti, R., Gupta, A., Chaturvedi, D., Guardiani, C., et al. (2016). VDAC3 as a sensor of oxidative state of the intermembrane space of mitochondria: the putative role of cysteine residue modifications. *Oncotarget* 7, 2249–2268. doi: 10.18632/oncotarget.6850

Reina, S., and De Pinto, V. (2017). Anti-cancer compounds targeted to VDAC: potential and perspectives. *Curr. Med. Chem.* 24, 4447–4469. doi: 10.2174/0929867324666170530074039

Reina, S., Palermo, V., Guarnera, A., Guarino, F., Messina, A., Mazzoni, C., et al. (2010). Swapping of the N-terminus of VDAC1 with VDAC3 restores full activity of the channel and confers anti-aging features to the cell. *FEBS Lett.* 584, 2837–2844. doi: 10.1016/j.febslet.2010.04.066

Reinhardt, C., Arena, G., Nedara, K., Edwards, R., Brenner, C., Tokatlidis, K., et al. (2020). AIF meets the CHCHD4/Mia40-dependent mitochondrial import pathway. *Biochim. Biophys. Acta* 1866:165746. doi: 10.1016/j.bbadis.2020.165746

Ren, D., Kim, H., Tu, H. C., Westergard, T. D., Fisher, J. K., Rubens, J. A., et al. (2009). The VDAC2-BAK rheostat controls thymocyte survival. *Sci. Signal.* 2:ra48. doi: 10.1126/scisignal.2000274

Roos, G., and Messens, J. (2011). Protein sulfenic acid formation: From cellular damage to redox regulation. *Free Radic. Biol. Med.* 51, 314–326. doi: 10.1016/j.freeradbiomed.2011.04.031

Rope, A. F., Wang, K., Evjenth, R., Xing, J., Johnston, J. J., Swensen, J. J., et al. (2011). Using VAAST to identify an X-linked disorder resulting in lethality in male infants due to N-terminal acetyltransferase deficiency. *Am. J. Hum. Genet.* 89, 28–43. doi: 10.1016/j.ajhg.2011.05.017

Rose, P., Moore, P. K., and Zhu, Y. Z. (2017). H2S biosynthesis and catabolism: new insights from molecular studies. *Cell. Mol. Life Sci.* 74, 1391–1412. doi: 10.1007/s00018-016-2406-8

Rostovtseva, T. K., Gurnev, P. A., Protchenko, O., Hoogerheide, D. P., Yap, T. L., Philpott, C. C., et al. (2015). α-synuclein shows high affinity interaction with voltage-dependent anion channel, suggesting mechanisms of mitochondrial

regulation and toxicity in Parkinson disease. *J. Biol. Chem.* 290, 18467–18477. doi: 10.1074/jbc.M115.641746

Roth, A. F., Wan, J., Bailey, A. O., Sun, B., Kuchar, J. A., Green, W. N., et al. (2006). Global analysis of protein palmitoylation in yeast. *Cell* 125, 1003–1013. doi: 10.1016/j.cell.2006.03.042

Saletti, R., Reina, S., Pittalà, M. G. G., Belfiore, R., Cunsolo, V., Messina, A., et al. (2017). High resolution mass spectrometry characterization of the oxidation pattern of methionine and cysteine residues in rat liver mitochondria voltage-dependent anion selective channel 3 (VDAC3). *Biochim. Biophys. Acta Biomembr.* 1859, 301–311. doi: 10.1016/j.bbamem.2016.12.003

Saletti, R., Reina, S., Pittalà, M. G. G., Magrì, A., Cunsolo, V., Foti, S., et al. (2018). Post-translational modifications of VDAC1 and VDAC2 cysteines from rat liver mitochondria. *Biochim. Biophys. Acta Bioenerg.* 1859, 806–816. doi: 10.1016/j.bbabio.2018.06.007

Sampson, M. J., Decker, W. K., Beaudet, A. L., Ruitenbeek, W., Armstrong, D., Hicks, M. J., et al. (2001). Immotile sperm and infertility in mice lacking mitochondrial voltage-dependent anion channel type 3. *J. Biol. Chem.* 276, 39206–39212. doi: 10.1074/jbc.m104724200

Sampson, M. J., Lovell, R. S., and Craigen, W. J. (1997). The murine voltage-dependent anion channel gene family. Conserved structure and function. *J. Biol. Chem.* 272, 18966–18973. doi: 10.1074/jbc.272.30.18966

Santo-Domingo, J., Wiederkehr, A., and De Marchi, U. (2015). Modulation of the matrix redox signaling by mitochondrial Ca^{2+}. *World J. Biol. Chem.* 6, 310–323. doi: 10.4331/wjbc.v6.i4.310

Sasaki, K., Donthamsetty, R., Heldak, M., Cho, Y. E., Scott, B. T., and Makino, A. (2012). VDAC: old protein with new roles in diabetes. *Am. J. Physiol. Cell. Physiol.* 303, C1055–C1060. doi: 10.1152/ajpcell.00087.2012

Schmitt, S., Prokisch, H., Schlunck, T., Camp, D. G., Ahting, U., Waizenegger, T., et al. (2006). Proteome analysis of mitochondrial outer membrane from Neurospora crassa. *Proteomics* 6, 72–80.

Schredelseker, J., Paz, A., López, C. J., Altenbach, C., Leung, C. S., Drexler, M. K., et al. (2014). High resolution structure and double electron-electron resonance of the zebrafish voltage-dependent anion channel 2 reveal an oligomeric population. *J. Biol. Chem.* 289, 12566–12577. doi: 10.1074/jbc.M113.497438

Shakir, S., Vinh, J., and Chiappetta, G. (2017). Quantitative analysis of the cysteine redoxome by iodoacetyl tandem mass tags. *Anal. Bioanal. Chem.* 409, 3821–3830. doi: 10.1007/s00216-017-0326-6

Shimizu, H., Schredelseker, J., Huang, J., Lu, K., Naghdi, S., Lu, F., et al. (2015). Mitochondrial Ca^{2+} uptake by the voltage-dependent anion channel 2 regulates cardiac rhythmicity. *eLife* 4:e04801.

Shimizu, S., Matsuoka, Y., Shinohara, Y., Yoneda, Y., and Tsujimoto, Y. (2001). Essential role of voltage-dependent anion channel in various forms of apoptosis in mammalian cells. *J. Cell Biol.* 152, 237–250. doi: 10.1083/jcb.152.2.237

Shoshan-Barmatz, V., De Pinto, V., Zweckstetter, M., Raviv, Z., Keinan, N., and Arbel, N. (2010). VDAC, a multi-functional mitochondrial protein regulating cell life and death. *Mol. Aspects Med.* 31, 227–285. doi: 10.1016/j.mam.2010.03.002

Shu, Z., Jung, M., Beger, H. G., Marzinzig, M., Han, F., Butzer, U., et al. (1997). pH-dependent changes of nitric oxide, peroxynitrite, and reactive oxygen species in hepatocellular damage. *Am. J. Physiol.* 273, 1118–1126. doi: 10.1152/ajpgi.1997.273.5.G1118

Sobotta, M. C., Liou, W., Stocker, S., Talwar, D., Oehler, M., Ruppert, T., et al. (2015). Peroxiredoxin-2 and STAT3 form a redox relay for H_2O_2 signaling. *Nat. Chem. Biol.* 11, 64–70. doi: 10.1038/nchembio.1695

Soubannier, V., Rippstein, P., Kaufman, B. A., Shoubridge, E. A., and McBride, H. M. (2012). Reconstitution of mitochondria derived vesicle formation demonstrates selective enrichment of oxidized cargo. *PLoS One* 7:e52830. doi: 10.1371/journal.pone.0052830

Spadaro, D., Yun, B. W., Spoel, S. H., Chu, C., Wang, Y. Q., and Loake, G. J. (2010). The redox switch: dynamic regulation of protein function by cysteine modifications. *Physiol. Plant.* 138, 360–371. doi: 10.1111/j.1399-3054.2009.01307.x

Spickett, C. M., and Pitt, A. R. (2012). Protein oxidation: role in signalling and detection by mass spectrometry. *Amino Acids* 42, 5–21. doi: 10.1007/s00726-010-0585-4

Stipanuk, M. H., Ueki, I., Dominy, J. E. Jr., Simmons, C. R., and Hirschberger, L. L. (2009). Cysteine dioxygenase: a robust system for regulation of cellular cysteine levels. *Amino Acids* 37, 55–63. doi: 10.1007/s00726-008-0202-y

Stojanovski, D., Müller, J. M., Milenkovic, D., Guiard, B., Pfanner, N., and Chacinska, A. (2008). The MIA system for protein import into the mitochondrial intermembrane space. *Biochim. Biophys. Acta* 1783, 610–617. doi: 10.1016/j.bbamcr.2007.10.004

Subedi, K. P., Kim, J. C., Kang, M., Son, M. J., Kim, Y. S., and Woo, S. H. (2011). Voltage-dependent anion channel 2 modulates resting Ca^{2+} sparks, but not action potential-induced Ca^{2+} signaling in cardiac myocytes. *Cell Calcium* 49, 136–143. doi: 10.1016/j.ceca.2010.12.004

Sugiura, A., McLelland, G. L., Fon, E. A., and McBride, H. M. (2014). A new pathway for mitochondrial quality control: mitochondrial-derived vesicles. *EMBO J.* 33, 2142–2156. doi: 10.15252/embj.201488104

Summa, D., Spiga, O., Bernini, A., Venditti, V., Priora, R., Frosali, S., et al. (2007). Protein-thiol substitution or protein dethiolation by thiol/disulfide exchange reactions: the albumin model. *Proteins* 69, 369–378. doi: 10.1002/prot.21532

Teijido, O., Ujwal, R., Hillerdal, C. O., Kullman, L., Rostovtseva, T. K., and Abramson, J. (2012). Affixing N-terminal α-helix to the wall of the voltage-dependent anion channel does not prevent its voltage gating. *J. Biol. Chem.* 287, 11437–11445. doi: 10.1074/jbc.M111.314229

Terziyska, N., Grumbt, B., Bien, M., Neupert, W., Herrmann, J. M., and Hell, K. (2007). The sulfhydryl oxidase Erv1 is a substrate of the Mia40-dependent protein translocation pathway. *FEBS Lett.* 581, 1098–1102. doi: 10.1016/j.febslet.2007.02.014

Tienson, H. L., Dabir, D. V., Neal, S. E., Loo, R., Hasson, S. A., Boontheung, P., et al. (2009). Reconstitution of the mia40-erv1 oxidative folding pathway for the small tim proteins. *Mol. Biol. Cell* 20, 3481–3490. doi: 10.1091/mbc.E08-10-1062

Tomasello, F. M., Guarino, F. M., Reina, S., Messina, A., and De Pinto, V. (2013). The voltage-dependent anion selective channel 1 (VDAC1) topography in the mitochondrial outer membrane as detected in intact cell. *PLoS One* 8:e81522. doi: 10.1371/journal.pone.0081522

Truong, T. H., Ung, P. M., Palde, P. B., Paulsen, C. E., Schlessinger, A., and Carroll, K. S. (2016). Molecular basis for redox activation of epidermal growth factor receptor kinase. *Cell Chem. Biol.* 23, 837–848. doi: 10.1016/j.chembiol.2016.05.017

Ujwal, R., Cascio, D., Colletierc, J. P., Fahama, S., Zhanga, J., Torod, L., et al. (2008). The crystal structure of mouse VDAC1 at 2.3 A resolution reveals mechanistic insights into metabolite gating. *Proc. Natl. Acad. Sci. U.S.A.* 105, 17742–17747. doi: 10.1073/pnas.0809634105

Urmey, A. R., and Zondlo, N. J. (2020). Structural preferences of cysteine sulfinic acid: the sulfinate engages in multiple local interactions with the peptide backbone. *Free Radic. Biol. Med.* 148, 96–107. doi: 10.1016/j.freeradbiomed.2019.12.030

Vahsen, N., Cande, C., Briere, J. J., Benit, P., Joza, N., Larochette, N., et al. (2004). AIF deficiency compromises oxidative phosphorylation. *EMBO J.* 23, 4679–4689. doi: 10.1038/sj.emboj.7600461

Valdez Taubas, J., and Pelham, H. (2005). Swf1-dependent palmitoylation of the SNARE Tlg1 prevents its ubiquitination and degradation. *EMBO J.* 24, 2524–2532. doi: 10.1038/sj.emboj.7600724

Vander Heiden, M. G., Li, X. X., Gottleib, E., Hill, R. B., Thompson, C. B., and Colombini, M. (2001). Bcl-xL promotes the open configuration of the voltage-dependent anion channel and metabolite passage through the outer mitochondrial membrane. *J. Biol. Chem.* 276, 19414–19419. doi: 10.1074/jbc.m101590200

Vögtle, F. N., Burkhart, J. M., Rao, S., Gerbeth, C., Hinrichs, J., Martinou, J. C., et al. (2012). Intermembrane space proteome of yeast mitochondria. *Mol. Cell. Proteomics* 11, 1840–1852. doi: 10.1074/mcp.M112.021105

Walker, S., Ullman, O., and Stultz, C. M. (2012). Using intramolecular disulfide bonds in tau protein to deduce structural features of aggregation-resistant conformations. *J. Biol. Chem.* 287, 9591–9600. doi: 10.1074/jbc.M111.336107

Wallace, D. C., Fan, W., and Procaccio, V. (2010). Mitochondrial energetics and therapeutics. *Annu. Rev. Pathol.* 5, 297–348. doi: 10.1146/annurev.pathol.4.110807.092314

Wan, J., Roth, A. F., Bailey, A. O., and Davis, N. G. (2007). Palmitoylated proteins: purification and identification. *Nat. Protoc.* 2, 1573–1584. doi: 10.1038/nprot.2007.225

Wang, Y., Peterson, S., and Loring, J. (2014). Protein post-translational modifications and regulation of pluripotency in human stem cells. *Cell Res.* 24, 143–160. doi: 10.1038/cr.2013.151

Weckbecker, D., Longen, S., Riemer, J., and Herrmann, J. M. (2012). Atp23 biogenesis reveals a chaperone-like folding activity of Mia40 in the IMS of mitochondria. *EMBO J.* 31, 4348–4358. doi: 10.1038/emboj.2012.263

Wei, P. C., Hsieh, Y. H., Su, M. I., Jiang, X., Hsu, P. H., Lo, W. T., et al. (2012). Loss of the oxidative stress sensor NPGPx compromises GRP78 chaperone activity and induces systemic disease. *Mol. Cell* 48, 747–759. doi: 10.1016/j.molcel.2012.10.007

Wu, C., Dai, H., Yan, L., Liu, T., Cui, C., Chen, T., et al. (2017). Sulfonation of the resolving cysteine in human peroxiredoxin 1: a comprehensive analysis by mass spectrometry. *Free Radic. Biol. Med.* 108, 785–792. doi: 10.1016/j.freeradbiomed.2017.04.341

Xiong, Y., Uys, J. D., Tew, K. D., and Townsend, D. M. (2011). S-Glutathionylation: from molecular mechanisms to health. *Antioxid. Redox Signal.* 15, 233–270. doi: 10.1089/ars.2010.3540

Xu, X., Decker, W., Sampson, M. J., Craigen, W. J., and Colombini, M. (1999). Mouse VDAC isoforms expressed in yeast: channel properties and their roles in mitochondrial outer membrane permeability. *J. Membr. Biol.* 170, 89–102. doi: 10.1007/s002329900540

Yamamoto, T., Yamada, A., Watanabe, M., Yoshimura, Y., Yamazaki, N., Yoshimura, Y., et al. (2006). VDAC1, having a shorter N-terminus than VDAC2 but showing the same migration in an SDS-polyacrylamide gel, is the predominant form expressed in mitochondria of various tissues. *J. Proteome Res.* 5, 3336–3344. doi: 10.1021/pr060291w

Yang, W., Di Vizio, D., Kirchner, M., Steen, H., and Freeman, M. R. (2010). Proteome scale characterization of human *S*-acylated proteins in lipid raft-enriched and non-raft membranes. *Mol. Cell. Proteomics* 9, 54–70. doi: 10.1074/mcp.M800448-MCP200

Young, M. J., Bay, D. C., Hausner, G., and Court, D. A. (2007). The evolutionary history of mitochondrial porins. *BMC Evol. Biol.* 7:31. doi: 10.1186/1471-2148-7-31

Zhang, D., Du, J., Tang, C., Huang, Y., and Jin, H. (2017). H2S-induced sulfhydration: biological function and detection methodology. *Front. Pharmacol.* 8:608. doi: 10.3389/fphar.2017.00608

Zhang, E., Al-Amily, I. M., Mohammed, S., Luan, C., Asplund, O., Ahmed, M., et al. (2019). Preserving insulin secretion in diabetes by inhibiting VDAC1 overexpression and surface translocation in β cells. *Cell Metab.* 29, 64–77. doi: 10.1016/j.cmet.2018.09.008

Zhao, Q., Yu, J., and Tan, L. (2015). S-Nitrosylation in Alzheimer's disease. *Mol. Neurobiol.* 51, 268–280. doi: 10.1007/s12035-014-8672-2

Zhu, C., Tian, L., Yang, H., Chen, P., Li, Y., and Liu, Y. (2019). Mitochondrial outer membrane voltage-dependent anion channel is involved in renal dysfunction in a spontaneously hypertensive rat carrying transfer RNA mutations. *Eur. J. Pharm.* 865:172622. doi: 10.1016/j.ejphar.2019.172622

Zhuang, J., Wang, P. Y., Huang, X., Chen, X., Kang, J. G., and Hwang, P. M. (2013). Mitochondrial disulfide relay mediates translocation of p53 and partitions its subcellular activity. *Proc. Natl. Acad. Sci. U.S.A.* 110, 17356–17361. doi: 10.1073/pnas.1310908110

Conflict of Interest: The authors declare that the research was conducted in the absence of any commercial or financial relationships that could be construed as a potential conflict of interest.

7. Unpublished data

(Tables S and Figures S in Appendix)

7.1 Identification of succination in human VDAC isoforms

Human VDAC isoforms were prepared as reported in the section ”Materials and Methods” of “Article 2”. Also liquid chromatography and tandem mass spectrometry (LC-MS/MS) analysis were performed as in the previous work. In Database search, the cysteine succination was included in the variable modifications.

The regions not identified in hVDAC2 and hVDAC3 through mass spectrometry analysis (see Article 2) do not containe cysteine residues and therefore, spectral data have not been analyzed for the presence of selenocysteine residues. Instead, spectral data were analyzed in order to detect the occurrence of cysteine succination. Succinated cysteines were not found in hVDAC1 and hVDAC2 whereas in hVDAC3 Cys 8 was found to be succinated (Table S1, Figure S1) in considerable amount (the ratio Cys Succinat/Cys normal is about 0.2) (Table 2) as Cys 8 in rVDAC3.

Table 2. Comparison of the absolute intensities of molecular ions of succinated peptides found in the analysis of hVDAC3 reduced with DTT, carboxyamidomethylated and digested in-solution.

Peptide	Position in the sequence	Measured monoisotopic m/z	Absolute intensity	Ratio Succinat/Norm
*<u>***C**</u>NTPTY<u>**C**</u>DLGK	2-12	715.2848 (+2)	$3.97 \cdot 10^5$	0.2
*<u>***C**</u>NTPTY<u>***C***</u>DLGK		685.7897 (+2)	$2.29 \cdot 10^6$	

*C: N-terminal acetylated; ***C***: cysteine carboxyamidomethylated; <u>**C**</u>: cysteine succinated.

7.2 Phosphorylation

Phosphorylation in rat VDAC isoform

The presence of Ser, Thr and Tyr residues in the phosphorylated form was verified in VDAC proteins extracted from rat liver mitochondria.

Rat VDAC isoforms were prepared as reported in the section "Article 1". Also liquid chromatography and tandem mass spectrometry (LC-MS/MS) analysis were performed as in the previous work. In Database search, the phosphorylations of serine, threonine, tyrosine were included in the variable modifications.

Phosphorylated residues were found in rVDAC1 and rVDAC2. In particular, in rVDAC1, Thr 19 was found to be phosphorylated (Table S2 and Figure S2) in a remarkable amount (the ratio Thr phosphorylated/Thr in normal form is 0.1) (Table 3), whereas Ser 101 and Ser 104 are phosphorylated (Table S2, Figures S3 and S4) in very low amount (Table 3).

In rVDAC2, Ser 116 is phosphorylated (Table S3 and Figure S5) with a ratio Ser phosphorylated/Ser in normal form of 0.2 (Table 4) whereas Tyr 130 (Table S3 and Figure S6) is predominantly present in the phosphorylated form (the ratio Tyr phosphorylated/Tyr in normal form is 2.5) (Table 4).

In rVDAC3 were not detected phosphorylated residues.

Table 3. Comparison of the absolute intensities of molecular ions of phosphorylated peptides found in the analysis of rVDAC1 reduced with DTT, carboxyamidomethylated and digested in-solution.

Peptide	Position in the sequence	Measured monoisotopic m/z	Absolute intensity	Ratio Phospho/Norm
DVF**T**KGYGFGLIK	16-28	762.8785 (+2)	$4.71 \cdot 10^5$	0.1
DVFTKGYGFGLIK		722.8958 (+2)	$4.16 \cdot 10^6$	
GLKLTFD**S**SFSPNTGKK	94-110	636.3152 (+3)	$1.60 \cdot 10^6$	0.04
GLKLTFDSSFSPNTGKK		913.9852(+2)	$3.63 \cdot 10^7$	
LTFDSSF**S**PNTGKK	97-110	804.8690 (+2)	$6.55 \cdot 10^5$	0.02
LTFDSSFSPNTGKK		764.8865 (+2)	$4.17 \cdot 10^7$	

T: threonine phosphorylated; **S**: serine phosphorylated.

Table 4. Comparison of the absolute intensities of molecular ions of phosphorylated peptides found in the analysis of rVDAC2 reduced with DTT, carboxyamidomethylated and digested in-solution.

Peptide	Position in the sequence	Measured monoisotopic m/z	Absolute intensity	Ratio Phospho/Norm
LTFDTTF**S**PNTGKK	109-122	818.8859 (+2)	$5.08 \cdot 10^4$	0.2
LTFDTTFSPNTGKK		778.9023 (+2)	$2.15 \cdot 10^5$	
IKSA**Y**KR	126-132	473.2534 (+2)	$1.17 \cdot 10^6$	2.5
IKSAYKR		433.2663 (+2)	$4.65 \cdot 10^5$	

S: serine phosphorylated**; Y**: tyrosine phosphorylated.

Phosphorylation in human VDAC isoform

The presence of Ser, Thr and Tyr residues in the phosphorylated form was verified also in VDAC proteins extracted from HAP1 cell mitochondria.

Human VDAC isoforms were prepared as reported in the section “Article 2”. Also liquid chromatography and tandem mass spectrometry (LC-MS/MS) analysis were performed as in the previous work. In Database search, the phosphorylations of serine, threonine, tyrosine were included in the variable modifications.

Phosphorylated residues were found in hVDAC1 and hVDAC2. In particular, in hVDAC1, Ser 104 residue was found to be phosphorylated (Table S4 and Figure S7) in low amount (Table 5); in hVDAC2 Ser 115 and Thr 118 residues are phosphorylated (Table S5 and Figures S8, S9) though in low amounts (Table 6).

In hVDAC3 were not detected phosphorylated residues.

Table 5. Comparison of the absolute intensities of molecular ions of phosphorylated peptides found in the analysis of hVDAC1 reduced with DTT, carboxyamidomethylated and digested in-solution.

Peptide	Position in the sequence	Measured monoisotopic *m/z*	Absolute intensity	Ratio Phospho/Norm
GLKLTFDSSF**S**PNTGKK	94-110	636.3153 (+3)	$8.78 \cdot 10^6$	0.02
GLKLTFDSSFSPNTGKK		609.6604 (+2)	$4.12 \cdot 10^8$	

S: serine phosphorylated.

Table 6. Comparison of the absolute intensities of molecular ions of phosphorylated peptides found in the analysis of hVDAC2 reduced with DTT, carboxyamidomethylated and digested in-solution.

Peptide	Position in the sequence	Measured monoisotopic *m/z*	Absolute intensity	Ratio Phospho/Norm
LTFDTTF**S**PNTGKK	108-121	818.8870 (+2)	$2.69 \cdot 10^4$	0.01
LTFDTTFSPNTGKK		519.6043 (+3)	$2.55 \cdot 10^6$	
LTFDTTFSPN**T**GKK	108-121	546.2587 (+3)	$3.15 \cdot 10^4$	0.01
LTFDTTFSPNTGKK		519.6043 (+3)	$2.55 \cdot 10^6$	

T: threonine phosphorylated; **S**: serine phosphorylated.

7.3. Possible significances of succination and phosphorylation in VDAC isoforms

There is only a very limited number of studies directed at PTMs of VDAC, including that of phosphorylation, by means mass spectrometry. A possible reason for the limited number of studies is that VDACs are highly hydrophobic integral OMM proteins and difficult to work with. The development of the new “in solution digestion” protocol coupled with the high resolution in mass spectrometry has permitted to overcome these difficulties.

The phosphorylated sites on rat and human VDAC isoforms and the candidate protein kinases involved are listed in Table 7. The identification of candidate protein kinases and the relative score was obtained using NetPhos 3.1 Server. This tool predicts Ser, Thr or Tyr phosphorylation sites in eukaryotic proteins using ensembles of neural networks. Both generic and kinase specific predictions are performer. In general the higher the score, the higher the confidence of the prediction and the higher the similarity to one or more of the phosphorylation sites. A score close to the threshold value of 0.500 indicates that the confidence for this site being a true phosphorylation site is quite low whereas a score close to 1.000 indicates a very likely phosphorylation site.

It is important to observe that some phosphorylation sites are conserved in rat and human VDAC isoforms. In particular Ser 104 residue is phosphorylated in rVDAC1 and hVDAC1 with a egual ratio (Ser phosphorylated/Ser in normal form) of about 0.02 (Tables 3 and 5). In VDAC2, Ser 116 of rat isoform and the corresponding Ser 115 in

human isoform are also present both in the phosphorylated and in normal form with the ratio of about 0.2 and 0.01, respectively (Tables 4 and 6). In rVDAC2, Tyr 130 residue is predominantly present in the phosphorylated form.

No phosphorylated residues were found in VDAC3. In rat instead, this isoform presents three Cys residues in the succinated form (Cys 8, Cys 36 and Cys 229) with one of them (Cys 8) in significant amount compared to the others (see Article 1). This PTM is conserved also in hVDAC3 where Cys 8 is succinated in a comparable amount to rVDAC3 (Table 2) (see Article 1). Whereas in rVDAC2 only Cys residue (Cys 48) is succinated in low amount (see Article 1).

Table 7. Phosphorylation sites of rat and human VDAC isoforms and candidate protein kinases. The scores that indicate the confidence for these sites are reported.

Isoform	Phosphorylation site	Candidate protein kinases	Score
rVDAC1	Thr 19	**PKC**	0.570
	Ser 101	**PKA**	0.462
	Ser 104	**Unspec** **CKI** **p38MAPK**	0.970 0.616 0.538
rVDAC2	Ser116	**CKI** **Unspec** **p38MAPK**	0.606 0.594 0.531
	Tyr 130	**INSR**	0.483
hVDAC1	Ser 104	**Unspec** **CKI** **p38MAPK**	0.970 0.616 0.538
hVDAC2	Ser 115	**CKI** **Unspec** **p38MAPK**	0.606 0.594 0.531
	Thr 118	**PKC** **Unspec** **CKI**	0.896 0.826 0.558

PKC: Protein Kinase C; **PKA**: Protein Kinase A; **Unspec**: Unspecific Kinase; **p38MAPK**: p38 Mitogen-Activated Protein Kinase; **INSR**: Insulin Receptor Tyrosine Kinase; **PKI**: Protein Kinase Inhibitor.

Generally, in VDAC proteins high levels of phosphorylation are associated with degradation and pro-apoptotic pathways[93,111]. At variance with the proposed pro-apoptotic feature of VDAC phosphorylation are findings in studies on mammalian NIMA-related protein kinase (Nek1) that appears to protect against cell death. The

authors of these studies have found that protection against apoptosis is contingent on VDAC1 phosphorylation on Ser residue 193, which is easily accessible from the cytosolic side of the OMM. Indeed Nek1 is localized predominantly in the cytosol while a significant fraction is found associated with mitochondria. Furthermore, the direct physical interaction between Nek1 and VDAC1 was demonstrated[112]. However, in my mass data, I have not found Ser 193 residue in phosphorylated form neither in rat nor in human isoforms.

In addition to the aforementioned studies, another work demonstrated, *in vitro,* that VDAC phosphorylation, in particular by cAMP dependent protein kinase (PKA) and Glycogen synthase kinase-3β (GSK3β), is an important determinant of its interaction with dimeric tubulin[113]. Recently, tubulin was found to be a uniquely potent regulator of VDACs because it induces reversible blockage of these channels.

Phosphorylation of VDACs has been reported to occur in pathological conditions. Indeed, several studies suggest that VDAC1 phosphorylation is involved in the genesis of apoptosis in brain of Alzheimer disease and Down syndrome patients[114].

The specific role of succination in VDACs is not known. However, this PTM could be associated with a general disregulation of mitochondrial metabolism due to fumarate accumulation.

7.4 Disulfide Bridges of rat VDAC3 isoform

Preparation of VDACs enriched fractions from rat liver mitochondria

Rat liver mitochondria were prepared as reported in the section "Materials and Methods" of "Article 1". All subsequent steps were carried out under controlled pH conditions, in the range between 6.5 and 7 (slightly acidic or at most neutral). Indeed, in a pH range 7.5-8.5, undesirable disulfide reshuffling can occur during sample handling (nota). . 5 mg of intact mitochondria have been washed in 10 mM Tris-HCl, 1 mM EDTA at pH 6.5 to eliminate any residue of the extraction buffer. The suspension was then centrifuged for 30 minutes at 10,000 x g at 4 °C, and at the end, after removing the supernatant, the pellet, containing the intact mitochondria, were lysed in buffer A (10 mM Tris-HCl, 1 mM EDTA, 3% Triton X-100 at pH 6.5) in ratio 5:1 (mitochondria mg/buffer volume mL) for 30 minutes on ice and then centrifuged at 17,400 x g for 30 minutes at 4 °C. The supernatant containing mitochondrial proteins was subsequently loaded onto a homemade glass column 5 x 80 mm, packed with 0.6 g of dry HTP (Bio-Gel, Biorad). Column was eluted with buffer A at 4 °C and fractions of 500 µL were collected and tested for protein content by a fluorometer assay (Invitrogen Qubit^{TM} Protein Assay Kit, ThermoFisher Scientific, Milan, Italy). Fractions containing proteins were pooled and dried under vacuum until 100 µL. The HTP eluate, enriched in VDAC proteins, was purified from non-protein contaminating molecules with the PlusOne 2-D Clean-Up Kit (GE Healthcare Life Sciences, Milan, Italy) according to the manufacturer's instructions.

In-solution digestion protocol of the HTP eluate

The desalted protein pellet obtained was suspended in 100 µL of 50 mM ammonium bicarbonate pH 7.0. Protein amount was determined to be 30 µg using a fluorometer assay. This solution containing hydrophobic proteins was divided in two aliquots each of 50 µL . One aliquot was directly alkylated by addition of iodoacetamide for blocking free cysteines and then in-solution digested. Another aliquot was incubated at 4°C in ice for 15 minutes. Next, 50 µL of 0.2% RapiGest SF (Waters, Milan, Italy), in 50 mM

ammonium bicarbonate pH 7.0, were added and the sample was kept at 4°C for 30 minutes. Subsequently also this aliquot was alkylated with iodoacetamide and in-solution digested. Alkylations were performed in 50 mM ammonium bicarbonate pH 7.0 by addition of iodoacetamide at the 2:1 M ratio over an average number of disulfide bridges equal to 10 for 1 h in the dark at 25 °C. Digestions were carried out using modified porcine trypsin in 50 mM ammonium bicarbonate pH 7.0 at an enzyme-substrate ratio of 1:50, at 37 °C for 4 h. The protein digests were then dried under vacuum, dissolved in 25 µL of 5% FA, diluted 1:2 (sample with RapiGest SF) or 1:5 (sample directly alkylated) and analyzed by nano UHPLC/High Resolution ESI-MS/MS:

Liquid chromatography, tandem mass spectrometry (LC–MS/MS) analysis and database search

Liquid chromatography and tandem mass spectrometry (LC-MS/MS) analysis were performed as in the previous work (see Article 1). LC–MS/MS data were processed by PEAKS software (v. 8.5, Bioinformatics Solutions Inc., Waterloo, ON Canada). Data were searched against the SwissProt database (release July 2016, containing 550,552 entries) using the MASCOT algorithm (Matrix Science, London, UK, version 2.5.1). The search was performed against *Rattus* sequences database (7,961 sequences). Full tryptic peptides with a maximum of 3 missed cleavage sites were subjected to bioinformatics search. Cysteine carboxyamidomethylation was set as fixed modification, whereas acetylation of protein N-terminal, trioxidation of cysteine, oxidation of methionine and transformation of N-terminal glutamine and N-terminal glutamic acid residue in the pyroglutamic acid form were included as variable modifications. The precursor mass tolerance threshold was 10 ppm and the max fragment mass error was set to 0.6 Da. Peptide spectral matches (PSM) were validated using Target Decoy PSM Validator node based onq-values at a 0.1% FDR.

Results

In rVDAC3 isoform the N-terminal segment was found with Cys 2 acetylated and a intra-peptide disulfide bridge between Cys 2 and Cys 8 (Table 8, Figure S10).

After calculating the m/z monoisotopic value of the peptide containing the disulfide bridge, the full scan spectrum (in high resolution) and the corresponding MS/MS spectrum (in low resolution) were searched manually by analyzing the raw data using the Xcalibur v.3.0.63 software.

Table 8. Peptides linked by disulfide bridge found in rVDAC3 tryptic digest after carboxyamidomethylation.

In the Table the respective retention time, experimentally measured and calculated monoisotopic m/z of the molecular ions, the position in the sequence, the peptide sequences and the absolute intensity of modified fragments present in the tryptic digest of carboxyamidomethylated rVDACs are reported. The sequence was confirmed by MS/MS.

Rt (min)	Monoisotopic m/z		Position in the sequence	Peptide sequences	Absolute intensity
	Measured	Calculated			
48.99	614. 2551 (+2)	614. 2547	2-12	*<u>**C**</u>STPTY<u>**C**</u>DLGK	$3.94 \cdot 10^5$

*C: N-terminal acetylated; <u>**C**</u>: cysteine residues linked by disulfide bridge.

Discussion

The presence of the disulfide bridge between Cys 2 and Cys 8 at the N-terminal of VDAC3 isoform had already been highlighted through the use of a digestion protocol under alkaline pH condition[49]. But in this condition, the presence of free sulfhydryl groups can induce undesired sulfhydryl-disulfide reshuffling[57]. Conversely, under neutral or acidic pH conditions. In fact, the alkylation with iodoacetamide and digestion with trypsin are reactions that occur optimally at pH 8.3. Also the solubilization with RapiGest SF detergent requires the same pH. The use of iodoacetamide is fundamental because, under physiological condition, it reacts with free Cys residues not engaged in disulfide bonds and thus present in the reduced form. Therefore carboxyamidomethylated Cys residues will not be taken into consideration for the research of disulfide bridges.

Disulfide reshuffling can be reduced by lowering the pH to 6.0 to 7.0 during tryptic digestion and using the enzyme pepsin under acidic conditions for proteolytic

digestion. Unfortunately, trypsin becomes less efficient and less specific at more acidic pH, and pepsin, which has an optimal pH range of 1-3, tremendously increases the complexity of both protein digests and data analysis.

In general, the “in solution digestion” protocol for the study of disulfide bridges has been developed using as a model system the chicken lysozyme, a small protein of 129 amino acids whose three-dimensional structure, with four disulfide bridges is well known. Although using this "simple" model protein, digestion with pepsin has produced a very complex peptide mixture, making it impossible to search for disulfide bridges under these conditions.

After several attempts we found the right conditions (listed above) to carry out digestion with trypsin in non-alkaline pH conditions. Also alkylation with iodoacetamide was carried out under the same conditions whereas the addition of RapiGest SF at pH 7 does not seem to improve VDAC proteins solubility. Probably the RapiGest SF functions exclusively in alkaline conditions of pH.

The VDAC3 disulfide bridge between Cys 2 and Cys 8 was simulated by molecular dynamics (MD) to investigate the functional consequences of the bond[52]. In the MD simulation, the bend induced by the covalent disulfide bond causes the whole N-terminal to stay closely packed to the wall of the barrel (strands 3-9). The N-tail bending determines a certain level of obstruction of the channel. Assuming that this model is coherent with the physiological state of the pore, the ion current in the S-S bridged VDAC3 should be only slightly lower with respect to the form with the same cysteines in reduced state.

8. General discussion

8.1 Development of a new “in solution digestion” protocol

The characterization of VDACs presents challenging issues due to an extremely hydrophobicity, low solubility, the difficulty of isolating each single isoform and separating them from other mitochondrial protein of similar hydrophobicity. Consequently, it is necessary to analyze them as components of a relatively complex mixture. However, high resolution mass spectrometry provided a powerful tool to overcome these difficulties.

The idea of studying the oxidation states of sulfur amino acids was born from the observation of Cys residues position in VDAC3 models (figure 8). Most of these residues are located in loops that are oriented towards the mitochondrial IMS, a highly oxidizing environment.

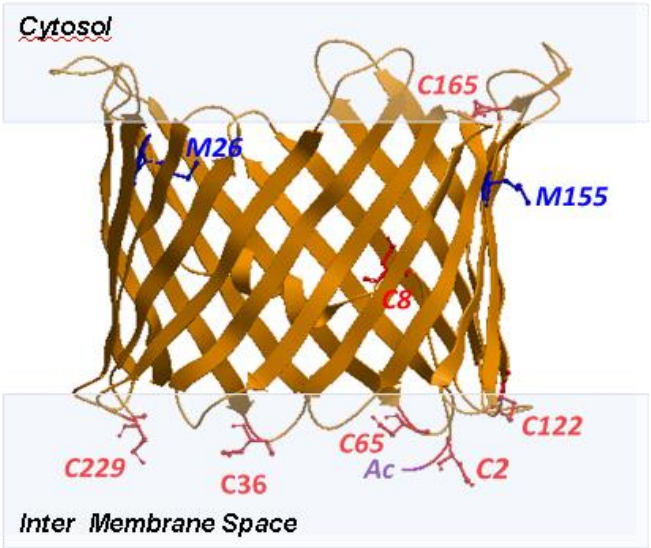

Figure 8. A structural model of human VDAC3. Side view of rat VDAC3 where the cysteine and methionine positions have been indicated. The structure was predicted by homology modelling, using mouse VDAC1 structure (pdb: 3EMN) as a template.

Rat liver VDAC3 was the first isoform we characterized by mass spectrometry in an attempt to understand its different behavior compared to the other two isoforms. VDAC3 is still poorly understood both in its structure and in its function. Indeed, it has not yet been crystallized or analyzed by NMR and only three dimensional models, obtained by homology structures on the other isoforms, are available. Moreover,

VDAC3 is the least abundant among the isoforms, as determined in expression level analysis by Real-Time PCR. In addition, while VDAC1 and 2 are mainly co-localized within the same area of the OMM, VDAC3 is distributed all over the surface of the mitochondrion and it is more abundant only in some tissues, such as celebral cortex, liver, heart, testis and, togheter with VDAC2, in spermatozoa. From a functional point, VDAC3 is not able to complement the *Δpor1* yeast growth defect on not-fermentable carbon sources at 37 °C and has proved to be inserted with difficulty in artificial membranes or liposomes and only in particular conditions (such as in the presence of DTT). Many small channels with a very low conductance are detected upon insertion of VDAC3 in the membrane. The starting hypothesis was that the oxidation state of the cysteine residues could modulate its insertion in the membrane and explain the apparent functional anomalies of isoform 3, perhaps opening the way to new interpretations that could define a specific function of this isoform particularly in the control of damage induced by oxidative stress (VDAC3 as a sort of damage sensor).

The first proteomic approach used for the study of VDAC3, extracted from rat liver mitochondria, was the bottom-up approach[51]. Mitochondria were extracted in normal conditions from tissues and subsequently lysated with 3% Triton X-100 at pH 7.0. The VDAC proteins were purified by HTP chromatography, technique that allows to obtain a VDAC isoforms enriched fraction but containing also other mitochondria hydrophobic proteins[115]. The eluates of several chromatographic columns were combined and protein fractions were precipitated with 9 volumes of cold acetone for 30 minutes. The protein pellet, recovered by centrifugation, was solubilized in SDS sample buffer without reducing agents and loaded on a polyacrylamide gel (SDS-PAGE). Therefore, to try to obtain a starting sample that was the more "purest" possible, several tests have been carried out, in order to improve the procedures of purification and separation by electrophoresis using precast gels with different content of acrylamide (12% and 17.5%). The definition of an adequate and effective method allowing the separation of the three VDAC isoforms, in itself would be an important milestone for the study of these proteins. Furthermore, the electrophoretic mobility of the three isoforms is slightly different and this could also be related to the presence of particular post-translational modifications.

After SDS-PAGE separation of the proteins, the bands were manually cut in small pieces and subjected to reduction whit DTT and alkylation with IAA, after having undergone several washing cycles alternatively with water and ACN. Finally, in gel-digestions, using trypsin or chymotrypsin, were performed.

In gel-digestion procedure has some disadvantages. First, larger peptides can get trapped between the gel meshes and lost during the extraction phase of the peptides from the gel. Second, the electrophoresis procedure itself could (due to possible over heating linked to the voltage applied and to the presence of residual quantities of the catalysts used for the polyacrylamide polymerization reaction) damage the samples and alter the redox state of the sulfur amino acids. In particular, we have shown in our works[51] that heating could slightly vary the redox state of Met residues while it has no effect on over oxidations of Cys to sulfonic acid. Furthermore, electrophoresis requires a greater quantity of sample and the use of dyes, such as Comassie Blue, and detergent, such as SDS, that could invalidate subsequent analyses because these compounds are difficult to eliminate even after successive and repeated washing with water and ACN. Furthermore, the lack of a further purification step, after the precipitation with acetone, determines the presence of intense signals in the chromatograms relating to Triton X-100 detergent. On the other hand, the advantage of electrophoresis is to work with gel-bands containing a reduced number of proteins and VDAC isoforms are particularly concentrated only in some bands at a molecular weight of about 30 KDa, based on the presence or absence of a reducing reagent during the run. Afterwards, to exclude the possibility that any unspecific and undesired oxidation could happen during the purification protocol, reduction and alkylation reactions of proteins were carried out before VDACs purification from the mitochondria. Moreover, the precipitation with acetone, in subsequent experiments, was eliminated to avoid interference with the subsequent analysis in mass spectrometry.

The 2-D-electrophoresis could have been a useful alternative to 1-D-electrophoresis to improve the separation of VDAC isoforms but its utilization presented other problems. Typical buffers for isoelectric focusing such as SDS, urea, thiourea and CHAPS can interfere with mass spectrometry analysis. In addition, 2-DE is a technique requiring

large quantities of sample, long analysis times (up to 24 hours or more per run) and higher applied voltages (15,000 V) compared to 1-DE analysis[116,117].

However, despite all the problems discussed above, the bottom-up approach has allowed to obtain for rat VDAC3 isoform, a good sequence coverage and to detect several peptide containing cysteine and methionine residues in the oxidized form[51].

An improvement of the VDAC3 results in mass spectrometric analysis was obtained following the introduction of the gel-free Shotgun proteomic approach or "MuDPIT". This approach allows to avoid electrophoresis separation of the samples because all proteins present in the HTP eluate are digested, producing a very complex peptide mixture. In this case, the experimental procedure is easier but the processing of the data is more difficult for the complexity of the system. The resulting proteolytic mixture can be subsequently analyzed by UHLC/High-Resolution mass spectrometry.

The reduction, alkylation and digestion reactions occur by adding, in order and distributed over time, the reagents (DTT, IAA and protease) to the sample dissolved in an appropriate buffer at pH 8.0.

This same proteomic approach has been used for mass spectrometry analysis of VDAC1 and VDAC2 isoforms from rat liver mitochondria (see Article 1). The introduction of other important procedures, from sample preparation to final analysis, has allowed us to develop a new "in solution-digestion" protocol.

In particular, the improvement of the results is due to the introduction of a purification step carried out on HTP chromatographic eluate by using the PlusOne 2D-Clean Up kit and a solubilization phase using RapiGest SF surfactant.

Kit reagents quantitatively precipitate proteins while leaving interfering substances (detergents, salts, lipids, phenolics, and nucleic acids) in solution, and, thanks the presence of a surfactant, improves the solubility of hydrophobic proteins and therefore the in solution-digestion process. In particular, RapiGest SF helps solubilize proteins making them more susceptible to enzymatic cleavage without significantly inhibiting enzyme activity and is heat stable for higher temperature digestions. Unlike other commonly used denaturants (e.g., SDS or Urea), RapiGest SF does not modify peptides or suppress endoprotease activity. Moreover, the RapiGest SF surfactant is compatible with enzymes such as trypsin or chymotrypsin and does not influence subsequent analysis because can be easily removed by treating the sample with FA. The Shotgun

proteomic approach, the development of a particular in “solution-digestion” protocol and the high resolution mass spectrometry analysis have permitted to overcome the difficulties associated with the analysis of membrane proteins and bypass the SDS-PAGE with its potential unwanted oxidations. The experimental utilized methods have allowed to investigate the primary structures and oxidation levels of peptides containing sulfur residues in rat VDAC1 and 2. Subsequently, by means of this same approach, this structural characterization was extended to human VDACs extracted from HAP1 cells (see Article 2).

Finally, the improvement of a proteomic analysis is associated with the availability of ever more performing software for data analysis. LC-MS/MS data of rVDAC3 were processed by Proteome Discoverer v. 1.4.1.14 that uses the MASCOT algorithm whereas LC-MS/MS data of rVDAC1/2 and hVDACs were processed using both Proteome Discoverer v. 1.4.1.14 and PEAKS software v. 8.5 that in addition to its own algorithm allows to perform the data analysis by the MASCOT algorithm using its *inChorus* function[101].

Using this new “in solution-digestion” protocol associated to UHLC/High Resolution mass spectrometry, a wide information about rat and human VDAC isoforms was obtained. Total sequence coverage of rat and human VDAC1 and the almost complete sequences of rat and human VDAC2 and VDAC3 were also obtained. Unfortunately, a short sequence stretch containing one genetically encoded cysteine was not covered both in rVDAC2 and in rVDAC3 whereas the sequences not identified in hVDAC2 and in hVDAC3 do not contain Cys and Met residues but correspond to small tryptic or chymotryptic peptides or even single amino acids, which cannot be detected in LC/MS analysis.

8.2 Possible significances of Cys-Ox PTMs in VDAC isoforms

The careful examination of the position of Cys residues in structures and predictive models of rat and human VDAC isoforms shows that the oxidation of such residues follows a specific targeting: a group of Cys is typically always found in a reduced form; another group is detected in a variable oxidation state; a third group was found in the

irreversible, over-oxidized form of sulfonic acid. This pattern is conserved among the mammalian species under study. These groups of Cys residues could have specific roles in the function of VDAC isoforms: the reduced group, exposed to the IMS or residing inside the channel, could be even utilized to form disulfide bridges with the aim of modulating the useful diameter for channelling water soluble molecules; the girdle of Cys residues located in the turns connecting the β-strands and exposed again to the IMS (in VDAC2 and VDAC3 isoforms) presents variable oxidative states of the sulphur group, thus can work as an oxidation buffer located on the inner surface of the OMM with the function to counteract excess of ROS produced by the OXPHOS; the third group is that of the heavily, irreversibly oxidized state.

This last group is the less abundant but the residue always found in such a chemical state is present only in VDAC1 and VDAC2, not in VDAC3, and it is exposed to the hydrophobic layer of the OMM. This is an apparent paradox, since such a bulky, hydrophilic moiety should not stay there: unless it has a function as a spot for structure intended to docking the OMM.

Thus the pattern of cysteines oxidation could be the key to understand the evolution of the three VDAC isoforms: VDAC1 has only two Cys (both human and rat), one of them in sulfonic state (in human isoform), and exposed to the hydrophobic layer of the OMM; human VDAC2 has 9 Cys (11 in rat isoform), in the three categories we described above, thus it has also the over-oxidized one; human VDAC3 has again 6 Cys (7 in rat), but in the human isoform lacks the category of over-oxidized one.

In this regard, it seems plausible the hypothesis[34], already mentioned in the introduction, where the authors proposed that the transient formation of a disulfide bond between VDAC3 cysteine residues located in the N-terminal region with those at the bottom of the pore could change its permeability,albeit the nature of such hindrance to the conductance is not clear yet. Molecular dynamic simulations shave shown that disulfide bonds between the closest cysteine residues available did not affect the pore diameter, but rather changed the electrical charge disposition on the protein surface[24,52].

Interesting, the insertion of negative charges due to SO_3H formation, can provoke electric repulsions inside the chain or toward phospholipids, and next modify the protein conformation.

Some authors suggested that these conformational changes can initiate protein incorporation into Mitochondria-Derived Vesicles (MDVs), subsequently targeted to lysosomes. The production of MDVs is a process stimulated by the mitochondrial stress[118]. In a recent work where the MDV pathway has been dissected and characterized, it was demonstrated that MDVs are enriched in oxidized proteins derived from mitochondria and in particular from the outer membrane. VDAC1 was found among the proteins in MDVs[119]. Unfortunately, the oxidation state of cysteines was not investigated nor the presence of VDAC3.

Post-translational removal of N-terminal Met leaves VDAC3 Cys 2 as the first amino acid. All proteomic analysis revealed this residue as completely acetylated, a PTM that, beside significantly influencing protein stability, activity, folding, and localization triggers the degradation of specific proteins by the Ac/N-degron pathway. The functions of this branch of the N-End Rule pathway include quality control and the regulation of input protein stoichiometries *in vivo*[120]. Any dysregulation of Nt-acetylation, that protects cysteine against irreversible oxidation, results in severe pathological conditions such as cancers, X-linked genetic disorders, hypertension and neurodegenerative diseases. Overall, it is tempting to speculate that the quantitative extent of VDAC oxidative modifications on the mitochondrial surface can be used as a signal of oxidation load, allowing the monitoring of the ROS amounts in each mitochondrion or mitochondrial network section.

9. Conclusions and future perspectives

The results of the high resolution mass spectrometry analisys demonstrate that the mitochondrial VDAC proteins, in physiological state, contain methionines both in normal form and oxidized to methionine sulfoxide. Furthermore, Cys residues are present in different oxidation state from the reduced state to the irreversible sulfonic acid state. The structural features elucidated by the present work may be helpful for a better understanding of the functional role of VDAC isoforms in the control of OMM permeability, in the response to the ROS oxidative pressure on IMS and in general of the mitochondrial quality control.

In the future I want to study the oxidation pattern of sulfur amino acids in neurodegenerative disease model systems (such as NSC-34 SOD1 G93A cells, model of Amyotrophic Lateral Sclerosis) and other Ox-PTMs such as persulfhydration or S-nitrosylation that are induced by the presence of the gaseous signaling molecules, hydrogen sulfide and nitric oxide, respectively.

Finally, the quest for the complete identification of disulfide bridges, through the correct interpretation of the full scan and MS/MS spectra, will be the next, highly challenging from the technical point of view, goal of this research.

10. List of figures

Figure S10. MS/MS spectrum of the doubly charged molecular ion at m/z 614.2551 (calculated 614.2547) of the N-terminal acetylated tryptic peptide of VDAC3 from *Rattus norvegicus* containing the disulfide bridge between Cys residues 2 and 8. The inset shows the full scan mass spectrum of molecular ion.

11. List of tables

12. List of Publications

1. R. Saletti, S. Reina, M. G. G. Pittalà, R. Belfiore, V. Cunsolo, A. Messina, V. De Pinto, S. Foti. High resolution mass spectrometry characterization of the oxidation pattern of methionine and cysteine residues in rat liver mitochondria voltage-dependent anion selective channel 3 (VDAC3). *Biochimica et Biophysica Acta, Biomembranes* (2016), 1859, 301-311.

2. R. Saletti, S. Reina, M. G. G. Pittalà, A. Magrì, V. Cunsolo, S. Foti, V. De Pinto. Post-translational modifications of VDAC1 and VDAC2 cysteines from rat liver mitochondria. *Biochimica et Biophysica Acta, Bioenergetics* (2018), 1859, 806-816.

3. M. G. G. Pittalà, R. Saletti, S. Reina, V. Cunsolo, V. De Pinto, S. Foti. A high resolution mass spectrometry study reveals the potential of disulfide formation in human mitochondrial Voltage-Dependent Anion Selective Channels isoforms (hVDACs). *International Journal of Molecular Sciences* (2020), 21, 1468.

4. S. Reina, M. G. G. Pittalà, V. De Pinto, S. Foti, R. Saletti. Cysteine oxidations in mitochondrial membrane proteins: the case of VDAC isoforms in mammals. *Frontiers*, *Cell and Developmental Biology* (2020), 8:397.

13. Conference contributions

1. S. Reina, R. Saletti, V. Cunsolo, R. Belfiore, M. G. G. Pittalà, S. Foti, V. De Pinto. OXIDATION STATES OF HUMAN RECOMBINANT AND RAT LIVER MITOCHONDRIA VDAC3 INVESTIGATED BY MASS SPECTROMETRY. 9thAnnual Congress of European Proteomics Association – EuPA, Milano 23-28 June 2015, Abstract book pag. 95.

2. M. G. G. Pittalà, S. Reina, R. Saletti, S. Foti, V. De Pinto. POST TRANSLATION MODIFICATIONS OF VDAC ISOFORMS SUGGEST A SPECIFIC ROLE OF THESE PROTEINS IN FUNCTIONAL OR REGULATORY ACTIVITIES OF MITOCHONDRIA. Emerging Concepts in Mitochondrial Biology, February, 4-8, 2018, Weizmann Institute of Science, Rehovot Israel, Abstract book pag. 87.

3. R. Saletti, S. Reina, M. G. G. Pittalà, A. Messina, V. Cunsolo, V. De Pinto, S. Foti. CARATTERIZZAZIONE DELLE MODIFICHE POST-TRADUZIONALI NELLE PROTEINE VDAC MEDIANTE SPETTROMETRIA DI MASSA AD ALTA RISOLUZIONE**.** Congresso Congiunto delle Sezioni Sicilia e Calabria SCI 2018, Catania 9-10 February 2018, Abstract book pag. 66.

4. M. G. G. Pittalà, R. Saletti, P. Risiglione, S. Cubisino, S. Foti, V. De Pinto. CHARACTERIZATION OF POST-TRANSLATION MODIFICATIONS OF VDAC ISOFORMS FROM RAT LIVER MITOCHONDRIA BY HIGH RESOLUTION MASS SPECTROMETRY. Bio-energetics, Metabolism and Nutrition: from molecules to systems, Bologna 25-26 June 2018, Abstract book pag. 12.

5. R. Saletti, M. G. G. Pittalà, P. Risiglione, V. Cunsolo, V. De Pinto, S. Foti. HIGH RESOLUTION MASS SPECTROMETRY CHARACTERIZATION OF THE OXIDATION PATTERN OF METHIONINE AND CYSTEINE RESIDUES IN HUMAN MITOCHONDRIA VOLTAGE-DEPENDENT ANION SELECTIVE CHANNEL ISOFORMS. XXII International Mass Spectrometry Conference, Firenze 26-31 August 2018, Abstract book pag. 662.

6. M. G. G. Pittalà, R. Saletti, P. Risiglione, S. Foti, V. De Pinto. POST-TRANSLATIONAL MODIFICATIONS OF VOLTAGE DEPENDENT ANION SELECTIVE CHANNEL (VDAC) ISOFORMS FROM RAT LIVER MITOCHONDRIA. XV FISV Congress, Roma 18-21 September 2018, Abstract book pag. 153.

7. M. G. G. Pittalà, R. Saletti, S. Reina, V. Cunsolo, V. De Pinto, S. Foti. OXIDATION STATE OF METHIONINE AND CYSTEINE RESIDUES IN HUMAN MITOCHONDRIAL VOLTAGE-DEPENDENT ANION SELECTIVE CHANNEL ISOFORMS (hVDACs) INVESTIGATED BY HIGH RESOLUTION MASS SPECTROMETRY. GIBB INTERNATIONAL Congress, Vieste 13-15 June 2019, Abstract book pag. 18.

8. M. G. G. Pittalà, A. Magrì, L. Mela, P. Risiglione, S. Cubisino, A. Messina. POST-TRANSLATIONAL ANALYSIS OF VDAC1 REVEALED A MARGINAL ROLE OF KINASE NEK1 IN THE PHOSPHORYLATION OF THE PORE. GIBB INTERNATIONAL Congress, Vieste 13-15 June 2019, Abstract book pag. 35.

9. M. G. G. Pittalà, R. Saletti, S. Reina, V. Cunsolo, V. De Pinto, S. Foti. HIGH RESOLUTION MASS SPECTROMETRIC CHARACTERIZATION OF THE METHIONINE AND CYSTEINE RESIDUES OXIDATION STATE IN HUMAN MITOCHONDRIAL VOLTAGE –DEPENDENT ANION SELECTIVE CHANNEL ISOFORMS (hVDACs). ItPA and HPS International XIV Congress, Catanzaro 25-27 June 2019, Abstract book pag. 87.

10. M. G. G. Pittalà, R. Saletti, S. Reina, V. Cunsolo, V. De Pinto, S. Foti. CHARACTERIZATION OF THE OXIDATION STATE OF METHIONINE AND CYSTEINE RESIDUES IN HUMAN MITOCHONDRIA VOLTAGE-DEPENDENT ANION CHANNEL ISOFORMS BY HIGH RESOLUTION MASS SPECTROMETRY. Membrane proteins: structure, function and regulation, Cosenza, 27-28 June 2019, Abstract book pag. 23.

11. M. G. G. Pittalà, R. Saletti, S. Reina, V. Cunsolo, V. De Pinto, S. Foti. HUMAN MITOCHONDRIAL VOLTAGE-DEPENDENT ANION CHANNELSCARRY OXIDIZED AND OVER-OXIDIZED METHIONINE AND CYSTEINE RESIDUES AS DETECTED BY HIGH RESOLUTION MASS SPECTROMETRY. 25th International symposium on glycoconjugates, Milano, 25-31 August 2019, Abstract book pag. 360 (Glycoconjugate Journal, Volume 36, Number 4, August 2019, Page 360).

12. P. Risiglione, M. G. G. Pittalà, S. Cubisino, R. Saletti, S. Foti, V. De Pinto. VDAC2 AND VDAC3 HAVE A SIMILAR REDOX PATTERN OF CONSERVED CYSTEINE RESIDUES. SIB 2019 60th Congress, Lecce, 18-20 September 2019, Abstract book pag.138.

13. S. Conti Nibali, S. Reina, M. G. G. Pittalà, V. De Pinto. UNRAVELING THE FUNCTION OF VDAC3 CYSTEINE RESIDUES ON MITOCHONDRIAL ACTIVITY: *IN VITRO* AND *IN CELLULO* STUDIES. National Ph.D Meeting 2020, Salerno, 19-21 March 2020, Submitted.

14. Acknowledgments

The present work was performed thanks a collaboration between the Molecular Biology Laboratory leaded by Prof. Vito De Pinto and the Organic Mass Spectrometry Laboratory by Prof. Salvatore Foti.

I would like to thank all the people who contributed to the accomplishment of this thesis and supported me during this year. First of all, my tutor Prof. Vito De Pinto for giving me the opportunity to work on this project and for his continuous support and encouragement.

I would especially like to extend my sincere gratitude to Prof. Rosaria Saletti for her motivation and patience during my PhD. Her knowledge and continuos advice helped me in each moment of my research.

I thank Prof. Angela Messina for her advice and for giving me some of her passion for scientific research.

Moreover, I would like to thank Prof. Salvatore Foti for giving me the possibility to work in his laboratory and for his precious advice, suggestions and comments.

I would also like to thank the research group in the Laboratory of Molecular Biology (in particular Prof. Francesca Guarino, Dr Simona Reina, Dr Andrea Magrì, Dr Maria Carmela Di Rosa and all the other PhD colleagues) and the research group in the Laboratory of Organic Mass Spectrometry (Prof. Vincenzo Cunsolo, Dr Vera Muccilli, Dr Antonella Di Francesco, Dr Annamaria Cucina and Dr Valentina Giglio) for helping me in various stages of my work and for contributing to create a friendly and collaborative environment. Their support was essential in my reasearch.

I would like to thank Prof. Massimo Masserini and Prof. Francesca Re who hosted me for eight months in their laboratory at the Amypopharma, spin off in the University of Milano-Bicocca, and Prof. Francisco Wandosell Jurado who hosted me for six months in his laboratory at the Centre of Molecular Biology “Severo Ochoa”, University of Madrid.

I wish to thank Bionanotech research and innovation tower (BRIT) for the availability of the Orbitrap Fusion Tribrid (Q-OT-qIT) mass spectrometer (Thermo Fisher Scientific, Bremen, Germany).

15. Appendix

Table S1. Succinated peptides found in hVDAC3 tryptic digest after DTT reduction and carboxyamidomethylation.

In the Table the respective retention time, experimentally measured and calculated monoisotopic m/z of the molecular ions, the position in the sequence and the peptide sequence of modified fragments present in the tryptic digest of reduced and carboxyamidomethylated hVDAC3 are reported. The sequence was confirmed by MS/MS.

Frag. n.	Rt (min)	Monoisotopic m/z		Position in the sequence	Peptide sequence
		Measured	Calculated		
1	47.89	715.2848 (+2)	715.2844	2-12	*CNTPTY<u>C</u>DLGK

*C: N-terminal acetylated; ***C***: cysteine carboxyamidomethylated; **C**: cysteine succinated.

Table S2. Phosphorylated peptides found in rVDAC1 tryptic digest after DTT reduction and carboxyamidomethylation.

In the Table the respective retention time, experimentally measured and calculated monoisotopic m/z of the molecular ions, the position in the sequence and the peptide sequence of modified fragments present in the tryptic digest of reduced and carboxyamidomethylated rVDAC1 are reported. All sequences were confirmed by MS/MS.

Frag. n.	Rt (min)	Monoisotopic m/z		Position in the sequence	Peptide sequence
		Measured	Calculated		
1	61.69	762.8785 (+2)	762.8788	16-28	DVF**T**KGYGFGLIK
2	47.49	636.3152 (+3)	636.3155	94-110	GLKLTFD**S**SFSPNTGKK
3	45.29	804.8690 (+2)	804.8692	97-110	LTFDSSF**S**PNTGKK

T: threonine phosphorylated; **S**: serine phosphorylated.

Table S3. Phosphorylated peptides found in rVDAC2 tryptic digest after DTT reduction and carboxyamidomethylation.

In the Table the respective retention time, experimentally measured and calculated monoisotopic m/z of the molecular ions, the position in the sequence and the peptide sequence of modified fragments present in the tryptic digest of reduced and carboxyamidomethylated rVDAC2 are reported.

Frag. n.	Rt (min)	Monoisotopic m/z		Position in the sequence	Peptide sequence	MS/MS
		Measured	Calculated			
1	50.46	818.8859 (+2)	818.8848	109-122	LTFDTTF**S**PNTGKK	Yes
2	37.75	473.2534 (+2)	473.2534	126-132	IKSA**Y**KR	No

S: serine phosphorylated**; Y**: tyrosine phosphorylated.

Table S4. Phosphorylated peptides found in hVDAC1 tryptic digest after DTT reduction and carboxyamidomethylation.

In the Table the respective retention time, experimentally measured and calculated monoisotopic m/z of the molecular ions, the position in the sequence and the peptide sequence of modified fragments present in the tryptic digest of reduced and carboxyamidomethylated hVDAC1 are reported.

Frag. n.	Rt (min)	Monoisotopic m/z		Position in the sequence	Peptide sequence
		Measured	Calculated		
1	79.93	636.3153 (+3)	636.3156	94-110	GLKLTFDSSF**S**PNTGKK

S: serine phosphorylated.

Table S5. Phosphorylated peptides found in hVDAC2 tryptic digest after DTT reduction and carboxyamidomethylation.

In the Table the respective retention time, experimentally measured and calculated monoisotopic m/z of the molecular ions, the position in the sequence and the peptide sequence of modified fragments present in the tryptic digest of reduced and carboxyamidomethylated hVDAC2 are reported.

Frag. n.	Rt (min)	Monoisotopic m/z		Position in the sequence	Peptide sequence
		Measured	Calculated		
1	57.93	818.8870 (+2)	818.8848	108-121	LTFDTTF**S**PNTGKK
2	47.42	546.2587 (+3)	546.2592	108-121	LTFDTTFSPN**T**GKK

T: threonine phosphorylated; **S**: serine phosphorylated.

Figure S1. MS/MS spectrum of the doubly charged molecular ion at m/z 715.2848 (calculated 715.2844) of the N-terminal acetylated tryptic peptide of VDAC3 from HAP1 cells containing Cys residue 2 in the carboxyamidomethylated form and Cys residue 8 in the succinated form. The inset shows the full scan mass spectrum of molecular ion. Fragment ions originated from the neutral loss of H_2O are indicated by an asterisk.

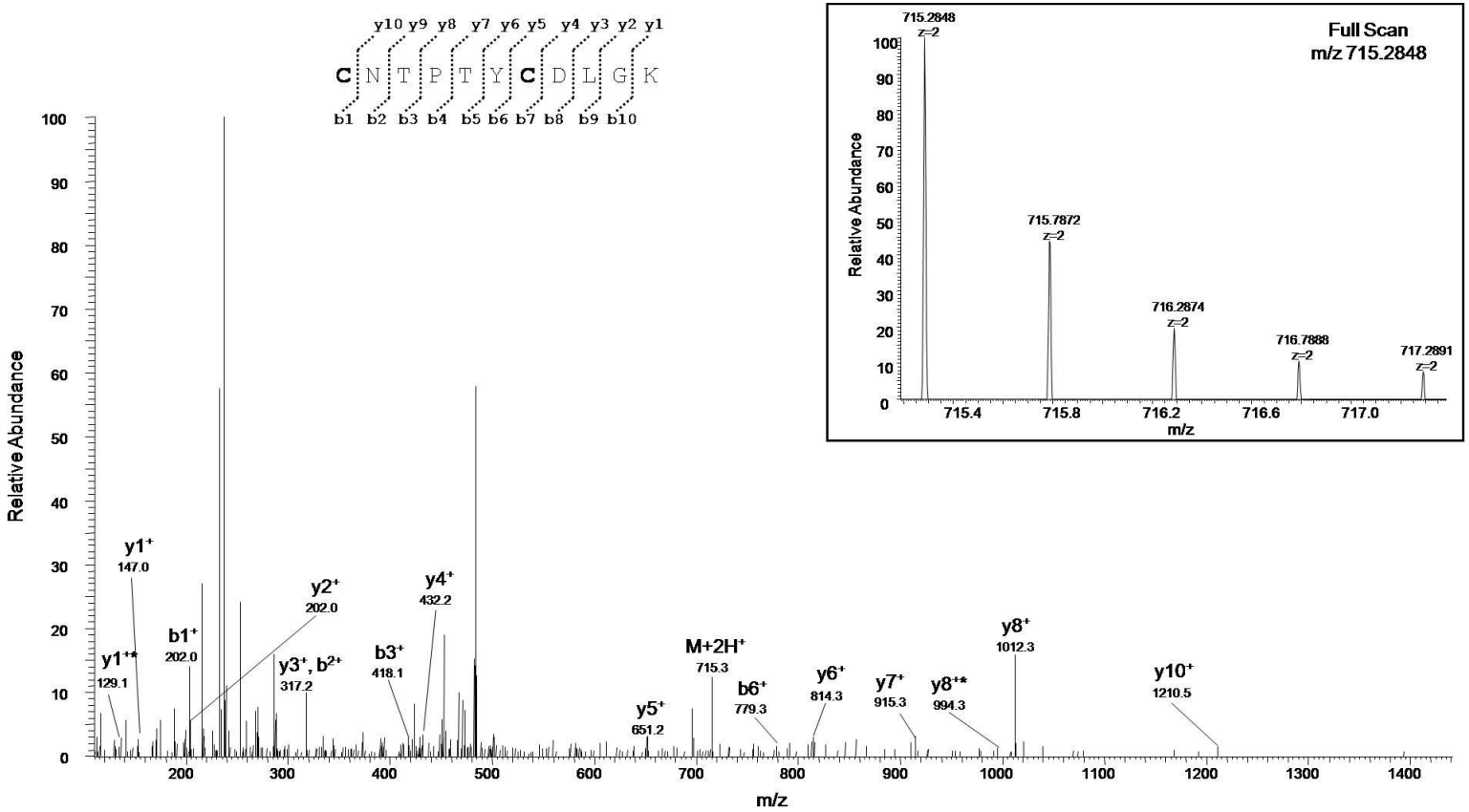

Figure S2. MS/MS spectrum of the doubly charged molecular ion at m/z 762.8785 (calculated 762.8788) of the VDAC1 tryptic peptide from *Rattus norvegicus* containing Thr residue 19 in the phosphorylated form.The inset shows the full scan mass spectrum of molecular ion. Fragment ions originated from the neutral loss of NH_3 are indicated by two asterisks. Fragment ions originated from the neutral loss of phosphoric acid (H_3PO_4, 98 Da) are indicated (fragment –P).

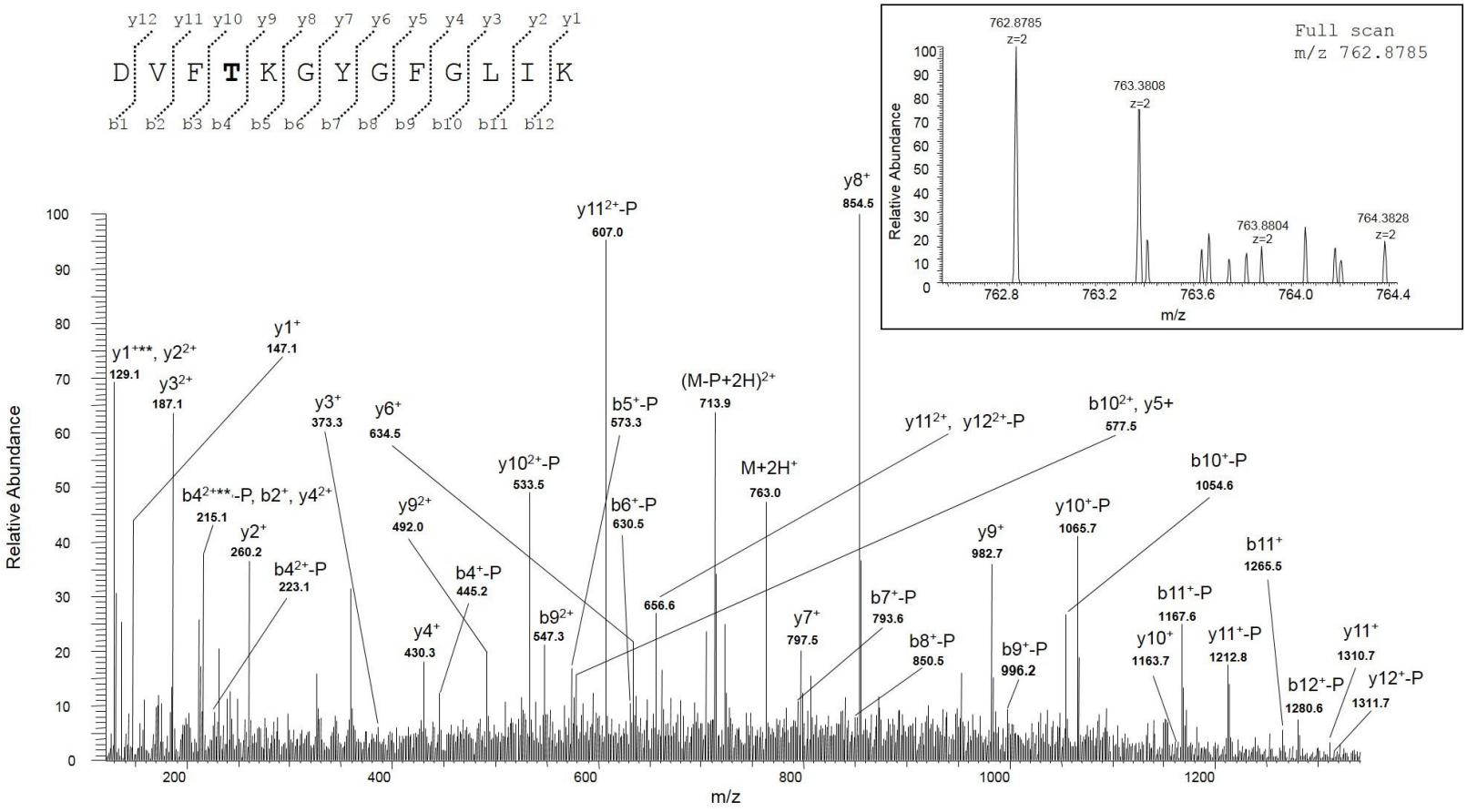

Figure S3. MS/MS spectrum of the doubly charged molecular ion at m/z 636.3152 (calculated 636.3155) of the VDAC1 tryptic peptide from *Rattus norvegicus* containing Ser residue 101 in the phosphorylated form.The inset shows the full scan mass spectrum of molecular ion. Fragment ions originated from the neutral loss of H_2O are indicated by one asterisk. Fragment ions originated from the neutral loss of phosphoric acid (H_3PO_4, 98 Da) are indicated (fragment –P).

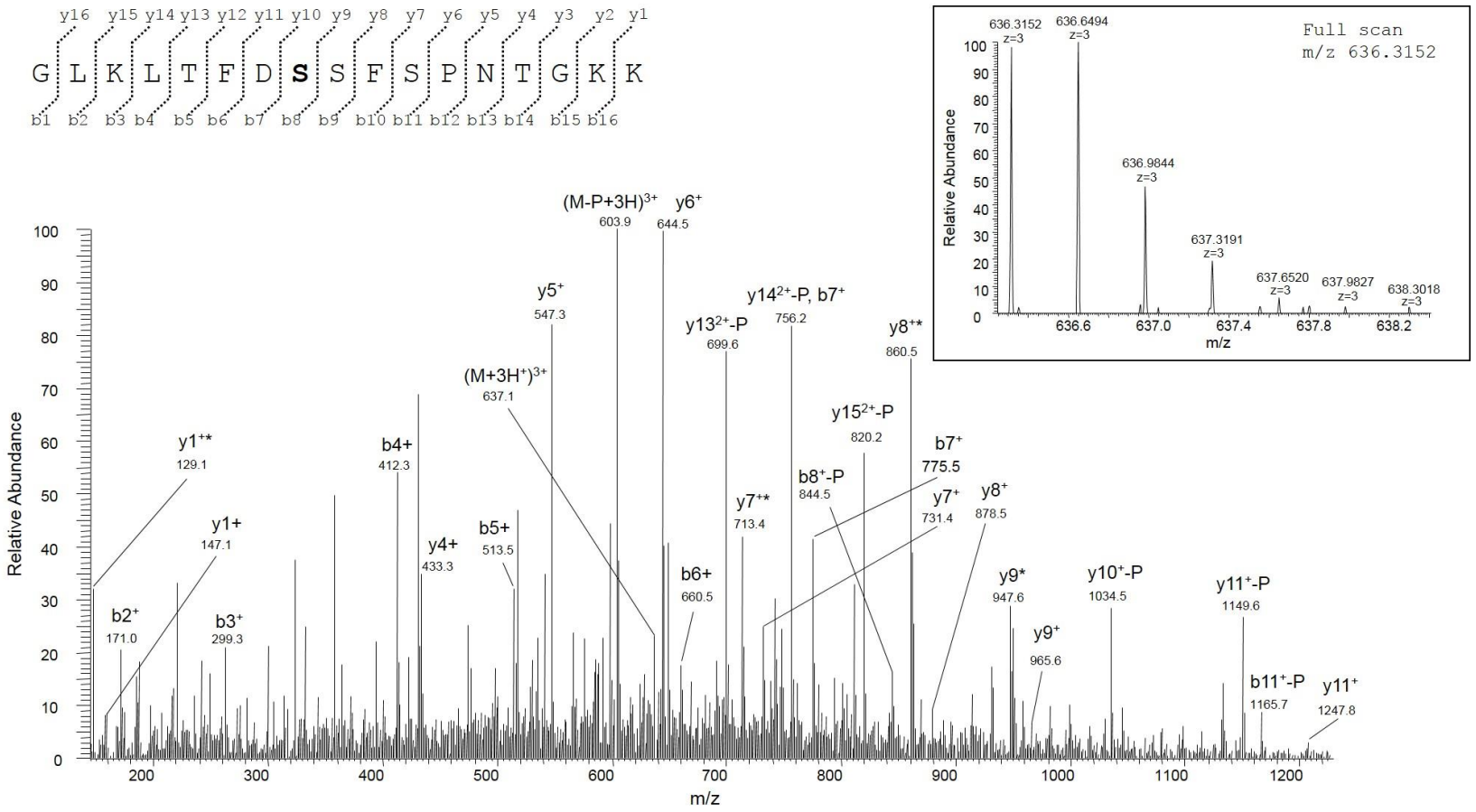

Figure S4. MS/MS spectrum of the doubly charged molecular ion at m/z 804.8690 (calculated 804.8692) of the VDAC1 tryptic peptide from *Rattus norvegicus* containing Ser residue 104 in the phosphorylated form.The inset shows the full scan mass spectrum of molecular ion. Fragment ions originated from the neutral loss of H_2O are indicated by one asterisk. Fragment ions originated from the neutral loss of NH_3 are indicated by two asterisks. Fragment ions originated from the neutral loss of phosphoric acid (H_3PO_4, 98 Da) are indicated (fragment –P).

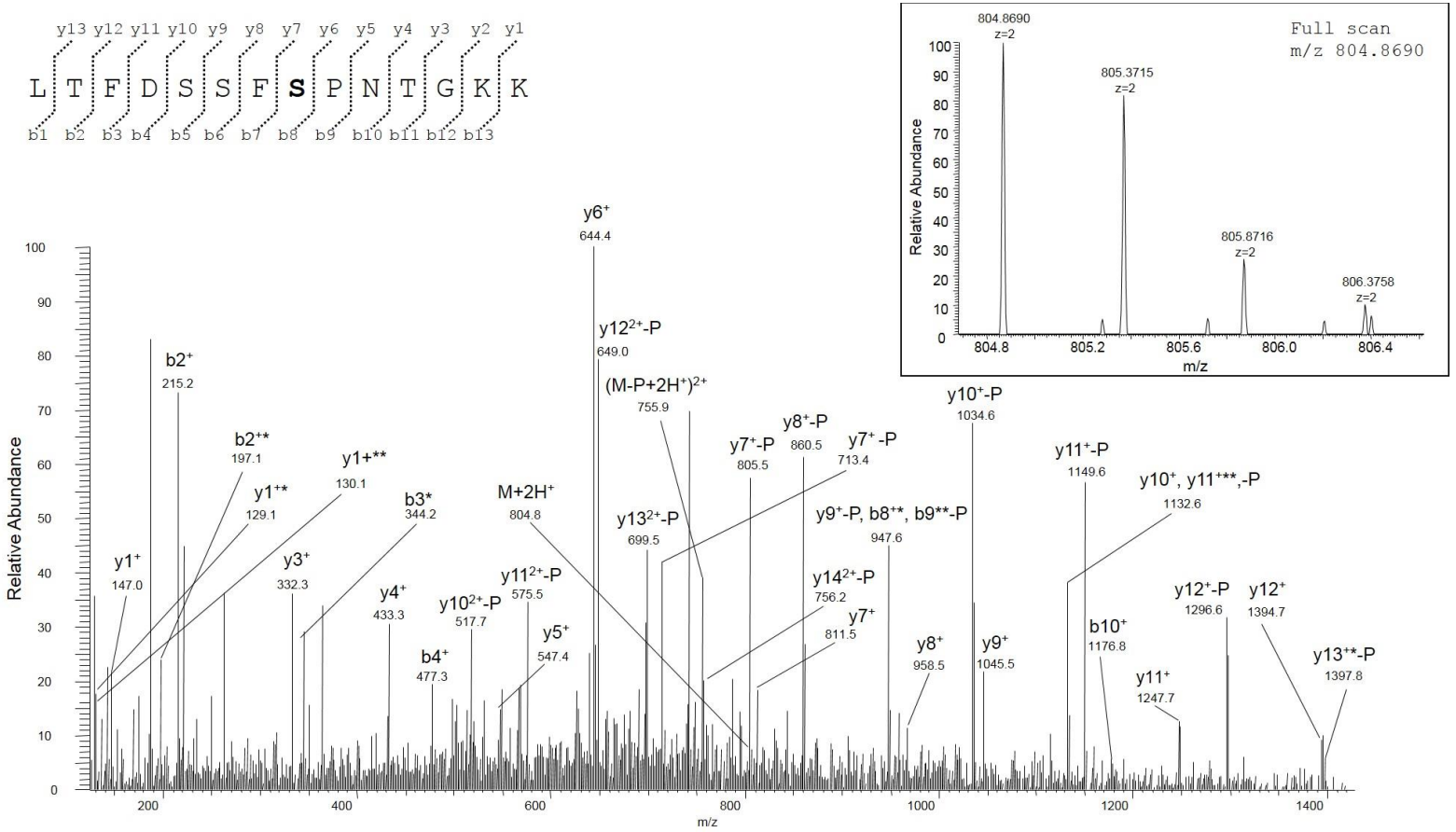

Figure S5. MS/MS spectrum of the doubly charged molecular ion at m/z 804.8690 (calculated 804.8692) of the VDAC2 tryptic peptide from *Rattus norvegicus* containing Ser residue 116 in the phosphorylated form.The inset shows the full scan mass spectrum of molecular ion. Fragment ions originated from the neutral loss of H_2O are indicated by one asterisk. Fragment ions originated from the neutral loss of NH_3 are indicated by two asterisks. Fragment ions originated from the neutral loss of phosphoric acid (H_3PO_4, 98 Da) are indicated (fragment –P).

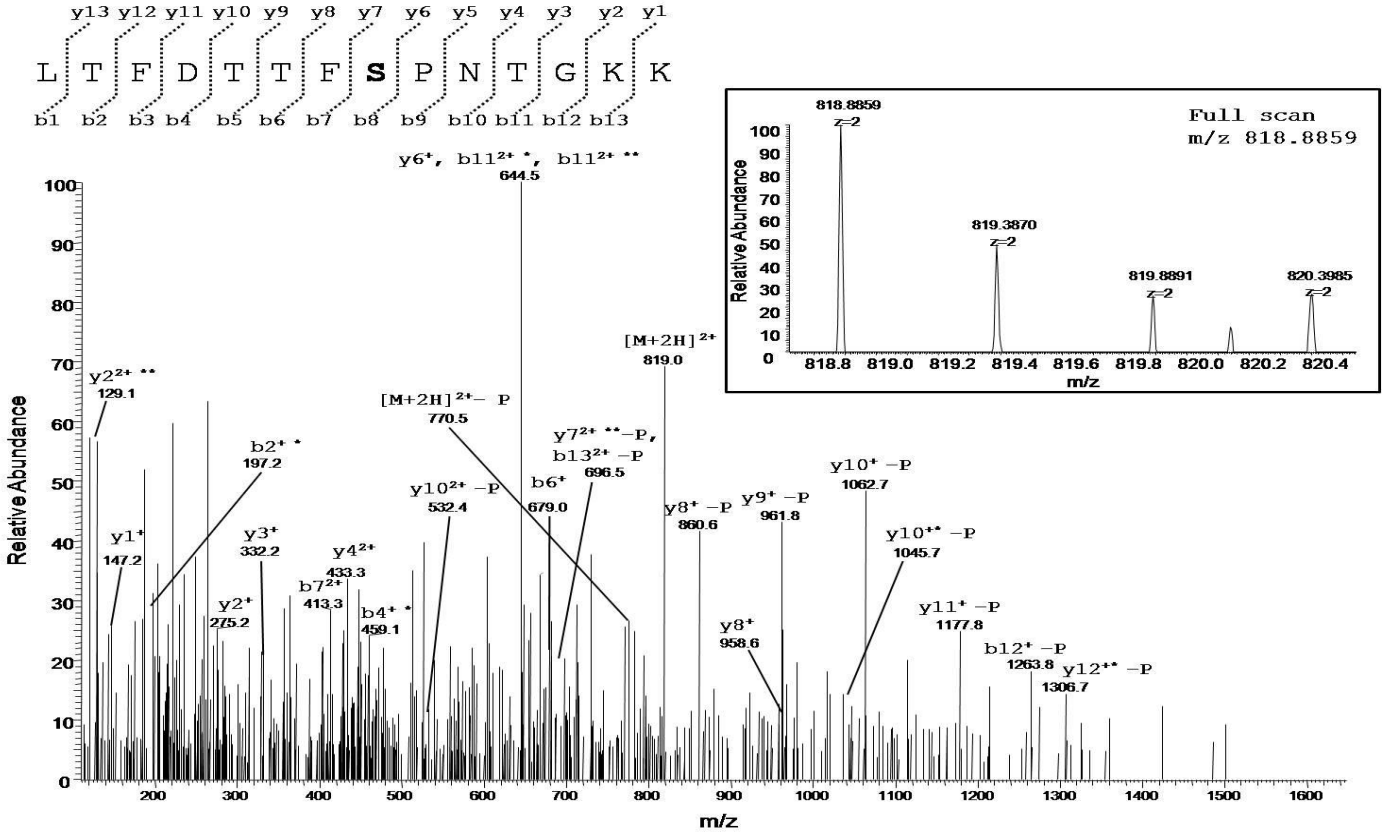

Figure S6. Full scan mass spectrum of the doubly charged molecular ion at m/z 473.2534 (calculated 473.2534, peptide sequence YKSA**Y**KR) of the VDAC2 tryptic peptide from from *Rattus norvegicus* containing Tyr residue 130 in the form phosphorylated form. MS/MS spectrum not found.

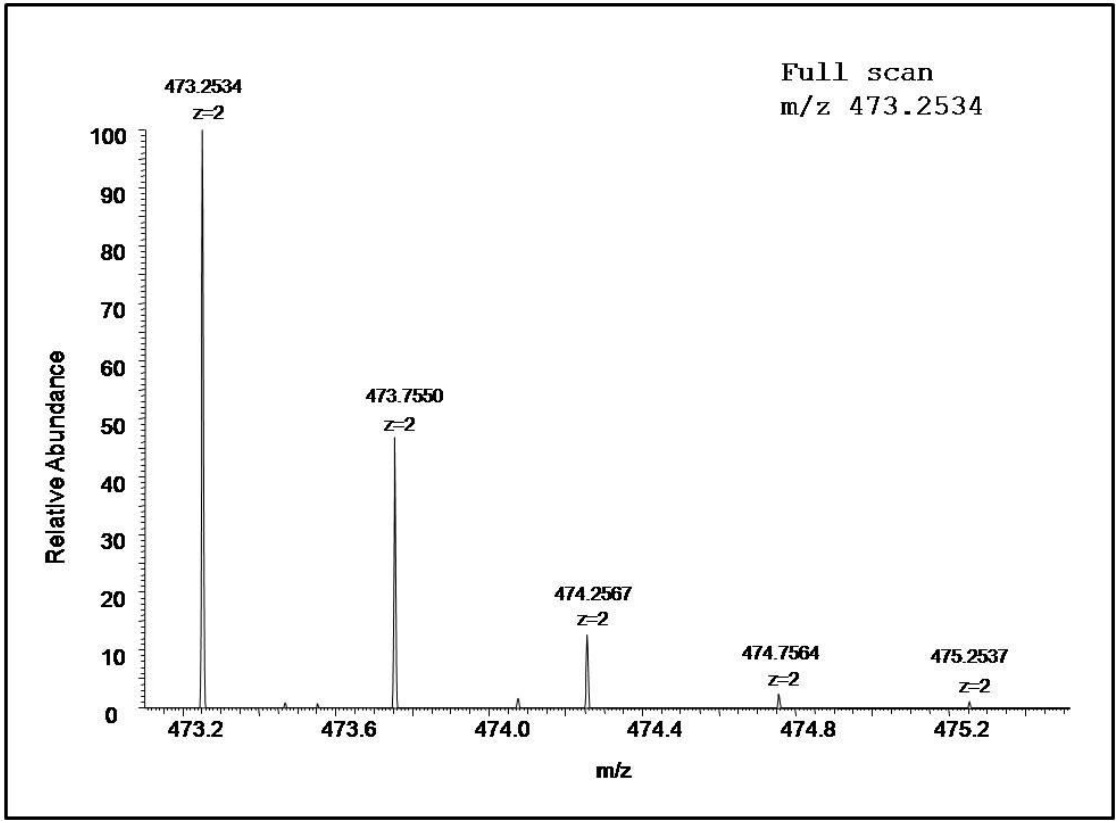

Figure S7. MS/MS spectrum of the triply charged molecular ion at m/z 636.3153 (calculated 636.3156) of the VDAC1 tryptic peptide from HAP1 cells containing Ser residue 104 in the phosphorylated form. The inset shows the full scan mass spectrum of molecular ion. Fragment ions originated from the neutral loss of phosphoric acid (H_3PO_4, 98 Da) are indicated (fragment –P).

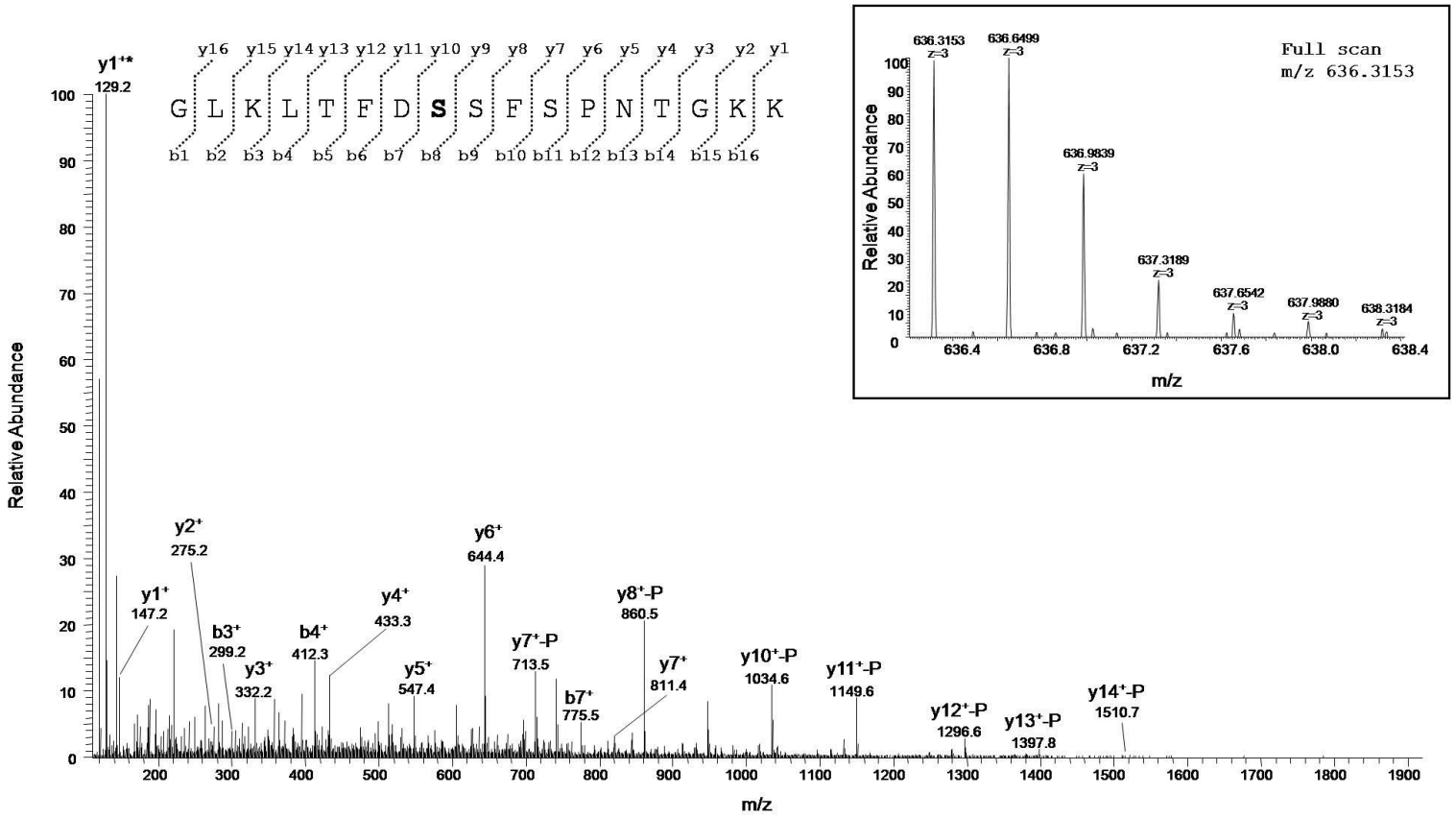

Figure S8. MS/MS spectrum of the doubly charged molecular ion at m/z 818.8870 (calculated 818.8848) of the VDAC2 tryptic peptide from HAP1 cells containing Ser residue 115 in the phosphorylated form.The inset shows the full scan mass spectrum of molecular ion. Fragment ions originated from the neutral loss of H_2O are indicated by one asterisk. Fragment ions originated from the neutral loss of phosphoric acid (H_3PO_4, 98 Da) are indicated (fragment –P).

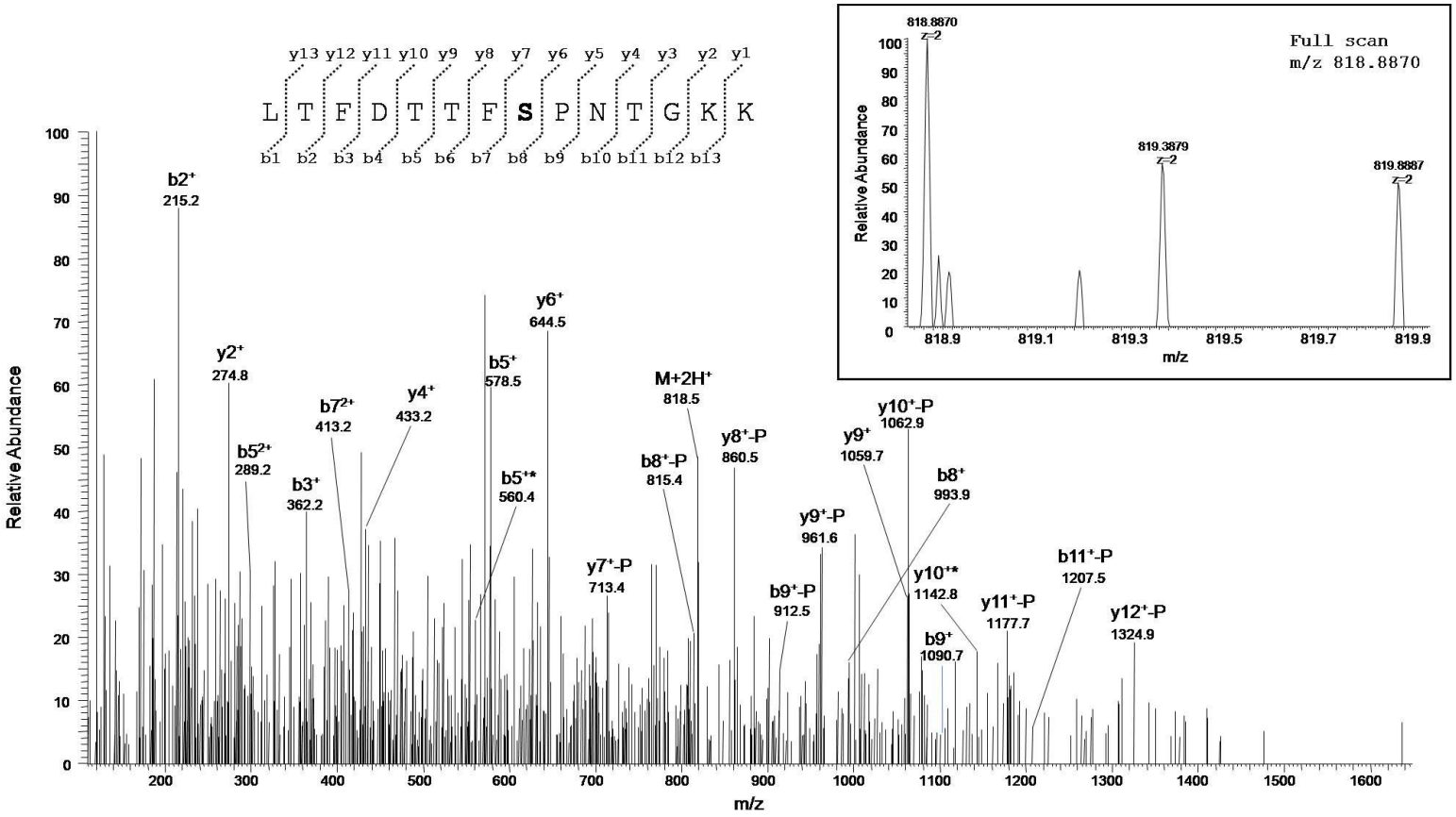

Figure S9. MS/MS spectrum of the triply charged molecular ion at m/z 546.2587 (calculated 546.2592) of the VDAC2 tryptic peptide from HAP1 cells containing Thr residue 118 in the phosphorylated form. The inset shows the full scan mass spectrum of molecular ion. Fragment ions originated from the neutral loss of phosphoric acid (H_3PO_4, 98 Da) are indicated (fragment –P).

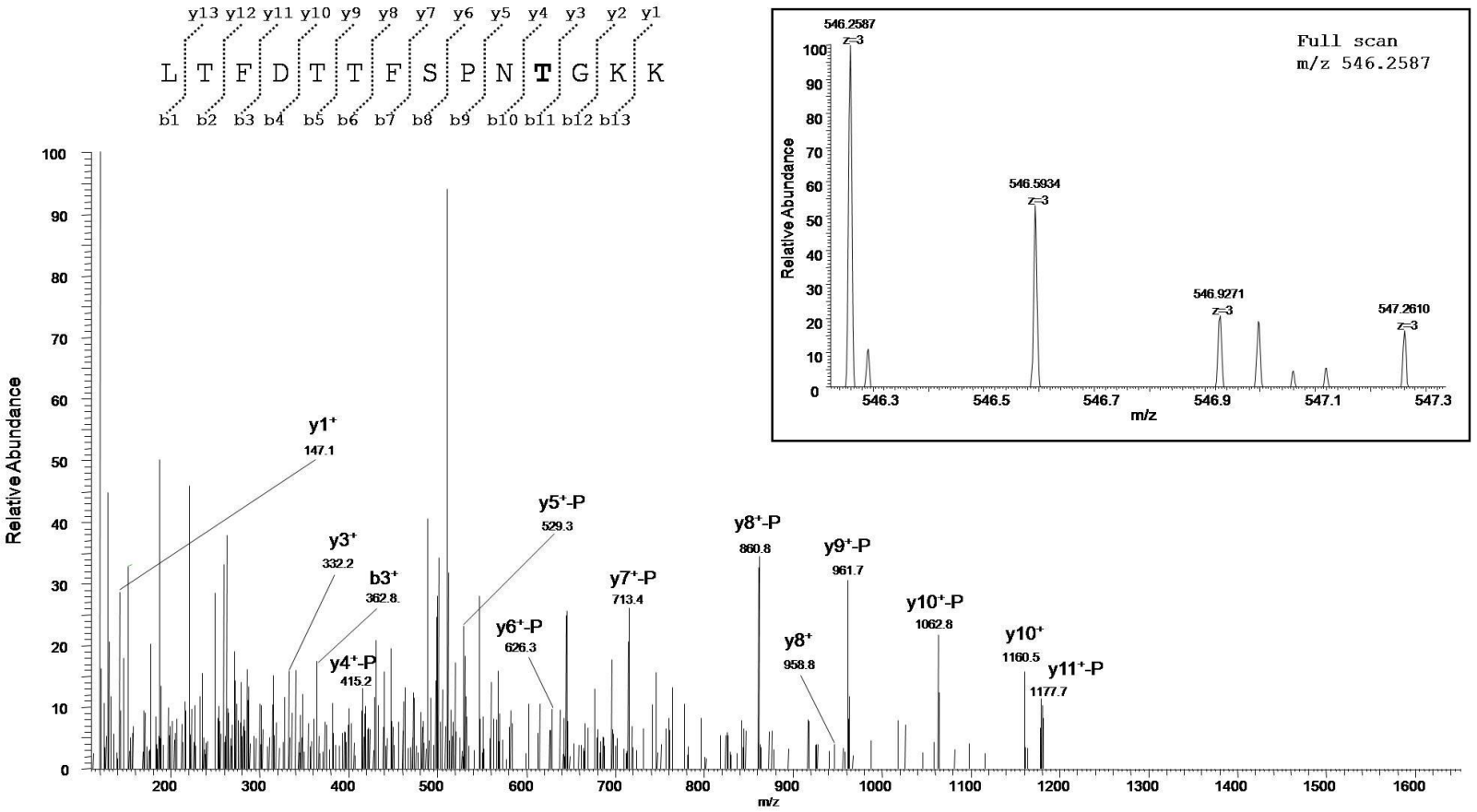

Figure S10. MS/MS spectrum of the doubly charged molecular ion at m/z 614.2551 (calculated 614.2547) of the N-terminal acetylated tryptic peptide of VDAC3 from *Rattus norvegicus* containing the disulfide bridge between Cys residues 2 and 8. The inset shows the full scan mass spectrum of molecular ion. Fragment ion originated from the neutral loss of H_2O is indicated by one asterisk. Fragment ions originated from the cleavage of S-S bond are indicated by three asterisks. Ac: Acetyl group.

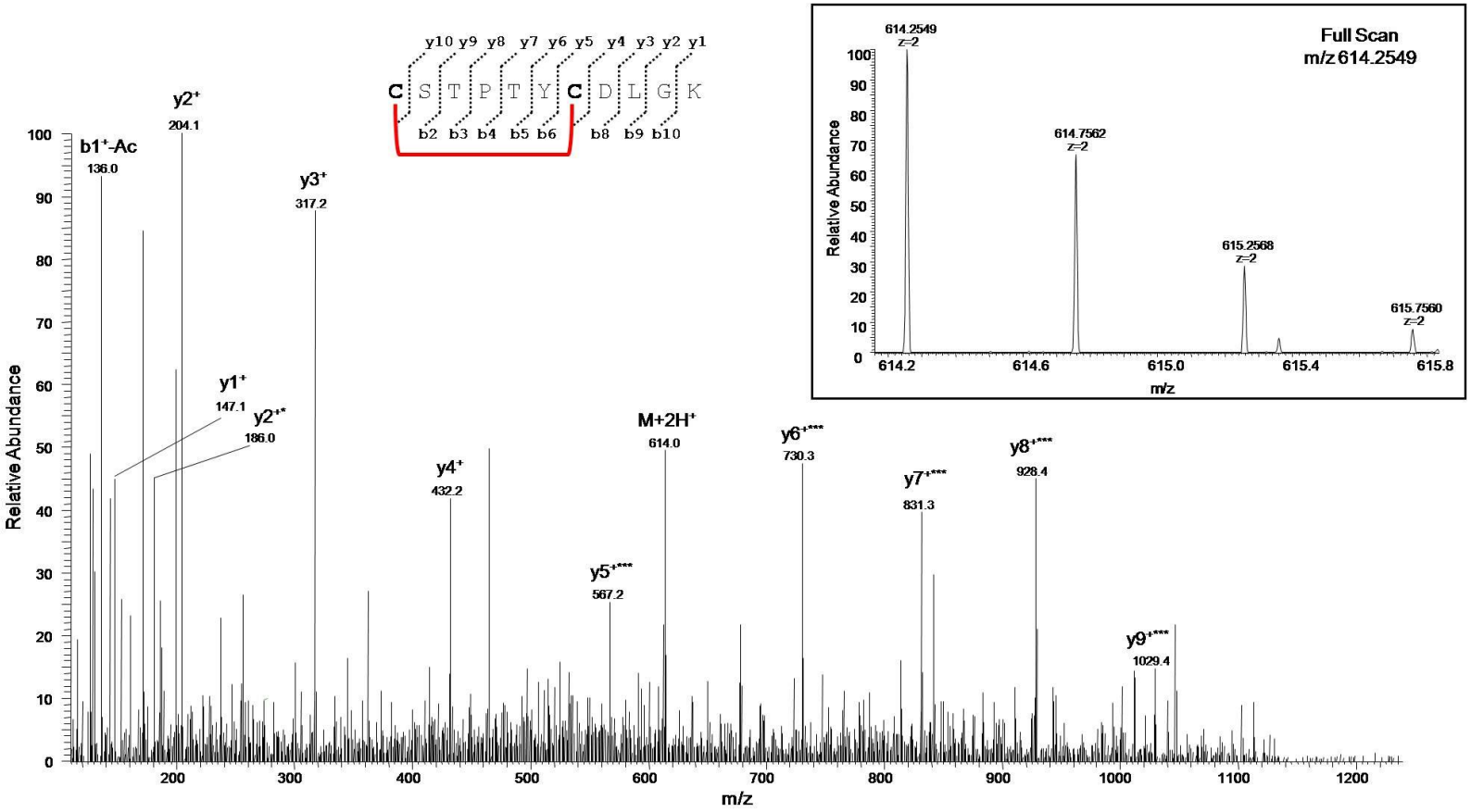

16. General list of References

[1] G. C. Brown. Control of respiration and ATP synthesis in mammalian mitochondria and cells. *Biochemical Journal* (1992), 284, 1-13.

[2] M. Crompton. The mitochondrial permeability transition pore and its role in cell death. *Biochemical Journal* (1999), 341, 233-249.

[3] G. Kroemer, L. Galluzzi, C. Brenner. Mitochondrial membrane permeabilization in cell death. *Physiological Reviews* (2007), 87, 99-163.

[4] L. A. Loeb, D. C. Wallace, G. M. Martin. The mitochondrial theory of aging and its relationship to reactive oxygen species damage and somatic mtDNA mutations. *PNAS* (2005), 102, 18769-18770.

[5] J. D. Cortese, A. L. Voglino, C.R. Hackenbrock. The ionic strength of the intermembrane space of intact mitochondria is not affected by the pH or volume of the intermembrane space. *Biochimica et Biophyisica Acta, Bioenergetics* (1992), 1100, 189-197.

[6] J. Hu, L. Dong, C. E. Outten. The redox environment in the mitochondrial intermembrane space is maintained separately from the cytosol and matrix. *Journal of Biological Chemistry* (2008), 283, 29126-29134.

[7] C. A. Mannella. Structure and dynamics of the mitochondrial inner membrane cristae. *Biochimica and Biophysica Acta, Molecular Cell Research* (2006), 1763 (5-6), 542-548.

[8] C. L. Bigarella, R. Liang, S. Ghaffari. Stem cells and the impact of ROS signalling. *Development* (2014), 141, 4206-4218.

[8] D. A. Bota, K. J. A. Davies. Lon protease preferentially degrades oxidized mitochondrial aconitase by an ATP-stimulated mechanism. *Nature Cell Biology* (2002), 4, 674-680.

[10] L. Milane, M. Trivedi, A. Singh, M. Talekar, M. Amiji. Mitochondrial biology, targets, and drug delivery. *Journal of Controlled Release* (2015), 207, 40-58.

[11] E. P. Leites, V. A. Morais. Mitochondrial quality control pathways: PINK1 acts as a gatekeeper. *Biochemical and Biophysical Research Communications* (2018), 500, 45-50.

[12] Y. Sun, A. A. Vashisht, J. Tchieu, J. A. Wohlschlegel, L. Dreier. Voltage-dependent Anion Channels (VDACs) recruit Parkin to defective mitochondria to promote mitochondrial autophagy. *Journal of Biological Chemistry* (2012), 287 (48), 40652-40660.

[13] M. Caterino, M Ruoppolo, A. Mandola, M. Costanzo, S. Orrù, E. Imperlini.Protein-protein interaction networks as a new perspective to evaluatedistinctfunctionalroles of voltage-dependentanionchannel isoforms. *Molecular BioSystems* (2017), 13 (12), 2466-2476.

[14] R. Benz. Permeation of hydrophilic solutes through mitochondrial outer membranes: review on mitochondrial porins. *Biochimica et Biophysica Acta, Biomembranes* (1994), 1197 (2), 167-196.

[15] A. H. Delcour, B. Martinac, J. Adler, C. Kung. Voltage-sensitive ion channel of Escherichia coli. *The Journal of Membrane Biology* (1989), 112, 267-275.

[16] M. J. Young, D. C. Bay, G. Hausner, D. A. Court. The evolutionary history of mitochondrial porins. *BioMed Central Evolutionary Biology* (2007), 7, 31.

[17] A. Messina, S. Reina, F. Guarino, V. De Pinto.VDAC isoforms in mammals. *Biochimica et Biophysica Acta, Biomembranes* (2012), 1818, 1466-1476.

[18] V. Shoshan-Barmatz, V. De Pinto, M. Zweckstetter, Z. Raviv, N. Keinan, N. Arbel. VDAC, a multi-functional mitochondrial protein regulating cell life and death. *Molecular Aspects of Medicine* (2010), 31, 227-285.

[19] S. Hiller, R.G.Garces,T.J. Malia, V.Y.Orekhov, M.Colombini, G.Wagner.Solution Structure of the Integral Human Membrane Protein VDAC-1 in Detergent Micelles. *Science* (2008), 32, 1206-1210.

[20] M. Bayrhuber, T. Meins, M. Habeck, S. Becker, K. Giller, S. Villinger, C. Vonrhein, C. Griesinger, M. Zweckstetter, K. Zeth. Structure of the human voltage-dependent anion channel. *PNAS* (2008), 105 (40), 15370-15375.

[21] R. Ujwal, D. Cascio, J. P. Colletier, S. Faham, J. Zhang, L. Toro, P. Ping, J. Abramson. The crystal structure of mouse VDAC1 at 2.3 Å resolution reveals mechanistic insights into metabolite gating. *PNAS* (2008), 105 (46), 17742-17745.

[22] M. Colombini. The published 3D structure of the VDAC channel: native or not? *Trends in Biochemical Sciences* (2009), 34 (8), 382-389.

[23] Schredelseker, A. Paz, C. J. Lopez, C. Altenbach, C. S. Leung, M. K. Drexler, J. N. Chen, W. L. Hubbell, J. Abramson.High resolution structure and double electron-electron resonance of the zebrafish voltage-dependent anion channel 2 reveal an oligomeric population. *The Journal of Biological Chemistry* (2014), 289 (18), 12566-12577.

[24] G. F. Omodeo, M. A. Scorciapino, A. Messina, V. De Pinto, M. Ceccarelli. Charged residues distribution modulates selectivity on the open state of human isoforms of the voltage dependent anion-selective channel. *PloS ONE* (2014), 9 (8), e103879.

[25] S. Majumder, H. A. Fisk.VDAC3 and Mps1 negatively regulate ciliogenesis. *Cell Cycle* (2005), 12 (5), 849-858.

[26] V. De Pinto, F. Guarino, A. Guarnera, A. Messina, S. Reina, F. M. Tomasello, V. Palermo, C. Mazzoni. Characterization of human VDAC isoforms: a peculiar function for VDAC3? *Biochimica et Biophysica Acta, Bioenergetics* (2010), 1797 (6-7), 1268-1275.

[27] B.C. Yoo, M. Fountoulakis, N. Cairns, G. Lubec. Changes of voltage-dependent anion selective channel proteins VDAC1 and VDAC2 brain levels in patients with Alzheimer's disease and Down syndrome. *Electrophoresis* (2001), 22, 172-179.

[28] P. H. Reddy. Is the mitochondrial outermembrane protein VDAC1 therapeutic targetfor Alzheimer's disease? *Biochimica et Biophysica Acta, Molecular Basis of Disease* (2013), 1832, 67-75.

[29] A. Asmarinah, A. Paradowska-Dogan, R. Kodariah, B. Tanuhardja, P. Waliszewski, C. A. Mochtar, W. Weidner, E. Hinsch. Expression of the Bcl-2 family genes and complexes involved in the mitochondrial transport in prostate cancer cells. *International Journal of Oncology* (2014), 45, 96-1489.

[30] S. Naghdi, P. Várnai, G. Hajnóczky. Motifs of VDAC2 required for mitochondrial Bak import and tBid-induced apoptosis. *PNAS* (2015), 112 (41), E5590-E5599.

[31] M. J. Sampson, W. K. Decker, A. L. Beaudet, W. Ruitenbeek, D. Armstrong, M. J. Hicks, W. J. Craigen. Immotile sperm and infertility in mice lacking mitochondrial voltage-dependent anion channel type 3. *Journal of Biological Chemistry* (2001) 276, 39206–39212.

[32] X. Xu, W. Decker, M. J.Sampson, W. J.Craigen, M. Colombini. Mouse VDAC isoforms expressed in yeast: channel properties and their roles in mitochondrial outer membrane permeability. *The Journal of Membrane Biology* (1999), 170, 89-102.

[33] V. Checchetto, S. Reina, A. Magrì, I. Szabò, V. De Pinto. Recombinant human Voltage Dependent Anion Selective Channel Isoform 3 (hVDAC3) forms pores with a very small conductance. *Cellular Physiology and Biochemistry* (2014), 34, 842-853.

[34] M. Okazaki, K. Kurabayashi, M. Asanuma, Y. Saito, K. Dodo, M. Sodeoka. VDAC3 gating is activated by suppression of disulfide-bond formation between the N-terminal region and the bottom of the pore. *Biochimica et Biophysica Acta, Biomembranes* (2015), 1848, 3188-3196.

[35] S. Reina, A. Magrì, M. Lolicato, F. Guarino, A. Impellizzeri, E. Maier, R. Benz, M. Ceccarelli, V. De Pinto, A. Messina. Deletion of β-strands 9 and 10 converts VDAC1 voltage-dependence in an asymmetrical process. *Biochimica et Biophysica Acta, Bioenergetics* (2013), 1827, 793-805.

[36] S. Reina, V. Palermo, A. Guarnera, F. Guarino, A. Messina, C. Mazzoni, V. De Pinto. Swapping of the N-terminus of VDAC1 with VDAC3 restores full activity of the channel and confers anti-aging features to the cell. *FEBS Letters* (2010), 584, 2837–2844.

[37] M. J. Sampson, R. S. Lovell,W. J. Craigen. The murine voltage-dependent anion channel gene family. Conserved structure and function. *Journal of Biological Chemistry* (1997), 272, 18966-18973.

[38] V. De Pinto, S. Reina, A. Gupta, A. Messina, R. Mahalakshmi. Role of cysteines in mammalian VDAC isoforms' function. *Biochimica et Biophysica Acta, Bioenergetics* (2016), 1857, 1219-1227.

[39] L. Bleier, I.Wittig, H. Heide,M. Steger, U. Brandt, S. Dröse. Generator-specific targets of mitochondrial reactive oxygen species. *Free Radical Biology and Medicine* (2015), 78, 1-10.

[40] L. Aram, S. Geula, N. Arbel, V. Shoshan-Barmatz. VDAC1 cysteine residues: topology and function in channel activity and apoptosis. *Biochemical Journal* (2010), 427, 445-454.

[41] S. Geula, H. Naveed, J. Liang, V. Shoshan-Barmatz. Structure-based analysis of VDAC1 protein: defining oligomer contact sites. *Journal of Biological Chemistry* (2012), 287, 2179–2190.

[42] T. Yamamoto, A. Yamada, M.Watanabe, Y. Yoshimura, N. Yamazaki, Y. Yoshimura, T. Yamauchi, M. Kataoka, T. Nagata, H. Terada, Y. Shinohara. VDAC1, having a shorter N-terminus than VDAC2 but showing the same migration in an SDS polyacrylamidegel, is the predominant form expressed in mitochondria of various tissues. *Journal of Proteome Research* (2006), 5, 3336–3344.

[43] B. Mertins, G. Psakis,W. Grosse, K.C. Back, A. Salisowski, P. Reiss, U. Koert, L.O. Essen. Flexibility of the N-terminal mVDAC1 segment controls the channel's gating behavior. *PLoS One* (2012), 7, e47938.

[44] S. Geula, D. Ben-Hail, V. Shoshan-Barmatz. Structure-based analysis of VDAC1: N-terminus location, translocation, channel gating and association with anti-apoptotic proteins. *Biochemical Journal* (2012), 444, 85–475.

[45] S. R. Maurya, R.Mahalakshmi. N-helix and cysteines inter-regulate human mitochondrial VDAC-2 function and biochemistry. *The Journal of Biological Chemistry* (2015), 290 (51), 30240-30252.

[46] C. Guardiani, M. A. Scorciapino, G. F. Amodeo, J. Grdadolnik, G. Pappalardo, V. De Pinto, M. Ceccarelli, M. Casu. The N-terminal peptides of the three human isoforms of the mitochondrial voltage-dependent anion channel have different helical propensities. *Biochemistry* (2015), 54, 5646-5656.

[47] S. R. Maurya, R. Mahalakshmi. Modulation of human mitochondrial voltage-dependent anion channel 2 (hVDAC-2) structural stability by cysteine-assisted barrel-lipid interactions. *The Journal of Biological Chemistry* (2013), 288 (35), 25584-25592.

[48] S. R. Maurya, D. Chaturvedi, R. Mahalakshmi. Modulating lipid dynamics andmembrane fluidity to drive rapid folding of a transmembrane barrel. *Scientific Reports* (2013), 3, 1989.

[49] S. Reina, V. Checchetto, R. Saletti, A. Gupta, D. Chaturvedi, C.Guardiani, F.Guarino,M. A. Scorciapino, A. Magrì, S. Foti, M. Ceccarelli, A. A. Messina, R. Mahalakshmi, I. Szabo, V. De Pinto. VDAC3 as a sensor of oxidative state of the intermembrane space of mitochondria: the putative role of cysteine residue modifications. *Oncotarget* (2016), 7, 2249–2268.

[50] S. R. Maurya, R. Mahalakshmi. Cysteine residues impact the stability and micelle interaction dynamics of the human mitochondrial β-barrel anion channel hVDAC-2. *PLoS ONE* (2014), 9, e92183.

[51] R. Saletti, S. Reina, M. G. G. Pittalà, R. Belfiore, V. Cunsolo, A. Messina, V. De Pinto, S. Foti. High resolution mass spectrometry characterization of the oxidation pattern of methionine and cysteine residues in rat liver mitochondria voltage-dependent anion selective channel 3 (VDAC3). *Biochimica et Biophysica Acta, Biomembranes* (2016), 1859 301-311.

[52] C. Guardiani, L. Leggio, M. A. Scorciapino, V. De Pinto, M. Ceccarelli. A computational study of ion current modulation in hVDAC3 induced by disulfide bonds. *Biochimica et Biophysica Acta, Biomembranes* (2016), 1858, 813–823.

[53] T. Tasaki, Y. T. Kwon. The mammalian N-end rule pathway: new insights into its components and physiological roles. *Trends in Biochemical Sciences* (2007), 32 (11), 520-528.

[54] T. Tasaki, S. M. Sriram, K. Soo Park, Y. Tae Kwon. The N-End Rule Pathway. *Annual Review of Biochemistry* (2012), 81, 261-289.

[55] K. G. Reddie, K. S. Carroll. Expanding the functional diversity of proteins through cysteine oxidation. *Current Opinion in Chemical Biology* (2008), 12, 746-754.

[56] H. Liu, K. May. Disulfide bond structures of IgG molecules: structural variations, chemical modifications and possible impacts to stability and biological function. *MAbs* (2012), 4, 17-23.

[57] F. Liu, B. van Breukelen and A. J. R. Heck. Facilitating protein disulfide mapping by a combination of pepsin digestion, Electron Transfer Higher Energy Dissociation (EThcD), and a dedicated Search Algorithm SlinkS. *Molecular e Cellular Proteomics* (2014) 13, 2776-2786.

[58] H. Xu, L. Zhang, M. A. Freitas. Identification and characterization of disulfide bonds in proteins and peptides from Tandem MS Data by Use of the MassMatrix MS/MS Seaech Engine. *Journal of Proteome Research* (2008), 7(1), 138-144.

[59] J. J. Gorman, T. P. Wallis, J. J. Pitt. Protein disulfide bond determination by mass spectrometry. *Mass Spectrometry Reviews* (2002), 21, 183-216.

[60] D. Stojanovski, J. M. Müller, D. Milenkovic, B. Guiard, N. Pfanner, A. Chacinska. The MIA system for protein import into the mitochondrial intermembrane space. *Biochimica et Biophysica Acta* (2008), 1783, 610-617.

[61] L. B. Poole, K. J. Nelson. Discovering mechanisms of signalling-mediated cysteine oxidation. *Current Opinion in Chemical Biology* (2008), 12 (1), 18-24.

[62] J. Yang, V. Gupta, K. S. Carroll, D. C. Liebler. Site-specific mapping and quantification of protein S-sulfenylation in cells. *Nature Communications* (2015), 5, 4776.

[63] C. E. Paulsen, K. S. Carroll. Cysteine-mediated redox signalling: chemistry, biology, and tools for discovery. *Chemical Reviews* (2013), 113, 4633-4679.

[64] T. J. Phalen, K. Weirather, P. B. Deming, V. Anathy, A. K. Howe, A. van derVliet, T. J. Jönsson, L. B. Poole, N. H. Heintz. Oxidation state governs structural transitions in peroxiredoxin II that correlate with cell cycle arrest and recovery. *The Journal of Cell Biology* (2006), 175, 779–789.

[65] J. Fang, T. Nakamura, D. H. Cho, Z. Gu, S. A. Lipton. S-nitrosylation of peroxiredoxin 2 promotes oxidative stress-induced neuronal cell death in Parkinson's disease. *Proceeding of the National Academy of Sciences of the United States of America* (2007), 104, 18742–18747.

[66] E. A. Veal, A. M. Day, B. A. Morgan. Hydrogen peroxide sensing and signaling. *Molecular Cell* (2007), 26, 1–14.

[67] H. A. Woo, S. W. Kang, H. K. Kim, K-S Yang, H. Z. Chae, S. G. Rhee. Reversible oxidation of the active site cysteine of peroxiredoxins to cysteine sulfinic acid. Immunoblot detection with antibodies specific for the hyperoxidized cysteine-containing sequence. *The Journal of Biological Chemistry* (2003), 278, 47361–47364.

[68] Z. A. Wood, L. B. Poole, P. A. Karplus. Peroxiredoxin evolution and the regulation of hydrogen peroxide signaling. *Science* (2003), 300, 650–653.

[69] T. S. Chang, W. Jeong, H. A. Woo, S. M. Lee, S. Park, S. G. Rhee. Characterization of mammalian sulfiredoxin and its reactivation of hyperoxidized peroxiredoxin through reduction of cysteine sulfinic acid in the active site to cysteine. *The Journal of Biological Chemistry* (2004), 279, 50994–51001.

[70] M. Lo Conte, K, S. Carroll. The redox biochemistry of protein sulfenylation and sulfinylation. *The Journal of Biological Chemistry* (2013), 288, 26480–26488.

[71] J. Blackinton, M. Lakshminarasimhan, K. J. Thomas, R. Ahmad, E. Greggio, A. S. Raza, M. R. Cookson, M. A. Wilson. Formation of a stabilized cysteine sulfinic acid is critical for the mitochondrial function of the parkinsonism protein DJ-1. *The Journal of Biological Chemistry* (2009), 284, 6476–6485.

[72] B. C. Dickinson, C. J. Chang. Chemistry and biology of reactive oxygen species in signaling or stress responses. *Nature Chemical Biology* (2011), 7, 504–511.

[73] S. Akter, L. Fu, Y. Jung, M. Lo Conte, J. R. Lawson, W. T. Lowther, R. Sun, K. Liu, J. Yang, K. S. Carroll. Chemical proteomics reveals new targets of cysteine sulfinic acid reductase. *Nature Chemical Biology* (2018), 14 (11), 995-1004.

[74] J. C. Lim, H.-I. Choi, Y. S. Park, H. W. Nam, H. A. Woo, K.-S. Kwon, Y. S. Kim, S. G. Rhee, K. Kim, H. Z. Chae. Irreversible oxidation of the active-site cysteine of Peroxiredoxin to cysteine sulfonic acid for enhanced molecular chaperone activity. *The Journal of Biological Chemistry* (2008), 283 (43), 28873-28880.

[75] E. Wagner, S. Luche, L. Penna, M. Chevallet, A, Van Dorsselaer, E. Leize-Wagner, T. Rabilloud. A method for detection of overoxidation of cysteines: peroxiredoxins are oxidized in vivo at the active-site cysteine during oxidative stress. *The Biochemical Journal* (2002), 366, 777-785.

[76] J. S. O'Neill, A. B. Reddy. Circadian clocks in human red blood cells. *Nature* (2011), 496, 09702.

[77] C. Colussi, M. C. Albertini, S. Coppola, S. Rovidati, F. Galli,L. Ghibelli. H_2O_2-induced block of glycolysis as an active ADP-ribosylation reaction protecting cells from apoptosis. *The FASEB Journal* (2000), 14, 2266-2276.

[78] F. Meng, D. Yao, Y. Shi, J. Kabakoff, W. Wu, J. Reicher, Y. Ma, B. Moosmann, E. Masliah, S. A Lipton, Z.Gu. Oxidation of the cysteine-rich regions of parkinperturbs its E3 ligase activity and contributes to protein aggregation. *Molecular Neurodegeneration* (2011), 6, 34.

[79] N. Fujiwara,M. Nakano, S. Kato, D. Yoshihara, T. Ookawara, H. Eguchi, N. Taniguchi, K. Suzuki. Oxidative modification to cysteine sulfonic acid of Cys 111 in Human Copper-Zinc Superoxide Dismutase. *The Journal of Biological Chemistry* (2007), 282 (49), 35933-35944.

[80] S. Nagano, Y. Takahashi, K. Yamamoto, H. Masutani, N. Fujiwara, M. Urushitani, T. Araki. A cysteine residue affects the conformational state and reuronal toxicity of mutant SOD1 in mice: relevance to the pathogenesis. *Human molecular genetics* (2015), 24 (12), 3427-3439.

[81] C. A. Strott. Sulfonation and molecular action. *Endocrine Reviews* (2002), 23 (5), 703-732.

[82] A. A. Turanov, X.-M. Xu, B. A. Carlson, M.-H. Yoo, V. N. Gladyshev, D. L. Hatfield. Biosynthesis of Selenocysteine, the 21st amino acid in the genetic code, and a novel pathway for cysteine biosynthesis. *Advances in nutrition* (2011), 2, 122-128.

[83] J. Gonzalez-Flores, S. P. Shetty, A. Dubey,P. R. Copeland. The molecular biology of Selenocysteine. *Biomolecular concepts* (2013), 4 (4), 349-365.

[84] L. Johanssona, G. Gafvelinb, E. S. J. Arner. Selenocysteine in proteins: properties and biotechnological use. *Biochimica et Biophysica Acta* (2005), 1726, 1-13.

[85] M. Blatnik, S. R. Thorpe, J. W. Baynes. Succination of proteins by Fumarate. Mechanism of inactivation of Glyceraldehyde-3-Phosphate Dhydrogenase in diabetes. *Annals of the New York Academy of Sciences* (2008), 1126, 272-275.

[86] L. Hening, S. Xiaoyang, H. Bin. Protein lysine acylation and cysteine succination by intermediates of energy metabolism. *American Chemical Society, Chemical Biology* (2012), 7, 947-960.

[87] N. Frizzell, M. Lima, J. W. Baynes. Succination of proteins in diabetes. *Free Radical Research* (2011), 45 (1), 101-109.

[88] E. D. Merkley, T. O. Metz, R. D. Smith, J. W. Baynes,N. Frizzell. The succinated proteome. *Mass Spectrometry Reviews* (2014), 33, 98-109.

[89] E. Linster, M. Wirtz. N-terminal acetylation: an essenzial protein modification emerges as an important regulator of stress responses. *Journal of Experimental Botany* (2018), 69 (19), 4555-4568.

[90] T. Arnesen, P. Van Damme, B. Polevoda, K. Helsens, R. Evjenth, N. Colaert, J. E. Varhaug, J. Vandekerckhove, J. R. Lillehaug, F. Sherman, K. Gevaert. Proteomics analyses reveal the evolutionary conservation and divergence of N-terminal acetyltransferases from yeast and humans. *PNAS* (2009), 106 (20), 8157-8162.

[91] T. Arnesen. Towards a functional understanding of protein N-terminal acetylation. *PLOS Biology* (2011), 9 (5), e1001074.

[92] J. Li, J. A. Paulo, D. P. Nusinow, E. L. Huttlin, S. P. Gygi. Investigation of proteomic and phosphoproteomic responses to signaling network perturbations reveals functional pathway organizations in yeast. *Cell Reports* (2019), 29, 2092-2104.

[93] J. Kerner, K. Lee, B. Tandler, C. L. Hoppel. VDAC proteomics: post-translation modifications. *Biochimica et Biophysica Acta* (2012), 1818 (6), 1520-1525.

[94] R. L. Levine, J. Moskovitz, E. R. Stadtman. Oxidation of methionine in proteins: roles in antioxidant defence and cellular regulation. *IUBMB Life* (2000), 50, 301-307.

[95] E.R. Stadtman, J. Moskovitz, R.L. Levine. Oxidation of methionine residues of proteins:

biological consequences. *Antioxidants & Redox Signaling* (2003), 5, 577–582.

[96] E. R. Stadtman. Protein oxidation and aging. *Free Radical Research* (2006), 40, 1250–1258.

[97] A. Koc, A. P. Gasch, J. C. Rutherford, H.-Y. Kim, V. N. Gladyshe. Methionine sulfoxide reductase regulation of yeast lifespan reveals reactive oxygen species-dependent and –independent components of aging. *PNAS* (2004), 101 (21), 7999-8004.

[98] D. J. Bigelow, T. C. Squier. Redox modulation of cellular signaling and metabolism through reversible oxidation of methionine sensors in calcium regulatory proteins. *Biochimica et Biophysica Acta* (2005), 1703, 121-134.

[99] N. Ugarte, I. Petropoulos, B. Friguet. Oxidizedmitochondrial protein degradation and repair in aging and oxidative stress. *Antioxidants & Redox Signaling* (2010), 13, 539–549.

[100] R. L. Levine, L. Mosoni, B. S. Berlett, E. R. Stadtman. Methionine residues as endogenous antioxidants in proteins. *National Academy of Sciences of the United States of America* (1996), 93, 15036–15040.

[101] S. Tan, H. Tong Tan, M. C. M. Chung. Membrane proteins and membrane proteomics. *Proteomics* (2008), 8, 3924-3932.

[102] K. Smolders, N. Lombaert, D. Valkenborg, G. Bargerman , L. Arckens. An effective plasma membrane proteomics approach for small tissue samples. *Scientific reports* (2015), 5, 10917.

[103] Y. Bledi, A. Inberg, M. Linial. Proceed: a proteomic method for analyzing plasma membrane proteins in living mammalian cells. *Briefings in Functional Genomics and proteomics* (2003), 2 (3), 254-265.

[104] Y. Zhao, W. Zhang, Y. Kho, Y. Zhao. Proteomic analysis of integral plasma membrane proteins. *Analytical Chemistry* (2004), 76, 1817-1823.

[105] X. Wang, S. Liang. Sample preparation for the analysis of membrane proteomes by mass spectrometry. *Protein Cell* (2012), 3 (9), 661-668.

[106] J. P. Whitelegge. Integral membrane proteins and bilayer proteomics. *Analytical Chemistry* (2013), 85, 2558-2568.

[107] J. M. Gilmore, M. P. Washburn. Advances in shotgun proteomics and the analysis of membrane proteins. *Journal of proteomics* (2010), 73, 2078-2091.

[108] C. Valle, M. T. Carrì. Cysteine modifications in the pathogenesis of ALS. *Frontiers in Molecular Neuroscience* (2017), 10, 5.

[109] T. K. Rostovtseva, P. A. Gurnev, O. Protchenko, D. P. Hoogerheide, T. L. Yap, C. C. Philpott, J. C. Lee, S. M. Bezrukov. α-Synuclein shows high affinity interaction with Voltage-dependent Anion Channel, suggesting mechanisms of mitochondrial regulation and toxicity in Parkinson Disease. *The Journal of Biological Chemistry* (2015), 290 (30), 18467–18477.

[110] A. Magrì, R. Belfiore, S. Reina, M. F. Tomasello, M. C. Di Rosa, F. Guarino, L. Leggio, V. De Pinto A. Messina. Hexokinase I N-terminal based peptide prevents the VDAC1-SOD1 G93A interaction and re-establishes ALS cell viability. *Scientific Reports* (2016), 6, 34802.

[111] C. P. Baines, R. A. Kaiser, T. Sheiko, W. J. Craigen, J. D. Molentkin. Voltage-dependent anion channels are dispensable for mitochondrial cell death. *Nature Cell Biology* (2007), 9, 550-555.

[112] Y. Chen, W. J. Craigen, D. J. Riley. Nek1 regulates cell death and mitochondrial membrane permeability through phosphorylation of VDAC1. *Cell Cycle* (2009), 8, 257-267.

[113] K. L. Sheldon, E. N. Maldonado, J. J. Lemasters, T. K. Rostovtseva, S. M. Bezrukov. Phosphorylation of Voltage-Dependent Anion Channel by serine/threonine kinases governs its interaction with tubulin. *Plos One* (2011), 6 (10), e25539.

[114] B. C. Yoo, M. Fountoulakis, N. Cairns, G. Lubec. Changes of Voltage-Dependent Anion-Selective Channel proteins VDAC1 and VDAC2 brain levels in patients with Alzheimer's disease and Down syndrome. *Electrophoresis* (2001), 22, 172-179.

[115] De Pinto, G. Prezioso, F. Palmieri. A simple and rapid method for the purificationof the mitochondrial porin from mammalian tissues. *Biochimica et Biophysica Acta* (1987), 905, 499–502.

[116] T. Yamamoto, A. Yamada, M. Watanabe, Y. Yoshimura, N. Yamazaki, Y. Yoshimura, T. Yamauchi, M. Kataoka, T. Nagata, H. Tereda, Y. Shinohara. VDAC1, having a shorter N-terminus than VDAC2 but showing the same migration in SDS-Polyacrylamide gel, is the predominant form expressed in mitochondria of various tissues. *Journal of Proteome Research* (2006), 5, 3336-3344.

[117] V. A. Menzel, M. C. Cassarà, R. Benz, V. De Pinto, A. Messina, V. Cunsolo, R. Saletti, K.-D. Hinsch, Elvira Hinsch. Molecular and functional characterization of VDAC2 purified from mammal spermatozoa. *Bioscience Reports* (2009), 29, 351-362.

[118] A. Sugiura, G. L. McLelland, E. A Fon, H.M. McBride. A new pathway for mitochondrial quality control: mitochondrial-derived vesicles. *The EMBO Journal* (2014), 33, 2142–2156.

[119] V. Soubannier, P. Rippstein, B. A. Kaufman, E. A. Shoubridge, H.M. McBride. Reconstitution of mitochondria derived vesicle formation demonstrates selective enrichment of oxidized cargo. *PLoS One* (2012), 7, e52830.

[120] M. Eldeeb, R. Fahlman. The-N-end rule: the beginning determines the end. *Protein & Peptide Letters* (2016), 23, 343–348.

La borsa di dottorato è stata cofinanziata con risorse del
Programma Operativo Nazionale Ricerca e Innovazione 2014-2020 (CCI 2014IT16M2OP005),
Fondo Sociale Europeo, Azione I.1 “Dottorati Innovativi con caratterizzazione Industriale”

UNIONE EUROPEA
Fondo Sociale Europeo